TEHNIČKI GLASNIK

TECHNICAL JOURNAL

TEHNIČKI GLASNIK / TECHNICAL JOURNAL – GODIŠTE / VOLUME 13 – BROJ / NUMBER 2

LIPANJ 2019 / JUNE 2019 – STRANICA / PAGES 81-164

/

SVEUČILIŠTE SJEVER / UNIVERSITY NORTH – CROATIA – EUROPE

ISSN 1846-6168 (PRINT) / ISSN 1848-5588 (ONLINE)

ISSN 1846-6168 (Print) ISSN 1848-5588 (Online)

TEHNIČKI GLASNIK - TECHNICAL JOURNAL

Scientific-professional journal of University North

Volume 13 Number 2
Varaždin, June 2019 Pages 81–164

Editorial Office:
Sveučilište Sjever – Tehnički glasnik
Sveučilišni centar Varaždin
104. brigade 3, 42000 Varaždin, Hrvatska
Tel. ++385 42 493 328, Fax.++385 42 493 333
E-mail: tehnickiglasnik@unin.hr
https://tehnickiglasnik.unin.hr
https://www.unin.hr/djelatnost/izdavastvo/tehnicki-glasnik/
https://hrcak.srce.hr/tehnickiglasnik

Founder and Publisher:
Sveučilište Sjever / University North

Print:
Centar za digitalno nakladništvo, Sveučilište Sjever

All manuscripts published in journal have been reviewed.
Manuscripts are not returned.

The journal is free of charge and four issues per year are published.
Circulation: 100 copies

Journal is indexed and abstracted in:
Web of Science Core Collection (Emerging Sources Citation Index - ESCI), EBSCOhost Academic Search Complete, EBSCOhost – One Belt, One Road Reference Source Product, ERIH PLUS, CITEFACTOR – Academic Scientific Journals, Hrčak - Portal znanstvenih časopisa RH

Registration of journal:
The journal "Tehnički glasnik" is listed in the HGK Register on the issuance and distribution of printed editions on the 18th October 2007 under number 825.

Preparation ended:
June 2019

Legend:
(1) University North, (2) Mechanical Engineering Faculty in Slavonski Brod, (3) Faculty of Graphic Arts Zagreb, (4) Faculty of Civil Engineering Osijek, (5) Faculty of Engineering Rijeka, (6) Faculty of Mechanical Engineering and Naval Architecture Zagreb, (7) Faculty of Metallurgy Sisak, (8) Tomas Bata University in Zlín, (9) Department of Physics of the University of Josip Juraj Strossmayer in Osijek, (10) Faculty of Humanities and Social Sciences Osijek, (11) Karlovac University of Applied Sciences, (12) University of Applied Sciences Velika Gorica, (13) Department of Polytechnics - Faculty of Humanities and Social Sciences Rijeka, (14) Faculty of Electrical Engineering and Computer Science - University of Maribor, (15) Faculty of Civil Engineering - University of Maribor, (16) University College of Teacher Education of Christian Churches Vienna/Krems, (17) Mechanical Engineering Faculty Tuzla, (18) Mechanical Engineering Faculty Sarajevo, (19) University of Travnik - Faculty of Technical Studies, (20) Higher Education Technical School of Professional Studies in Novi Sad, (21) University of Novi Sad - Faculty of Technical Sciences, (22) Faculty of Mechanical Engineering - University of Montenegro, (23) Brno University of Technology, (24) Odessa State Academy of Civil Engineering and Architecture, (25) Faculty of Civil Engineering - University of Mostar, (26) Faculty of Manufacturing Technologies with the seat in Prešov - Technical University in Košice

Note from the Editor-in-Chief

Dear readers,

In June, as it is the case every year, all journals indexed in the SCI bases await the official announcement of the impact factor (JCR IF) for the previous year. The Technical Journal is still not indexed in such bases, even though it is in the WoS (Web of Science - Emerging Sources Citation Index) citation base, which is why the unofficial impact factor has to be calculated. When calculated, for 2018, IF would be 0.123.

In the ranking evaluation, the journal is most often concentrated on the IF indicator. However, there are also many other indicators for journal ranking. One of the more commonly used is the SJR (***S****CImago* ***J****ournal* ***R****ank*) indicator. The official SJR index for 2018 was recently published and it was based on the data from the Scopus database. In the calculations, the IF takes into account the previous two years (the number of citations in the current year is divided by the total number of published papers in the previous two years), while the SJR index refers to the previous three years. Hence, the important difference between those two indicators is actually the data that they rely on in their calculations. WoS is a more selective database because it includes a smaller number of journals compared to the Scopus database, which encompasses a significantly larger number of journals. However, unlike the IF where each citation is equally taken into consideration (citation = citation), SJR weighs citations in such a way that more significance is given to those from more prestigious (more highly ranked) journals. Consequently, it is not possible to directly compare the IF and SJR indicators, and they should be perceived as an alternative to each other. The Technical Journal has been registered at Scopus, Ei Compendex and Inspec, where it awaits its evaluation.

When it comes to the developments related to our magazine, I highlight the traditional annual meeting of the editors of 12 technical journals from Croatia (5), Austria (1), Slovenia (2) and Serbia (4). This year, the meeting was held on 24 May 2019 at the Faculty of Mechanical Engineering in Maribor and it was organized by the *International Journal of Simulation Modeling* and *Advances in Production Engineering & Management*. At this fifth meeting, the Technical Journal participated for the first time, and it was presented by its Editor-in-Chief. It was a unique opportunity to discuss the difficulties that technical journals encounter on a day-to-day basis in their work, especially their editorial boards, which succeed in maintaining the reputation of the magazine with tremendous efforts and numerous difficulties, from the financial and organizational ones to providing a sufficient number of quality publications. The next meeting will take place in 2020 and will be organized by the *International Journal of Industrial Engineering and Management* at the Faculty of Technical Sciences in Novi Sad.

In terms of classified articles, in this issue we published 7 original scientific papers, 2 preliminary communications, 2 review papers and 3 professional papers from various technical fields.

At the end, as always, we invite you, our dear authors and readers, to contribute with your articles to our work and thereby help retain the quality of our joint journal.

Best regards,

Milan Kljajin
Editor-in-Chief of **Technical Journal**

ISSN 1846-6168 (Print), ISSN 1848-5588 (Online)
https://doi.org/10.31803/tg-20180116174952

Original scientific paper

THE EIGENVALUES OF ONE-SPEED NEUTRONS IN A SLAB WITH FORWARD AND BACKWARD SCATTERING

Ökkeş EGE, Hakan ÖZTÜRK

Abstract: The eigenvalue spectrum is studied for one-speed neutrons in a slab with forward and backward scattering. First, the transport equation describing the interaction of neutrons in a system with general geometry is given. Then, the scattering function in transport equation is chosen as the forward-backward-isotropic (FBI) scattering model. The resultant transport equation is solved using the Legendre polynomials expansion (P_N method) and the Chebyshev polynomials of second kind expansion (U_N method) in neutron angular flux. Then, the P_N and U_N moments of the equations are obtained using the properties of the Legendre and the Chebyshev polynomials of the second kind. Finally, the eigenvalues for various values of the collision and scattering parameters are calculated using different orders of the presented methods and they are given in the tables for comparison.

Keywords: eigenvalue spectrum; forward and backward scattering; slab geometry; U_N method; transport equation

1 INTRODUCTION

The criticality problem of a multiplying system is among the important problems in calculations of the neutron transport theory. There are many studies in literature about the solution of one-speed neutron transport equation with isotropic and anisotropic scattering for bare or reflected slabs and spheres. The scattering reactions from material atoms strongly affect the distribution and the interaction of the neutrons and thus the continuity of the fission chain reaction in the reactor system. Therefore, in the solution of the problems of neutron transport theory, the scattering of neutrons through the media should be as detailed as possible.

The series expansion of the angular flux or scattering function is commonly used in the problems of transport theory. In these approximations, neutron angular flux is expanded in two parts; the spatial and angular parts. The angular part of it is represented by an orthogonal polynomial. Among the orthogonal polynomials, the Legendre polynomials are the most widely used ones in the angular part of the neutron angular flux. This technique is known as the P_N method in literature. However, this does not indicate the validity of this method for all cases and problems. In some of the studies using P_N approximation, it is reported to be a rather poor representation of the angular flux especially near material boundaries [1]. Therefore, the Chebyshev polynomials of first kind (T_N method) have been tried instead of Legendre polynomials. Ultimately in case of anisotropic scattering and extrapolated end point calculations, it was observed that better results were obtained in using the Chebyshev polynomials rather than the Legendre polynomials [2-4]. In recent years, since these polynomials are in the same family, i.e. Jacobi polynomials, the second kind of Chebyshev polynomials approximation (U_N method) was used in criticality and diffusion length calculations for isotropic and anisotropic scattering in vacuum and reflecting boundary conditions. From those studies, it was observed that compatible results have been obtained in all cases [5-9]. As it is well known, an analytic or a numerical method can be used for all kinds of problems in science without hesitation. Therefore, in order to see the sustainability of the U_N method in different problems, it is still worth to use it in transport theory. In this study, eigenvalue spectrum for one-speed neutrons in a slab with forward, backward and isotropic scattering is studied using the present U_N method. The researchers in all areas may be interested in the solution algorithm followed in this study to apply it to their problems and thus an alternative method can be added to the literature.

The scattering function in transport equation is very important since it describes the interaction types of the neutron with the material boundaries. It should be as comprehensive as possible to represent the neutron interactions with the materials inside the system. There are many scattering functions in literature used for the neutron scattering function in transport equations. Among them, the forward-backward-isotropic (FBI) scattering model is one of the commonly used models in problems of transport theory [10, 11].

In the first part of the study, in order to compare the results obtained from the essential U_N method, the Legendre polynomials expansion (P_N method) is used for the solution of the eigenvalue problem with forward and backward scattering. This is done because the results obtained from the P_N method are seen to be benchmark in many cases.

Then, in the second and the essential part of this study, the U_N method, in which the angular part of the neutron flux is represented by the second kind of Chebyshev polynomials, is used for the solution of the same problem.

In both methods, after expanding the angular part of the neutron flux in terms of the Legendre and the second kind of Chebyshev polynomials respectively, P_N and U_N moments of the equations are obtained using the orthogonality and the recurrence relations of those polynomials precisely. Then, eigenvalue equations are derived by offering a general solution for the neutron flux. The numerical results for the eigenvalues are calculated and thus the eigenvalue spectrum

is obtained for using various values of the scattering parameters; collision and the forward and backward scattering parameters.

Calculated numerical results obtained by both methods are listed in the tables side by side. It can be observed from the derivations of the equations and the tabulated results that the U_N method is one of the most efficient methods among the polynomial expansion-based techniques with its rapid convergence and comparatively simple algebraic equations for the problems of transport theory.

2 THE METHODS

Many methods are developed for the solution of the neutron transport equation in literature. Some of them are stochastic and the others are deterministic. In this study, the approximation of the Chebyshev polynomials of second kind (U_N method) is preferred since it is one of the most powerful methods among the polynomial expansion based techniques and it is hoped to be used in other problems of applied mathematics. In addition, the eigenvalue problem is derived using the spherical harmonics (P_N method), i.e. a conventional, most commonly used and effective method for the solutions of the problems of transport theory. Therefore, the results obtained from both methods can easily be compared with each other.

2.1 Solution with P_N Method

The conservative form of the time-independent stationary transport equation for one-speed neutrons can be given as [10],

$$\begin{aligned}&\boldsymbol{\Omega}\cdot\nabla\psi(r,\boldsymbol{\Omega})+\sigma_T\psi(r,\boldsymbol{\Omega})=\\&=c\sigma_T\int\psi(r,\boldsymbol{\Omega}')\,f(\boldsymbol{\Omega}'\cdot\boldsymbol{\Omega})\,\mathrm{d}\boldsymbol{\Omega}'\end{aligned}\tag{1}$$

While $\boldsymbol{\Omega}'$ represents the unit vector along the neutron velocity before (and $\boldsymbol{\Omega}$ after) a scattering collision, σ_T represents the probability of all interactions of neutrons with materials; the total macroscopic cross-section. $\psi(r, \boldsymbol{\Omega})$ represents the neutron angular flux at position r and direction $\boldsymbol{\Omega}$. c is the secondary neutron numbers and $f(\boldsymbol{\Omega}\cdot\boldsymbol{\Omega}')$ can be forward-backward-isotropic (FBI) scattering model for the scattering function describing all kind of interaction of the neutrons with materials,

$$\begin{aligned}&f(\boldsymbol{\Omega}'\cdot\boldsymbol{\Omega})=\frac{1-\alpha-\beta}{4\pi}+\\&+\frac{\alpha}{2\pi}\delta(\boldsymbol{\Omega}'\cdot\boldsymbol{\Omega}-1)+\frac{\beta}{2\pi}\delta(\boldsymbol{\Omega}'\cdot\boldsymbol{\Omega}+1)\end{aligned}\tag{2}$$

where α and β coefficients can be seen as the forward and backward scattering probabilities, respectively; $0 \le \alpha, \beta \le 1$, $\alpha + \beta \le 1$ [11].

First, the scattering function given in Eq. (2) is inserted in Eq. (1) and then the one-dimensional transport equation can be written as,

$$\begin{aligned}&\mu\frac{\partial\psi(x,\mu)}{\partial x}+\sigma_T(1-\alpha c)\psi(x,\mu)=\\&=\frac{c\sigma_T}{2}(1-\alpha-\beta)\times\int_{-1}^{1}\psi(x,\mu')\mathrm{d}\mu'+\beta c\sigma_T\psi(x,-\mu)\end{aligned}\tag{3}$$

The neutrons are assumed to have same speed and thus the energy and the slab is assumed to be finite, homogeneous and having a thickness of $2a$ extending from $x = -a$ to $x = a$. The free space boundary and symmetry conditions are assumed:

$$\psi(a,\mu)=0\,,\tag{4a}$$

$$\psi(x,\mu)=\psi(-x,\mu),\quad \mu>0\,,\tag{4b}$$

In P_N method, the neutron angular flux in one-dimensional case is expanded in terms of the Legendre polynomials,

$$\begin{aligned}&\psi(x,\mu)=\sum_{m=0}^{\infty}\frac{2m+1}{4\pi}\Phi_m(x)\,P_m(\mu),\\&-a\le x\le a,\ -1\le\mu\le 1.\end{aligned}\tag{5}$$

The orthogonality and the recurrence relations of the Legendre polynomials are,

$$\int_{-1}^{1}P_n(\mu)P_m(\mu)\mathrm{d}\mu=\frac{2}{2n+1}\delta_{n,m}\,,\tag{6}$$

$$(2m+1)\mu P_m(\mu)=(m+1)P_{m+1}(\mu)+mP_m(\mu)\,.\tag{7}$$

In the next solution process, Eq. (5) is inserted into Eq. (3). Then, the resultant equation is multiplied by $P_n(\mu)$ and integrated over $\mu \in [-1, 1]$ by means of Eqs. (6) and (7). Ultimately, P_N moments of equations are obtained;

$$\begin{aligned}&(n+1)\frac{\mathrm{d}\Phi_{n+1}(x)}{\mathrm{d}x}+n\frac{\mathrm{d}\Phi_{n-1}(x)}{\mathrm{d}x}+\\&+\sigma_T(2n+1)\left\{1-c\left[\alpha+(-1)^n\beta\right]\right\}\Phi_n(x)=\\&=c\sigma_T(2n+1)(1-\alpha-\beta)\Phi_0(x)\delta_{n,0}.\end{aligned}\tag{8}$$

$n \ge 0$. Conventionally, the general solutions to Eq. (6) are employed of the form [10],

$$\Phi_n(x)=G_n(\nu)\exp\left(\frac{\sigma_T x}{\nu}\right).\tag{9}$$

This solution is inserted into Eq. (6) for obtaining the eigenvalue equations and thus the eigenvalues,

$$\begin{aligned}&(n+1)G_{n+1}(\nu)+nG_{n-1}(\nu)+\\&+\nu(2n+1)\left\{1-c\left[\alpha+(-1)^n\beta\right]\right\}G_n(\nu)=\\&=\nu c(2n+1)(1-\alpha-\beta)G_0(\nu)\delta_{n,0},\end{aligned}\tag{10}$$

where $G_{-1}(\nu) = 0$ and $G_0(\nu) = 1$. As the requirement of the method one can set $G_{N+1}(\nu) = 0$ to obtain the discrete and the continuum ν eigenvalues using various values of c, α and β. As an example for P_1 approximation, an expression for the eigenvalues can easily be derived from Eq. (10) by solving the coupled equations for $n = 0$ and 1 together,

$$\nu_{1,2}=\pm\frac{1}{\sqrt{3(1-c)\left[1-c(\alpha-\beta)\right]}}.\tag{11}$$

2.1 Solution with U_N Method

In some of recent studies, the following function is used as angular flux in transport equation and compatible results are reported to be obtained in various problems of neutron transport [5, 6]:

$$\begin{aligned}&\psi(x,\mu)=\frac{2}{\pi}\sqrt{1-\mu^2}\sum_{n=0}^{N}\Phi_n(x)U_n(\mu),\\&-a\le x\le a,\quad -1\le\mu\le 1\end{aligned}\tag{12}$$

As in the derivation of the equations in P_N method, prior to starting the applications, the orthogonality and recurrence relations of the Chebyshev polynomials of second kind are needed [12],

$$\int_{-1}^{1}U_n(\mu)U_m(\mu)\sqrt{1-\mu^2}\,\mathrm{d}\mu=\frac{\pi}{2}\delta_{n,m},\tag{13}$$

$$U_{n+1}(\mu)-2\mu U_n(\mu)+U_{n-1}(\mu)=0.\tag{14}$$

Indeed, the same procedure with the P_N method is valid for the U_N method. In order to obtain the U_N moments of the angular flux Eq. (12) is needed to be inserted into Eq. (3). Then if one multiplies the resultant equation by $U_m(\mu)$ and integrates it over $\mu \in [-1,1]$:

$$\frac{\mathrm{d}\Phi_1(x)}{\mathrm{d}x}+2\sigma_T(1-c)\Phi_0(x)=0\tag{15a}$$

$$\begin{aligned}&\frac{\mathrm{d}\Phi_{n+1}(x)}{\mathrm{d}x}+\frac{\mathrm{d}\Phi_{n-1}(x)}{\mathrm{d}x}+2\sigma_T\left\{1-c\left[\alpha+(-1)^n\beta\right]\right\}\Phi_n(x)=\\&=c\sigma_T(1-\alpha-\beta)\left\{\frac{1+(-1)^n}{n+1}\Phi_0(x)\right\},\end{aligned}\tag{15b}$$

$n \ge 1$. The ansatz solution for neutron flux given in Eq. (9) is substituted into Eqs. (15). One can easily obtain the following system of algebraic equations for $G_n(\nu)$:

$$G_1(\nu)=-2\nu(1-c)G_0(\nu),\tag{16a}$$

$$\begin{aligned}&G_{n+1}(\nu)+G_{n-1}(\nu)+2\nu\left\{1-c\left[\alpha+(-1)^n\beta\right]\right\}G_n(\nu)=\\&=\nu c(1-\alpha-\beta)\left\{\frac{1+(-1)^n}{n+1}G_0(\nu)\right\},\quad n\ge 1,\end{aligned}\tag{16b}$$

By following the same procedure described in P_N approximation, the discrete and continuum ν eigenvalues are computed by setting $G_{N+1}(\nu) = 0$ for various values of c, α and β. As an example for U_1 approximation, an expression for the eigenvalues can easily be derived from Eqs. (16),

$$\nu_{1,2}=\pm\frac{1}{2\sqrt{(1-c)\left[1-c(\alpha-\beta)\right]}}.\tag{17}$$

After computing the discrete eigenvalues, since all eigenvalues correspond to a linear independent eigenfunction, the linear combination of the eigenfunctions can be written as the n^{th} Chebyshev moment of angular flux for odd numbers of N,

$$\begin{aligned}&\Phi_n(x)=\sum_{k=1}^{\frac{N+1}{2}}\lambda_k G_n(\nu_k)\left[\begin{array}{l}\exp\left(\dfrac{\sigma_T x}{\nu_k}\right)\\+(-1)^n\exp\left(\dfrac{-\sigma_T x}{\nu_k}\right)\end{array}\right]\\&n=1,\ldots,N,\ -a\le x\le a\end{aligned}\tag{18}$$

where λ_k are the linear combination coefficients and they can be determined from the physical boundary conditions. The parity property of $G_n(-\nu) = (-1)^n G_n(\nu)$ is also used.

3 NUMERICAL RESULTS

The U_N method which is one of the most powerful methods improved for the solution procedure of the transport equation is used for the solution of the eigenvalue problem for one-speed neutrons in a homogeneous slab with forward and backward scattering. Before starting to apply the U_N method to the problem, in order to establish a benchmark list for the comparison of the results, first the conventional P_N method is applied to the transport equation for the solution of the problem. The function given in Eq. (5) is used for the neutron angular flux in Eq. (3) in P_N method. At the end of the operation of the conventional P_N method to the transport equation, Eq. (10) is obtained for calculating the eigenvalues for various values of the scattering parameters. This operation has been done to illustrate the similarity of the methodology derived by both methods. This similarity is expected since the functions used in both methods have the same definition interval and they are in

the same polynomial family.

Then, in the main part of this study, the function involving the Chebyshev polynomials of second kind given in Eq. (12) is used for the neutron angular flux in transport equation together with the FBI scattering model given in Eq. (2) to obtain the U_N moments of equations. Thereafter, a general solution is employed to the moment equations and analytic expressions for a system of algebraic equations of the eigenvalues are obtained and they are given in Eqs. (16). Numerical results for the eigenvalues are calculated by setting $G_{N+1}(\nu) = 0$ in Eqs. (16) as in P_N approximation for various values of the collision parameter c, forward scattering parameter α and backward scattering parameter β. Although these results are computed up to an order of $N = 5$, the order of approximation can be extended to $N > 5$. In all cases, the total macroscopic cross section is assumed to be its normalized value, $\sigma_T = 1$ cm^{-1}.

4 CONCLUSIONS

The numerical results for the eigenvalues are computed for the values of c ranging from 0.90 to 1.20. They are calculated in the cases of isotropic scattering ($\alpha = 0.0$; $\beta = 0.0$), forward scattering ($\alpha = 0.3$; $\beta = 0.0$) and backward scattering ($\alpha = 0.0$; $\beta = 0.3$) using both P_N and U_N methods.

Table 1 Eigenvalue spectrum for isotropic scattering ($\alpha = 0.0$; $\beta = 0.0$)

c	P_1	U_1	P_3	U_3	P_5	U_5
0.90	1.82574	1.58114	0.48657 1.90273	0.41811 1.89082	0.30333 0.80588 1.90320	0.27959 0.74313 1.90252
0.95	2.58199	2.23607	0.49688 2.63507	0.42556 2.62721	0.30775 0.81133 2.63515	0.28348 0.74840 2.63493
0.99	5.77350	5.00000	0.50506 5.79673	0.43152 5.79343	0.31132 0.81526 5.79673	0.28664 0.75231 5.79671
1.01	5.77350i	5.00000i	5.75054i 0.50912	5.75373i 0.43450	5.75054i 0.31311 0.81709	5.75052i 0.28823 0.75417
1.10	1.82574i	1.58114i	1.75703i 0.52692	1.76555i 0.44777	1.75665i 0.32127 0.82437	1.75620i 0.29547 0.76176
1.20	1.29099i	1.11803i	1.20016i 0.54547	1.20976i 0.46209	1.19830i 0.33041 0.83089	1.19723i 0.30364 0.76887

Table 2 Eigenvalue spectrum for forward scattering ($\alpha = 0.3$; $\beta = 0.0$)

c	P_1	U_1	P_3	U_3	P_5	U_5
0.90	2.13687	1.85058	0.65609 2.26245	0.56524 2.24245	0.41111 1.09787 2.26390	0.37910 1.01227 2.26229
0.95	3.05352	2.64443	0.68920 3.14223	0.59103 3.12885	0.42794 1.13179 3.14250	0.39429 1.04385 3.14197
0.99	6.88592	5.96338	0.71721 6.92541	0.61294 6.91977	0.44230 1.15912 6.92542	0.40726 1.06958 6.92537
1.01	6.91549i	5.98899i	6.87613i 0.73170	6.88158i 0.62431	6.87613i 0.44978 1.17285	6.87608i 0.41402 1.08259
1.10	2.23050i	1.93167i	2.10923i 0.80037	2.12318i 0.67895	2.10778i 0.48622 1.23547	2.10666i 0.44699 1.14242
1.20	1.61374i	1.39754i	1.45011i 0.88174	1.46395i 0.74581	1.44269i 0.53228 1.30738	1.43994i 0.48889 1.21169

In Tab. 1, the eigenvalues for isotropic scattering are given. While the eigenvalues for forward scattering are given in Tab. 2, the eigenvalues for backward scattering are given in Tab. 3. As can be followed from all tables, all eigenvalues are real when $c < 1$. These eigenvalues can be used for diffusion theory (diffusion coefficient or diffusion length) or calculation of scalar flux. On the other hand, imaginary eigenvalues are seen when $c > 1$ as expected. Since this situation corresponds to supercritical reactor, the eigenvalues for $c > 1$ are used in criticality problems. It is seen from tables 1 through 3, the numerical results for the eigenvalues obtained from both methods exhibit the same behaviour. Although it is not shown in the results in tables, one can easily understand that the tabulated eigenvalues are in pairs as they are felt in Eq. (11) and Eq. (17).

Table 3 Eigenvalue spectrum for backward scattering ($\alpha = 0.0$; $\beta = 0.3$)

c	P_1	U_1	P_3	U_3	P_5	U_5
0.90	1.62008	1.40303	0.49742 1.71530	0.42854 1.70013	0.31169 0.83236 1.71640	0.28742 0.76746 1.71517
0.95	2.27773	1.97257	0.51410 2.34390	0.44087 2.33392	0.31922 0.84424 2.34410	0.29412 0.77864 2.34371
0.99	5.06955	4.39036	0.52803 5.09863	0.45126 5.09448	0.32563 0.85337 5.09863	0.29983 0.78744 5.09860
1.01	5.05786i	4.38024i	5.02908i 0.53515	5.03306i 0.45661	5.02907i 0.32897 0.85780	5.02904i 0.30281 0.79179
1.10	1.58312i	1.37102i	1.49705i 0.56807	1.50695i 0.48189	1.49602i 0.34510 0.87689	1.49523i 0.31726 0.81085
1.20	1.10702i	0.95871i	0.99476i 0.60487	1.00426i 0.51162	0.98968i 0.36514 0.89686	0.98779i 0.33537 0.83121

In this study, the neutrons are assumed to be scattered isotropically in forward and backward directions in a homogeneous slab. Eq. (12) which is expanded in a series of the Chebyshev polynomials of second kind is used as the angular neutron flux in transport equation. The derived equations for the U_N moments are solved for the eigenvalue spectrum of the neutrons. These eigenvalues can be extended for requested collision and scattering parameters and they can be used in many problems of transport theory such as the criticality calculations, diffusion theory or scalar flux calculations. The method used in this study has already been used in other studies and the applicability and validity of it were proven from the results [5-7]. In addition, the traditional P_N method is also applied to the problem and the results obtained from this method are given in tables for comparison. From the tabulated results, one can easily realize that the U_N method is an effective method for the transport equation and thus it can be used in other problems of science and engineering. In near future, this study can be extended to the cases with anisotropic scattering and reflecting boundary conditions.

5 REFERENCES

[1] Lee, C. E. & Dias, M. P. (1984). Analytical solutions to the moment transport equations-I; one-group one-region slab and sphere criticality. *Ann. Nucl. Energy*, 11, 515-530. https://doi.org/10.1016/0306-4549(84)90076-8

[2] Aspelund, O. (1958). On a new method for solving the (Boltzmann) equation in neutron transport theory. *PICG*, 16, 530-534.
[3] Conkie, W. R. (1959). Polynomial approximations in neutron transport theory. *Nucl. Sci. Eng.,* 6, 260-266. https://doi.org/10.13182/NSE59-A28841
[4] Yabushita, S. (1961). Tschebyscheff polynomials approximation method of the neutron transport equation. *J. Math. Phys.*, 2, 543-549. https://doi.org/10.1063/1.1703739
[5] Öztürk, H., Anlı, F., & Güngör, S. (2007). Application of the U_N method to the reflected critical slab problem for one-speed neutrons with forward and backward scattering. *Kerntechnik*, 72, 74-76. https://doi.org/10.3139/124.100321
[6] Öztürk, H. (2008). The reflected critical slab problem for one-speed neutrons with strongly anisotropic scattering. *Kerntechnik*, 73, 66-74. https://doi.org/10.3139/124.100532
[7] Öztürk, H. (2008). Study of the effect of anisotropic scattering on the critical slab problem in neutron transport theory using Chebyshev polynomials. *Kerntechnik*, 73, 284-287. https://doi.org/10.3139/124.100572
[8] Öztürk, H. (2011). Modified U_N method for the reflected critical slab problem with forward and backward scattering. *Kerntechnik*, 76, 142-145. https://doi.org/10.3139/124.110126
[9] Öztürk, H. (2014). The effect of strongly anisotropic scattering on the critical size of a slab in one-speed neutron transport theory: Modified U_N method. *Ann. Nucl. Energy*, 65, 24-29. https://doi.org/10.1016/j.anucene.2013.10.021
[10] Davison, B. (1958). *Neutron transport theory*. London: Oxford University Press. https://doi.org/10.1063/1.3062414
[11] Sahni, D. C., Sjöstrand, N. G., & Garis, N. S. (1992). Criticality and time eigenvalues for one-speed neutrons in a slab with forward and backward scattering. J. Phys. D: Appl. Phys., 25, 1381-1389. https://doi.org/10.1088/0022-3727/25/10/001
[12] Arfken, G. (1985). *Mathematical methods for physicists*. London: Academic Press, Inc.

Authors' contacts:

Ökkeş EGE, MsC student
Osmaniye Korkut Ata University,
Faculty of Arts and Sciences,
Department of Physics,
Osmaniye, 80000, Turkey
Tel. +90 328 8251818
E-mail: okkesege@gmail.com

Hakan ÖZTÜRK, PhD, Full Professor
(Corresponding author)
Osmaniye Korkut Ata University,
Faculty of Arts and Sciences,
Department of Physics,
Osmaniye, 80000, Turkey
Tel. +90 328 8251818
E-mail: hakanozturk@osmaniye.edu.tr

ISSN 1846-6168 (Print), ISSN 1848-5588 (Online)
https://doi.org/10.31803/tg-20180310210604

Original scientific paper

INFLUENCE OF REINFORCED CONCRETE FORMING FEATURES ON MECHANICAL CHARACTERISTICS

Marina DRAPALUK

Abstract: The article found that defects in cement and aggregate grains can not only cause stress concentration and contribute to cracking, but also can stop their propagation. It was determined that, in addition to zones with reduced strength, a zone with an increased viscosity can become a brake on the path of a growing crack, having a modulus of elasticity much less than the modulus of elasticity of the base material. The influence of moulding of reinforced concrete structures on its mechanical characteristics was revealed. It can be stated that mineral additives of various nature, regardless of hydraulic activity degree, optimize the deformative properties of cement stone and concrete with practically constant compressive strength.

Keywords: cement stone; defects; mineral additives; shrinkage cracks

1 INTRODUCTION

The main mechanism that establishes the cracks propagation in concrete on a dense aggregate is the failure of adhesion at the interface of "cement stone - aggregate". These assumptions were confirmed by numerous studies of the interface. This area is usually weaker than the mortar part and is the site of microcrack formation as a result of water separation and shrinkage. On the other hand, the analysis of stresses from an external load showed the presence of places with a high concentration of stresses, which cause the development of initial microcracks in the main separation crack. From this it follows that the interface of the "cement stone - aggregate" is capable of blocking the developing crack only in the event that there is sufficient adhesion of the aggregate to the cement stone. With low adhesive strength, this surface is the area from which cracks develop, which determine the nature of the general destruction of concrete.

2 ANALYSIS OF RECENT RESEARCH

The dual role of various defects (pores, initial shrinkage cracks) in cement and aggregate grains was noticed by Popovich [1], highlighting that, first of all, they can cause stress concentration and contribute to the appearance of cracks; secondly, they can suspend their propagation. He noticed that when compressing, pores in the concrete prevent propagation of cracks to a greater extent than when stretching. That is why, in his opinion, increase in porosity will worsen the strength of concrete at compression more than its tensile or bending strength. The role of the aggregate in inhibiting the growth and quenching of brittle cracks is convincingly enough characterized by the data of many researchers, in particular, Sytnik and Ivanov [2], who discovered that the destruction of cement stone occurs suddenly. Parametric levels of cracks formation for it are not observed, i.e. they coincide with the ultimate strength. Ya. Tanigawa and E. Hosaka [3] came to the same conclusion when investigating the cracking of cement stone. They found that the samples break down immediately after propagation of macrocracks along the longitudinal axis because there is no aggregate in the cement stone that stops their propagation. When studying the mechanism of crystalline bodies destruction, Frenkel [4] noted that development and growth of cracks could be effectively inhibited by fine pores present in the material, as well as inclusions with less strength or modulus of elasticity. Consequently, in addition to zones with reduced strength, zones with increased viscosity may become an effective brake in the path of a growing crack, having a modulus of elasticity much less than the modulus of elasticity of the base material. In addition to high viscoplastic properties, said zones should also possess excellent adhesion to the base material.

3 PURPOSE AND OBJECTIVES

At present, there are known studies and experience in the use of mineral and organic weakly rigid porous components (additives) of various dispersity in concrete mixtures: from dispersity of binding one to the size of fine and coarse aggregates [5]. It is portland cement with mineral additives and pozzolanic portland cement, mortars and concretes on mixed and combined aggregates. The listed materials are characterized by savings in the clinker part (when using finely dispersed mineral additives), reduced density of concrete with mixed aggregates), increased crack resistance, frost resistance, in some cases - tensile strength [6]. Summarizing the results of studies carried out to date in this field, it is expedient to differentiate such components depending on their dispersion. In accordance with this, it is possible to isolate finely dispersed components (additives) with a specific surface of 50-300 m^2/kg [6]; components with dimensions of fine aggregate - sand; components with dimensions of coarse aggregate. Therefore, it is important to determine the ways to optimize the structure of concrete in order to increase the crack resistance and durability.

4 OBJECTS AND METHODS OF RESEARCH

In case of uniaxial and triaxial compression of ordinary concrete, the initial cracks are formed mainly under the

grains of coarse aggregate even before loading [7]. It weakens the contact layer, breaks monolithic, reduces the uniformity and strength of concrete as a whole. The weakness of the contact layer is determined by sedimentation processes in freshly laid concrete and the development of shrinkage cracks in it during hardening. First, as a result of internal water separation, water accumulates under the grains of aggregate, resulting in the formation of pores, partially or completely filled with water [7]. During the hardening of concrete, the defectiveness of the contact layer is enhanced by the appearance of shrinkage stresses and, as a consequence, the formation and development of shrinkage cracks localized mainly at the interfaces of phases with different stiffness. At the same time, defects in cement and aggregate grains can, firstly, serve as a cause of stress concentration and contribute to the appearance of cracks; secondly, they can suspend their propagation [7]. It was noted that when compressing the pores in the concrete, the crack propagation is prevented more than by stretching [7].

Mechanism of inhibition of destruction processes of concrete is determined by the presence in it of "weak" elastoviscous and layered inclusions, which reduce local stresses and extinguish energy of cracks growth. Such layered inclusions include hydrosilicates and calcium hydroxide, as well as additives of polymers and expanded vermiculite.

In addition, viscous catalysts for brittle fracture of concrete are closed air pores, which, on the one hand, reduce the effective cross-section of the material, and on the other they are able to redistribute local stresses in concrete among its components with different elasticity.

5 SCIENTIFIC RESULTS

As a result of analysis of the degree of technological factors influence on the processes of moulding the operational properties of the concrete being developed, it is established that it is expedient to use dry concrete moulding technology.

However, transporting and placement of a concrete mixture in a mould for a dry concrete mix becomes very important due to delamination during transportation, placement in a mould, and distribution in a mould. The experience of transporting dry mixtures in bags and sealed containers for the factory production of reinforced concrete products is not economically justified [8].

Other technical solutions, with the exception of the proposal to supply the feeder of the concrete paver with a protective casing and equip the loading panel with a reciprocating drive, are not available.

An important technological conversion is solidification. The average density of a dry concrete mixture of different composition was solidified when it was solidified by vibrating, impact method and rolling, the mixtures were solidified layer by layer of different thickness.

The parameters of solidification - amplitude and frequency of oscillations (impacts) were also varied; the intensity of the load and vibration and impact solidification time; speed of movement and linear pressure of the roller with a rolling seal.

Based on the conducted studies, it was concluded that the highest quality of solidification was achieved when the concrete mix was placed with vibrating and loading [9].

The influence of vibration parameters on the workability of modified concrete mixtures of dry moulding of different compositions was determined under the conditions of mixture distribution by shape and vacuuming. For this purpose, several compositions of dry concrete mixtures with a cement content in the mortar part of $C/(C + S) = 0.3$; 0.7; 1.0 and with the same ratio of the mass of the mortar part to the total mass of the concrete mix $S/(S + L)$. In order to simulate the processes of efflux and compaction of modified concrete dry moulding, a viscometer was used in the mold. Four modes of vibrocompaction were set: frequency $f = 50$ Hz, acceleration Ag = 1.5g; 2.5g; 3.5g; 4.5g. The results of the experiments are given in Tab. 1.

Table 1 Influence of vibration intensity on the workability of modified concrete mixes of dry molding during vibrating compaction and vibrodistribution their form

Item No.	The composition of the mixture		The distribution and compaction time of the mixture τ_1 and τ_2, c, during acceleration							
	$\frac{C}{C+S}$	$\frac{S}{S+L}$	1,5g		2,5g		3,5g		4,5g	
			τ_1	τ_2	τ_1	τ_2	τ_1	τ_2	τ_1	τ_2
1	0	0.3	32	56	24	47	18	30	12	25
2	0	0.7	54	63	35	55	25	35	20	28
3	0	1.0	57	65	35	60	30	36	24	35
4	0.3	0.3	52	68	30	37	23	25	18	25
5	0.3	0.7	61	77	32	37	25	32	21	27
6	0.3	1.0	64	89	40	45	28	40	23	30
7	0.7	0.3	55	63	33	47	25	30	20	28
8	0.7	0.7	63	81	40	52	30	40	26	40
9	0.7	1.0	70	92	49	60	27	43	25	41
10	1.0	0.3	60	68	35	60	24	39	20	25
11	1.0	0.7	67	79	40	63	28	47	23	40
12	1.0	1.0	70	90	47	62	30	46	25	37

Table 2 Influence of vibration intensity on the workability of modified dry-formed concrete mixes with vibratory vacuum compaction with expiry

Item No.	The composition of the mixture		The distribution and compaction time of the mixture τ_1 and τ_2, c, during acceleration							
	$\frac{C}{C+S}$	$\frac{S}{S+L}$	1.5g		2.5g		3.5g		4.5g	
			τ_1	τ_2	τ_1	τ_2	τ_1	τ_2	τ_1	τ_2
				50	26	21	16	25	12	20
				60	65	52	39	50	31	43
				52	38	23	20	32	14	26
				38	04	34	07	42	06	29
				58	43	22	27	34	19	27
1	0	0.3	27	55	33	42	27	34	19	25
2	0	0.7	46	33	47	70	20	31	18	52
3	0	1.0	48	52	24	42	27	29	17	25
4	0.3	0.3	45	66	89	09	20	39	17	42
5	0.3	0.7	49	53	34	41	19	32	11	25
6	0.3	1.0	50	95	54	48	28	35	18	52
7	0.7	0.3	47	63	34	42	27	32	11	25
8	0.7	0.7	50	06	69	91	27	25	19	42
9	0.7	1.0	53	63	35	52	30	35	12	28
10	1.0	0.3	47	77	42	23	30	43	02	33
11	1.0	0.7	47	73	35	52	19	30	12	21
12	1.0	1.0	45	09	97	70	90	34	01	12
				63	52	50	27	34	18	25
				53	01	52	04	40	18	52
				63	35	42	27	40	19	82
				55	44	52	19	40	29	32
				66	54	31	26	30	20	22

As can be seen in Tab. 1, as the amount of sand and cement in the mixture increases, the hardness τ_1 increases from 32 to 57 and 70 s with an acceleration of 1.5g, and from 12 to 24 and 25 s with an acceleration of 4.5g. The time for reaching the maximum density τ_2 also increases. The data Tab. 1 allows us to predict the rigidity and assign the time of vibrocompaction of modified concrete mixes of dry moulding, depending on the composition of the mixture and the intensity of vibration, but this is for normal moulding conditions.

To determine the rational modes of vibrovacuum moulding, the experiment was repeated with a vacuum of 0.09 MPa on the same mixing gauge, but with the vacuum-bag installed. The results of the experiment are given in Tab. 2.

From the comparison of Tabs. 1 and 2, it is evident that vacuuming reduces the time of distribution and compaction of modified dry-formed concrete mixes with a high content of sand and cement by about 20%.

Methods of water saturation of the concrete mixture, in particular, the condensation of water vapour, are also important. At the same time, the process is carried out either independently of other technological processes, or in the process of heat and moisture treatment (Tab. 3).

Table 3 Influence of impregnation methods and modes on the wetting rate of a dry sample (cylinder diameter and height 15 cm)

Impregnation method	Impregnation mode	Duration of impregnation, min
Capillary suction	Immersion in water at a temperature of 20 °C	328
	The same, 2% solution of PFM-BS	275
	The same, 2% fleeceflower extract solution	294
	The same, in liquid glass, ρ = 1.2 kg/dm^3	more than 12 h
	The same, hot water 80 °C	275
Pressure filtration	One-sided water injection at a pressure of 0.05 MPa	Channel formation
	The same, 2% solution of PFM-BS	54
	The same, 2% fleeceflower extract solution	77
	The same, hot water 80 °C	62
	Single-side suction of water with a vacuum of 0.005 MPa	4.0
	The same, of water at 80 °C	2.4
	Injection of liquid glass ρ = 1.2 kg/dm^3 with a pressure of 0.1 MPa	124
	Suction of liquid glass ρ = 1.2 kg/dm^3 with a pressure of 0.1 MPa	27
	Suction-injection of liquid glass ρ = 1.2 kg/dm^3 with a pressure of 0.1 MPa and a vacuum of 0.1 MPa	5.0
	The same at 80 °C	3.5
Condensation	Volumetric steam injection with a pressure of 0.1 MPa	63
	Volumetric suction of steam with a pressure of 0.1 MPa	2.0
	Injection of steam with a pressure of 0.1 MPa into the previously evacuated dry mixture	less than 2 min

Saturation of a dry concrete mixture with steam condensate in the process of heat and moisture treatment leads to the wetting of the surface of the layer of all the product facets, in connection with it, the air in the volume of the mixture is entrapped, and the saturation of the product is extremely difficult. For a more complete impregnation, it is also suggested to apply hot water to the surface of the product after steam is applied and a "crust" is formed, and then again steam. However, it does not change the mechanism of air entrapment in the volume of the product and, moreover, has limited application. It is also proposed to use steam for the water saturation in the process of heat and moisture treatment with a pressure of 0.5 MPa.

It reduces the impregnation time to 3-13.5 min. However, in this case, the effect of air entrapment in the volume is preserved, and complete moistening of the sample is not guaranteed. It is also possible to carry out water saturation under pressure, which, depending on the thickness of the product, should be from 0.2 to 0.6 MPa (0.2 for a 10 cm layer, 0.6 for a 40 cm layer).

Preference is given to the use of hot water, since with increasing temperature its dynamic viscosity decreases. When the pressure is increased from 0.1 to 1.0 MPa, the saturation time of the layer of the concrete mixture 10 cm thick is reduced from 28 to 2.8 minutes. For a layer of 30 cm, the saturation time of the sample at a pressure of 0.3 MPa is 46 minutes. Thus, the most effective way of water saturation is water saturation at a pressure of 0.3-0.5 MPa. However, there is a danger of washing through channels in a disconnected semidry mixture. For real products, where local inhomogeneities are unavoidable due to large sizes (in the density of the dry mix, in the density of the filtering elements, etc.), this method is not possible. Another important issue is selection of the dry-formed concrete composition. When calculating the composition of water-based mixtures, they are first set by the flow of water, which then allows the calculation of the amount of cement. With dry moulding, the water flow cannot be set, since it is a function of the density of the mixture, and density is a function of the consumption of cement, sand, gravel. Therefore, the absolute volume method for dry mixtures is unacceptable.

At present, there are three main methods for designing dry concrete composition. Gusev et al. [10] suggest starting the calculation with the choice of an astringent whose activity should correspond to the brand of concrete. Calculation is based on the dependence of the strength (grade) of concrete on the packing density of solid-phase components. To find the optimal ratio of components, it is proposed to make mixtures of components and to determine experimentally the optimum ratio of components [10]. The authors do not give acceptable formulas for the calculation.

The empirical dependence of the strength of dry-formed concrete on the packing density of solid-phase components [11] is also based on the calculation proposed by

Ovchinnikov.

The method of designing the composition of dry concrete is most fully described in [11]. According to this method, the average density is first assigned, depending on the type of construction and the method of solidification. Then, according to the known strength and average density, the required binder activity is determined. Finally, from the experimental graphs, water demand and cement consumption are determined, and then the aggregate consumption and the proportion of sand in it are calculated. However, this method does not provide for taking into account the specific properties of the components and, in addition, it assumes the possibility of a free choice of the cement brand, which is impracticable.

In connection with the above, we have proposed a method for assigning a dry concrete mix, based on the following theoretical considerations.

1) The strength of concrete depends on the water-cement ratio, and the water-cement ratio in dry concrete is directly determined by the ratio of cement and sand. As the cement is saturated with voids in the sand, the voidness of the solution, and therefore, the water-cement ratio decreases. After filling with a volume of voids in the sand, the cement becomes densified with a further decrease in voidness and water-cement ratio. When the cement packing density reaches its maximum value, a further increase in its consumption leads to a proportional increase in the volume of intergranular voids. The porosity and the subsequent water content increase, while in the water-cement ratio it remains constant.

2) At a given ratio of cement and sand, the minimum cement consumption will be in the case where the packing density of solid phase components is maximum.

To check this reasoning, a series of experiments was carried out, the purpose of which was to establish a quantitative relationship between the cement fraction in the solution mixture $C/(C+S)$, the water-cement ratio, and the strength of the concrete. The results are shown in Tab. 4, from which it follows that as the cement content increases, the density of the mixture first increases sharply with a maximum at $C = 500$ kg/m^3, and then decreases. The strength first increases sharply from 30 to 70 MPa and stabilizes at water-cement ratio = 0.27-0.25 (Tab. 4).

Table 4 Dependence of the water-cement ratio and strength on the cement content in the solution component of concrete

Item No.	Initial data			Comparable data		
	C, kg/m^3	S, kg/m^3	K_u	$C/(C+S)$	W/C	f_{cc}, MPa
1	300	975	0.814	0.239	0.62	39.8
2	400	880	0.844	0.312	0.39	53.8
3	500	775	0.854	0.408	0.292	69.2
4	550	710	0.854	0.436	0.265	79.3
5	600	600	0.846	0.500	0.256	81.2

Remark: $R_c = 43$ MPa.

Thus, the correlation between $C/(C+S)$ and water-cement ratio, and therefore between $C/(C+S)$ and R_b, is expressed quite clearly, and the task is only to quantify this relationship for the conditions of use of different materials. To solve this problem, another series of experiments was carried out on three different types of cements, two types of sands and two types of crushed stone. Firstly, the densest compositions with different contents of cement were selected for this, a cement-sand mixture with a different sand-cement ratio was prepared. Then, crushed stone was added in portions to the resulting mixture, and after adding each portion, the mixture was solidified, the average density was determined. The amount of crushed stone, at which the mixture with a given C/S ratio acquired the maximum density, was considered optimal. Cylinders with a diameter and height of 15 cm were formed from this mixture. The samples were saturated with water at a temperature of 80 °C. After thermo-axial aging for 4-6 h, the samples were lifted and placed in a normal hardening chamber for 28 days. The solidification was produced by vibration with a frequency of 50 Hz and an acceleration of 3.0 g, the value of the load was 0.09 MPa, and the depth of vacuum was 0.09 MPa. The moulding mode is taken from Tab. 4. In the results of the determination of the samples strength, it follows that the strength of the dry-formed concrete increases with an increase in the C/S ratio, and after a certain C/S ratio, the value of which depends on the sand porosity, the strength increase sharply slows down. This is due to the fact that initially the packing density of the cement particles in the intervals between the grains of sand increases with C/S ration rising, and porosity of dry and water content of the saturated concrete decrease. After reaching the maximum packing density of cement grains approximately 1700-1800 kg/m^3, further increase in cement consumption is accompanied by a corresponding increase in the amount of water. The water-cement ratio remains constant, which is confirmed by the results of the experiments and the calculation given in Tab. 4. It has also been found that the more porosity there is, the faster its maximum density is achieved with a larger cement content, and the more porosity of crushed rock there is, the more cement-sand mixture is required to achieve the maximum density and strength of concrete.

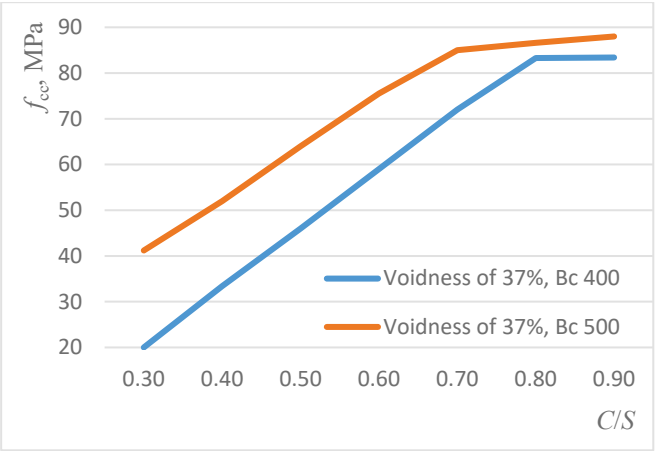

Figure 1 Nomogram for the purpose of cement-sand ratio of dry-formed concrete (with increasing (decreasing) of sand porosity by 1%, C/S ratio increases (decreases) by 0.01).

In accordance with the above provisions, the following procedures for the designation of dry concrete are proposed.

1) From the graph in Fig. 1 the required C/S ratio depending on the given brand of concrete R_b, cement activity

R_c and sand porosity S_p can be found.

2) A dry mixture of cement and sand should be prepared in a predetermined ratio and this mixture should be saturated with crushed stone until the maximum density is achieved.

3) For the maximum average density and the ratio of dry components, their consumption per 1 m^3 of concrete is found.

4) Concrete samples are to be prepared and tested, and if their strength is more than 10% of the required one, the resulting strength value is to be marked on the vertical line corresponding to the found *C*/*S* ratio, a line parallel is to be drawn to the strength lines until it meets the required concrete strength and a new value of *C*/*S* ratio is to be found. The proposed method favourably differs from the known ones in that it takes into account the properties of specific materials and the conditions for manufacturing the samples. For the design of the composition by this method, it is not necessary to determine the properties of materials, it is only necessary to know the activity of cement (Fig. 1).

It has been found that with dry moulding, the traditional way of lubricating forms with water-emulsion compounds is not always acceptable. When placing a dry mixture in a lubricated mould, the lubricant film partially passes from the mould to the mixture, moulding spots on the finished product. In order to solve the problem in a complex way, a material was chosen for moulds that had zero adhesion to the concrete and did not need lubrication. The technique consisted in determining the strength of the adhesion of concrete to a plate of this material, concreted in the neck of the figure-eight. The results of testing the samples for axial tension are shown in Tab. 5.

Table 5 Adhesion of dry concrete with various materials (impregnation with a liquid glass solution with a density of 1.2 kg/dm³)

Material	R_{ad}, MPa, at the age, days			
	7	14	28	After SVS 80 °C
Stone (granite)	1.15	2.0	4.31	3.48
Epoxy resin ED-20	0.11	0.24	0.47	0.81
Wood (pine)	0.82	1.56	3.92	3.33
Carbon steel St3sp	0.65	1.34	3.00	3.05
Stainless steel 14G2	0.28	0.42	0.75	0.87
Rubber	0.15	0.25	0.62	0.77
Polyethylene (film)	0.00	0.00	0.00	0.09
Polyvinyl chloride (film)	0.10	0.2	0.5	0.82

It has been established by trials that the optimal material for moulds is polyethylene. Samples with a liner from it were spontaneously separated during excavation from moulds, so the preparation of the formwork for dry moulding consisted of pasting the mould with a polyethylene film. A film with a thickness of 0.3 mm and a waterproofing enamel consisting of a solution of chlorosulfonated polyethylene in toluene with the addition of a stabilizer was used. Before coating, the moulds were cleaned with a sandblaster, then the enamel layer was applied with a brush. The same layer of enamel was applied to one side of the film and after 30-40 minutes the film was stuck to the surface of the mould.

The technology of manufacturing moulds and matrices with polyethylene coating was proposed in [12].

Introduction of additives into the concrete, which reduce concentration of stresses at the interface with different elastic characteristics, significantly reduces the swing range and limits of changes in the maximum and minimum deformation and stresses during the destruction of concrete. The presence of elastic-viscous inclusions in the structure of the concrete - low-modulus additives as internal stress relaxers and energy absorbers of cracks - provides an increase in the strength, fracture toughness and frost resistance of concrete.

It was noted that "heterogeneity of concrete, creating the appearance of microcracks, delays their degeneration into dangerous macrocracks, and presence of stress concentrators in the material structure makes it insensitive to both external concentrators and to newly emerged internal ones." It can be stated that mineral additives of various nature, regardless of the hydraulic activity degree, optimize the deformative properties of cement stone and concrete with practically constant compressive strength. This is due to the reduced rigidity of mineral additives. This additive, in its function, performs in the concrete the role of closed air pores, the effectiveness of which is determined by the theoretical considerations discussed above about the ability of a "weak" surface to energetically quench the growth of a fragile crack.

6 CONCLUSIONS AND PROSPECTS FOR FURTHER RESEARCH

Based on the general principles governing the structural and mechanical heterogeneity of the concrete cement matrix, the positive effect of the dry moulding method with slightly hard additives on the structure of concrete and its physical and mechanical characteristics is determined by three factors: at the stage of structure formation, reduction of shrinkage stresses, including the most dangerous tear stresses at the "aggregate-cement matrix" boundary and tensile stresses in the cement matrix; when loaded, frozen and thawed - by equalizing the stresses in the concrete structure and redistributing them among the concrete components with a different modulus of elasticity; inhibition of growth and cracking. It was also established that the reduction of the modulus of elasticity of the aggregate should be within the elasticity modulus of the cement matrix, since a significant decrease in the rigidity of the aggregate will lead to an overload of the cement component and a loss of strength when compressing concrete.

Manifestation of a factor that determines the mechanism of damping cement matrix and concrete largely depends on two parameters of the damping component: its stiffness (modulus of elasticity) and size (dispersion).

1) Reduction of the concrete aggregates hardness due to the use of dense aggregates of medium hardness (such as limestone crushed stone) and light aggregates (slag pumice, expanded clay).

2) Reducing the concentration of dense aggregates due to the expansion of the grains of a large aggregate by cement-sand mortar and small one by cement stone.

3) Increasing the aggregate adhesion strength to the cement stone by increasing the purity and the dense aggregates surface roughness, as well as the use of porous aggregates.

4) The use of concretes on mixed coarse and fine

aggregates, as well as combined concrete, as binder, which uses portland cement with mineral additives, slag portland-cement, pozzolanic and other types of mixed cements.

7 REFERENCES

[1] Popovics, S. (1989). Fracture Mechanism in Concrete: How Much Do We Know? *J. Eng. Mech. Div. Proc. Amer. Soc. Eng.*, 95(3), 531-544. (Russian).

[2] Sytnik, V. I. & Ivanov, Yu. A. (1989). Investigation of micro crack formation in high-strength concretes. *Stroitelnye konstruktsii: Respmezhved. nauch.-tekhn. sb. NII stroitelnykh konstruktsiy*, Kiev, 12, 42-48 (Russian).

[3] Tanigawa, Ya. & Hosaka, Ye. (1987). *Mekhanizm razvitiya treshchin i razrusheniya betona kak kompozitsionnogo materiala*, 90 p. (VTsP No. 89/70795)(Translation from English).

[4] Frenkel, Ya. I. (1968). *Staticheskaya fizika*. Izd. AN SSSR, 760 p. (English).

[5] Batyanovskiy, E. I. (1982). Effektivnost primeneniya sukhikh betonnykh smesey. *Promyshlennoe stroitelstvo i inzhenernye sooruzheniya*, 6, 27-32. (Russian).

[6] Taiji, S., Suenory, A., Shigehisa, T., & Mikio, N. (1980). Effect of Coars Aggregate and Mortal Matrix of the Impact Compressive Strength of Concrete. *Rev. 34th Gen. Meet. Cem. Ass. Jap. Techn. Sess.*, Tokyo, 147-149. (Japanese).

[7] Holland, T. C. (1998). High-Performance Concrete: As High as It Gets. *The Concrete Producer, 16*(7), 501-505.

[8] Bataynowski, E. I. (1982). Efektiwnost primenenia suhih betonnuch smesey. *Promuchlennoe stroitelstwo i ingenernue soorujenia*, 6, 27-32. (Russian).

[9] Drapaluk, M. V. (2009). Technologia betona polusuhogo formovania dla elementow gidrotechnicheskih soorugeniy. *Westnik Dnipropetrowskogo nacionalnogo uniwersitetu zaliznuchnogo transportu imeni akademika V. Lazarana*, 27, 178-180. (Ukrainian).

[10] Gusew, B. V., Deminov, A. D., & Krukov, B. I. (1982). *Udarno-wibracionnaj technologia uplotnenia betonnuh smesey*. Stroyizdat, 150 p. (Russian).

[11] Owchinnikow, P. F. (1983). *Vibroreologia*, Kiev: Naukova dumka, p. 270. (Russian).

[12] Prozorow, A. S., Goldman, F. A., & Karimov, P. D. (1994). Ispolzowanie form s polimernum pokrutiem dla poluchenia konstrukcii s relefnoy poverchnostu. *Beton i zhelezobeton*, 5, 11-13.

Author's contact:

Marina DRAPALUK, Ass. Prof., PhD
Odessa State Academy of Civil Engineering and Architecture,
Didrikhsona St., 465029 Odessa, Ukraine
Tel.: +380 990474585
E-mail: drapalukmarina@meta.ua

ISSN 1846–6168 (Print), ISSN 1848–5588 (Online)
https://doi.org/10.31803/tg-20180516131304

Original scientific paper

CAST IRON ROLLS – AN OVERVIEW ON THE PROPER HARDNESS ASSURED BY THE MANUFACTURING PROCESS

Imre KISS

Abstract: The manufacturing process of the rolling rolls, as well as the quality of materials used in casting them, can have an important influence upon the quality and the safety of the exploitation. Our approaches to the issue of quality assurance of the rolling rolls, from the viewpoint of the quality of materials that are featured, can cause duration and safety in the rolling exploitation. This research is required because of the numerous flaws that cause rejection, since the phase of melting of these irons is intended to cast rolls. According to the industrial analysis in the cast iron rolls foundries, the results show that one of the main rejection categories is due to the inadequate hardness of the rolls. One of the parameters that will determine the cast iron's structure is the chemical composition, and this factor could assure the exploitation properties of each roll in all the stands of rolling mill. In this sense, the paper presents an overview of industrial and laboratory research regarding the assurance of the chemical composition of the irons (with nodular graphite) destined for the half–hard rolls casting, and tries to draw some remarks upon the proper correlations of these irons. This study analyses iron rolls cast in combined moulds (iron chill, for the barrel and moulding sand, for the necks of rolls) and includes charges of rolls from half–hard classes, with definite structure and nodular graphite, obtained in simplex cast processes. It presents, in graphical form, the influence of the chemical composition of these irons on the hardness, measured on the barrel. The proper solution is determined through some mathematical restrictions to the input data that the mathematical modelling is initiated with. It will be determined through regression equations, which describe the mathematical dependency between the hardness and the elements of chemical composition – the basic elements (Carbon [C], Manganese [Mn] and Silicon [Si]), the particulate elements (Sulphur [S], Phosphorus [P] and Magnesium [Mg]) and the main alloying elements (Nickel [Ni], Molybdenum [Mo] and Chrome [Cr]). The main results and the graphical addenda are presented.

Keywords: cast iron rolls; chemical composition; hardness; half-hard class; regression surfaces; modelling

1 INTRODUCTIVE NOTES

In the process of rolls casting, in spite of the most accurate guidance of the technological phases, the performance factor remains relatively low [1, 2]. The requirements, which are imposed to the cast iron rolls in service, are very different and often contradictory [1–6]. The rolls must have adequate mechanical resistance and high working temperature stability. Also, they must present a relative lower hardness in the core and on the necks, and a higher hardness on the roll's barrel (surface). [1, 2]

To assure these properties, in the core of rolls the structure of irons must contain graphite, whereas the barrel's hardness is guaranteed by the quantity of cementite [1, 2]. This peculiar structure will assure roll's good resistance at the thermal fatigue, the high wear resistance in dried friction conditions as well as the stability at unexpected temperature variations in the steels rolling process [1–10]. Overall, the rolls must present high service requirements, which are the peculiar hardness, the higher resistance in the various thermal and wear regimes, and stability at the high working temperature [1–6]. Also, the rolls must assure the steels clamping in the rolling process, as well as the high surface quality of the various rolled by–products [1–10].

In this sense, obtaining the various properties in different points of the same foundry product – i.e. cast iron rolls – meets difficult technological problems in manufacturing (in different process phases like iron melting, alloying, modification treatment of the graphite, moulding and mould's drying, casting, cooling and solidification in the combined moulds), which supposes to consider many technological factors [1, 2, 5, 6]. One of the main parameters that will determine the cast iron's peculiar structure is the chemical composition, which must assure the service requirements of each cast roll [1, 2].

First of all, the roll's barrel hardness achievement, fixed strictly by the requirements for each roll's type, is conditioned by the irons peculiar structure's achievement, which contains pearlite, cementite and nodular graphite. The macrostructure is not imposed by requirements (except for the nodular graphite irons, where a spherical shape of the graphite is strictly required), conditioned by the adequate quantities of cementite in the barrel, respectively the adequate quantities of graphite in core and on necks [1–6]. As a result of the spheroidal form of the graphite, the gradual fall in hardness is an added advantage of these types of rolls being much stronger than he clear–chill type rolls [1, 2]. They are used in conditions in which the first essential requirement is the toughness, rather than the resistance at wear, e.g. rolls for heavily loaded roughing stands. [1, 2, 10]

Overall, not respecting the chemical composition, the rolls will be rejected [1, 2]. An important group of defects, which lead to rolls rejection (approximately 9–10% of total rejection in foundries), consists of inadequate depths of the hard barrel. These technological defects may consist of insufficient or excessive thickness of the rolls barrel (i.e. on the rolling surface). [1, 2, 4]

The uneven thickness on the barrel's height leads to rejection, too [1, 2]. In other 5–6% of the situations, the rejection is caused by structural defects [1, 2]. Avoiding these in rolls casting is an extremely complex task, which requires an adequate consideration of manufacturing, especially the accurate guidance of rolls melting–alloying processes, close to the preparation of the combined chill for casting. [1, 2]

2 METHODOLOGY & TECHNICAL AREA

The iron rolls cast in the simplex procedure, in combined moulds (iron chill, for the barrel and moulding sand, for the necks of the rolls) are studied. [1, 2, 4]

The study included rolls from the half–hard classes (0, 1 and 2 classes), which required hardness between 33–59 Shore (219–347 Brinell) and 59–75 Shore (347–550 Brinell) for the hardest class [1, 2]. The required hardness is presented in Tab. 1. [1, 2, 4]

Table 1 The Required Hardness of the Half–Hard Cast Iron Rolls

Roll's Type	Class of Hardness	Required Rolls Hardness			
		on Barrel (Surface)		in Core / on Neck's	
		[Shore Hardness]	[Brinell Hardness]	[Shore Hardness]	[Brinell Hardness]
FNS	0	33–42	218–286	30–40	195–271
FNS	1	43–59	294–347	30–40	195–271
FS	2	59–68	420–491	35–45	218–309
FNS	2	69–75	499–550	35–45	218–309

Table 2 The Required Chemical Composition of the Half–Hard Cast Iron Rolls

Roll's Type	The Chemical Composition, (%)								
	C	Si	Mn	P	S	Ni	Cr	Mo	Mg
FS	2.9–3.6	0.3–1.2	max 0.6	max 0.15	max 0.1	max 0.6	max 0,5	0.3–0.5	–
FNS	3.0–3.5	1.2–2.5	0.1–0.7	max 0.15	max 0.02	1.5–2.5	max 0.8	0.3–0.5	0.02–0.04

The recommended chemical compositions for the half–hard class rolls, cast from lamellar graphite iron (type FS) and nodular graphite iron (type FNS) in Tab. 2 are presented. [1, 2] The rolls' chemical composition includes the basic elements ([C], [Si], [Mn], [S] and [P]), the alloying elements ([Cr], [Ni] and [Mo]), as well as the Magnesium [Mg] content (in the case of nodular irons). [1, 2, 4] In special cases, these irons can contain up to 0.15–0.2% Vanadium [V] [1, 2]. Also, in the case of irons with nodular graphite, destined to casting rolls (type FNS), is accepted a higher content of Phosphorus [P], because this participates at the roll's surface hardening [1,2].

The research includes half–hard cast rolls from nodular graphite irons (type FNS), hardness class 1 and 2, with the half–hard barrel of 40–150 mm depth [1, 2]. The lot of analysed rolls is representative for the half–hard category as the chemical composition and the measured hardness of that is presented in Tab. 3 [1,2]. The hardness checking (on the two necks, respectively on barrel), is done in equidistant points, according to the standard stipulation.

The value of the equivalent Carbon [C_{ech}], calculated by the formula (I), is recommended to be maximum 4.3%, for cast iron rolls. Also, for this value's calculation, the formula (II) is accepted, too. [1, 2]

$$[C]_{ech} = [C] + 0.3([Si] + [P]) - 0{,}03[Mn] + \\ + 0.4[S] + 0.07[Ni] + 0.05[Cr]\ (\%) \quad (I)$$

$$[C]_{ech} = [C] + 0.33[Si] + 0.1[Ni]\ (\%) \quad (II)$$

Table 3 The Chemical Composition and the Measured Hardness of the Half–Hard Cast Iron Rolls

Chemical Composition, (%)	
Carbon [C]	3.22–3.42
Silicon [Si]	1.72–2.19
Manganese [Mn]	0.62–0.79
Phosphorus [P]	0.130–0.165
Sulphur [S]	0.011–0.024
Nickel [Ni]	1.49–2.22
Chrome [Cr]	0.36–0.72
Molybdenum [Mo]	0.18–0.28
Magnesium [Mg]	0.021–0.029
Equivalent Carbon value, (%)	
Equivalent Carbon [C_{ech}]	3.952–4.219
Hardness, [Brinell units]	
on the Necks	219–276
on the Barrel	282–352

We applied the mathematical modelling [1, 2, 7] taking into consideration the industrial data obtained from the rolls industry, as well as the cast iron roll's requirements. Using the mathematical correlations (double and triple) is really helpful in the rolls manufacturing. Basically, it allows us to determine the chemical composition variation boundaries, in view the obtaining a proper rolls hardness [1–6, 9].

Therefore, we suggest a mathematical approach on influence of the basic elements (Carbon [C], Manganese [Mn] and Silicon [Si]), the particulate elements (Sulphur [S], Phosphorus [P] and Magnesium [Mg]) and the main alloy elements (Nickel [Ni], Molybdenum [Mo] and Chrome [Cr]) over the hardness on the rolls rolling surface.

Finally, we determine mathematically the equations of the hyper surfaces in the 3 and 4 dimensional space, the average values and average square aberrations (presented in Tabs. 4–6). [1, 2]

Table 4 The variable's limits of variation, the average values and the variable's deviation from the average values. Case of the Carbon [C], Silicon [Si] and Manganese [Mn] contents

The variables	Limits of variation	Average values	Variable's deviation
Carbon [C], (%)	3.14–3.52	3.2861	0.0852
Silicon [Si], (%)	1.48–1.92	1.7191	0.1303
Manganese [Mn], (%)	0.42–0.73	0.5683	0.0755
Hardness on barrel, $[HB]_{barrel}$	355–486	421.2211	36.8652

Table 5 The variable's limits of variation, the average values and the variable's deviation from the average values. Case of the Phosphorus [P], Sulphur [S] and Magnesium [Mg] contents

The variables	Limits of variation	Average values	Variable's deviation
Phosphorus [P], (%)	0.106–0.141	0.1199	0.0075
Sulphur [S], (%)	0.008–0.032	0.0191	0.0063
Magnesium [Mg], (%)	0.021–0.031	0.0255	0.0029
Hardness on barrel, $[HB]_{barrel}$	355–486	421.2211	36.8652

Table 6 The variable's limits of variation, the average values and the variable's deviation from the average values. Case of the Chrome [Cr], Nickel [Ni] and Molybdenum [Mo] contents

The variables	Limits of variation	Average values	Variable's deviation
Chrome [Cr], (%)	0.30–0.97	0.4978	0.1314
Nickel [Ni], (%)	0.81–2.68	1.3535	0.4779
Molybdenum [Mo], (%)	0.18–0.71	0.3722	0.1502
Hardness on barrel, $[HB]_{barrel}$	355–486	421.2211	36.8652

By processing the data obtained in foundry practice, we obtained equations of correlation between the chemical composition of the rolling rolls iron and the hardness distribution on the roll's barrel [1, 2, 7]. The main results and the graphical addenda are presented below, in synthesis.

3 RESULTS & GRAPHICAL ADDENDA

3.1 Correlation between the Basic Elements

The main basic element of the iron composition is Carbon [C]. In the case of the half–hard iron rolls, this varies between 3.0–3.5% that assures the recommended 220–420 Brinell hardness (on the barrel) and 220–300 Brinell hardness (in core and on the necks) [1,2]. After the melting period, the Carbon [C] content fits in the established values (3.22–3.42%), while the hardness, measured on the different points of roll's barrel, is between 222–352 Brinell [1,2].

The Silicon [Si] has influence upon the refinement of graphite, being one of the elements that have graphitising effect and favours the presence of graphite in the core. The Silicon [Si] percentage is in close dependence with the content of Carbon [C]. Their action is similar, but the separate effect of each of them is stronger when one of the elements is in a smaller or a larger proportion accordingly. With the growth of Silicon [Si] and Carbon [C] content, it will increase the graphite's quantity, and therefore the half–hard barrel's thickness is narrowed.

The analyses showed that the Silicon [Si] varied between 1.64–2.19%, which is technically accepted (1.2–2.5% being the limits stipulated by these rolls requirements). Following the data, we can remark the hardness diminution with the growth of Silicon [Si] content, the general variation being similar to a Carbon [C] variation.

At a lower limit of Manganese [Mn] content, this element has a strong anti–graphitising effect. Above the 0.7% Manganese [Mn] content, carbides are stabilised and the hardness is increasing. We also know, above 1.0% Manganese [Mn] content, this element acts like an alloying element, stabilises the cementite, and implicitly hardens the irons [1, 2].

$$[HB]_{(barrel)} = 638.14[C]^2 - 241.48[Si]^2 + 1975.15[Mn]^2 - \\ - 687.68[C]\cdot[Si] + 310.44[Si]\cdot[Mn] + 142.35[Mn]\cdot[C] + \\ + 3363.00 - 2995.15[C] + 3009.10[Si] - 3135.56[Mn] \quad (1)$$

The correlation coefficient of Eq. (1) is $rf = 0.7667$ and the deviation from the regression surface is $sf = 32.5612$.

3.2 Correlation between the Particulate Elements

Having an unfavourable effect upon the mechanical properties, the Sulphur [S] content is recommended to be in minimal quantities. The hardness as well as the strength decrease while the Sulphur [S] content grows. Also, the Sulphur [S] affects the graphite nodularity, so there is a need to reduce it to the minimum, strictly restricted to be at maximum 0.02%. Above this value, the Sulphur [S] has a negative value upon the mechanical properties.

In the case of half–hard rolls, the Phosphorus [P] content is limited to a maximum of 0.2–0.3% [1, 2]. Since this chemical element shapes tough compounds, which are needed in the rolling surface, Phosphorus [P] does not have an effect, if limited in this interval. The increase of hardness can be observed, together with growth of the Phosphorus [P] percentage.

Magnesium [Mg] plays a special part, as it is the element with which the ladle inoculation has been made. The graphite's nodularity assures the higher mechanical properties, by eliminating several inconveniences found at the rolls cast from irons with lamellar graphite. [1, 2]

$$[HB]_{(barrel)} = -331.55[S]^2 + 883.11[P]^2 + 188.87[Mg]^2 + \\ + 469.14[S]\cdot[P] - 793.68[P]\cdot[Mg] - 774.06[Mg]\cdot[S] - \\ - 236.72[S] - 10470.29[P] + 173.81[Mg] + 1028.50 \quad (2)$$

The correlation coefficient of Eq. (2) is $rf = 0.7471$ and the deviation from the regression surface is $sf = 24.5054$.

3.3 Correlation between the Alloying Elements

The irons intended for these cast rolls are alloyed especially with Nickel [Ni], Molybdenum [Mo] and Chrome [Cr], in reduced contents, being low alloyed irons [1,2].

The requirements firmly state the elements required to rise the rolls quality, the contents of these elements being between large limits. Also, the contents of these alloying elements can be reduced due to the strong effect of the Magnesium [Mg] from the nodulising agent, upon the structure and the graphite's form.

The Nickel [Ni] addition leads to the improvement of the mechanical properties. If we do not allow this element to increase the graphitisation degrees and the white solidification in the barrel, this content can be considerably reduced. Accordingly, the Silicon [Si] content can be varied, as this element replaces Nickel [Ni].

In the case of the half–hard cast iron rolls, the Chrome [Cr] has a less important influence than in the case of hard and extra–hard rolls, as in their case the Chrome [Cr] proves to be the most efficient alloying element to regulate the crust depth. The half–hard rolls have Chrome [Cr] content, which is preserved at low limits (a maximum of 0.6%), although this content still assures the necessary hardness on the barrel. An increase of the hardness is to notice, together with a growth of the Chrome [Cr] content.

Also, Chrome [Cr] content is in close accordance with the Nickel [Ni] content, to favour the formation of the perlitical structure, without the massive and rough carbides. Both are added simultaneously, because the addition of Chrome [Cr] compensates the graphitising effect of the Nickel [Ni]. The proportion between Nickel [Ni] and Chrome [Cr] is situated in a 2–4 value of ratio.

Molybdenum [Mo] is a carburigenous element, but this effect is relevant only at percentage above 0.6%. Below this value, fine structures are obtained, also an increase of the mechanical properties (especially the high temperature stabilities). In these irons, contents beyond a percentage of 0.15 % Molybdenum [Mo], are not recommended, because a part of Molybdenum [Mo] is lost through the combination with Phosphorus [P], therefore Molybdenum [Mo] losing a part of its alloying behaviour.

In the case of half–hard rolls, the content of Molybdenum [Mo] does not pass this limit, and is imposed to 0.1–0.3%. The analyses showed that the Molybdenum [Mo] content varies between 0.18–0.28%. Although the marks seem dispersed, it is easy to notice the growth of hardness as the content of Molybdenum [Mo] increases in this interval.

$$[HB]_{(barrel)} = 63.55[Ni]^2 + 660.05[Mo]^2 - 449.63[Cr]^2 - \\ -84.71[Ni]\cdot[Mo] + 177.74[Mo]\cdot[Cr] - 253.52[Cr]\cdot[Ni] - \\ -13.60[Ni] - 291.23[Mo] + 817.36[Cr] + 260.62 \quad (3)$$

The correlation coefficient of Eq. (2) is $rf = 0.7066$ and the deviation from the regression surface is $sf = 26.0834$.

3.4 Drawing the Correlation Diagrams

Since the surfaces (described by equation 1–3) cannot be represented in a 3–dimensional space, the independent variables were successively replaced with their average values (Tabs. 4–6) and by mathematical restrictions to the input values, the proper solution is determined. Is searched to constraint average values, inclusively to dependent variables, desired to achieve through the proper chemical composition.

Starting from the Eq. (1) and the average values from Tab. 4, we obtain the following double correlations:

$$[HB]_{(barrel)}[C]_{med} = -241.49[Si]^2 + 1975.15[Mn]^2 + \\ +310.44[Si]\cdot[Mn] + 749.31[Si] - 2667.77[Mn] + 411.57 \quad (4a)$$

$$[HB]_{(barrel)}[Si]_{med} = 1975.15[Mn]^2 + 638.14[C]^2 + \\ +142.35[Mn]\cdot[C] - 2601.87[Mn] - 4177.37[C] + 7822.34 \quad (4b)$$

$$[HB]_{(barrel)}[Mn]_{med} = 638.14[C]^2 - 241.48[Si]^2 - \\ -687.68[C]\cdot[Si] - 2914.25[C] - 3185.51[Si] - 2219.00 \quad (4c)$$

Starting from the Eq. (2) and the average values from Tab. 5, we obtain the following double correlations:

$$[HB]_{(barrel)}[S]_{med} = 883.11[P]^2 + 188.87[Mg]^2 - \\ -793.69[P]\cdot[Mg] - 1529.54[P] + 2648.74[Mg] + 458.36 \quad (5a)$$

$$[HB]_{(barrel)}[P]_{med} = 188.87[Mg]^2 - 331.55[S]^2 - \\ -774.06[Mg]\cdot[S] - 777.41[Mg] + 326.38[S] + 1042.66 \quad (5b)$$

$$[HB]_{(barrel)}[Mg]_{med} = -331.55[S]^2 + 883.11[P]^2 + \\ +469.14[S]\cdot[P] - 434.77[S] - 307.22[P] + 2707.26 \quad (5c)$$

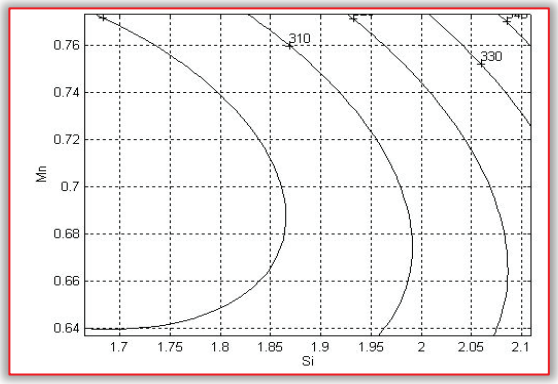

a)

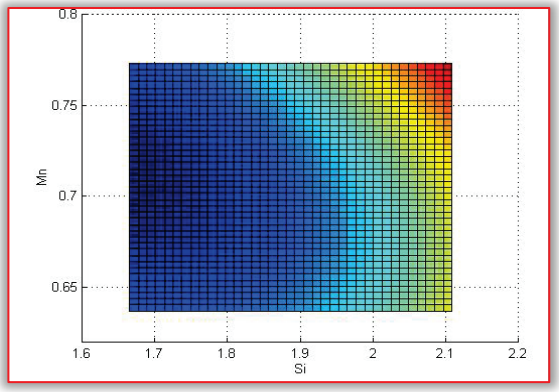

b)

Figure 1 The Hardness [HB] dependence with the Carbon [C], Silicon [Si] and Manganese [Mn] contents at the Half–hard Cast Iron Rolls. Case of Carbon [C] at the calculated average value: $[HB]_{barrel}(C_{med}, Si, Mn)$

Starting from the Eq. (3) and the average values from Tab. 6, we obtain the following double correlations:

$$[HB]_{(barrel)}[Ni]_{med} = -449.63[Cr]^2 + 660.05[Mo]^2 + \\ +177.74[Mo]\cdot[Cr] + 474.22[Cr] - 541.23[Mo] + 358.69 \quad (6a)$$

$$[HB]_{(barrel)}[Cr]_{med} = 660.05[Mo]^2 + 63.55[Ni]^2 - \\ -184.71[Ni]\cdot[Mo] - 202.75[Mo] - 139.81[Ni] + 556.09 \quad (6b)$$

$$[HB]_{(barrel)}[Mo]_{med} = 63.55[Ni]^2 - 449.63[Cr]^2 - \\ -253.52[Cr]\cdot[Ni] - 82.34[Ni] + 883.51[Cr] + 243.66 \quad (6c)$$

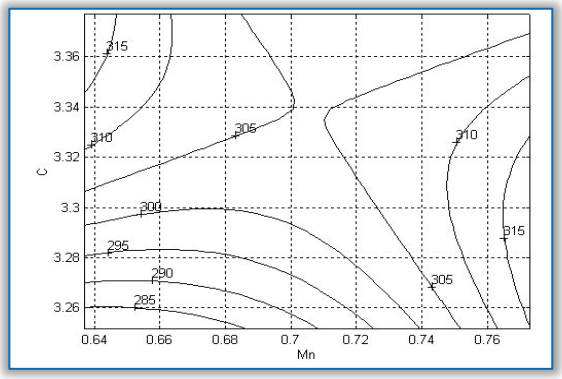

a)

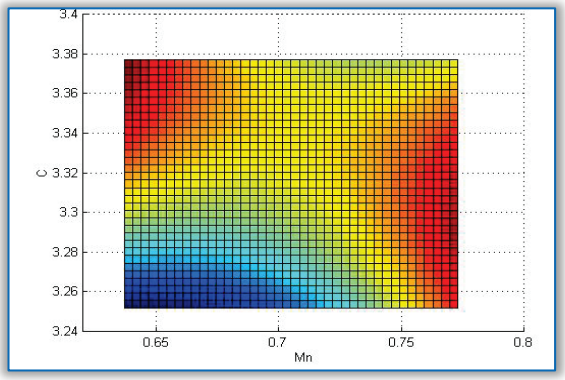

b)

Figure 2. The Hardness [HB] dependence with the Carbon [C], Silicon [Si] and Manganese [Mn] contents at the Half–hard Cast Iron Rolls. Case of Silicon [Si] at the calculated average value: $[HB]_{barrel}(C, Si_{med}, Mn)$

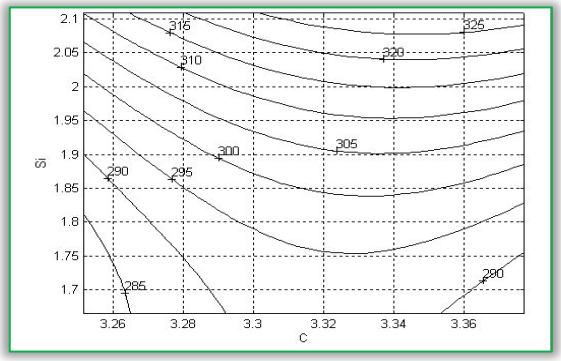

a)

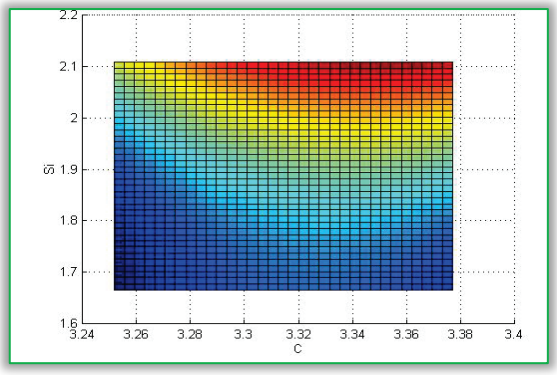

b)

Figure 3. The Hardness [HB] dependence with the Carbon [C], Silicon [Si] and Manganese [Mn] contents at the Half–hard Cast Iron Rolls. Case of Manganese [Mn] at the calculated average value: $[HB]_{barrel}(C, Si, Mn_{med})$

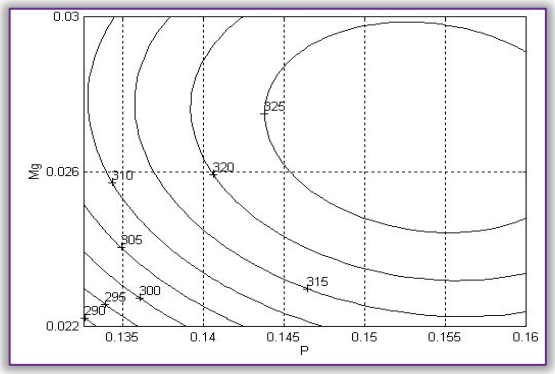

a)

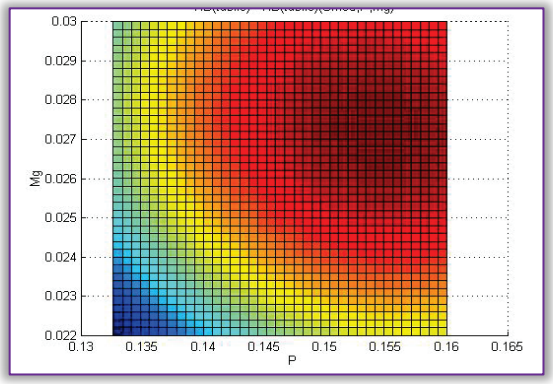

b)

Figure 4. The Hardness [HB] dependence with the Phosphorus [P], Sulphur [S] and Magnesium [Mg] contents at the Half–hard Cast Iron Rolls. Case of Phosphorus [P] at the calculated average value: $[HB]_{barrel}(P_{med}, S, Mg)$

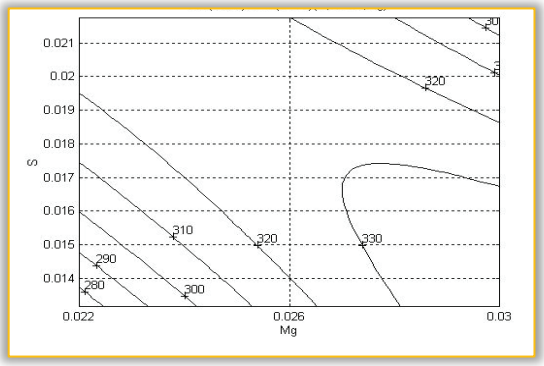

a)

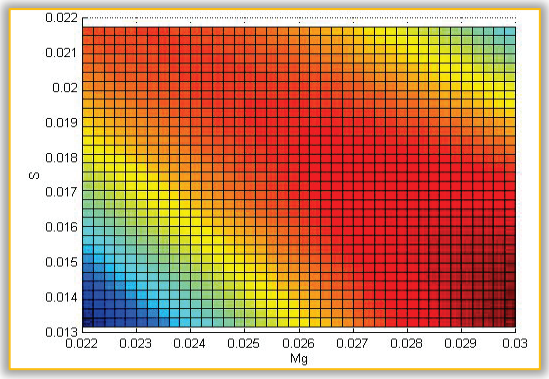

b)

Figure 5. The Hardness [HB] dependence with the Phosphorus [P], Sulphur [S] and Magnesium [Mg] contents at the Half–hard Cast Iron Rolls. Case of Sulphur [S] at the calculated average value: $[HB]_{barrel}(P, S_{med}, Mg)$

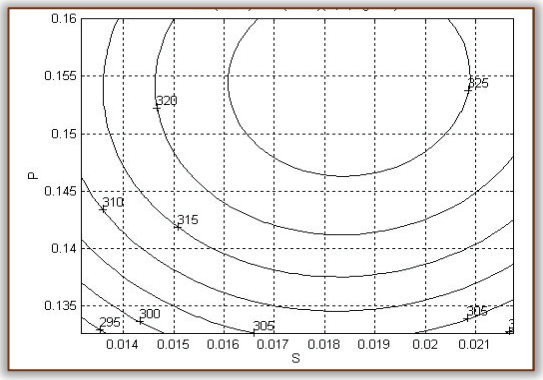

a)

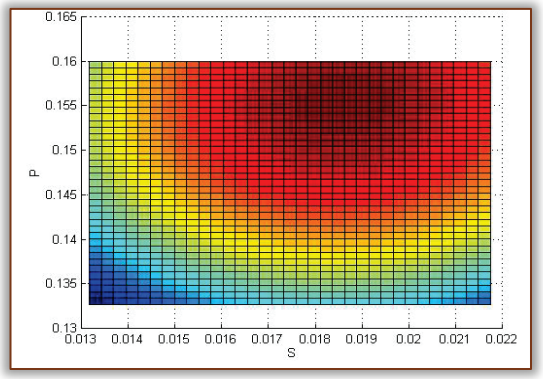

b)

Figure 6 The Hardness [HB] dependence with the Phosphorus [P], Sulphur [S] and Magnesium [Mg] contents at the Half–hard Cast Iron Rolls. Case of Magnesium [Mg] at the calculated average value: $[HB]_{barrel}(P, S, Mg_{med})$

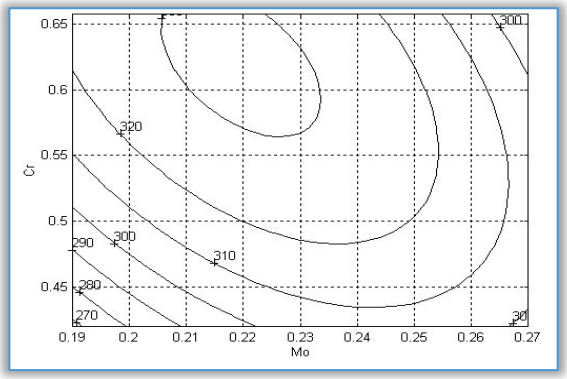

a)

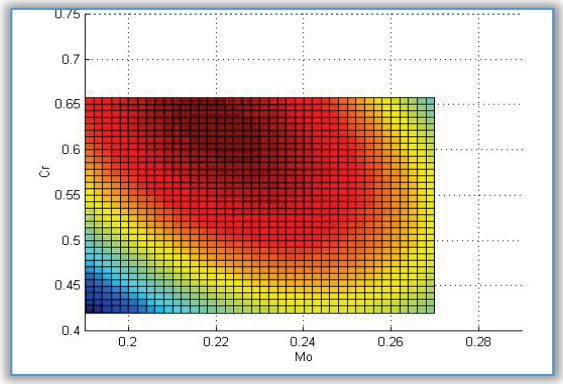

b)

Figure 8 The Hardness [HB] dependence with the Chrome [Cr], Nickel [Ni] and Molybdenum [Mo] contents at the Half–hard Cast Iron Rolls. Case of Nickel [Ni] at the calculated average value: $[HB]_{barrel}(Cr, Ni_{med}, Mo)$

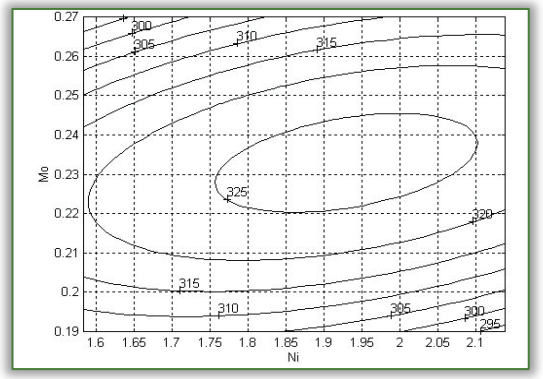

a)

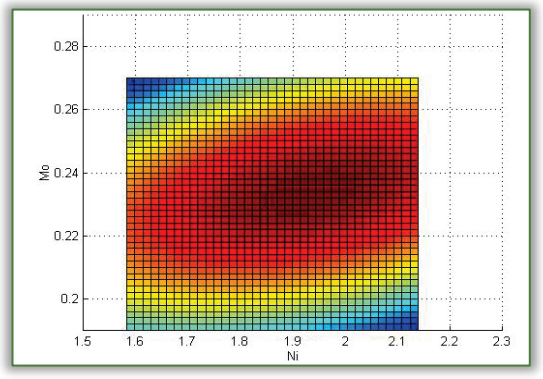

b)

Figure 7 The Hardness [HB] dependence with the Chrome [Cr], Nickel [Ni] and Molybdenum [Mo] contents at the Half–hard Cast Iron Rolls. Case of Chrome [Cr] at the calculated average value: $[HB]_{barrel}(Cr_{med}, Ni, Mo)$

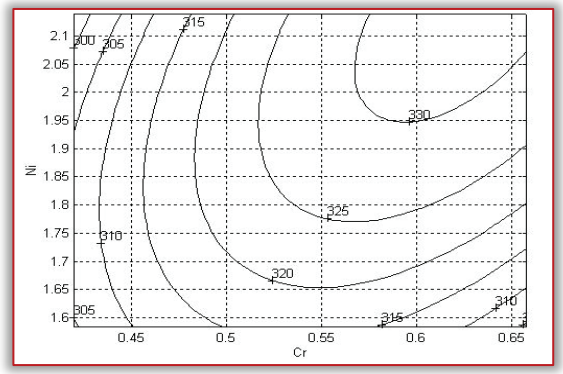

a)

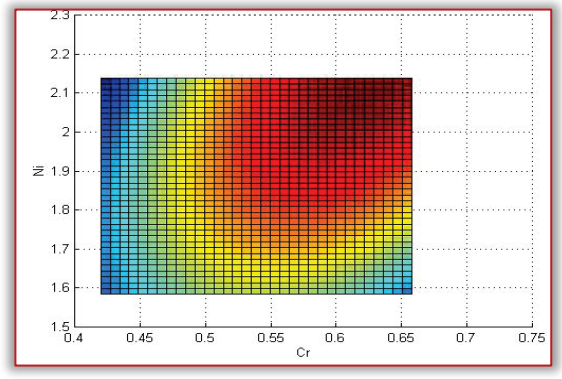

b)

Figure 9 The Hardness [HB] dependence with the Chrome [Cr], Nickel [Ni] and Molybdenum [Mo] contents at the Half–hard Cast Iron Rolls. Case of Molybdenum [Mo] at the calculated average value: $[HB]_{barrel}(Cr, Ni, Mo_{med})$

Therefore, the Eqs. (4)a–c, (5)a–c and (6)a–c were obtained, which describe the correlations between the elements, belonging to the 3–dimensional space.

These regression surfaces, described by the Eqs. (4)a–c, (5)a–c and (6)a–c can be represented as correlation diagrams (Figs. 1–9) and, therefore, can be interpreted by the manufacturers. Using these diagrams is really helpful in the foundry practice, as it allows us to determine variation boundaries for the chemical composition, in view of obtaining the proper hardness.

5 DISCUSSIONS & TECHNOLOGICAL REMARKS

Particularly, the following comments can be made:

- the relation between the variables can be illustrated graphically, too (Figs. 1–9). These variation domains, described by the Eqs. (4)–(6)a–c, which governed on the roll's barrel, belonging to the 3–dimensional space can be reproduced and therefore interpreted by manufacturers.
- knowing the level curves (isolines, presented in Figs. 1a–9a) which determine the technological domains for the half–hard rolls barrel (presented in Figs. 1b–9b), allows the proper addition of basic, particulate and alloying elements. Therefore, we can obtain a desired hardness within the required limits.
- the proper values of the chemical composition in the main elements of this irons destined to the cast of the half–hard rolls (Carbon [C], Manganese [Mn] and Silicon [Si]) are to be found on the diagrams on Figures 1–3, in a double correlation. According to them the proper addition of each main element can be noticed, which will assure the proper hardness on the barrel.
- a proper proportion between the Silicon [Si] and the Manganese [Mn] contents is needed both from the basic metallic charges and from the ferro–alloy addition (Fe–Si, Fe–Mn, Si–Mn);
  - ≡ for a narrower half–hard barrel, a supplementary addition of Fe–Si is made, which released the Silicon [Si] content, thus segregating supplementary quantities of graphite in the barrel area and narrowing the barrel;
  - ≡ for increased depth of barrels, a supplementary addition of carbides is made to heighten the quantity of the tough formation cementite;
- additionally, the content of the nodulising agent (Magnesium [Mg]) will be correlated with the [S] and [P] content, found on the correlation diagrams on Figs. 4–6, in a triple correlation; in the triple dependency of Phosphorus [P], Sulphur [S] and Magnesium [Mg], besides an proper ratio of Silicon [Si] and Carbon [C] contents. A special importance is needed to be given to the Sulphur [S], as it can affect the graphite's nodularity;
- the proper values of the chemical composition in the alloying elements (Molybdenum [Mo], Nickel [Ni] and Chrome [Cr]) are to be found in the double correlation graphs, on Figs. 7–9. According to them, the proper content of each main element can be noticed, values that can assure the adequate hardness. Thus, the proper additions of alloying elements can be used in practice in order to assure the proper hardness.
- a proper proportion between the Chrome [Cr], Nickel [Ni] and Molybdenum [Mo] contents is needed both from the metallic charges and from the ferro–alloy used for alloying (Fe–Cr, Fe–Ni, Fe–Mo);
- the main chemical composition must be correlated with further addition of alloying elements, respecting the adequate proportions between Silicon [Si] and Nickel [Ni] or between Manganese [Mn] and Chrome [Cr], besides a proper ratio of Carbon [C] and Silicon [Si];
- the smooth decrease of hardness and its maintaining on the depth is performed through the proper and exactly determined proportions between all the elements (basic, particulate and alloying).

6 CONCLUSIONS

As general conclusion, it can be noted that in the melting phase of the irons, the proper hardness can be obtained through the qualities of metallic charge and addition materials (nodulising agent – Magnesium [Mg] and ferro–alloys – Fe–Si, Fe–Mn, Si–Mn, Fe–Cr, Fe–Ni and Fe–Mo). as well as through a proper guidance of melting, alloying and nodulising processes.

In the cast–iron rolls, all the structural constituents are to be found, each of them having its own hardness, well determined. One of the basic factors that determine the structure is the chemical composition, basic Carbon [C], Manganese [Mn] and Silicon [Si]), particulate (Phosphorus [P], Sulphur [S] and Magnesium [Mg]) and the alloying (Molybdenum [Mo], Nickel [Ni] and Chrome [Cr]), too. The non–compliance of each sort of rolls chemical composition will lead to rejection of them.

Based on the experiments, on the results obtained from the manufacturing data processing, we concluded that realization of the proper chemical compositions of the cast–iron can constitute a technically efficient way to assure the exploitation properties, the roll's material having an important role in this sense.

Mathematical modelling establishes a methodology for determination of process parameter's of rolls manufacturing, for which a mechanical feature is the proper values. Because it has the actual data, the model optimization is carried out on industrial data, collected on cast rolls.

The investigations are described in the context of recovery from a technical point of view of the manufacturing and exploitation of the cast iron rolls, for which there is concern the casting sectors (cast iron rolls foundries) and the rolling mill stands, aimed at determining the quality's assurance and increase the durability in service.

This research opens the way of irons chemical compositions analyses, intended for all cast iron rolls. Implementation of these results in the industrial practice also provides guarantees on quality assurance of the cast rolls.

Acknowledgement

At the fundament of this study are several scientific works in which the author is involved, through his experience gained as an engineer in a well–known factory for its iron rolling mills rolls production. The research includes the own studies and analyses, experiments and research, regarding the quality improvement of the iron rolls [1–6, 9].

7 REFERENCES

[1] Kiss, I. (2008). *Rolling rolls – Approaches of quality in the multidisciplinary research*, Mirton, Timisoara.
[2] Kiss, I. (2005). *Quality of rolling–mill rolls cast by iron with nodular graphite*, Mirton, Timisoara.
[3] Kiss, I. (2008). Research upon the quality assurance of the rolling–mill rolls and the variation boundaries of the chemical composition. *Revista de Metalurgia, 44*(4), 335–342. https://doi.org/10.3989/revmetalm.2008.v44.i4.125
[4] Kiss, I. & Maksay, St. (2008). Graphical addenda in the technological area of the nodular iron cast rolls production. *Acta Polytechnica Hungarica, 5*(4), 15–27.
[5] Kiss, I., Alexa, V., Ratiu, S. A., & Cioata, V. G. (2014). The quality assurance in the rolling industry: Methods, approaches and tendencies. Machine Design, 6(4), 131–136.
[6] Kiss, I., Cioata, V. G., & Alexa, V. (2010). Increasing the rolling–mill rolls quality in some multidisciplinary research. *Acta Technica Corviniensis – Bulletin of Engineering, III*(2), 31–36.
[7] Ziadi, A., Belzunce, F. J., Rodríguez, C., & Fernández, I. (2005). Comportamiento en servicio de los aceros rápidos utilizados en la fabricación de los cilindros de trabajo de los trenes de bandas en caliente. *Revista de Metalurgia, 41*(2), 107–121. https://doi.org/10.3989/revmetalm.2005.v41.i2.194
[8] Mammeri, A., Belzunce, F. J., Rodríguez, C., Torre, M., Poveda, S., & García, J. (2003). Propiedades mecánicas de los aceros aleados al cromo utilizados en la fabricación de cilindros de apoyo de trenes de laminación. *Revista de Metalurgia, 39*(2), 107–110. https://doi.org/10.3989/revmetalm.2003.v39.i2.321
[9] Kiss, I., Cioata, V. G., Alexa, V., & Ratiu S. A. (2011). Technological behaviour and interpretations in some multidisciplinary approaches. *Annals of F. E. H. – International Journal of Engineering, IX*(4), 203–206.
[10] Krawczyk, J. (2011). Microstructure and tribological properties of mottled cast iron with different chemical composition. *Archives of Materials Science and Engineering, 51*(1), 5–15.

Author's contacts:

Imre KISS, Associate Professor
University Politehnica Timisoara,
Faculty of Engineering Hunedoara,
Department of Engineering and Management,
5, Revolutiei, 331128 Hunedoara, Romania
Tel.: +40254 207588
E–mail: imre.kiss@fih.upt.ro

ISSN 1846-6168 (Print), ISSN 1848-5588 (Online)
https://doi.org/10.31803/tg-20180528190453

Original scientific paper

IMPROVING RADAR PERFORMANCE WITH CONSTANT ENVELOPE MULTI-LEVEL CHIRP

Farhad BAHADORI-JAHROMI, Alireza HASSANNEJAD

Abstract: M-level Continuous Phase Chirp Modulation is considered for data transmission. In this article, we would like to propose a new approach to transmitting information with the help of multi-level wave guide signaling. The main problem with the classic chirp modulation system is that the final phase of the signal is not equal in each period to the initial phase of the next step, and this discontinuity is present in each data transmission period. The main objective of this paper is to improve the efficiency of chirp modulation, which is recommended for continuous phase multi-level scalar modulation, which results has a significant increase in system performance. In this new approach, for sending the M symbols, we use the M level to send the message. With the help of this idea, we simulate the telecommunication system and examine the probability of its bit error in the presence of additive white Gaussian noise and Rician fading.

Keywords: chirp signal; Multi-level Chirp Modulation; detection; phase modulation

1 INTRODUCTION

For the first time, the signal was taken into consideration at Bell phone Labs. The chirp signal is a signal whose frequency varies with time. If the frequency of this signal changes linearly with time, then it is called the linear trick signal or LFM; if its frequency is changed nonlinearly, it is called a non-linear tangle signal or NLFM. Linear jump signal was used for radar applications for the first time and afterwards it was widely used in radar and sonar systems because of its many advantages that have been researched alongside its uses. One of the main advantages of the chirp signal is the lack of full sensitivity to the Doppler shifter, as well as there is a variety of hardware to formulate and process it. In recent years, many studies have been carried out on the use of signal jig in telecommunication applications [1]. One of the most important issues in telephony is pulse shaping, since all the main characteristics of the telecommunications system include detection efficiency, distance separation and class. Initial factors that are effective in choosing pulse shapes include spacing coverage and Doppler, detection probability, resolution and measurement errors [2].

After the introduction of the use of the wave guide signal in telecommunications applications, many discussions have been presented to provide optimal modulation based on the chirp signal and its detection. Since the LFM signal has wide bandwidth, modulation based on the LFM signal is classified as a broad spectrum technique. This extension in the modulation bandwidth based on the screw signal causes this modulation to have advantages over the modulation of ASK and FSK. In 1999, Jassenda and his colleagues conducted a full study on various methods of detecting the wave guide signal in the time-frequency domain [3]. In 2002, Willet presented a new method for detecting a waveform signal based on the Huff transform, which uses the signal-signaling signal distribution, which is one of the frequency distributions of the signal [4]. In 2006 and 2007, Gelman and his colleagues presented two new methods for signal processing, which are based on basic functions that change the instantaneous phase signal of the base in then [5] and [6]. In 2008, a method was presented in [7], which is a combination of papers [3] and [6]. In 2005, Barbo and his colleagues presented a new method for classifying radar targets – in that paper, the fractional Fourier transform was used to improve the classification of sound waves and the results have been compared with Fourier transform results. In 2009, Schulli and his colleagues presented a new method for processing the chirp signal based on the Fourier transform, which used higher order statistics for this method [8]. In 2011, Gironjin and his colleagues introduced a new conversion called Chirp-z conversion, which was used to process SAR data and showed that this conversion is capable of greatly increasing the accuracy of suffering and Doppler at the same time [9]. In 2014, Cristalina and his colleagues changed the detection algorithms for radar applications that are mobile targets and the signal used by the chirp, which can estimate the speed of the targets with higher accuracy and less computational complexity. For that purpose they used the Chirp Scaling Algorithm or the CSA algorithm [10]. Then, Osama introduced a method called a discrete linear pulse transform, which used the compression of the signal and showed that this conversion has two degrees of greater freedom than the Fourier transform, as well as in applications where the combined signal of several components has a very high accuracy [11]. In 2018, the method introduced by Wei Wang and et al. [12].

2 MODULATED SIGNAL OF MULTI-LEVEL SCREW WITH FIXED FASTENING

The general relation for the fixed-tiered multi-level screw signal is as follows:

$$\xi_i(t) = \sqrt{\frac{2E_s}{\tau_s}}\cos\left[\omega_c t + \psi_i(t) + \varphi\right] \quad 0 \le t < \tau_s,\ i = 1, 2, ..., M \qquad (1)$$

Where E_s is the symbol's energy, τ_s the period of symbol, ω_c the carrier frequency, $\psi_i(t)$ contains the phase information

and ϕ the initial phase of the signal, and also the function $\psi_i(t)$ is defined as follows:

$$\psi_i(t) = I_i J(t) \tag{2}$$

So that

$$I_i = \begin{cases} +i & \text{if } i \text{ is odd} \\ -(i-1) & \text{if } i \text{ is even} \end{cases} \tag{3}$$

Which indicates that one of the M symbols or input level ±1, ±3,…, ±(M − 1) has been applied to the modulator. In addition, the phase signal function is specified as follows:

$$J(t) = \begin{cases} 0 & t \le 0,\ t > \tau_s \\ 2\pi \int_0^t f_I(\tau)\mathrm{d}\tau & 0 \le t \le \tau_s \\ \pi\eta = \pi(h-\omega) & t = \tau_s \end{cases} \tag{4}$$

Which $\pi\eta$ denotes the final phase of the signal at $t = \tau_s$ and $f_I(t)$ is the instantaneous frequency function, which is defined as follows:

$$f_I(t) = \begin{cases} 0 & t \le 0,\ t > \tau_s \\ \left(\frac{h}{2\tau_s}\right) - \left(\frac{\omega}{\tau_s^2}\right)t, & 0 \le t \le \tau_s \end{cases} \tag{5}$$

In the above relation, the variables h and w are dimensionless, and h represents the peak-to-peak frequency divider, and w represents the frequency change frequency divided by the symbol rate ($1/\tau_s$), and since h = (η + ω); (η, ω) are determined as parameters of signal modulation. It should be noted that in the M-surface scrolling modulation system, for each ±1, ±3,…, ±(M − 1), there is a curved signal with a specific frequency range. For example, for a binary system, an incremental gain signal for level −1 is defined and a trickle signal with decreasing frequency for the +1 level or vice versa. Block diagram of multi-level chirp system is shown in Fig. 1.

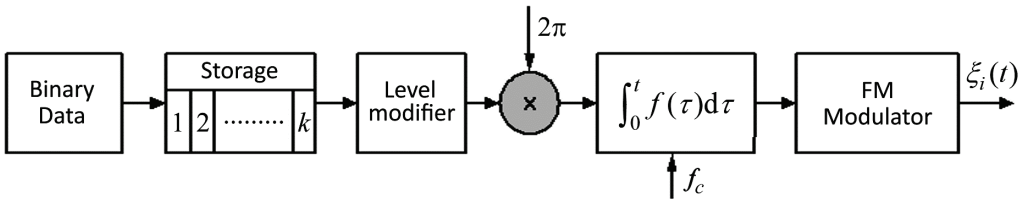

Figure 1 Block diagram of Multi-level Chirp Modulator System

3 CONTINUOUS PHASE MULTI-LEVEL MODULATION

The main objective of this paper is to improve the efficiency of chirp modulation, in which continuous multi-level scalar modulation is proposed. This adds a great deal to the system performance, as well as one of the advantages offered by the system and which can be introduced as a memory modulation – in each free space, it must store the initial and final phase information that can model a continuous phase modulation. In addition to introducing the proposed method, the receiver structure for optimal detection is also introduced, and the relationships required for obtaining the probability of error are extracted. The general relation for the continuous phase modulated multi-level wave guide signal is as follows

$$\xi(t, I) = \sqrt{\frac{2E_s}{\tau_s}} \cos\left[\omega_c t + \psi(t, I) + \varphi\right] \quad 0 \le t < \infty \tag{6}$$

Where E_s is the symbol's energy, τ_s the symbol period, ω_c the carrier frequency, $\psi_i(t, I)$ contains the phase information and ϕ the initial phase of the signal, and also the function $\psi_i(t, I)$ is defined as follows

$$\psi(t, I) = I_i J\left[t - (i-1)\tau_s\right] + \pi\eta \sum_{k=1}^{i-1} I_k, \quad (i-1)\tau_s \le t < i\tau_s \tag{7}$$

In addition, $I = I_1, I_2, I_3, \ldots$. in such a way that in a non-interpolated sequence a value d is one of the following values

$$I_i = \pm 1, \pm 3, ..., \pm(M-1) \tag{8}$$

So that

$$P(I_i) = \frac{1}{M};\ i = 1, 2, ... \tag{9}$$

In addition, the phase signal function is specified as follows

$$J(t) = \begin{cases} 0 & t \le 0,\ t > \tau_s \\ 2\pi \int_0^t f_I(\tau)\mathrm{d}\tau & 0 \le t \le \tau_s \\ \pi\eta = \pi(h-\omega) & t = \tau_s \end{cases} \tag{10}$$

And $f_I(t)$ is the instantaneous frequency function that is defined as follows

$$f_I(t) = \begin{cases} 0 & t \le 0,\ t > \tau_s \\ \left(\frac{h}{2\tau_s}\right) - \left(\frac{\omega}{\tau_s^2}\right)t, & 0 \le t \le \tau_s \end{cases} \tag{11}$$

According to Eq. (7), it is clear that the signal phase value depends not only on the amount of data in the desired symbol, but it is quite obvious that the phase value is dependent on the previous symbols that have entered the modulator (also the memory modulation system). In other words, the first expression is in the fuzzy relation (7), which is determined by the i^{th} symbol, and the second expression in this relation indicates that the phases associated with the previous symbols are also combined with the obtained phase. Since the signal phase is always a coefficient of 2π, one can obtain a new path for the phase tree by selecting each parameter η.

4 OPTIMAL RECEIVER STRUCTURE

The detection problem for the signal defined is as follows:

$$y(t) = \xi(t, I_\delta, A) + z(t), \quad 0 \le t \le n\tau_s \tag{12}$$

In Eq. (12), $A = (I_1, I_2, ..., I_{\delta-1}, I_{\delta+1}, ..., I_n)$ represents one of the M^{n-1} possible sequences of data symbols. Likelihood ratio test is used for detection, so that the correct function for the M-CPCM signal is calculated as follows:

$$CF_M = \int_A \exp\left\{\frac{2}{N_0}\int_0^{n\tau_s} y(t)\,\xi\left[t, I_\delta = -(M-1), A\right]\mathrm{d}t\right\} p(A)\,\mathrm{d}A \tag{13}$$

The distribution of the probability of parameter A is determined as follows:

$$p(A) = p(I_1)p(I_2)...p(I_{\delta-1})p(I_{\delta+1})...p(I_n) \tag{14}$$

$$p(I_i) = \frac{1}{M}\{\delta(I_i - 1) + \delta(I_i + 1) + ... \\ ... + \delta\left[I_i - (M-1)\right] + \delta\left[I_i + (M-1)\right]\} \tag{15}$$

In addition, the exponential function is obtained as follows

$$CF_M = 1/m\sum_{k=1}^{m} \exp\left\{\frac{2}{N_0}\int_0^{nT_S} r(t)\,\xi\left[t, I_\delta = -(M-1), A_k\right]\mathrm{d}t\right\} \tag{16}$$

Finally, the optimal receiver output is calculated by the following equation:

$$CF_k = \max\left\{CF_1, CF_2, ..., CF_M\right\} \tag{17}$$

5 SIMULATION RESULTS

In Fig. 2, the error rate diagram is shown in terms of the signal-to-noise ratio (N_b/N_0) for the proposed method for the number of different viewing intervals (n = 2, 3, 4, 5)for CPCM-32, as well as the comparison with the modulation of 32PSK and 32FSK.

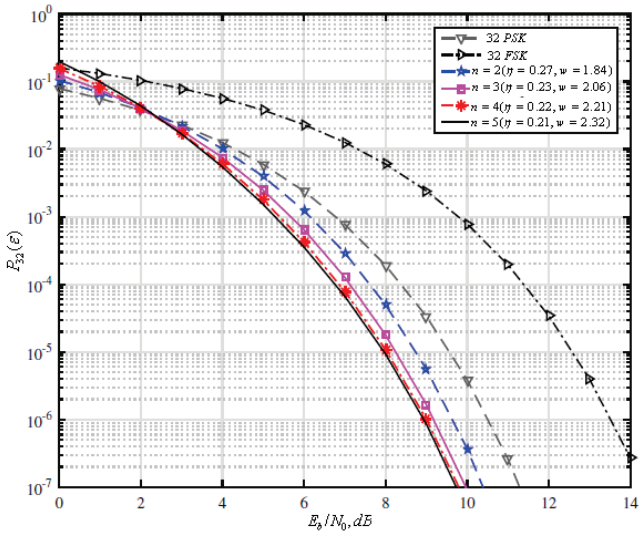

Figure 2 Error probability chart for SNR for system 32-CPCM

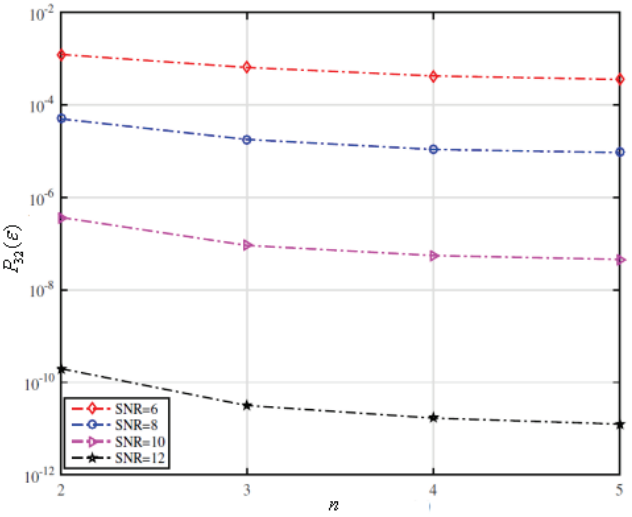

Figure 3 Error probability graph in terms of viewing interval for System 32-CPCM for different SNRs

As shown in Fig. 2, the proposed modulation performance is better than BPSK and FSK. In addition, with the increase in the number of observation intervals, the proposed algorithm improves, and this improvement is negligible with increasing computational complexity due to increasing the value of n. In Fig. 3, we draw the error probability in terms of the observation interval, which we consider to be more precise in reducing the error by increasing the viewing distance.

As shown in Fig. 3, for low SNRs (6 dB and 8 dB), the error rate is reduced slightly with increasing intervals, but for the higher SNRs this improvement (line reduction) is more visible. As SNR = 12 dB, the error rate is at least less of a 0.01. On the other hand, by increasing the amount of n, the computational volume increases exponentially.

6 CONCLUSION

In this paper, we introduced a new approach for transmitting information using a fixed-tiered multi-level chirp signal, and designed an optimal receiver for its detection. In this new approach, we used the M-symbol to send a different surface. With the help of this idea, we simulate the telecommunication system, and the simulation results show that the proposed modulation function has better performance than classical modulations. In addition, with the increase in the number of observation intervals, the proposed algorithm improves, and this improvement is negligible with increasing computational complexity due to increasing the value of n.

7 REFERENCES

[1] Alsharef, M., Hamed, A. M., & Rao, R. K. (2015). Error rate performance of digital chirp communication system over fading channels. *Lecture Notes in Engineering and Computer Science: Proceedings of The World Congress on Engineering and Computer Science 2015*, 21-23 October, 2015, San Francisco, USA, 727-732.

[2] Khyam, Md. O., Noor-A-Rahim, Md., Li, X., Ritz, C. H., Guan, Y. L., & Ge, S. S. (2018). Design of Chirp Waveforms for Multiple-access Ultrasonic Indoor Positioning. *IEEE Sensors Journal*, (99), 1-1, June. https://doi.org/10.1109/JSEN.2018.2846481

[3] Chassande-Mottin, E. & Flandrin, P. (1999). On the Time-Frequency Detection of Chirps. *Applied and Computational Harmonic Analysis*, 6, 252–281. https://doi.org/10.1006/acha.1998.0254

[4] Hamed, A. M., Alsharef, M., & Rao, R. K. (2015). Bit error probability performance bounds of CPFSK over fading channels. *Electrical and Computer Engineering (CCECE), 2015 IEEE 28th Canadian Conference on*, 1329-1334, 3-6 May. https://doi.org/10.1109/CCECE.2015.7129471

[5] Gelman, L. and Ottley, M. (2006). New processing techniques for transient signals with non-linear variation of the instantaneous frequency in time. *Mechanical Systems and Signal Processing*, July, p. 1254. https://doi.org/10.1016/j.ymssp.2004.10.002

[6] Alsharef, M. & Rao, R. K. (2016). Multi-mode multi-level continuous phase chirp modulation: coherent detection. *Accepted for Presentation in IEEE CCECE 2016*, Vancouver, Canada, 15-18 May. https://doi.org/10.1109/CCECE.2016.7726777

[7] Li, X. & Bi, G. (2008). A New Transform for Chirp Detection. *International Symposium on Information Theory and its Applications, ISITA2008*. https://doi.org/10.1109/ISITA.2008.4895439

[8] Qin, Y., Wenyao, L., Shouli, Z., & Hairong, H. (2009). Detection of Chirp Signal by Combination of Kurtosis Detection and Filtering in Fractional Fourier Domain. *Proceedings of the 2009 2nd International Congress on Image and Signal Processing, CISP'09*. https://doi.org/10.1109/CISP.2009.5301566.

[9] Engen, G. & Larsen, Y. (2011). Efficient Full Aperture Processing of TOPS Mode Data Using the Moving Band Chirp Z-Transform. *IEEE Transactions on Geosciences and Remote Sensing, 49*(10). https://doi.org/10.1109/TGRS.2011.2145384

[10] Cristallini, D., Pastina, D., Colon, F., & Lombardo, P. (2012). Efficient Detection and Imaging of Moving Targets in SAR Images Based on Chirp Scaling. *IEEE Transactions on Geoscience and Remote Sensing,* 51, 2403-2416. https://doi.org/10.1109/TGRS.2012.2210556

[11] Liu, G.-G., Zhang, L.-R., Liu, N., Chen, G.-F., & Zhang, Y. (2013). Focusing Highly Squinted Using the Extended Nonlinear Chirp Scaling Algorithm. *IEEE Geosciences and Remote Sensing Letters, 10*(2), 342-346. https://doi.org/10.1109/LGRS.2012.2203785

[12] Wang, W., Du, J., & Gao, J. (2018). Multi-Target Detection Method Based on Variable Carrier Frequency Chirp Sequence. *Sensors Journal*, 8(10), 3386. https://doi.org/10.3390/s18103386

Authors' contacts:

Farhad BAHADORI-JAHROMI,
Department of Electrical and Computer Engineering,
Fasa Branch, Islamic Azad University, Fasa, Iran
E-mail: bahadori.fr@gmail.com

Alireza HASSANNEJAD,
Department of Electrical and Computer Engineering,
Fasa Branch, Islamic Azad University, Fasa, Iran
E-mail: a.hassani9831@yahoo.com

ISSN 1846-6168 (Print), ISSN 1848-5588 (Online)
https://doi.org/10.31803/tg-20180926113107

Original scientific paper

ONLINE CONTROL OF COMBINE REEL HEIGHT IN PRESENCE OF FARM ROUGHNESS USING AN ON-OFF CONTROLLER

Nadia ZENDEHDEL, Younes SHAMORADI

Abstract: Adjusting the harvesting combine reel height in presence of the farm rough surface reduces the harvest losses, prevents possible damage to the headland and increases gravel harvest. Regarding the importance of the issue, in this study, the dynamics of the reel height control system of the John Deere1055 combine was modeled and the controllability and observability of the obtained transfer function is determined in state space. After that, with the aim of cutting the stem from a suitable point, an on-off controller is designed to keep the reel height from the ground in a permitted range. At this stage, a reduced model system is used as an approximated system to design a controller. The designed controller is simulated in MATLAB. In this simulation, the roughness of the ground was considered as the control loop noise with the normal probability distribution function. The results confirm that the reel height change is kept in the specified range against the farm roughness. The laboratory sample was also constructed using an independent excitation circuit DC motor, an optical distance sensor, and a micro controller. The experimental test shows that the height control system responses to changes in surface height at an appropriate speed without any oscillation in range.

Keywords: combine headland, on-off controller, reel height, roughness of the farm

1 INTRODUCTION

Considering the strategic value of cereals such as wheat and barley, it is necessary to pay attention to reduce the harvest loss. Cutting stems from a proper height is an important factor in preventing cluster falling out, increasing the straw harvest and decreasing the amount of uncropped cluster at farm level. In the John Deere 1055 combine, the headland system settings, including the height of the reel from the ground, are adjusted by the operator outside the farm, before starting the harvest process. But the reel height is changed continuously in presence of farm roughness, during the harvesting process and combine movement. This not only affects the quality of cereal harvesting, but sometimes leads to a collision of reel into the ground and damaging it.

Studies on casualties during harvesting of some oilseeds and cereals show the combine headland have a significant role in harvesting quality [1]. One of the factors influencing the combine failure is the operation of the cutting machine [2]. The adaptation of these settings to the conditions of the products and the land characteristics significantly reduces the loss of harvest [3].

The study on the cutting headland has shown that 79.6% of the combine problems are related to reel and cutting blades [4]. In a local study, wheat harvest losses in Khorramabad were estimated at 21.5%, such that 65% of the estimated loss is related to the natural casualties and 56.4% of it is return to the combine losses [5]. In Chaharmahal va Bakhtiari, the highest losses at harvesting stage were determined by John Deere combine 955 and 1055 in 6.8% of Omid wheat and 3.46% of Sardari wheat cultivar, respectively [6]. Due to the importance of improving the harvesting process, many researchers have been focusing on this issue in recent years. For example, a laboratory sample of the combine headland system was designed with the aim of minimizing the loss of rapeseed in harvesting stage [7].

In this sample model, the speed of the combine, the shear speed and the linear velocity of the reel are optimally determined. In order to prevent the excess losses of the John Deere 955 combine, using the concept of fuzzy control, the settings for controlling the reel round speed and the cutting speed of the cutting blade are optimized considering the speed of the combine while working in the field [8]. The presented system is introduced only to alert the driver. Additionally, the cutting height of the stem is not considered.

Regarding the fact that a suitable adjustment of combine head factors reduces wheat harvest loss as 50% in an experimental study [9], the effect of reel kinematic index factors, cutting height, vertical distance of the reel from the shoulder cut and the horizontal distance of the carousel from the shoulder on head loss were identified, respectively. Then, based on the results, a neuro-fuzzy controller was designed in simulink and used to determine the relevant variables.

In the study of [10], with the help of fuzzy logic, the automated adjustment of factors which affect the performance of the end of the John Deere 955 combine has been studied and has not been addressed to harvesting stages.

In our country, mechanized harvesting of cereals is often done by combines that their headland adjustments should be done intuitively by operator, out of the field and before the start of the process. Due to the ruggedness of the farm's surface, during the harvest, the height of the carousel changes from the surface of the earth and some adjustments should be done.

In this research, with the aim of controlling the height of the carousel and clipping of the cluster stem from the appropriate height, a controller is designed and the control system is simulated in the Simulink environment. The proposed control system samples the vertical height of the carousel using some sensors and compares it with a reference height. If the error exceeds the allowable tolerance, the control loop moves reel shaft on the headland to maintain the carousel height changes in a stable and acceptable tolerance.

To this "end" an "on-off" controller controls the peripheral rotation of a DC motor. This rotary motion is converted to the linear motion by power screw to drive the carriage shaft to the optimum level up or down.

2 MATERIALS AND METHODS

In the proposed control system, the required tensile force which is necessary move the reel system is prepared by the kinetic energy of a DC engine. The force is applied to the reel after changing from rotary to tensile. Therefore, the rotational movement of the engine should be controlled in response to the change in the height of the combine head, which is measured by a sensor. Since the reel height should be maintained in a given range, an on-off controller is suitable to be design.

2.1 Research Theory

2.1.1 The Independent Excitation DC Motor Dynamical Behaviour

The engine is a machine that is responsible for converting electrical energy into mechanical energy. In this study, the required motional energy is provided by the mechanical energy of an independent excitation DC motor which is controlled by the armature voltage. With the assumption of the constant current of the armature circuit (i_f), the linear model of rotor torque (T) is calculated from Eq. (1). In this relation (k) is the conversion coefficient.

$$T = ki_f \tag{1}$$

Using the Newton's second law, the dynamic equation of engine angular rotation is obtained in accordance with Eq. (2).

$$J\frac{\mathrm{d}\theta^2(t)}{\mathrm{d}t^2} = ki_f(t) - f\frac{\mathrm{d}\theta(t)}{\mathrm{d}t} \tag{2}$$

θ represents the engine angular rotation. J and f respectively indicate shaft inertia and friction. In addition, the voltage of the input loop of the excitation field is also determined according to Eq. (3).

$$e_f(t) = R_f i_f + L_f\frac{\mathrm{d}i_f(t)}{\mathrm{d}t} \tag{3}$$

R_f and L_f indicate the resistivity and inductance of the armature circuit, i_f and e_f respectively, the excitation field current and voltage. The transfer function of the motor with the armature voltage as its input and the rotor rotation as the output variable is determined using the Laplace transform of relations (2) and (3). After linearization, the transfer function is calculated as it is formulated by Eq. (4). In Eq. (4), N shows the number of armature windings.

$$G(s) = \frac{Q(t)}{E_f(t)} = \frac{\frac{N}{\pi}}{s\left[(JL_f)s^2 + (R_fJ + L_ff)s + (R_ff)\right]} \tag{4}$$

Regarding the angular rotational relationship and linear displacement, the transfer function of the motor is changed as Eq. (5).

$$G(s) = \frac{x(s)}{E_f(s)} = \frac{\frac{Nr}{\pi}}{s\left[(JL_f)s^2 + (R_fJ + L_ff)s + (R_ff)\right]} \tag{5}$$

The values of coefficients in Eq. (5) are set based on the experimental characteristics of an independent excitation motor with a nominal voltage of 24 V and a nominal speed of 20 rpm. The factors obtained in the laboratory are given in Tab. 1. The mass of the rotor shaft in presence of power screw is considered 10 kg. In calculating these parameters, the John Deere 1055 combine headland angle is considered 45 degrees and the weight of the carriage is 20 kilograms. From the mechanical point of view, due to the weight of the moving structure and its distance from the center of gravity, two inertial and frictional forces are presented as two opposing forces. The effect of these two forces can be minimized by using a ball bearing or power screw, and the speed of the system is increased. With this in mind, the coefficient of friction movement is considered 0.64.

Table 1 Parameters of DC motor and combine headland

J (kg·m^2)	f	N	r (m)	L_f (mH)	R_f (mΩ)	parameter
19.27	0.64	2000	0.02	27.5	164	value

With respect to the values of engine parameters and reel, the engine transfer function is obtained as Eq. (6).

$$G(s) = \frac{x(s)}{E_f(s)} = \frac{12.73}{0.53s^3 + 3.18s^2 + 0.11s} = \frac{24}{s^3 + 6s^2 + 0.21s} \tag{6}$$

2.1.2 Investigating the Features of Open Loop and Closed Loop Systems

According to Eq. (6), system is type one and marginal stable. In other words, the system will have a bounded output in response to a bounded input. Figs. 1 and 2 indicate the step response of the closed loop and open loop system, respectively.

The closed-loop system shows a stable behavior, while the open-loop step response system has incremental behavior. Based on state space studies, the system is controllable and observable. Therefore, it is possible to use the on-off controller to keep the system's output changes in a desirable range.

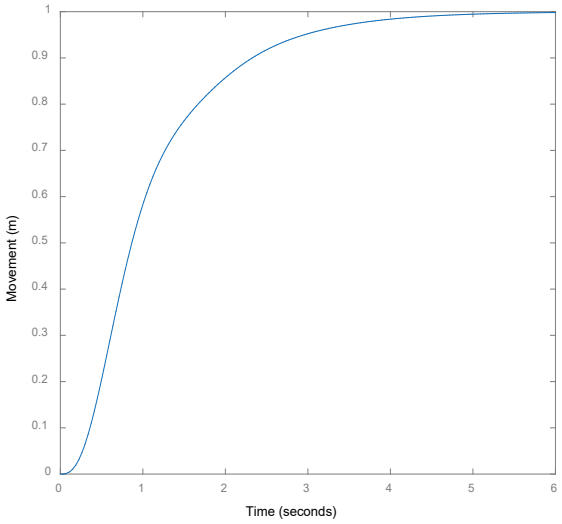

Figure 1 Closed-loop system step response

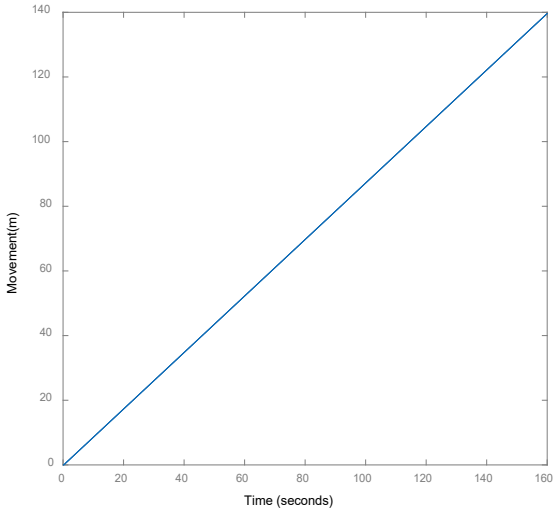

Figure 2 Open-loop system step response

2.1.3 Controlling the Reel Height with the Aim of Reducing Harvest Losses against Surface Roughness

In this section, controlling the reel height is discussed and an on-off controller is designed. To this end, the height change of the farm is monitored continuously during the combine movement. The controller drives a motor to change the reel height based on the measurements.

On-off controller is a non-linear and discrete controller that controls the duty cycle of the hysteresis relay operation. The system secures the closed-loop system output in terms of a reference point, within a permitted range of changes [11].

2.1.4 Model Reduction

Designing an on-off controller for a system of type 2 and above is a nonlinear, complex problem, with a heavy computing need. Since the reel height control system is type 3, it is necessary to approximate it by a model reduction system which is type 1. The constant gain (k) and the time constant (T) of a first order system transfer function $G(s)=\frac{K}{1+Ts}$ are calculated respectively, by relations (7) and (8).

$$S_1(\infty)=lim_{s\to 0}\, s\times\frac{1}{s}\times\frac{K}{1+Ts}=k \tag{7}$$

$$S_1(T)=0.632k \tag{8}$$

Based on the step response of the combine reel control system shown in Fig. 1, the reduced model is obtained by relation (9).

$$G(s)=\frac{24}{s^3+4.6s^2+27.51s+24}\equiv\frac{1}{1+1.09s} \tag{9}$$

Fig. 3 shows the step response of the original and approximated system. In this figure, the continuous line diagram is related to the step response of the reel control system and the dotted line diagram is the step response of the approximated system.

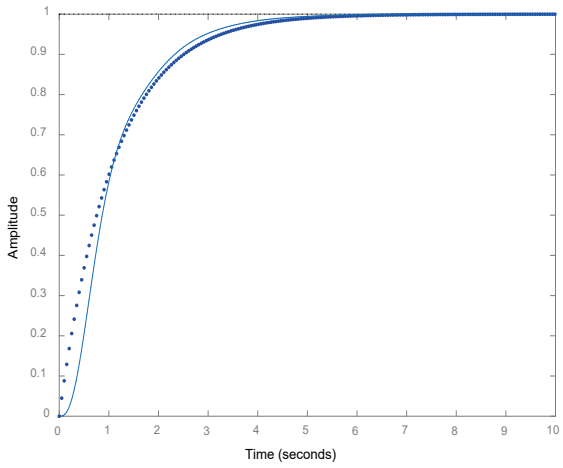

Figure 3 Step response of the reel height controlled system and approximated system

As it can be shown, the step response of the system and its approximation in the operating interval is the same.

2.1.5 On-off Controller Design

Based on the designing theory of an on-off controller, control input is determined by relation (10), using parameters such as the reference point and the allowable range of output variations, as well as the existence delay in relay operation.

$$p=\frac{x_1x_2\left(e^{\frac{T_0}{T}}-1\right)}{K\left(x_1e^{\frac{T_0}{T}}-x_2\right)} \tag{10}$$

The parameters x_2 and x_1 are the lower and upper bound of the reel height change interval. The parameter p is the voltage should be applied as input to motor. T_0 is also the operating time of the relay. Considering the relay operation time as 0.15 seconds, the optimum height as for cutting the stems of grain 0.75 m and an acceptable error as 0.05 m, the armature voltage is obtained 23.5 volts.

3 RESULTS AND DISCUSSION

3.1 Simulation and Numerical Results

The presented on-off controller is applied on the combine reel height control system in the simulink environment and its performance is tested in the presence of disturbances caused by farm roughness. In this section, the roughness of the earth is determined by a random function with a Gaussian probability distribution function with zero mean and the variance of 10. Fig. 4 shows the changes in moving combine reel because of the surface roughness over a period of 60 seconds.

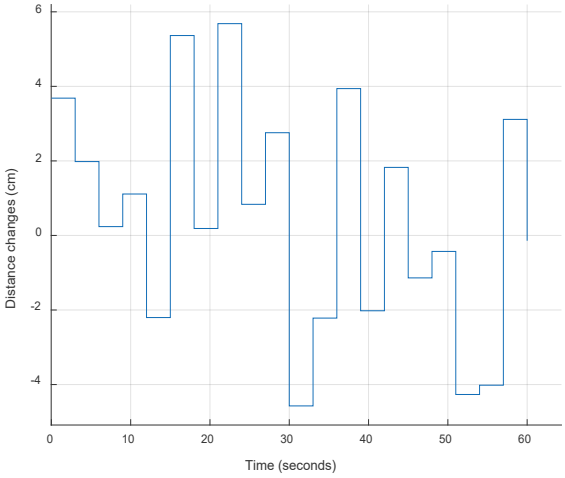

Figure 4 Changes in moving combine headland due to the surface roughness

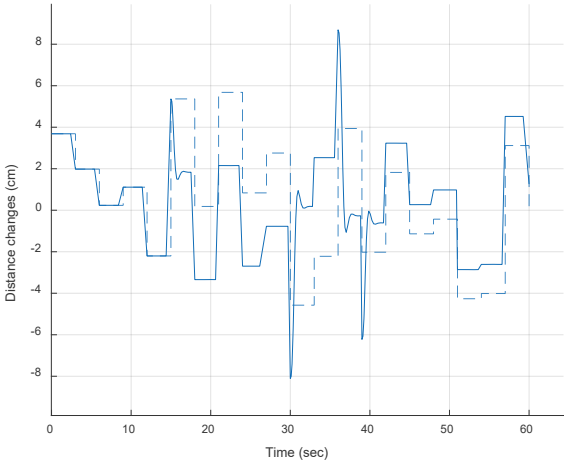

Figure 5 Controlled reel height changes (continuous line diagram), Combine head height changes because of farm roughness (doted diagram)

Considering the suitable height for cutting the stem of the wheat cluster as 0.75 m with tolerance of 0.05 m, the permitted height for the reel location is between 0.7 and 0.8 meters. As shown in Fig. 5, the controller, in response to the farm roughness, applies the voltage to the engine armature with an adjusted left / right direction and maintains the reel distance to the ground level in the desired range.

It is evident in Fig. 5 that when the moving combine passes above a tall roughness and the reel height changes more than 5 cm, the right-turned relay is activated and the voltage applied to the motor. So, the reel is returned to the permitted range.

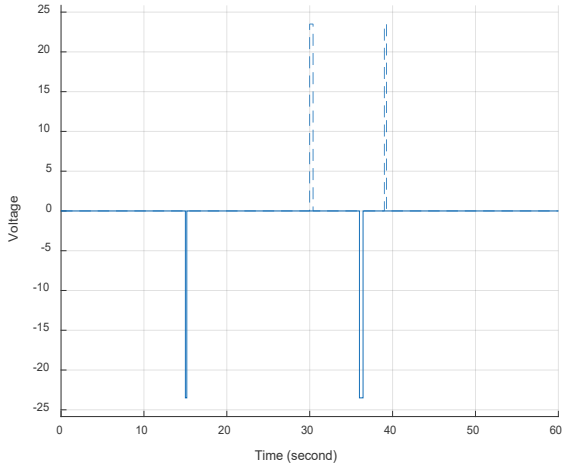

Figure 6 Right-turned relay operation (continuous line) and left-turned relay operation (dotted)

Fig. 6 shows the operation of the right and left-turned relays.

3.2 Performance of the On-Off Reel Height Controller

In the following, the performance of the reel height control system is discussed at time 15 seconds and 30 seconds. At 15 seconds, the combine is placed on a roughness, and the reel height rises as much as 5.36 cm from the base level. As a result of this change, the reel will also be at 80.36 cm above the base. This height is out of the acceptable tolerance which is defined for the on-off controller. Therefore, as shown in Fig. 6, the right –turned relay is actuated and the voltage is applied to armature. The height change shown in Figure 5 (continuous line) indicates that the reel moves to reduce the height and reel enters the permitted range.

Due to the rapid response of the motor after about 0.6 seconds, the reel enters the permissible height and the relay is turned off (Fig. 6). But due to the kinetic inertia of the motor, the reel moves downward after the relay is turned off for 1.38 seconds. Finally, the reel stops at 1.9 cm above the base level at 16.83 seconds.

On the other hand, analyzing the change of reel height at the moment of 30 seconds indicates that due to the roughness of the ground at that moment, the height of the headland decreases 4.6 cm. On the contrary, this height drop is also imposed on the reel and it is placed at 66.9 cm. At this time, the left-turned relay is activated at 0.4 second (Fig. 6), and

the voltage is applied to drive motor and return the reel to the permitted height interval. As shown in Fig. 6, the reel movement continues 1.9 seconds to reach a height 1.3 cm above the base. After that, the engine is placed in steady state mode.

3.3 On-Off Height Controller Simulation

The proposed control system is simulated in MATLAB. In this way, the operator can define the situation of the farm surface roughness and the allowable combine reel position respect to suitable stem cutting point. In the simulation, the position of the reel height changes in the block is applicable to the control loop through "Distance change" block. Additionally, the acceptable tolerance of the stem cutting point can be defined through "R-relay" and "L-relay" blocks. This section can be set by the operator according to the type of the grains. The "Transfer function" block contains the model reel height control system consisting DC motor and a part of combine head. This block is modeled completely depends on the type of combine and used motor. If necessary, its parameters can be adjusted in accordance with the combine. Finally, to show the simulation results the "Display1", "Display2" and "Display3" blocks are used. They respectively show the surface roughness sensor measurement, relay on-off state, and reel height compared to the reference level. Fig. 7 illustrates the control block diagram.

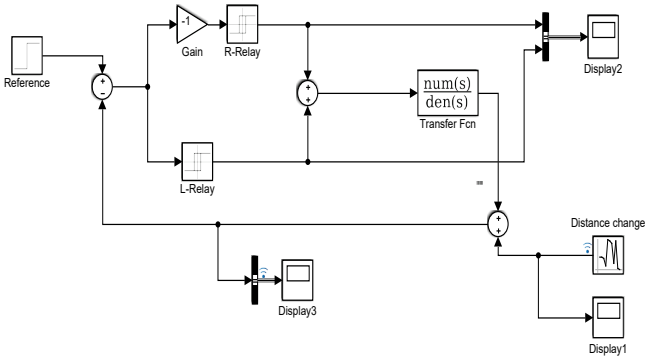

Figure 7 Simulation block diagram

The proposed control algorithm has outstanding features. It is based on the analytical control method and use the linear control theory. The designed controller is not expert based and it is independent of verbal rules. Therefore, it is free from human error. Additionally, the mentioned method is independent from the type of grains, land, and any experiences associated with them. So, it is easily usable and generalized in the process of harvesting a variety of grains or types of farms with different surfaces. Another important advantage of this controller is the high speed of response to the changing height of the moving combine head. The used relies capable to switch in response to the farm roughness with respect the speed of the combine (approx. 20 km / h). Using a gearbox and a power screw also makes it possible for the control system to change the reel position not only in the John Deere 1055 with a 20 kg reel weight, but also in other similar machines up to 50 kg weight. The proposed control method enables the setting parameter feature for the operators and it is guarantee the flexibility factor of the controller.

4 CONCLUSION

In this study, in order to guarantee the cutting of grain stems from a specific height with constant tolerance, an on-off controller was designed and used as a closed loop control method. Typically, a study was conducted on John Deere 1055 harvesting combine. Suitable height for cutting is considered as 0.75 m with an acceptable tolerance of 0.05 m. The controlled system is simulated in MATLAB. The results show a fast and appropriate response of the reel height control system against the farm roughness considered as a noise signal in simulation.

The controller acts human error-free and independent from the operator's experience. In addition, the control method can adapt with various types of harvest combine, grains and different levels of agricultural land.

5 REFERENCES

[1] Shahab-Zadeh, M. M. (2005). *Design, construction and evaluation canola harvest by helping the separator*. *Doctoral dissertation, Thesis*, Faculty of Agriculture, Shiraz University. (In Farsi)).

[2] Jalali, A. & Abdi, R. (2014). The Effect of Ground Speed, Reel Rotational Speed and Reel Height in Harvester Losses. *Journal of Agriculture and Sustainability*, *5*(2).

[3] Campbell, W. P. & Alswager, S. S. (2003). Adjusting equipment now can alleviate harvest losses. *Biological Systems Engineering.(402)*, 2472-3030.

[4] Quick, G. R. & Mills, W. M. (1978). High Capacity Narrow-Pitch Soybean Cutterbar. *Transactions of the ASAE*, *21*(2), 277-0280. https://doi.org/10.13031/2013.35289

[5] Rahmati, M., H. Rozdari, A. M., Ezadi, M., & Yousefian, S. H. (2014). Evaluation and comparison of wheat harvest losses for two common combines in Khorramabad Township. *Journal of Researches in Mechanics of Agricultural Machinery*, *3*(1).

[6] Mirasi, A., Asoodar, M. A., Samadi, M., & Kamran, E. (2014). The Evaluation of wheat losses harvesting in two conventional combine (John Deere 1165, 955) in Iran. *International Journal of Advanced Biological and Biomedical Research*, *2*(5), 1417-1425.

[7] Soleimani, M. & Kasraei, M. (2012). Optimum Adjustments of Cereal Combine Harvester Platform for Canola Harvesting by Using of a Simulated Platform. *Journal of Agricultural Machinery*.

[8] Javidi, M. (2005). Simulation of a control and alarm system for the harvesting combine. *Master thesis*. (In Farsi).

[9] Zareei, S. & Abdollahpour, S. (2016). Simulation of neuro-fuzzy model for optimization of combine header setting. *Journal of Agricultural Machinery*, *6*(2), 406-416.

[10] Lashgari, M., Mobli, H., Omid, M., Alimardani, R., Mohtasebi, S., & Hesamifard, R. (2008). Implementation and Evaluation of a Fuzzy Logic Controller for the Automatic Settings of a Combine Harvester. *Journal of Agricultural Engineering Research, 9*(3), 75-88.

[11] Merikh-Baiat, F. (2009). *Modelling and industrial control*. (In Farsi).

Authors' contacts:

Nadia ZENDEHDEL
Corresponding author
Faculty of Electrical and Computer Engineering,
Department of Electrical Engineering,
Quchan University of Technology,
Quchan, Iran
nadia.zendehdel@gmail.com

Younes SHAMORADI
Faculty of Electrical and Computer Engineering,
Department of Electrical Engineering,
Quchan University of Technology,
Quchan, Iran

ISSN 1846-6168 (Print), ISSN 1848-5588 (Online)
https://doi.org/10.31803/tg-20190417112619

Original scientific paper

NUMERICAL SIMULATION OF THE STRESS-STRAIN STATE OF COMPLEX-REINFORCED ELEMENTS

Olena KRANTOVSKA, Mykola PETROV, Liubov KSONSHKEVYCH, Matija OREŠKOVIĆ, Sergii SYNII, Nelli ISMAILOVA

Abstract: The article describes a developed technique of a numerical simulation of the stress-strain state of complex-reinforced elements, which allows you to create models of double-span continuous. The performed experimental and theoretical studies allowed us to carry out the testing of the developed design model and to justify the reliability of the proposed numerical simulation methodology. The results of the experimental studies were compared with those of the theoretical studies. The theoretical calculus algorithm was developed by using the finite element method. Theoretical calculations were performed by using the mathematical-graphical environment software system LIRA-SOFT and the mathematical and computer program MATLAB. On the basis of the experimental research, the iso-fields of displacements and stresses in the materials of an eccentrically compressed beam with a small bend of the slab were constructed, which collapse behind the inclined narrow strip of concrete and displacements and stresses in the materials of the eccentrically stretched beam, which is destroyed due to the yield of the upper mounting armature.

Keywords: deformation model; finite element modelling; LIRA-SOFT; stress-strain state

1 INTRODUCTIONS

One of the prominent factors in the design of beam-reinforced concrete elements in a complex stressed state is the resistance of the supporting areas, which remains unexplained due to the static uncertainty of this task.

The execution of experimental and theoretical studies with the aim of improving the existing and developing new, modern calculation models of complex stressed supporting areas of reinforced concrete elements is an important and actual task. At the same time, the application of the theory of plasticity, methods of the mechanics of deformation and destruction of the solid allow us to describe in detail the process of the deformation of experimental reinforced concrete elements.

The purpose of the study–development, based on the experimental and theoretical research, was numerical modelling of the stress-strain state (SSS) of complicated elements using numerical nonlinear finite-element calculations.

Today, the finite element method (FEM) [1] has taken the top position because of its obvious advantages, the possibility of bringing the problem to a system of linear or nonlinear algebraic equations.

The theory of M. I. Karpenko [2-4] showed high efficiency in the programmable modeling of the work of reinforced concrete with cracks based on the FEM, which were generalized by the V. I. Murashov theory for the case of a complex stressed state [5]. Works by L. Prandtl [6], E. Ries [7], A. A. Ilyushin and many others were devoted to the studies of the plasticity of materials with their complex SSS.

The theory of the plasticity of concrete and reinforced concrete proposed in [1] was substantially developed by A. I. Kozachevsky [8], V. M. Kruglov [9], S. F. Klovanich [10], V. I. Korsun [11] and others. Hereafter, M. I. Karpenko and his students developed the theory of small elastic-plastic deformations, in which concrete before and after the appearance of cracks is considered to be anisotropic.

2 RESEARCH METHODOLOGY

2.1 General Guidelines

In accordance with the developed methodology of experimental research, the items listed below have been tested:

- single-span beams of a rectangular cross-section with the dimensions of 100 × 200 mm with h_0 = 175 mm, span $l = 9 \cdot h_0$ = 575 mm and shear span a/h_0 = 1, 2, 3, made of the heavy concrete of classes C12/15, C20/25, C30/35, reinforced by two plain frames with the lower rebar 2⌀12, 14, 16 A500S, with the top rebar 2⌀8, 10, 12 A500S and with the transverse rebar 2⌀3, 4, 5 V_r-I;
- two-span continuous beams, respectively, $b \times h$ = 100 × 180 mm with h_0 = 155 mm, $l = 8 \cdot h_0$, a/h_0 = 1, 2, 3, C12/15, C20/25, C30/35, 2⌀10, 12, 14 500S, 2⌀10, 12, 14 A500S, 2⌀3, 4, 5 V_r-I.

Single-span beams were tested for eccentrically stretching at $N_{st}/(f_{ck} \cdot b \cdot h_0)$ = 0.05; 0.2; 0.35, eccentric compression $N_{st}/(f_{ck} \cdot b \cdot h_0)$ = 0.2; 0.4; 0.6, in a numerical experiment, modelled using a deformation method based on the results of previous field experiments, on eccentric compression with $N_{st}/(f_{ck} \cdot b \cdot h_0)$ = 0.05; 0.2; 0.35. The eccentricity of the application of the longitudinal force was changed: $e/h_0 = -0.25$; 0; +0.25. The continuous same beams were tested on the bending by two concentrated forces.

For the experiment, power plants were manufactured according to the schemes [12].

Experiments were performed on five-factor, close to the properties of the D-optimal plan of type N5, which provides the same accuracy of the prediction of the experimental value in the area described by a radius equal to 1 relative to the central "0" point (Experiment No. 27), as well for two-factor,

three-level, close to the properties of the D-optimal, plan B2 type for the study of eccentrically stretched beams [13].

2.2 Modelling of the Stress-Strain State of Reinforced Concrete Beams

Concrete and reinforcement in the experimental samples work together, but have different physical and mechanical properties characterized by the non-linear dependence between the stresses and strains. In this regard, for the implementation of finite-element models of experimental reinforced concrete elements in the LIRA-SOFT PC, additionally, the tested complete concrete deformation diagrams were introduced according to the data of the NIISK (A. M. Bambura) and two-line diagrams of the reinforcement [14, 15].

Calculations were made by only one-half of the beam due to the symmetry of the experimental elements and loads. The beams were conditionally broken into spatial octogenic iso parametric finite elements No. 236 with the dimensions of 1 × 1 × 1 cm for the convenience of the modelling of the reinforcement, and considering that in real beams, a large aggregate was crumbled by granite gravel fraction 5-10 mm. The number of elements in the model of the acontinuous beam were - 19600, nodes - 22725; the conventional and eccentrically compressed beam, respectively, 15800 and 18320.

The calculations used a stepwise and stepwise-iterative method using the piecewise linear dependence of the library number 14 according to the corresponding algorithm: if the value of the generalized deformation goes beyond the given fractured line, then the exclusion of the material ($E_i = 1$) of the elementary plane from the cross section is modeled. In the performance of real and numerical experiments, at first stages, eccentrically compressed, stretched load was applied, and then – transverse load in the form of two symmetrically located concentrated forces.

The adapted layered model of the deformation of the experimental elements and the execution of numerical experiments is realized in the MATLAB PC environment. According to [16], we adopt a deformation model of the beam in a discrete form: divide it into i-sections and j-layers up the height of a cross-section. Let us assume that the formed sites have the same SSS. The reinforcement of the stretched and compressed zones is tied to the cross-sectional faces at the level of the centres of gravity. The basis of the SSS simulation of the experimental beams is the traditional position for the deformation model.

The modelling of the SSS of the experimental beams is performed by the following algorithm:

1) Initial information is entered.
2) The geometric characteristics of the beam's cross-sections are determined by taking into account the real modulus of the deformation of cross sections at this stage:

$$(EA)_{red,i} = \sum_{j=1}^{j\max} (E_{cij} A_{cij} + E_{si} A_{si} + E'_{si} A'_{si}) \quad (1)$$

$$(ES)_{red,i} = \sum_{j=1}^{j\max} (E_{cij} A_{cij} y_{ij} + E_{si} A_{si} y_{si} + E'_{si} A'_{si} y'_{si}) \quad (2)$$

$$y_{0i} = \frac{(ES)_{red,i}}{(ES)_{red,i}} \quad (3)$$

$$(EI)_{red,i} = \sum_{j=1}^{j\max} \Big[E_{cij} A_{cij} (y_{0i} - y_{ij})^2 + \\ + E_{si} A_{si} (h_0 - y_{0i})^2 + E'_{si} A'_{si} (y_{0i} - a')^2 \Big] \quad (4)$$

where $E_{cij}(t)$, E_{si}, E'_{si} – cross-sectional deformation modules, respectively concrete, stretched and compressed reinforcement, which before the load are accepted as equal to the initial deformation modules; A_{cij} – area of the j^{th} layer of the i^{th} section of the beam; y_{ij} – distance from the compressed side of the beam to the centre of the gravity of the j^{th} layer of the i^{th} section of the beam.

3) The initial coordinate of the pole of the longitudinal force N is determined.

$$y_{P_0} = \left[\frac{h}{2} - y_{0i} \pm (e + e_{0ac.}) \right] \quad (5)$$

where e – eccentricity of applying a longitudinal stretching or compression force; $e_{0ac.}$ – accidental eccentricity,

$$e_{0ac.} = \frac{h}{30} \quad (6)$$

4) The stage of the load is given with the subsequent increase in the given magnitude of the longitudinal compressive (stretching) force $\Delta N = 0.1[N_{adm}]$ to a given or admissible value. For a continuous element, we define the transverse force with its subsequent increase on ΔV, and determine the corresponding spans and support moments and the transverse forces on the medium support. Before the appearance of a plastic hinge on the medium support, these moments are counted on a non-deformed scheme, according to the methods of construction mechanics.

The support and span moments are accepted:

$$M_{sup} = -0{,}236 \text{ V}; M_{sup} = -0{,}205 \text{ V}; M_{sup} = -0{,}130\text{V} \quad (7)$$

$$M_{sp} = 0.143 \text{ V}; M_{sp} = 0.079 \text{ V}; M_{sp} = 0.022 \text{ V}. \quad (8)$$

At this stage of the work of a continuous beam, the value of the transverse force on the medium support to the right and to the left of it is determined, respectively:

$$V_{sup,right} = \frac{M_{sp} - M_{sup}}{a} \quad (9)$$

$$V_{sup,left} = \frac{M_{sup} - M_{sp}}{a} \quad (10)$$

With the appearance of a plastic hinge over the middle support, the support moment reaches the maximum possible value of $M_{sup} = [M_{sup}]$, which can be sustained by the concrete cross-section over the support. Furthermore, there is a redistribution of internal forces with increasing span moments, which are:

$$M_{sp} = \frac{V \cdot d \cdot a - M_{sup} \cdot d}{L} \le \left[M_{sp} \right] \quad (11)$$

where $[M_{sp}]$ – the maximum admissible value of the span moment; d - the distance from the first support to the line of action of the concentrated force; a - is the distance from the line of action of the concentrated force to the medium support.

The transverse force on the support is determined after the appearance of a plastic hinge:

$$V_{ult} = \frac{\left[M_{sp} \right] - \left[M_{\sup} \right]}{a} \quad (12)$$

5) The deformations of concrete and reinforcement in the sections of the beam are determined:

$$\varepsilon_{cij} = \frac{N}{(EA)_{redi}} \cdot \left[1 + \frac{y_P \left(y_{ij} - y_{0i} \right) (EA)_{redi}}{(EI)_{redi}} \right] + \frac{M_i \left(y_{ij} - y_{0i} \right)}{(EI)_{redi}} \quad (13)$$

$$\varepsilon_{si} = \frac{N}{(EA)_{redi}} \cdot \left[1 + \frac{y_P \left(h - a_i - y_{0i} \right) (EA)_{redi}}{(EI)_{redi}} \right] + \frac{M_i \left(h - a_i - y_{0i} \right)}{(EI)_{redi}} \quad (14)$$

$$\varepsilon'_{si} = \frac{N}{(EA)_{redi}} \cdot \left[1 + \frac{y_P \left(a'_i - y_{0i} \right) (EA)_{redi}}{(EI)_{redi}} \right] + \frac{M_i \left(a'_i - y_{0i} \right)}{(EI)_{redi}} \quad (15)$$

$$y_{Pi} = y_{P_0} + y_{N(x)}, \quad (16)$$

where $y_N(x)$ – additional deflection or bend of the i^{th} section, due to the longitudinal force N, which is determined by the equation:

$$y_{N(x)} = \left[\frac{(\varepsilon_{si} - \varepsilon'_{b1})}{h_0} \right] \cdot \rho_{mNi} \cdot l^2 \quad (17)$$

where ρ_{mNi} – a coefficient that takes into account the effect of the moment on the longitudinal force N (or the effort of the previous tension) on the magnitude of its bend or buckling. It is determined by the length of the beam ($0 \le x \le l$) by the equation

$$\rho_{mNi} = \frac{l \cdot x - x^2}{2l^2} \quad (18)$$

6) If deformations in concrete and reinforcement do not exceed the maximum admissible values, then we remember them. Through this value, we determine the stresses according to the diagrams of the σ-ε concrete and reinforcement. Then we perform the correction of the cross-section modules of concrete deformation and reinforcement.

$$E_{cij} = \frac{\sigma_{cij}}{\varepsilon_{cij}} \quad (19)$$

$$E_{s_{i,low}} = \frac{\sigma_{si,low}}{\varepsilon_{si,low}} \quad (20)$$

$$E_{s_{i,up}} = \frac{\sigma_{si,up}}{\varepsilon_{si,up}} \quad (21)$$

Next, we determine the geometric characteristics of the beams' cross-sections for the specified values of the modules of the deformation of the cross-sections $(EA)_{red,i}$, $(EI)_{red,i}$.

7) Through the corrected geometric characteristics, specify the values of the deformations of concrete and reinforcement and compare them with the previous values. If their values are close (no more than 1% inaccuracy), then at this stage, the SSS of the beams is revealed and you can go to the definition of deflections and other parameters of the workability of the experimental beams.
8) According to the author's improved technique [14], we determine the size of the shear bearing capacity of the inclined cross-sections $[V_{ult}]$ of the experimental reinforced concrete beams.
9) After reaching the given or admissible value of the longitudinal stretch force $[N_{adm}]$, we turn to the consideration of the change of the SSS in the process of the proportional loading of a single-span beam by symmetrically disposed transverse forces F to the destruction of the element per a normal or inclined crack.
10) Determine the values of the bending moment and transverse force along the length of the beam.
11) Through the Eqs. (13)-(16), we determine the deformation of concrete and reinforcement, and also specify the coordinate of the pole of the force $[N_{adm}]$, taking into account an additional bending due to the action of transverse and longitudinal forces,

$$y_{Pi} = y_{P_0} + y_{tot,i} \quad (22)$$

where $y_{tot,i}$ – a complete deflection, which is defined as the algebraic sum of deflections due to bending deformations from the transverse and longitudinal loading, as well as the shear deformations:

$$y_{tot,i} = \left(\frac{\varepsilon_{si} - \varepsilon_{c1}}{h_0} \right) \cdot \left(\rho_{mNi} + \rho_{mMi} \right) l^2 \cdot \rho_{qi} \quad (23)$$

where ρ_{mMi} - a coefficient that takes into account the influence of the bending moment on the deflection of the beam in this cross section. It is counted within the shear span.

12) At each stage, the values of the increasing transverse force V near the medium support for the two-span beam and the destructive force V_{ult} are compared. If $V \geq V_{ult}$, then this means that the external load has reached a value at which the beam can be destroyed on the medium support section along the inclined cross-section.

3 RESULTS

The results of the numerical implementation of the experiments of an ordinary one-span (test task), eccentrically stretched and compressed, as well as the continuous reinforced concrete beams (five-factor experiments) are presented in Tab. 1.

Table 1 Destructive loading of experimental elements

№№	Eccentrically-compressed beams			Eccentrically stretched beams			Continuous double-span beams		
	$V_l^{exp.}$	LIRA-SOFT	MATLAB	$V_l^{exp.}$	LIRA-SOFT	MATLAB	$V_l^{exp.}$	LIRA-SOFT	MATLAB
1	77	82	77	19,5	22	21	118	130	112
2	117	123	120	43,1	53	45	140	140	121
3	124	127	123	136,7	140	135	103	115	95
4	57	57	54	48,8	51	49	60	70	50
5	135	142	137	32,0	48	34	193	205	165
6	69	70	69	13,8	23	16	91	100	61
7	65	70	62	54,4	56	54	64	80	60
8	106	114	106	155,3	102	146	82	90	85
9	140	145	140	65,2	79	78	139	150	171
10	50	58	49	13,5	22	9	83	90	88
11	63	71	62	42,8	52	43	88	95	62
12	108	112	110	122,6	128	121	118	130	80
13	144	150	146	143,3	145	131	165	170	169
14	54	58	54	48,5	52	49	68	85	62
15	59	62	57	9,8	10	3	93	105	90,5
16	104	111	105	54,0	70	67	99	115	92
17	50	66	60	38,3	44	37	83	95	85
18	133	137	123	101,6	102	102	130	145	145
19	95	101	97	55,7	63	55	100	110	115
20	81	88	79	55,6	61	55	80	80	76
21	93	97	91	59,5	62	59	91	105	101
22	84	89	86	51,3	57	51	89	100	88
23	96	102	93	18,0	27	20	102	105	112
24	85	92	88	76,9	70	77	78	85	86
25	102	105	93	50,1	53	50	104	105	109
26	74	87	83	60,0	66	61	76	85	97
27	89	92	89	55,4	62	55	90	100	99
$\upsilon = \frac{\sigma}{b_0} \cdot 100\ \%$		12	5.7		18	6.4		11.8	6.6

The use of this finite element calculation allows you to simulate the SSS of test beams at all stages of operation, up to destruction.

A sequential analysis of the iso-fields of the displacements and stresses (Figs. 1, 2) in the materials of real construction allows us to estimate the influence of the investigated factors and the factors of external influence on their bearing capacity, to predict the character of further deformations and destruction.

It was found that the stresses in transverse reinforcement reach, on average, 58% of the yield strength. Due to the two-axial compression of the concrete in the supporting area, strengthening is observed (in relation to the prism), on average, it is 22%, and its bearing capacity, respectively, is 43%. After the formation of the so-called "plastic hinge" over the medium support of the continuous beam with an increasing load, there is a known redistribution of moments (within the limits of 20 ... 30%) with the growth of the latter in the spans and the destruction of their supporting areas is completed by the achievement of all transverse reinforcement of the yield limit. The destruction, practically, of all continuous double-span beams occurred due to the punching shear over the middle support with the achievement of compressive stresses in concrete under the concentrated forces and over the support, respectively, $\sigma_{cx} \cong 0.72 f_{ck}$ and $1.03 f_{ck}$, $\sigma_{cz} \cong 0.96 f_{ck}$ and $0.66 f_{ck}$, $\tau_{cxz} \cong 0.47 f_{ck}$ with $x = l - a \ldots l$.

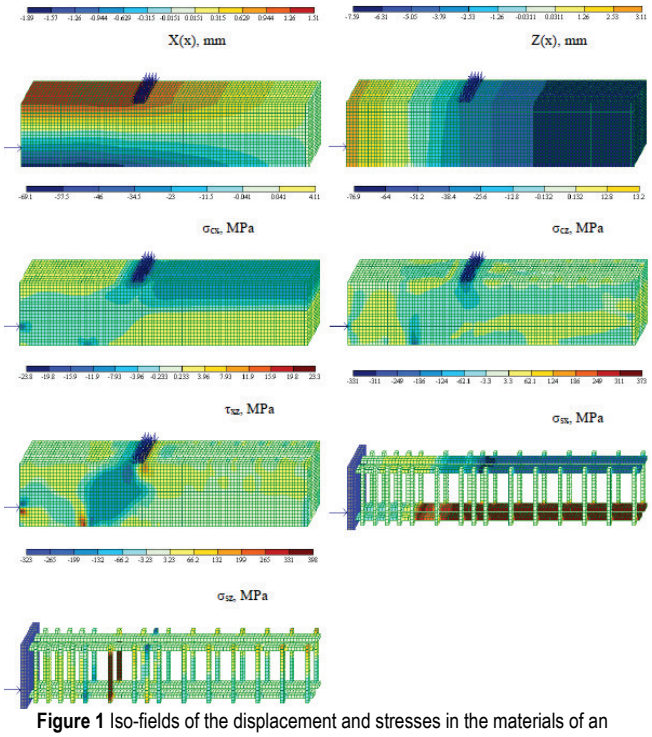

Figure 1 Iso-fields of the displacement and stresses in the materials of an eccentrically compressed beam with a small shear span which collapses per inclined compressed concrete strip (Experiment 8).

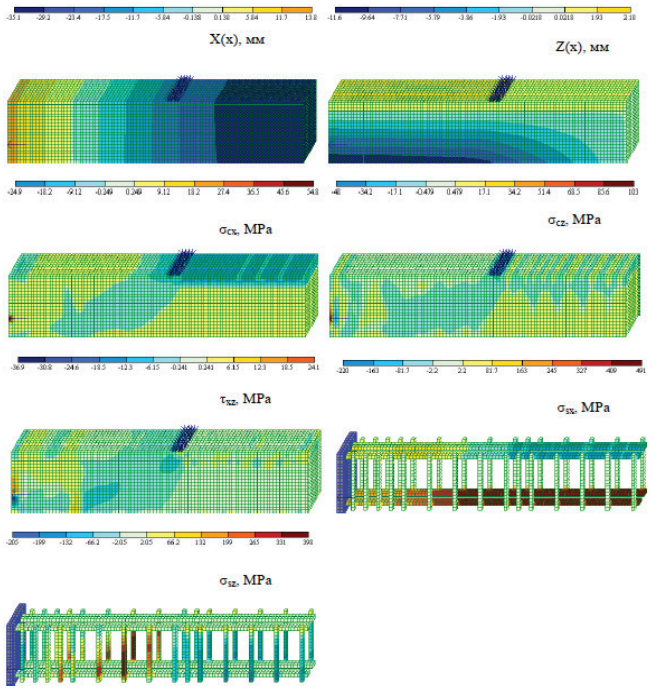

Figure 2 Iso-fields of the displacement and stresses in the materials of an eccentrically stretched beam which is destructed by the yielding flow of the upper reinforcement (Experiment 2).

4 CONCLUSIONS

The numerical modelling methodology of the SSS of complex-reinforced concrete elements with the help of a numerical nonlinear finite-element calculation based on the general mechanics of reinforced concrete is developed. The finite-element calculation was used to model the stress-strain state of the experimental beams at all stages of operation, up to destruction.

The adequacy of this method is confirmed by its comparison with the results of the conducted field experiments to determine the bearing capacity of an ordinary single-span, eccentrically stretched and compressed beam, as well as continuous reinforced concrete beams. Research have found that the stresses in armatures reach 58% of the limit of release. In the support area, the reinforcement averaged 22% and its bearing capacity was 43%.

The destruction of all continuous double-span beams occurred due to the punching shear over the middle support with the achievement of compressive stresses in the concrete. Theoretical calculations by using the PC LIRA-SOFT and MATLAB showed convergence with the experimental data in the range of the coefficient of variation of 6 ... 11.8%.

5 REFERENCES

[1] Klovanich S. F. & Mironenko I. N. (2007). *Method of Finite Elements in the Mechanics of Reinforced Concrete*, Izd-o ONMU, Odessa.

[2] Gvozdev, A. A. & Karpenko, N. I. (1965). The work of reinforced concrete with cracks under a plane stressed state. *Structural Mechanics and Analysis of Constructions*, 2, 20-23.

[3] Karpenko, N. I. (1996). *General models of mechanics of reinforced concrete*. Stroyizdat, Moscow.

[4] Karpenko, N. I. & Klovanich, S. F. (1983). Determining relations for reinforced concrete with cracks in thermosensitive effects. *Structural Mechanics and Analysis of Constructions*, 2, 6-11.

[5] Gorodetsky, A. S., Shmukler, V. S., & Bondarev, A. V. (2003). *Information technologies for calculating and designing building constructions*. NTU "KhPI", Kharkiv.

[6] Prandtl, L. (1924). Spannungsverteilung in plastischen Körpern. *Proc. of 1st Int. Congr. of Appl. Mech.*, 43-54.

[7] Reiss, E. (1948). Accounting for elastic deformation in the theory of plasticity. *Theory of plasticity*, 206-222.

[8] Kozachevsky, A. I. (1983). Modification of the deformation theory of plasticity of concrete and the plane stress state of reinforced concrete with cracks. *Structural Mechanics and Analysis of Constructions*, 4, 12-16.

[9] Kruglov, V. M. (1983). Nonlinear relations and criteria for the strength of concrete in a triaxial stress state. *Structural Mechanics and Analysis of Constructions*, 4, 12-16.

[10] Klovanich, S. F. (2004). The finite element method in nonlinear mechanic soil and concrete. *Building construction, 61*(1), 103-108.

[11] Korsun, V. I. (2005). Design constructions for temperature and force effects taking into account the inhomogeneity of the properties of materials, *dis. Dr. tech. Sciences*, DonNACEA, Makeevka.

[12] Krantovska, O., Petrov, M., Ksonshkevych, L., Synii, S., & Sunak, P. (2018). Improved engineering method for calculating the strength of the supporting areas of reinforced concrete elements. *MATEC Web of Conferences*, Kharkiv. https://doi.org/10.1051/matecconf/201823002014

[13] Voznesensky, V. A. (1981). Static methods of experiment planning in technical and economic research. *Finance and Statistics*, Moscow.

[14] Dorofeev, V. S., Karpiuk, V. M., & Krantovska, E. N. (2010). Strength, crack resistance and deformability of continuous reinforced concrete beams (monograph). Even, Odesa.
[15] Dorofeev, V. S., Karpiuk, V. M., & Petrov, N. N. (2011). Strength, deformability and crack resistance of the support of inclined sections of eccentrically stretched, compressed of reinforced concrete beams (monograph). Even, Odesa.
[16] Blikharskyy, Z. Y. (2005). Onset-deformation of the mill-concrete constructions in the aggressive medium during the day, *dis. Dr. tech. Sciences*, LPNU, Lviv.

Authors' contacts:

Olena KRANTOVSKA
Odessa State Academy of Civil Engineering and Architecture,
Ditrikhson st. 4, 65029 Odesa, Ukraine
Tel: +380660474510

Mykola PETROV
Odessa National Academy of Telecommunications O. S. Popov,
Kovalska st. 1, 65029 Odesa, Ukraine
Tel: +380677630679

Liubov KSONSHKEVYCH
Odessa State Academy of Civil Engineering and Architecture,
Ditrikhson st. 4, 65029 Odesa, Ukraine
Tel: +380669170688

Matija OREŠKOVIĆ
University North, Department of Civil Engineering,
48000 Koprivnica, Croatia
E-mail: moreskovic@unin.hr

Sergii SYNII
Lutsk National Technical University,
Lvivska st. 75, 43018 Lutsk, Ukraine
E-mail: sergii.synii@gmail.com

Nelli ISMAILOVA
Odessa National Academy of Telecommunications O. S. Popov,
Kovalska st. 1, 65029 Odesa, Ukraine
Tel: +385508545585

ISSN 1846-6168 (Print), ISSN 1848-5588 (Online)
https://doi.org/10.31803/tg-20190427093441

Original scientific paper

PWM CONTROLLING OF A NEW MULTI DC-DC CONVERTER CIRCUIT

Erol CAN

Abstract: The design and development of DC-DC converter circuits are important for increasing and decreasing the direct current energy sources at operating the loads and systems. In this study, a multi DC-DC converter structure is described. The purpose of creating this circuit structure is to create a more effective circuit by offering a different circuit structure. For the proposed DC-DC converter, a circuit structure with five switches is created. This circuit structure is described by mathematical models according to the operation of the four parts PWMs in different time periods. After the mathematical analysis of the circuit structure, the proposed circuit and conventional circuit are operated in the Matlab Simulink. The obtained results are compared. According to the comparisons, the proposed circuit produces a higher output voltage than the traditional one and has a higher performance. Additionally, the circuit is operated for values of different loads using different switching times. Finally, voltages and currents are observed on loads.

Keywords: different switching times; multi DC-DC converter; the four parts PWM

1 INTRODUCTION

Nowadays, DC-DC converters are needed for many electrical devices used in the industry and social life. Hence, many designs have been focused on DC-DC converter circuits. Some studies [1, 2] show that the simple DC-to-DC converter structures have been used for the dc voltage conversion that a system needs. Some of the converter works have been done to regulate the electrical energy obtained from the solar systems and fuel [3-6]. Some converter studies have addressed the problem of applying a min-type control of a synchronous boost converter using the non-linear control switching surface used in the mixed control equations [7, 8]. It also offers the advantages of the switching surface of the start of the operation of the DC-DC converter and explores its potential use for output voltage regulation [9]. This article, unlike the studies listed in the literature, wishes to create a new DC-DC converter structure and mathematical model against the traditional DC-DC converter structures. The proposed circuit structure with its output voltage multiplexing capability offers superior hardware and a different mathematical model than the conventional converters [10-12]. Since it has a simpler structure than other cascade converters, it contains fewer circuit elements [13-17]. In this circuit structure, five IGBT switches are operated by four different PWMs in different time zones. After running the first stage of the PWM1 and PWM 2 DC-DC converter, PWM 3 and PWM4 manage the second stage cycle to re-increase the output voltage obtained. While the first inductor stores current, the second inductor stores the second inductor current. At the same time, the input source in the first cycle contributes again to the input voltage for the second cycle. At the end of the total cycle, the output voltage for the second stage multiplies the output voltage from the conventional DC-DC converter in the first stage. This circuit structure is described in the second section with a mathematical analysis. In the simulation studies, the circuit is operated after the proposed circuit structure has been created in Matlab Simulink. After the output, volt and coil currents are monitored by the oscilloscope, and the results are obtained. Then, the results obtained from the conventional DC-DC converters and the proposed circuits are compared. Additionally, the circuit is operated for different loads by using different switching times. According to the results obtained, while the proposed circuit provides the current of different loads from low current values to high current values, it provides a voltage of different loads from high voltage values to low voltage values. The results show that the proposed circuit is superior to other DC-DC converters.

2 PROPOSED CONVERTER CIRCUIT STRUCTURE

Fig. 1 shows the circuit structure of the converter. There are S1 to S5 switches on the circuit structure. There is one dc voltage source, two equal inductors which are L_1, L_2; two diodes which are D1, D2; two equal capacitors which are C_1, C_2. In Fig. 2, there is a four part pulse width modulation that controls these switches.

In the first stage, when the PWM-1 is active on the circuit, the circuit structure will be as in Fig. 3a. While PWM-2 is active on the circuit, the circuit structure is in Fig. 3b.

V_{dc} is $E \cdot V_{o1}$ is the converter output voltage for the first stage. T is the time period. D is the PWM value at the time period. PWM-1 operates the V_{dc} source and the L_1 inductor on the circuit by means of the S1 and S2 switches. In this case, the current through the inductor reaches its maximum value during the operation of PWM-1. PWM-2 operates the V_{dc} source and L_1 inductor on the circuit by means of the D1, S1, and S4 switches. In this case, the current through the inductor reaches its minimum value during the operation of the PWM-2. The maximum value of the current at this stage is equal to the negative value of the current as it goes down to the minimum. This gives the output voltage the equation known of the DC-DC converter as in Eq. (1).

$$V_{o1} = \frac{E}{(1-D)} \tag{1}$$

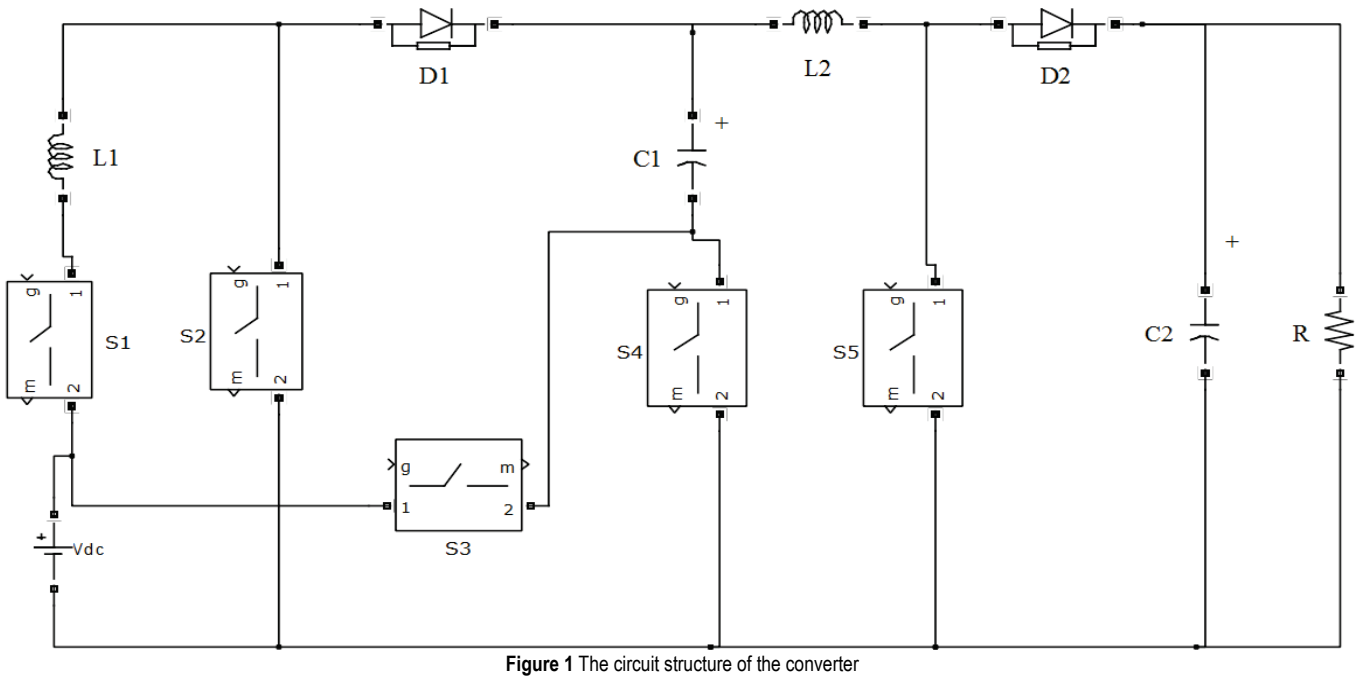

Figure 1 The circuit structure of the converter

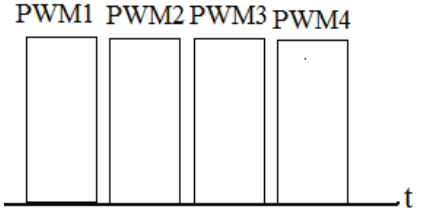

Figure 2 PWMs for the circuit structure of the converter

Since PWM1 and PWM2 constitute half of the total operating time of the PWM, the output voltage is half of the output voltage of the converter operating at full period. Eq. (2) can be written as Eq. (3).

$$V_{o1} = \frac{E}{2(1-D)} \tag{2}$$

In the second stage, when the PWM-3 is active on the circuit, the circuit structure will be as in Fig. 4a. While PWM-4 is active on the circuit, the circuit structure is in Fig. 4b.

V_{o1} is also the converter input voltage at the second stage, while V_{o1} is the converter output voltage for the first stage. PWM-3 operates the V_{dc} source, L_2, C_1 on the circuit by means of the S3 and S5 of the switches. In this case, the current through the inductor reaches its maximum value during the operation of the PWM-3. The current of the L_2 inductor from the minimum to the maximum value can be written as in Eq. (3).

$$\left(\begin{array}{l} \dfrac{E}{2(1-D)L_2} = \dfrac{\mathrm{d}i_2}{\mathrm{d}t} \\ I_{\min} - I_{\max} = \dfrac{E}{2(1-D)L_2} DT \end{array} \right) \tag{3}$$

PWM-4 operates the V_{dc} source, C_1, C_2 and L_2 on the circuit by means of the D2, S3 switches. In this case, the current through the inductor reaches its minimum value during the operation of PWM-4. The maximum value of the current at this stage is equal to the negative value of the current as it goes down to the minimum. The current of the L_2 inductor from the maximum to the minimum value can be written as in Eq. (4), Eq. (5), and Eq. (6).

$$\frac{E}{2(1-D)} = \frac{\mathrm{d}i_2}{\mathrm{d}t} L_2 + VC_2 \tag{4}$$

$$\frac{E}{2(1-D)L_2} - \frac{VC_2}{L_2} = \frac{\mathrm{d}i_2}{\mathrm{d}t} \tag{5}$$

$$I_{\min} - I_{\max} = \left(\frac{E}{2(1-D)L_2} - \frac{VC_2}{L_2} \right)(1-D)T \tag{6}$$

The negative value of Eq. (6) can be equalized to Eq. (3) and a common arrangement can be made as in Eq. (7) and Eq. (8).

$$DT\frac{E}{2(1-D)L_2} = -\frac{E}{2(1-D)L_2} + \frac{VC_2}{L_2}(1-D)T \tag{7}$$

$$D\frac{E}{2(1-D)L_2} = -\frac{E}{2(1-D)L_2} + \frac{VC_2}{L_2} + D\left(\frac{E}{2(1-D)L_2} - \frac{VC_2}{L_2} \right) \tag{8}$$

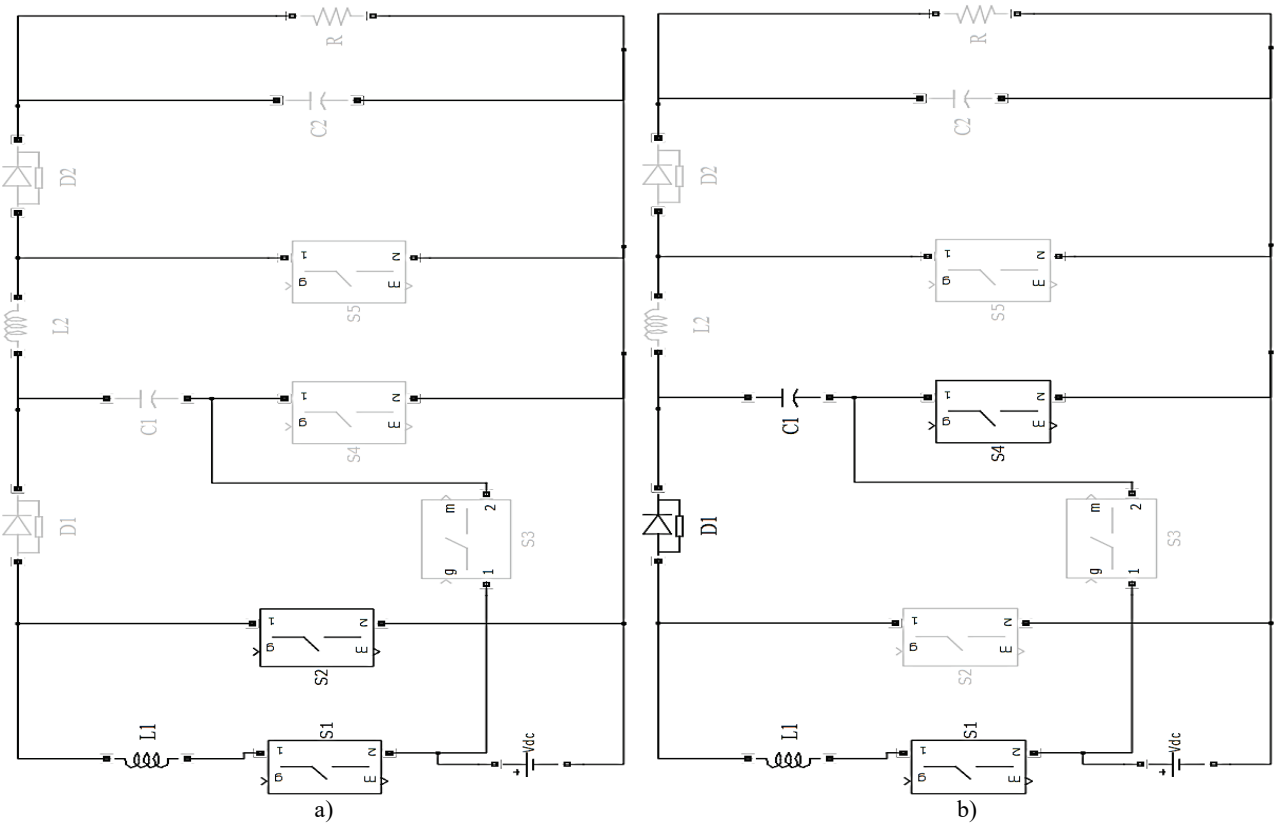

Figure3 a) the circuit structure for PWM-1, b) the circuit structure for PWM-2

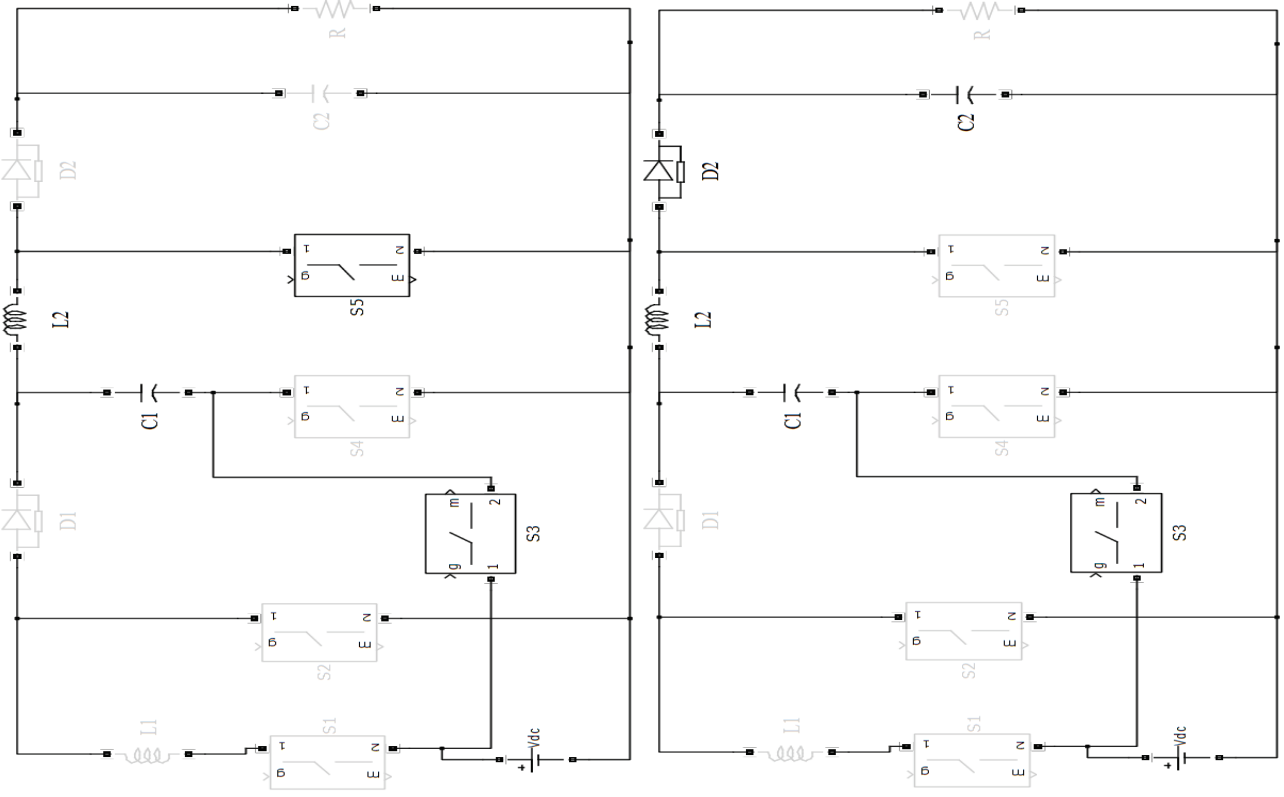

Figure 4 a) the circuit structure for PWM-3, b) the circuit structure for PWM-4

Eq. (8) can be arranged as the equations in Eq. (9), Eq. (10), and Eq. (11). Then, this gives the novel output voltage the equation of the DC-DC converter as in the equations below.

$$\frac{E}{2(1-D)L_2} = -D\frac{VC_2}{L_2} + \frac{VC_2}{L_2} \tag{9}$$

$$\frac{E}{2(1-D)} = (1-D)VC_2 \tag{10}$$

$$\frac{E}{2(1-D)^2} = VC_2 \tag{11}$$

The value of the dividing number in the equation that makes up the VC_2 can be different if the working times of the PWMs were changed. If the number of cycles in the circuit is increased, the number of multiplexes will increase. Hence, the force of $(1 - D)$ will increase with the increase of the cycle amount.

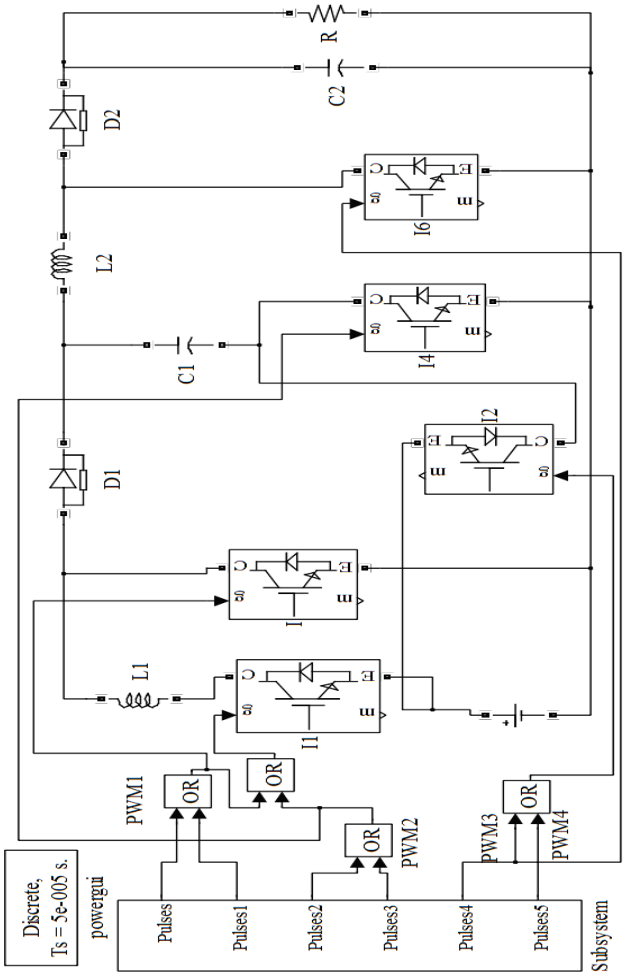

Figure 5 The circuit structure used in the simulation of the multi DC-DC converter

3 SIMULATION OF THE MULTIPLE DC-DC CONVERTOR

Fig. 5 shows the circuit structure used in the simulation for the multi DC-DC converter. The multi DC-DC converter has 5 IGBT switches. These switches are operated in 4 different time zones with 4 parts of PWMs that are shown in the Fig. 6. $L_1 = L_2 = 10$ mH, $C_1 = C_2 = 10$ mF, $R = 5$ Ohm. The switching time is 0.01 s.

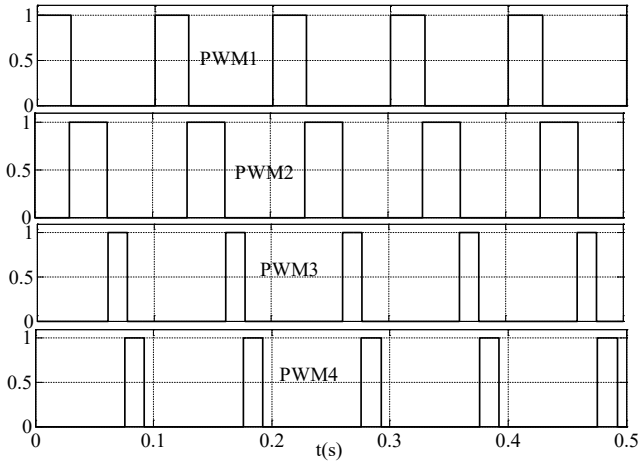

Figure 6 PWMs for the multi DC-DC converter at the simulation

When the proposed circuit is operated in the Matlab Simulink, the current occurring in the L_1 and L_2 inductors for 4 different time periods is as shown in Fig. 7.

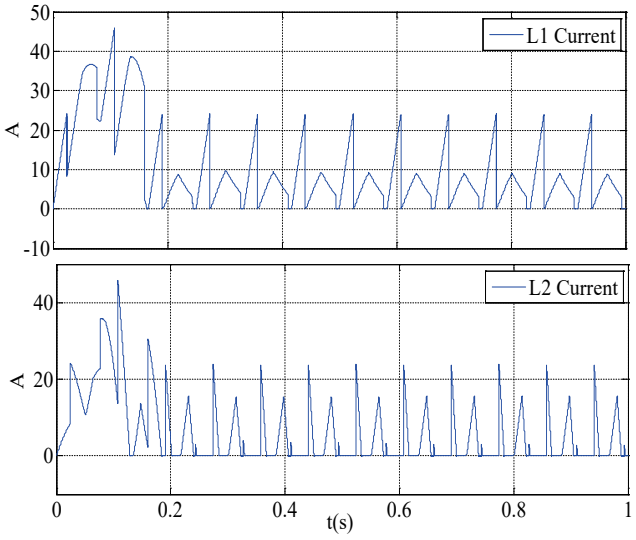

Figure 7 The current occurring in the L_1 and L_2 inductors for 4 different time periods

As seen in Fig. 7, the DC-DC converter structure provides two times the current storage on the coils in order to achieve a higher output voltage than the conventional converters. Current variations are provided in line with the working times of the PWMs on the inductors. The output voltages of conventional converters and multiple converters are shown in Fig. 8 for equal loads.

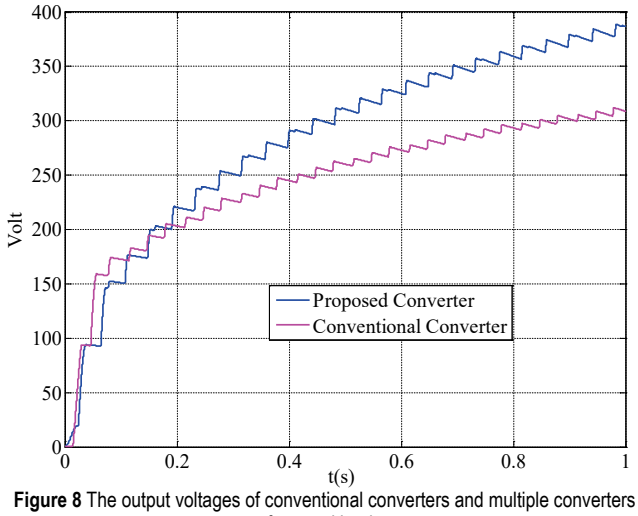

Figure 8 The output voltages of conventional converters and multiple converters for equal loads

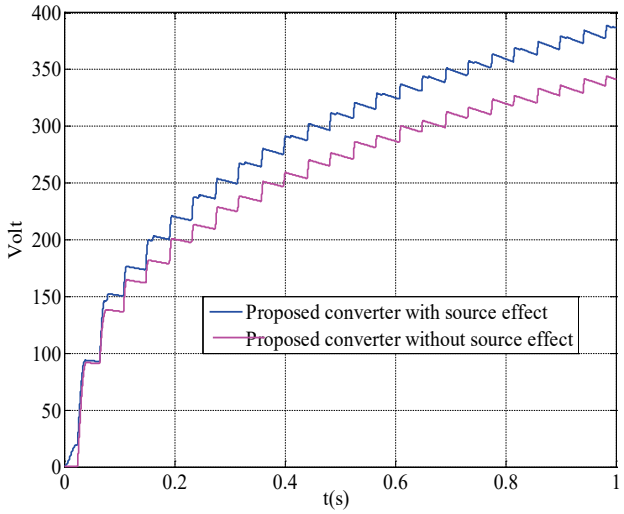

Figure 9 The effect of using the source twice on the output voltages

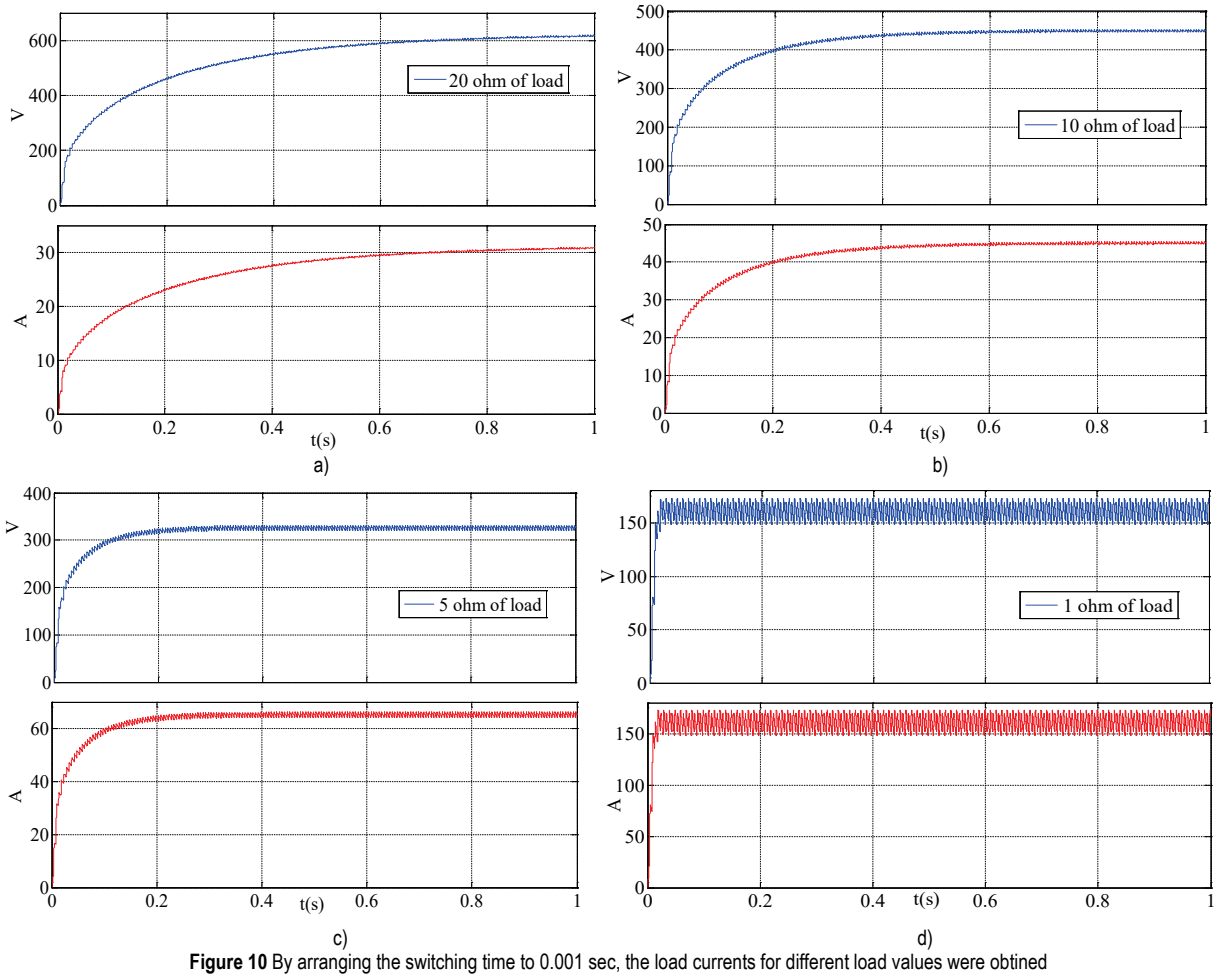

Figure 10 By arranging the switching time to 0.001 sec, the load currents for different load values were obtined

The conventional converter with an input voltage of 50 volts reaches 310 volts at the output voltage, while the multi-DC-DC converter with an input voltage of 50 volts reaches an output voltage of 380 volts. Therefore, the proposed converter structure with a single microcontroller is possible to obtain more output voltage than the conventional converter structure. Another advantage of the multiple DC-DC converter structure is that it uses a single input voltage source in the first stage, and it is used as the input source in the second multiplexing stage. Therefore, it contributes to a high output voltage. The output voltages, which show the effect of using this source twice, are given in Fig. 9.

In the circuit structure, when the input voltage source is used in the first cycle, the output voltage is 380 V. The output

voltage remains at 340 V when the source is not activated while multiplexing for the second time.

In this study, PWMs in the first cycle have 2 times of the periods according to the second cycle. Therefore, the increases on the output voltage are also percentages. According to a result of the circuit structure operation and results, it provides superiority to conventional converters. Compared to the cascade and the new generation of DC-DC converters, it has less circuit elements and less cost while the proposed converter has a different working order and hardware than them [18-20]. At the same time, it offers a new method of working for a different circuit structure and mathematical models.

By arranging the switching time to 0.001 sec, the switching frequency is increased and the load currents and voltages are shown in Fig. 10 for different load values.

For the simulations from 1ohm of load to 20 ohm of load, the L_1 and L_2 are replaced with 0.1mH in the converter circuit, while C_1 and C_2 are changed to 30 mF. When the circuit is operated for the 20 ohm load, the voltage on the load reaches 600 V and the current value is 30 A. While the circuit is operated for the 10 ohm load, the voltage on the load reaches 450 V and the current value is 45 A. At the 10 ohm load, according to the 20 ohm load, the current value is an increase of 15A, while a decrease of 150 V occurs. While the circuit is operated for the 5 ohm load, the voltage on the load reaches 340 V and the current value is 68 A. At the 5 ohm load, according to the 10 ohm load, the current value is an increase of 23 A, while a decrease of 110 V occurs. When the circuit is operating at the 1 ohm of load, the current and voltage values are 150 A, and 150 V. According to these results, the proposed circuit provides different current and voltage values for different loads.

4 CONCLUSION

This article described the structure of the multi DC-DC converter. The circuit structure of the converter, which has a more advanced structure than the conventional DC-DC converter structure, has been described and simulation studies have been made for this circuit structure. The results obtained from the proposed circuit were compared with the results obtained from the conventional DC-DC converter. While the 50-volt of the dc input voltage was increased to 310 V with the conventional DC-DC converter, the input voltage was increased to 380 volts with the proposed circuit. This was achieved through the current storage by operating in different time segments of two different inductors on the same circuit structure. Additionally, the circuit was operated for different loads using different switching times. When the circuit was operated for the 20 ohm of load, the voltage on the load reached 600 V and the current value was 30 A. While the circuit was operated for the 10 ohm of load, the voltage on the load reached 450 V and the current value was 45 A. At the 10 ohm of load, according to the 20 ohm of load, the current value faced an increase of 15A, while a decrease of 150V occurred. While the circuit was operated for the 5 ohm of load, the voltage on the load reached 340 V and the current value was 68 A. At the 5 ohm of load, according to the 10 ohm of load, the current value faced an increase of 23A while there was a decrease of 110V at the load. When the circuit was operating at the 1 ohm of load, the current and voltage values were 150 A, and 150 V. Thus, the DC-DC converter structure with superior new hardware and a mathematical model has been successfully implemented.

5 REFERENCES

[1] Sanghavi, B. M., Tejaswini, C., & Venkateshappa, V. (2019). DC/DC boost converter using DSP controller for fuel cell. *Perspectives in Communication, Embedded-systems and Signal-processing-PiCES*, *2*(10), 248-251.

[2] Duan, C. & Wu, D. (2019). Nonlinear Voltage Regulation Algorithm for DC-DC Boost Converter with Finite-Time Convergence. *Journal of Control Science and Engineering*. https://doi.org/10.1155/2019/6761784

[3] Suryadevara, R. & Parsa, L. (2019). Full-Bridge ZCS-Converter-Based High-Gain Modular DC-DC Converter for PV Integration with Medium-Voltage DC Grids. *IEEE Transactions on Energy Conversion*, *34*(1), 302-312. https://doi.org/10.1109/TEC.2018.2878964

[4] Chandrasekar, B., Nallaperumal, C., & Dash, S. S. (2019). A Nonisolated Three-Port DC–DC Converter with Continuous Input and Output Currents Based on CUK Topology for PV/Fuel Cell Applications. *Electronics*, *8*(2), 214. https://doi.org/10.3390/electronics8020214

[5] Venkatesan, C., Manickam, C., Reddy, M. J. B., Ganesan, S. I., & Chilakapati, N. (2019). Enhanced Power Output from the PV with Low Input Ripple DC-DC Converter. *Electric Power Components and Systems*, 1-12. https://doi.org/10.1080/15325008.2018.1466214

[6] Liu, J., Zheng, Z., Wang, K., & Li, Y. D. (2019). Comparison of boost and LLC converter and active clamp isolated full-bridge boost converter for photovoltaic DC system. *The Journal of Engineering*, *2019*(16), 3007-3011. https://doi.org/10.1049/joe.2018.8507

[7] Deaecto, G. S., Geromel, J. C., Garcia, F., & Pomilio, J. (2010). Switched affine systems control design with application to DC–DC converters. I*ET Control Theory & Applications, 4*(7), 1201-1210. https://doi.org/10.1049/iet-cta.2009.0246

[8] Albea-Sanchez, C., Garcia, G., & Zaccarian, L. (2015). Hybrid dynamic modeling and control of switched affine systems: application to DC– DC converters. T*he 54th Annual Conference on Decision and Control*. IEEE, 2264-2269. https://doi.org/10.1109/CDC.2015.7402544

[9] Sferlazza, A., Martínez-Salamero, L., Sanchez, C. A., Garcia, G., & Alonso, C. (2019). Min-Type Control Strategy of a DC-DC Synchronous Boost Converter. *IEEE Transactions on Industrial Electronics*.

[10] So, W. C., Tse, C. K., & Lee, Y. S. (1996). Development of a fuzzy logic controller for DC/DC converters: design, computer simulation, and experimental evaluation. *IEEE transactions on power electronics*, *11*(1), 24-32. https://doi.org/10.1109/63.484413

[11] Can, E. & Sayan, H. H. (2017). The performance of the DC motor by the PID controlling PWM DC-DC boost converter. *Tehnički glasnik*, *11*(4), 182-187.

[12] Can, E. & Sayan, H.H. (2016). SSPWM three phase inverter design and experimented on unbalanced loads. *Tehnički vjesnik, 23*(5), 1239-1244. https://doi.org/10.17559/TV-20150730222021

[13] Sanjeevikumar, P. & Rajambal, K. (2008). Extra-high-voltage DC-DC boost converters topology with simple control strategy. *Modelling and Simulation in Engineering*, 6. https://doi.org/10.1155/2008/593042
[14] Majeed, Y. E., Ahmad, I., & Habibi, D. (2019). A Multiple-Input Cascaded DC–DC Converter for Very Small Wind Turbines. *IEEE Transactions on Industrial Electronics*, *66*(6), 4414-4423. https://doi.org/10.1109/TIE.2018.2863214
[15] Hu, X., Ma, P., Wang, J., Tan, G., & Yao, Z. (2019). A Hybrid Cascaded DC-DC Boost Converter with Ripple Reduction and Large Conversion Ratio. *IEEE Journal of Emerging and Selected Topics in Power Electronics*. https://doi.org/10.1109/JESTPE.2019.2895673
[16] Yu, J., Liu, M., Song, D., Yang, J., & Su, M. (2019). A Soft-Switching Control for Cascaded Buck-Boost Converters without Zero-Crossing Detection. *IEEE Access*, *7*, 32522-32536. https://doi.org/10.1109/ACCESS.2019.2903841
[17] Can, E. (2019). The Design and Experimentation of the New Cascaded Dc-Dc Boost Converter for Renewable Energy. *International Journal of Electronics*, 106(9), 1374-1393. https://doi.org/ 10.1080/00207217.2019.1591529
[18] Lee, S. W. & Do, H. L. (2019). Quadratic Boost DC–DC Converter with High Voltage Gain and Reduced Voltage Stresses. *IEEE Transactions on Power Electronics*, *34*(3), 2397-2404. https://doi.org/10.1109/TPEL.2018.2842051
[19] Uno, M. & Shinohara, T. (2019). Module-Integrated Converter Based on Cascaded Quasi-Z-Source Inverter with Differential Power Processing Capability for Photovoltaic Panels Under Partial Shading. *IEEE Transactions on Power Electronics*. https://doi.org/10.1109/TPEL.2019.2906259
[20] Uno, M. & Shinohara, T. (2019). Module-Integrated Converter Based on Cascaded Quasi-Z-Source Inverter with Differential Power Processing Capability for Photovoltaic Panels Under Partial Shading. *IEEE Transactions on Power Electronics*. https://doi.org/10.1109/TPEL.2019.2906259

Author's contacts:

Dr. **Erol CAN**, Assistant Professor
School of Civil Aviation, Erzincan University,
Aviation Electrical Electronics, 24100 Erzincan, Turkey
E-mail: can_e@hotmail.com

ISSN 1846-6168 (Print), ISSN 1848-5588 (Online)
https://doi.org/10.31803/tg-20180717222848

Preliminary communication

INFORMATION SECURITY: THREAT FROM EMPLOYEES

Aleksandar ERCEG

Abstract: Information security inside the organization is becoming a major issue in the modern and global world. Information accessibility and security are a major issue where user behaviour plays an important role. Information security user behaviour is becoming an increasing threat to their organization information security. Since the organization is investing in and implementing information security systems, the issue of employees' behaviour has become increasingly important. This paper aims to show how workers treat information security and is looking upon so called "people problem". In the research, the personal behaviour of health care professionals and workers in a Croatian production company in relation to information security was tested. Results have shown that the overall behaviour of respondents in production company is more responsible and security awareness with proper use of passwords is associated with knowledge about the importance of security application in their work. Further research is recommended.

Keywords: business data; healthcare; information security; passwords; production company; security risk

1 INTRODUCTION

Information security involves people and technology. Up to 90% of companies and organizations encounter at least one information security incident during the business year [1]. In the last several years, there has been a significantly rising concern about information security and behaviour of people which is simply described by Schneier [2, p. 256] who stated to "tell prospective clients that the mathematics are impeccable, the computers are evincible, the networks are lousy, and the people are abysmal. I have learned a lot about the problems of securing computers and networks, but none that really helps solve the people problem."

Stanton et. al. [3] stated that although organizations tend to be concerned about external threats, the recent situation is showing that a substantial part of incidents is coming from inside of the organization. Today many believe that promotion of end user good behaviour is important to model for effective information security policies inside organizations. End user and their information security related behaviour can influence a total information security and therefore they can be of great benefit for managers, information technologists and others connected to assessing and/or influencing end user behaviour.

In this paper, the so called "people problem" will be examined and how employees threat potential information risks by sharing their passwords, making backups, etc., and how this can influence organization information security. The paper is divided into several parts. In the first part, the literature overview is given. In the second, the methodology is presented followed by data analysis and a discussion section where findings are shown. The last part contains the brief conclusion of the paper and implications for further research are provided.

2 INFORMATION SECURITY

Information is the most valuable asset an organization (private, public, government, nongovernment) can have. Therefore, it is of utmost importance to develop a combination of systems, operation and internal procedures for ensuring the integrity and secrecy of data and operational procedures in the organization [4]. Benefits of computerization are numerous both in health and in the business sector. The development of communication networks in the global communications area has destroyed all classic protection systems of information and communication, ranging from the protection system from the so-called "viruses" to unauthorized access to information. Information security is influenced by the environment in which information is exchanged and communicated. The rapid development of information and communication technology has further increased the complexity of the security environment over the past two decades [5]. Information security represents the protection of information systems and information from potential unauthorized access, use, disclosure, disruption, modification, perusal, inspection, recording or destruction. Thus, the information security becomes part of our lives. Information security is influenced by the people who use them and the same technologies that enable these processes in accordance with which it takes place. The increasing influence of thinking about information security policies indicates the width and complexity of the content that is being covered. Information security can be defined as a state of condition of confidentiality, integrity, and availability of data, which is achieved by applying certain standards and measures, and organizational support for business planning, implementation, verification, and updating of standards and measures [6]. The aim of information security activities is the detection and prevention of non-authorized information technology user activities [7]. Chang and Lin [8, p. 7] stated that information security is a social and organizational problem since technical systems must be operated and used by people.

Information and communication technologies users can significantly affect the information system security [9] and are still considered the weakest link of information security [8], [10]. A significant influence on the development of information security policies has additional factors that so far have not been considered, such as the structure of the

organization and its culture [5]. Kaushal and Khan [10] proposed an information security life cycle. (Fig. 1)

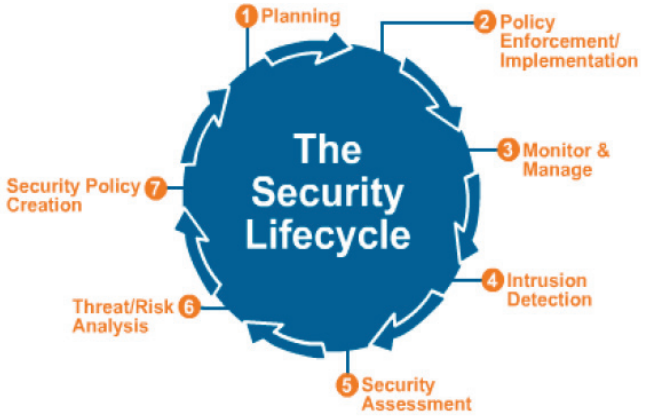

Figure 1 Information security life cycle [10, p. 123]

The previous figure presents information security life cycle with several important phases and it is necessary for successful management of information security programs. Every step shows the importance of the approach to information security. It is of utmost significance for the organization to recognize that this process is never-ending, and that organization needs to improve its behaviour during every cycle.

Information security is needed because the technology applied to information creates risks. In cases when information security risk is recognized and is stable, it is necessary to create a policy for information security. These policies can be divided into four categories: protection measures, detection measures, consequences response measures and measures to ensure the effectiveness of the consequences response.

3 LITERATURE OVERVIEW

In the previous ten years, research in the field of security technology has been increased. Most of these studies were focused on the impact of human factors and questions the usefulness of security mechanisms in information and communication technologies. Previous studies [11], [12] investigated the impact of human behaviour on information security in companies. Their results, among other things, pointed out the everyday behaviour of employees in relation to the use of information and communication technologies and the possibility of preventive behaviours to avoid problems. Research conducted in Germany [13] indicated that security measures whose aim is information security are necessary. These measures should be designed to address the key risks and their consequences. While organizations today rely significantly on information technology and information security is of increasing attention, today there are only a few strategies for information security practitioners [4].

Due to the increasing need for data protection that is mostly present and developed in the banking and financial sector, management of companies is increasingly considering information security management as their direct responsibility and that because of information security ignorance significant personal, financial and legal responsibility can occur. It is important to state that Gaunt [14] proposed information security awareness programs for improving information security behaviour in healthcare contexts. For this reason, we should not neglect the role of the user that can affect the level of system security with its risk behaviour [9] – according to statistical data it is proved that most of the security breaches in business organizations are caused unintentionally [15]. Therefore, the information security and its management have become an important business responsibility of the top-level company's management boards [16]. Almost 75% of big corporations have suffered security breaches because of staff related activities and 50% of the worst breaches were caused by human error [17]. Those security breaches were the result of unwitting security compromises.

The most common form of business communication is e-mail, with the recommendation of using a business address that is controlled by the institution and where all security requirements are met. According to Cyber security survey in 2017, more than 70% of security breaches were the result of staff receiving the fraudulent e-mail. The survey revealed that only 20% of staff attended information security training [18].

In addition to the e-mail communication security, it is necessary to reduce medical data security vulnerabilities, which may have a negative impact on health care data protection [19]. Research about the role of users related to information security is still rare, while previous studies usually focus on the password as the first line of defence in most information systems. Studies have shown that despite the recommendations on the password selection, users still tend to select those passwords that are simple and easy to remember or those concerning their personal data [20]. Despite the training, users still have the habit to share their passwords with their colleagues, write them in a visible place, or do not change them for a long time, which confirms that the user behaviour is a very common problem in the field of security and that education is still necessary [21]. Different techniques for estimation of user's risk behaviour have been developed, and one of the latest is the algorithm for evidential reasoning that is used to assess and compare the status of multiple systems [9].

But it seems that the awareness among users about the importance of the health care system (which in Croatia is the public service) may be worse in relation to the average user in the business sector. Although financial damage can be large-scale, security incidents with data from the electronic health record can cause long-term much higher, even material, damage to the individual person. Similar previous research on the awareness of ICT users in terms of safety and their behaviour are very scared and particularly on the issue of health care professionals.

Several researchers started with the development of different concepts and theories relevant to the influence of user behaviour to organization information security. Among them, Stanton et al. [3] in their research catalogued and

analysed a range of end user security behaviour in organizations (Fig. 2).

Expertise	Intentions	Title	Description
High	Malicious	Intentional destruction	Behavior requires technical expertise together with a strong intention to do harm to the organization's IT and resources. Example: employee breaks into an employer's protected files in order to steal a trade secret.2
Low	Malicious	Detrimental misuse	Behavior requires minimal technical expertise but nonetheless includes intention to do harm through annoyance, harassment, rule breaking, etc. Example: using company email for SPAM messages marketing a sideline business.
High	Neutral	Dangerous tinkering	Behavior requires technical expertise but no clear intention to do harm to the organization's IT and resources. Example: employee configures a wireless gateway that inadvertently allows wireless access to the company's network by people in passing cars.
Low	Neutral	Naïve mistakes	Behavior requires minimal technical expertise and no clear intention to do harm to the organization's information technology and resources. Example: choosing a bad password such as "password."
High	Beneficial	Aware assurance	Behavior requires technical expertise together with a strong intention to do good by preserving and protecting the organization's information technology and resources. Example: recognizing the presence of a backdoor program through careful observation of own PC.
Low	Beneficial	Basic hygiene	Behavior requires no technical expertise but includes clear intention to preserve and protect the organization's IT and resources. Example: a trained and aware employee resists an attempt at social engineering by refusing to reveal her password to a caller claiming to be from computer services.

Figure 2 Two factors taxonomy of security behaviour [21, p. 126]

The previous figure shows categories of possible user security behaviour in organizations that are arranged in two dimensions. This taxonomy can help with tasks in examining and controlling user information security behaviour in organizations. Siponen et al. [22] in their research confirm that major threats to information security are careless employees and they not only have to be aware of information security policies and procedures but also must comply with them. To influence information security related behaviour top management and information security staff should clearly state the importance of complying with organization information security policy. Ajzen [23] found that the intention to comply with information security policies can significantly impact behaviour; the stronger an intention to engage in behaviour is, it is more likely to be performed.

4 MATERIAL AND METHODS

The aim of this research was to determine whether there were differences in user information security behaviour among health care workers and workers in the private company situated in the same Croatian town.

The research was conducted by a certified survey of risk behaviour - Users' Information Security Awareness Questionnaire (UISAQ) which measures the level of information system's users' awareness on security matters, as general as possible. The UISAQ questionnaire has two main scales and six subscales: Potentially Risky Behaviour, Usual Behaviour, Personal Computer Maintenance, Borrowing Accessing Data, Knowledge and Awareness, Security in Communications, Secured Data, Backup Quality. These subscales describe user's behaviour, knowledge, and awareness [24].

UISAQ allows IT professionals' better analyses of information systems users and it helps them in identifying issues with the low security level. On the other side, UISAQ can help researchers in the better categorization of users in relation to their security awareness. This tool can be helpful in gaining a conclusion about user's risky behaviour, making correlations with security awareness level and potential identification of unsecure users.

A survey in this paper was used to determine user impact on the overall system security in hospital and in private company. The study was conducted on 152 respondents, of whom 88 (57.9%) were health care professionals (nurses/technicians, physicians) employed in Healthcare institution (hospital respondents) and 64 (42.1%) of respondents were employed in a Croatian production company (private company respondents).

5 RESULTS AND DISCUSSION

The average age of respondents working in hospital was 40 (IQR 30 – 48) years, without significant differences in relation to respondents from production company whose average age iwass 43 years (37 – 47). Women are more represented in the hospital (Fisher's exact test, $p = 0.003$), and there are significantly more employees with university degrees employed in production company (χ^2 test, $p < 0.001$). According to the educational program a total of 66 (43.7%) respondents completed graduate study, more are non-hospital employees (Fisher's exact test, $p < 0.001$). Although in both institutions in a time of employment, employees, when given username and password, signed the rules they need to comply, only 82 (55%) of respondents recalled having signed the document, significantly more from production company (Fisher's exact test, $p < 0.001$). When asked to write their password for analyses and assessment of the password quality, as many as 79 (52%) respondents wrote theirs, significantly more from production company (Fisher exact test, $p < 0{,}001$). Although production company employees have written their "passwords", it was impossible to check if the passwords were true. (Tab. 1)

Table 1 Groups scale mean scores

	Number of respondents (5)			p*
	Hospital	Private company	Total	
Gender				
Men	22.7	46.9	32.9	0.003
Women	77.3	53.1	67.1	
Education level				
High School	39.8	15.9	29.8	<0.001
College	28.4	11.1	21.2	
University	31.8	73	49	
Working place				
Higher management	0	3.1	1.3	0.222
Middle management	25.3	28.1	26.5	
Employee	74.7	68.8	72.2	
Educational program				
High school	39.8	15.9	29.8	<0.001
Professional study	18.2	9.5	14.6	
Undergraduate study	9.1	0	5.3	
Graduate study	27.3	66.7	43.7	
Post-graduate study	5.7	7.9	6.6	
Signed the rules for using the institution information system	40.5	75	55.4	<0.001
On the survey typed their password	38.6	70.3	52	<0.001

Respondent's behaviour was rated over 17 questions in three areas: lending, behaviour, and confidence. Sometimes 15 (9.9%) respondents lend official access data (username and password) to fellow work colleagues, who find themselves in need. Different passwords for different systems are always used by 35 (23.3%) respondents (i.e. for Facebook one, for e-mail another, for business system third password, etc.), 48 of respondents (32%) never used more than one e-mail address (i.e. private and official e-mail), and 97 (63.8%) never locked business computer during brief departure from the office, classroom, working place. 90 (59.6%) respondents never install various programs of unknown and less known manufacturers, which may be interesting but not necessary for work (i.e. different video players, multimedia accessories, web browsers). On social networks, 25 (16.4%) of respondents rarely leave personal information (i.e. private address, cell phone number, the message that they are on holiday, etc.). (Fig. 3)

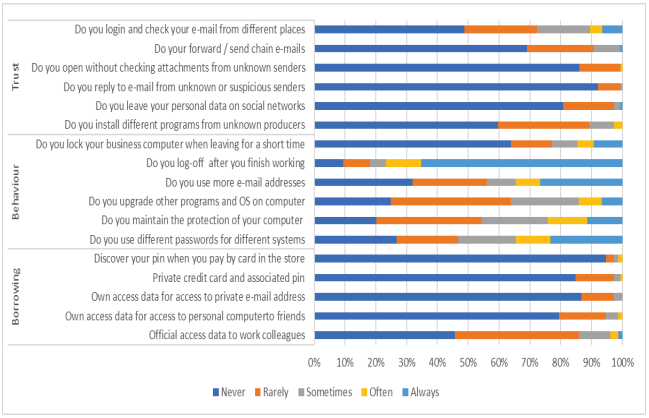

Figure 3 Respondents according to the behaviour scale

Communication over social networks is considered as totally insecure by 47 (30.9%) respondents, and 64 (42.1%) respondents stated mobile phone communication as quite insecure (talking and SMS). Correspondence over e-mail is considered quite insecure by 43 (28.3%) respondents. (Fig. 4)

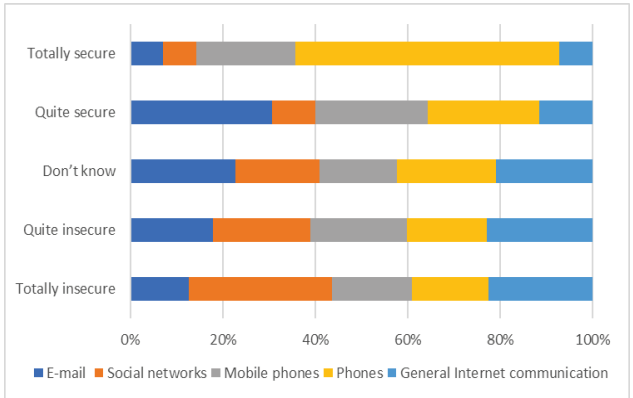

Figure 4 The distribution of answers according to the security level

According to the belief level, most respondents 59 (39.3%) are not convinced that someone will take money from their bank account, while 19 (12.6%) are convinced that someone will steal their identity on the internet (e-mail, e-banking, Facebook, etc.). (Fig. 5)

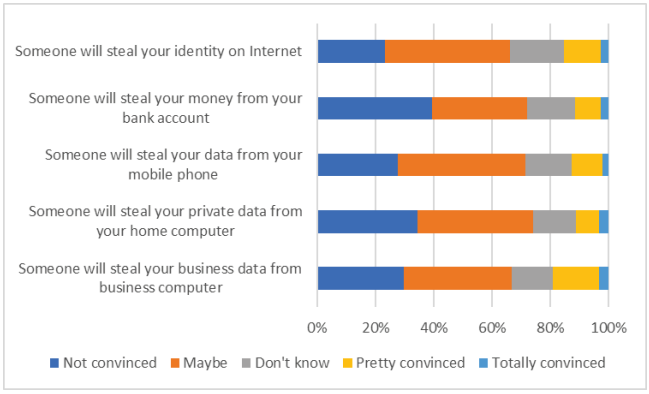

Figure 5 The distribution of answers according to the belief level

Unconditionally maintenance of their passwords is totally unimportant for 13 (8.6%) respondents and extremely important 66 (43.7%) respondents. Periodical replacement of their passwords with new ones, at least for important systems is quite important for 73 (48.3%) respondents, and 72 (47.7%) respondents stated that is extremely important to separate business from private computing resources (i.e. USB memory, e-mail, phone). (Fig. 6)

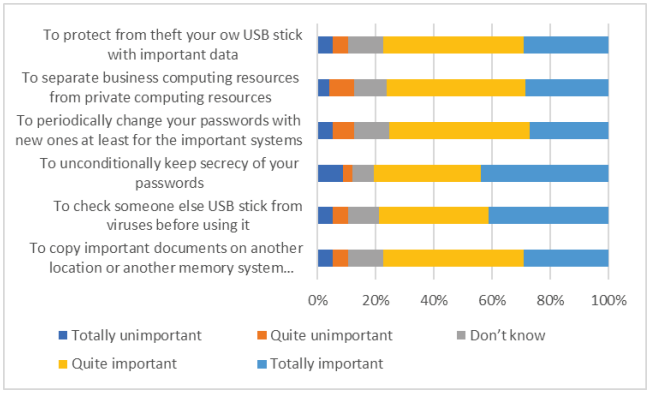

Figure 6 The distribution of answers according to the importance level

Behaviour scale means score 2 (interquartile range 1.8 – 2.2) is significantly worse with hospital respondents (Mann Whitney test, $p = 0.038$). Significant are differences in behaviour subscale where respondents from production company are acting as more responsible (Mann Whitney test, $p = 0.011$), with scale mean score 3 (interquartile range 2.3 – 3.6). With security and importance scale there is no significant difference between the mean scale score between the two groups. Belief scale mean score of 4 (3.3 – 4.4), is significantly higher with production company employees (Mann Whitney test, $p = 0.027$). (Tab. 2)

Personal data security has been determined by the time when the last backups of personal data and documents have been made and with the number of persons that know the respondent's password. Out of survey respondents, 28 of them (18.55%), of which 10 (11.5%) from hospital and 18 (28.1%) from production company, never made a backup of their documents. 30 (20%) participants stated that besides

them two more people knew their password, of whom significantly more, 17 (26.6%), from the production company. 26 (30.2%) participants from hospital stated that they were the only ones who knew their password, which is significantly less in relation to the participants from production company (Fisher exact test, $p = 0.020$). While comparing personal data security with those respondents who wrote their password in the survey there is significantly more respondents from production company – 20 (44.4%) and at the same time, they stated that they were the only ones that knew their password (Fisher exact test, $p = 0.046$). (Tab. 3)

Table 2 Groups scale mean scores

Mean rating	Median (interquartile range)			p*
	Hospital respondents	Private company	Total	
Behaviour scale	2.2	2.0	2.0	0.038
Borrowing	1.2.	1.2	1.2	0.988
Behaviour	3.3	3	3.2	0.011
Trust	1.2	1.3	1.3	0.078
Security scale	2.2	2.4	2.2	0.393
Belief scale	4	4.2	4	0.027
Importance scale	1.8	1.8	1.8	0.811

Table 3 Respondents according to answers about data security and groups

Personal data security	Number of respondents (%)			p*
	Hospital respondents	Company respondents	Total	
When was the last time the backup of personal data and documents made?				
Never	11,5	28.1	18.5	0.053
Don't' remember	43.7	32.8	39.1	
During last six months	23	26.6	24.5	
During last month	17.2	7.8	13.2	
Last week	4.6	4.7	4.6	
How many people know respondent's password for accessing e-mail system?				
More than 10	8.1	0	4.7	0.020
From 5 to 10	7	7.8	7.3	
Me and two more	15.1	26.6	20	
Me and one more	39.5	25	33.3	
Only me	30.2	40.6	34.7	
When did you make a backup of personal files and documents last time?				
Never	5.9	28.9	19	0.058
Don't remember	44.1	24.4	32.9	
During the last six months	29.4	33.3	31.6	
During last month	14.7	8.9	11.4	
Last week	5.9	4.4	5.1	
How many people know the password for accessing your own e-mail?				
More than 10	2.9	0	1.3	0.046
From 5 to 10	0	8.9	5.1	
Me and two more	20.6	26.7	24.1	
Me and one more	44.1	20	30.4	
Only me	32.4	44.4	39.2	

Through the research, it has been shown that the overall behaviour of respondents in production company ($p = 0.011$) is more responsible, which confirms previous research on the use of e-mail addresses according to which the respondents from technical scientific fields use more secure official e-mail addresses, as opposed to biomedical researchers. Different passwords for different systems are used by 23.3% of respondents, which is slightly less than it was found in research on 836 subjects [25], of whom 31% always use different passwords. The introduction of "single sign-on" (SSO) i.e. single logging into the system, which institutions began to implement [26], would reduce the burden on employees about remembering multiple passwords. Analyses [27] showed that the awareness of users toward to the information system security and proper use of passwords is associated with knowledge about the importance of security application in their work. The ratio of respondents to the question of personal data security proved to be very weak - 18.5% of respondents had never made a backup of their data, and 39.1% could not remember when they had done it the last time, where the distribution frequency of making backups among medical and electrical engineering students is very low.

Among all respondents, 28, of whom 10 (12%) are from the hospital and 18 (28%) are from the production company, have never made a copy of their documents. To question about password sharing, 30 (20%) respondents stated that two more people knew their password, of which significantly more, 17 (27%) from production company, while 26 (30%) of hospital respondents stated that they didn't share their password, which is significantly less than those not working in hospital (Fisher's exact test, $p = 0.020$). Comparing the security of personal data from those respondents who wrote their password in questionnaire there are significantly more respondents from production company - 20 of them (44%), while at the same time they claim that they are the only one which knows their password (Fisher's exact test, $p = 0.046$).

5 FINAL REMARKS AND CONCLUSION

Most research agrees that almost highest threat to an organization's information security comes from employees who do not follow set information security procedures. Employees must be aware of and follow information policies and procedures. Entire company (hospital, government, private) plays important role in presenting policies and procedures for user information security behaviour. Education of employees should be a major task in today's information era where everything is available to everyone; also, information must be treated as secure as possible when it is necessary.

Although user information security behaviour in different industrial sectors was compared in the research, there are similarities in the user behaviour. In both examined companies there are users that care about information security but also many of them do not think that information security is important for a company's efficiency. Research results have shown that employees in a private company behave better in relation to information security. They are more responsible and security aware regarding password usage and have better knowledge about the importance of security application in their work.

To conclude, it is appropriate to propose further research on information security behaviour and to check relation between different production companies in Croatia and their approach in solving so called "people problem" in dealing with information security since it was found in research that although employees signed a statement about information

security, not many of them remembered it and some of them did not comply with it.

6 REFERENCES

[1] Bagchi, K. &, Udo, G. (2003). An analysis of the growth of computer and Internet security breaches. *Communications of AIS*, 2, 684-700. https://doi.org/10.17705/1CAIS.01246

[2] Schneier, B. (2000). *Secrets and Lies: Digital Security in a Networked World*. New York: John Wiley & Sons, Inc.

[3] Stanton, J. M., Stam, K. R., Mastrangelo, P., & Jolton, J. (2005). Analysis of end user security behaviours. *Computers & Security, 24*(2), 124-133. https://doi.org/10.1016/j.cose.2004.07.001

[4] Hon, K., Chi, Y., Chao, L. P., & Tang, J. (2003). An integrated system theory of information security management. *Information Management and Computer Security, 11*(5), 243-248. https://doi.org/10.1108/09685220310500153

[5] http://www.fer.unizg.hr/download/repository/KvalifikacijskiDrIspit_AK_08022010.pdf (Accessed on April 2018)

[6] Narodne novine. (2007). Zakon o tajnosti podataka i informacijskoj sigurnosti (in Croatian).

[7] Gollmann, D. (1999). *Computer Security*, New York: John Wiley & Sons.

[8] Chang, S. E. & Lin, C. S. (2007). Exploring organizational culture for information security management. *Industrial Management & Data Systems, 107*(3), 438-458. https://doi.org/10.1108/02635570710734316

[9] Šolić, K., Jović, F., & Blažević, D. (2013). An Approach to The Assessment of Potentially Risky Behaviour of ICT System's Users, *Technical Gazette*, 20(2), 335-342.

[10] Kaushal, P. & Khan, R. (2018). A Review on Information Security. *International Journal of Advanced Research in Computer Science and Software Engineering, 8*(4), 122-124. https://doi.org/10.23956/ijarcsse.v8i4.646

[11] Bisset, J. K. & Shipton, G. (2000). Some Human Dimensions of computer virus creation and infection. *International Journal of Human-Computer Studies, 52*(5), 899-913. https://doi.org/10.1006/ijhc.1999.0361

[12] Marioani, M. G. & Zappala, S. (2014). PC Virus attacks in small firms: Effects of risks perceptions and information technology competence on preventive behaviours. *TPM, 21*(1), 51-65.

[13] https://www.dcsec.uni-hannover.de/uploads/tx_tkpublikationen/risk-survey-csf.pdf (Accessed on April 2018)

[14] Gaunt, N. (1998). Installing an appropriate information security policy in hospitals. *International Journal of Medical Informatics, 49*(1), 131-134. https://doi.org/10.1016/S1386-5056(98)00022-7

[15] https://www.bsi.bund.de/SharedDocs/Downloads/EN/BSI/Grundschutz/guidelines/IT-sec-guidelines_pdf.pdf?__blob=publicationFile (Accessed on March 2018)

[16] Von Solms, B. & Von Solms, R. (2005). From information to... business security? *Computer & Security, 24*(4), 271-273. https://doi.org/10.1016/j.cose.2005.04.004

[17] https://www.pwc.co.uk/assets/pdf/2015-isbs-technical-report-blue-03.pdf, (Accessed May 2018)

[18] https://assets.publishing.service.gov.uk/government/up-loads/system/uploads/attachment_data/file/609186/Cyber_Security_Breaches_Survey_2017_main_report_PUBLIC.pdf (Accessed May 2018)

[19] Dantu, R., Oosterwijk, H., Kolan, P., & Husna, H. (2007). Securing medical networks. *Network Security, 2007*(6), 13-16. https://doi.org/10.1016/S1353-4858(07)70055-7

[20] Taneski, V., Heričko, M., & Brumen, B. (2014). Password security – no change in 35 years? *Proceedings of 37th International Convention Information and Communication Technology, Electronics and Microelectronics*, Opatija, 1360-1365. https://doi.org/10.1109/MIPRO.2014.6859779

[21] Sedinić, I., Lovrić, Z., & Perušić, T. (2014). Costumer and User education as a tool to increase security level. *Proceedings of 37th International Convention Information and Communication Technology, Electronics and Microelectronics* Opatija, 1441-1445. https://doi.org/10.1109/MIPRO.2014.6859793

[22] Siponen, M., Pahnila, S. & Mahmood, A. (2014). Employees' Adherence to Information Security Policies: An Empirical Study. *Information & Management, 51*(2), 217-22. https://doi.org/10.1016/j.im.2013.08.006

[23] Ajzen, I. (1991). The Theory of Planned Behaviour. *Organizational Behaviour and Human Decision Processes, 50*(2), 179-211. https://doi.org/10.1016/0749-5978(91)90020-T

[24] Šolić, K., Velki, T., & Galba, T. (2015) Empirical study on ICT system's users' risky behaviour and security awareness. *Proceedings of 38th International Convention Information and Communication Technology, Electronics and Microelectronics*, Opatija, 1623-1626. https://doi.org/10.1109/MIPRO.2015.7160485

[25] Hoonakker, P., Bornoe, N., & Carayon, P. (2009). Password Authentication from a Human Factors Perspective: Results of a Survey among End-Users. *Proceedings of the Human Factors and Ergonomics Society Annual Meeting*, San Antonio, 53(6), 459-463. https://doi.org/10.1177/154193120905300605

[26] Sasse, M. A., Brostoffand, S., & Weirich, D. (2001). Transforming the 'weakest link' - a human/computer interaction approach to usable and effective security. *BT Technology Journal*, 19, 122-131. https://doi.org/10.1023/A:1011902718709

[27] Duggan, G. B., Johnson, H., & Grawemeyer, B. (2012). Rational Security: Modelling Everyday Password Use. *International Journal Human Computer Studies, 70*(6), 415-431. https://doi.org/10.1016/j.ijhcs.2012.02.008

Author's contacts:

Aleksandar ERCEG, Ph.D., Assistant Professor
J. J. Strossmayer University of Osijek,
Faculty of Economics in Osijek,
Trg Ljudevita Gaja 7, 31 000 Osijek, Croatia
aleksandar.erceg@efos.hr

ISSN 1846-6168 (Print), ISSN 1848-5588 (Online)
https://doi.org/10.31803/tg-20181123111226

Preliminary communication

THE DETERMINATION OF THE THERMAL RELIABILITY CRITERION FOR BUILDING ENVELOPE STRUCTURES

Gennadiy FARENYUK

Abstract: The paper presents the basic methodical principles for the time analysis of the variations of envelope structures' thermal insulation properties and for the substantiation of the thermal reliability criterion, which should allow the analysis of the actual parameters of heat losses during the operation of buildings. In the paper, the state of the envelope structures thermal failure, the concept of building thermal envelope thermal reliability and the principles of its rating are defined. The physical meaning and basic criterion of the envelope structure thermal reliability are formulated. The application of the thermal reliability criterion allows determining the probable variations in the thermal insulation properties during the building operation and, accordingly, the changes of the building energy performance over time.

Keywords: building envelope structure; criterion; thermal reliability

1 INTRODUCTION

A modern building is a system composed of a number of subsystems that can be considered as independent systems. The system of enclosing structures, which is a thermal envelope of a building, is a determining factor in the context of defining the energy performance indicators for a building. It is necessary to develop the methodological guidelines for this system to determine reliability. The structural design of the elements of the building thermal envelope determines the structural response to external influences and the nature of the formation of the relevant operating indicators for a building.

The possible decrease of the thermal engineering indicators of the envelope structures depends on the features of the heat and mass transfer processes defined by the thermophysical properties of the materials and the structural design of the envelope, as well as on the critical states of moisture within the structure thickness causing the structural variations in materials and construction elements and, consequently, the energy state deterioration in the entire system.

The consideration of a building as an object of human activity allows singling out its two main functions, namely, the spatial and thermal ones. The spatial function of a residential building envisages the creation of a certain space where a person can form his/her private living environment fully according to his/her own free choice with a relatively minimal influence of the society. For production and civic buildings, the spatial function is to allocate a special volume for performing definite technological operations. The human body can function normally in a narrow temperature range, therefore, it is necessary to protect the human beings from adverse climatic influences and create a specific thermal and gas environment, which is the second functional task of the house. This function implementation is a rather complicated engineering task. For its solution, a building must be equipped with a variety of communications and systems, the stable operation of which directly ensures the reliable and no-failure operation of the building. In this context, the state of the building, when the performance of at least one of the above-mentioned functions is not ensured, can be considered as the failed state.

The building must meet three main criteria as follows: (1) the overall reliability, which defines the protection degree for a human being as an individual and as a social group; (2) the comfort, which sets the parameters of the thermal, acoustic, light, gas environment; (3) the cost effectiveness, which determines the costs for ensuring the first two criteria. Additionally, there are certain architectural requirements conditioned by national traditions, time trends, manufacturing capabilities, etc. All these parameters of the building are majorly determined by its thermal envelope, which is composed of a system of enclosing structures, the structural solutions of which define the building performance.

The paper's goal is to determine the basic methodological principles for the analysis of the time variations of the thermal insulation properties of the envelope structures and to justify the thermal reliability criterion in order to analyze the actual parameters of heat losses during the building's operation.

As a science, the theory of reliability arose in the 1960s-1980s and was developed in the works of many scholars, including the Ukrainian specialists [1-7]. The provisions of theoretical studies, set forth in the referenced scientific works, were taken as a basis for the development of the rating method for the reliability of the buildings' thermal envelopes [8].

For the first time, the concept of the thermal reliability of envelope structures and the failures of building thermal insulation were considered in [9]. The failure as a reliability characteristic is an event that occurs when an object loses its ability to perform the assigned function in ensuring its serviceable condition. For a building, an event of failure is considered as a state when the fulfillment of prescribed (normalized or comfortable) heat and moist conditions in the building premises is not ensured.

2 THE VARIATIONS OF ENVELOPE STRUCTURES' THERMAL INSULATION PROPERTIES

The method for rating the thermal reliability of envelope structures is based on the principle of the design boundary states' determination, when the requirement of failure-free operation, i.e., of non-excess beyond the boundary state, is established by the inequality of the following type:

$$\Omega(w,T,R,R_g,z,\tau,\varepsilon,I,J,W) = \Omega(\Theta_j) \le \frac{\Gamma_{\aleph}}{\wp_{\aleph}} \quad (1)$$

where: $\Omega(\aleph_{j=1,\dots,J})$ is the parameter's function of the considered system (an envelope structure, a thermal envelope, etc.); (Θ_j) are the design values of the system's actions and characteristics; $\Gamma_{\aleph}$ - function limit by the operating parameter Θ_j; and $\wp_{\aleph}$ - coefficient of reliability taking into account the sensitivity of a structure for its survivability under the variations of the corresponding parameter Θ_j.

In the general theory of reliability, the construction failure [1] is seen as the crossing of the permissible region random boundary by a random path that reflects the construction behavior. The envelope structure behavior is characterized by a variation of its thermal insulation properties under the influence of climatic external factors and internal heat and moisture environment. Additionally, the installation factors also determine the random boundaries of the probable thermal state of the envelope structure.

The external influences affecting the thermal envelope and determining the limits of the boundary states of the enclosing structures include the following factors:

- the variations of the external and internal air temperature and humidity;
- atmospheric influences including solar radiation, rain, snow, wind; and
- the nature of temperature variations during the cold season.

The structural solutions of the enclosing structure and the thermal envelope of the building as a whole determine the structure response to the external influences and the nature of the corresponding operational indicators formation for the studied object. The probable reduction of the thermal engineering parameters of the enclosing structures depends on the specific features of the heat and mass transfer processes, which are defined by the thermophysical properties of the materials, the structural solution of the envelope, as well as the emergence of moisture critical states in the thickness of the structure, which lead to structural changes in materials and construction elements and, consequently, to the deterioration of the energy state of the general system. This causes the need for a thorough analysis of all components that affect the indicators of thermal reliability of structures and, accordingly, the energy performance of the building.

Failure is a condition which happens when object performance is interrupted. For enclosing structures, the state of thermal failure should be detected in the presence of at least one of the following parameters:

- a drop of the local values of the inner surface temperatures up to the temperature of air vapor condensation under the design thermal conditions (Fig. 1);
- accumulation of moisture in the thickness of the structure during the annual operating cycle (Fig. 2);
- the occurrence of layers of mold or fungal formations on the inner surface of the structure or under its decorative layers (Fig. 3-5).

a)

b)

Figure 1 The condensate (a) and hoarfrost (b) formation on the surfaces of transparent structures during tests under the design temperature conditions in the climatic chamber.

Figure 2 Accumulation of moisture in the external wall of the temple building during the annual operating cycle.

In its physical essence, the thermal failure of structures, thermal envelopes or buildings as a whole relates to partial failures, that is, to the loss of the structures' ability to perform the part of their functions. In the case of a thermal envelope thermal failure, a building does not lose its characteristics of the overall reliability, including the environmental protection of the people, etc. However, in such circumstances, the above listed criteria of the building's operational suitability are not met.

The thermal failure concept is directly related to the notion of the structure boundary state and in our case, it should be considered as the state of the building thermal envelope, in which further building operation is associated with the violations of normal human life conditions, increased economic costs and the structures' durability decrease.

The damage of some elements in civil structures affects the operational reliability of other elements of the unit. This general principle applies to the thermodynamic processes in multi-layered enclosing structures, in which, for instance, the failure in a form of a breach of vapor sealing properties of the corresponding structural layer results in the decrease of the insulating properties of the warmth-keeping layer. This makes it necessary to assess structure reliability, when the modern enclosing structure is considered as a system, the design and manufacture of which was carried out according to functional requirements [10], taking into account the mutual influences of its elements.

In the process of considering the thermal envelope of a whole building as a system, this principle remains unchanged and envisages that the failure of an envelope element (for instance, a window structure) leads to thermal damages of the wall opaque structures and of the entire system.

Therefore, the reliability rating for an object consisting of a system of interacting elements, such as a multilayered thermally heterogeneous structure or a building thermal envelope, should obviously be based on the characteristics of individual elements and the use of the statistical simulation method [2, 6]. In this case, the functioning of the system is presented as a sequence of random events associated with the individual elements of the system. The event points out any deterioration of the element operation quality. In the process of simulation, the interrelation of elements in the system is established by changing the characteristics of individual elements after the event for any of them. The simulation is carried out for a specific period, for instance, for the estimated warranty period, and so on.

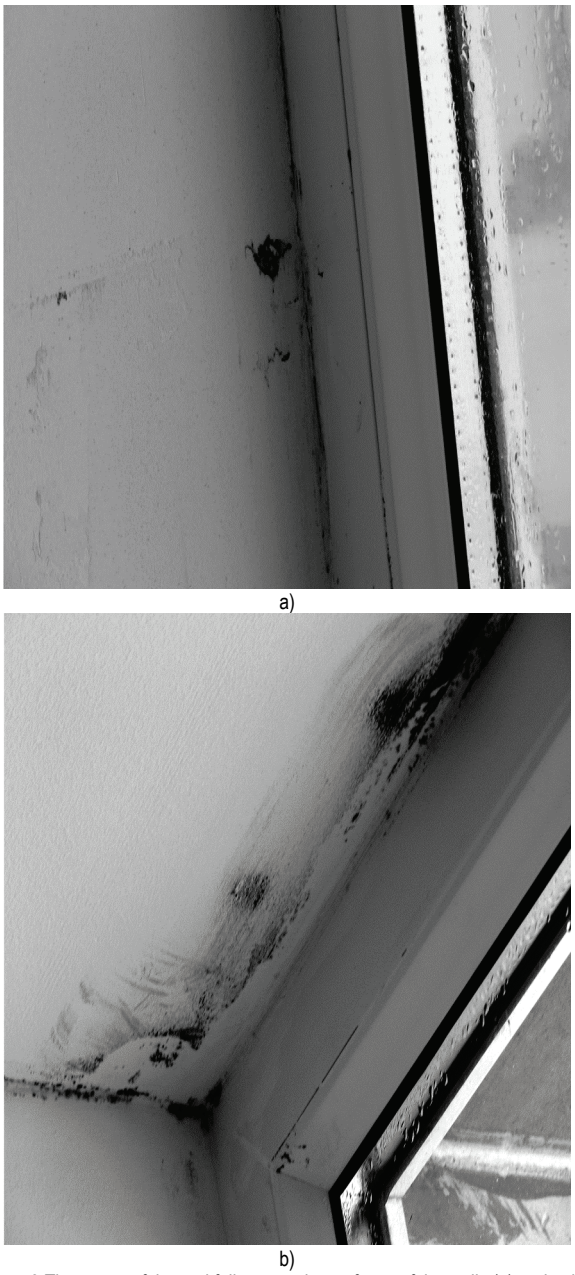

a)

b)

Figure 3 The states of thermal failures on the surfaces of the walls (a) and ceiling (b) of the living-room during the first cold period after the replacement of old windows with modern PVC windows with a one-chamber glass unit (4M-16-4M).

Every single simulation cycle can be reiterated, and the statistics of the system in various states can be collected with the various quantities of events for system elements. Based on such statistics, the reliability of the system is rated.

The simplest scheme of element connection is a multilayered construction consisting of elements connected in a series according to the heat flow resistance. In

compliance with the technical theory of reliability, the reliability-rating is carried out by the characteristic of the probability of a system failure-free operation with independent elements by means of the following equation:

$$P_s = \prod_{i=1}^{n} P_i \tag{2}$$

where P_i is the probability of an i^{th} element of a failure-free operation.

a)

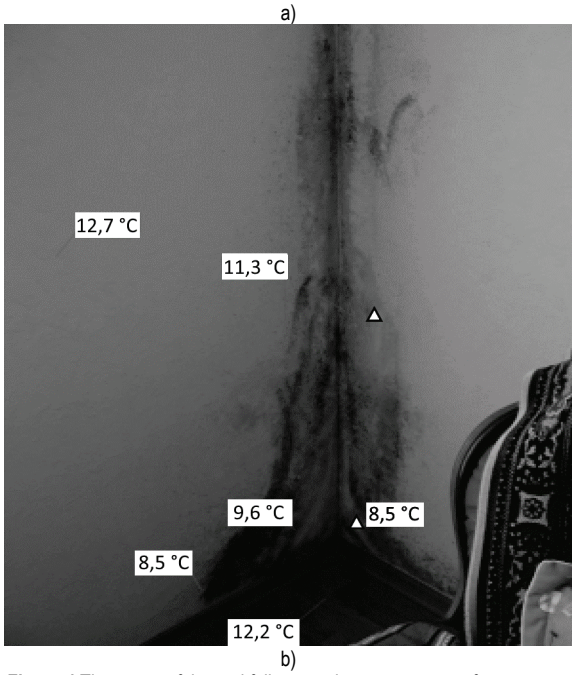

b)

Figure 4 The states of thermal failures at the corner areas of apartments

In the processes of heat transfer through the structure, the sequential scheme envisages a thermally homogeneous envelope structure. Real structures, especially the modern ones, are thermally heterogeneous, and the heat transfer is carried out according to a scheme that can be considered as two (or more) groups of series-connected elements on the assumption that the groups are connected in a parallel (Fig. 6), and the estimation of the failure-free operation probability of the system is carried out according to the Eq. (3).

$$P_s = 1 - \prod_{i=1}^{n} (1 - P_i) \tag{3}$$

The operational reliability of individual elements is characterized by the probability P_i of a failure-free operation of the corresponding element during the given period in the conditions, when other elements operate normally. An expert assessment is used for this characteristic. A set of respective probabilities for all elements constitutes the vector of reliability coefficients.

a)

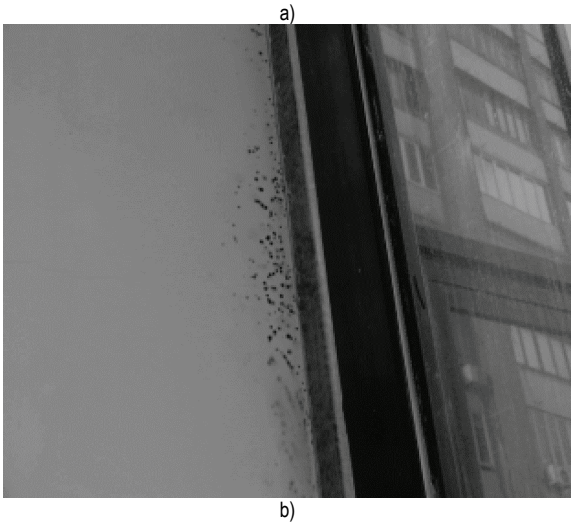

b)

Figure 5 Appearance of the façade element in a building (a) having the recorded state of the external walls' thermal failures after three months of operation (b).

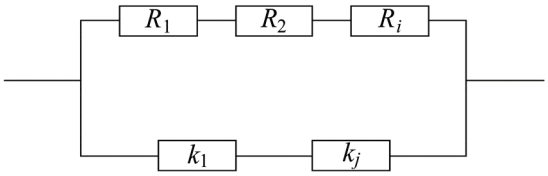

Figure 6 Conditional representation of the thermal work of thermal envelope structures (R_1, R_2 and R_i are the thermal resistances of the 1st, 2nd and i^{th} layers of the structure; k_1 and k_j are the thermal transfer linear coefficients of the 1st and j^{th} thermally conductive connections).

3 CRITERION OF THE THERMAL RELIABILITY OF THE ENVELOPE STRUCTURES

The assessment of the thermal insulation reliability has its own features. In radio engineering systems, the failure of one element results in system failure. The study of the reliability of load-bearing civil structures shows that the failure of one element can lead to the failure of the system. In this case, the element fail occurs once, and this failure is decisive for the system's further operability. In envelope structures, the thermal failures of elements may occur many times during the given time. The failures of the entire system can also be multiple. If this occurs, the construction does not lose its heat-insulating properties completely. Therefore, for assessing the thermal reliability of enclosing structures, it is insufficient to determine the failure-free operation probability and other frequency characteristics, but indicators that characterize the possibility of the changes of the building thermal envelope operational properties should be introduced.

The possible variations of the main characteristics of the thermal insulation, i.e., of the reduced total thermal resistance, can be taken as a criterion for the reliability of the system (building envelope, enclosing structure, etc.):

$$R_{\mathrm{r}} = 1 - \frac{R_{\Sigma\mathrm{pr}}(0) - R_{\Sigma\mathrm{pr}}(N)}{R_{\Sigma\mathrm{pr}}(0)} \tag{4}$$

where $R_{\Sigma\mathrm{pr}}$ is the reduced total thermal resistance of the enclosing structure.

The physical essence of this criterion is the determination of the envelope structure operational efficiency during its predetermined period of operation under the possible changes of the state of the structural elements because of the influence of various (climatic, assembling, operational, etc.) factors. The criterion can vary from one to near-zero values. In the first boundary state, the enclosing structure fully retains its thermal insulation properties during its predetermined lifetime. In the second boundary state, it completely loses its thermal insulation properties and is no longer an envelope structure, although it physically exists and is an obstacle to the external environment. The criterion of the reduced total thermal resistance characterizes the reliability of the building thermal insulation, because its value is determined by taking into account the effect of the possible failures of each element of the structure on the occurrence of failures in other elements and the corresponding change of the insulation properties of the structure (the system under consideration) after the cycle of probable climatic influences.

4 CONCLUSIONS

The developed method application for the statistical simulation of the processes of the heat failure of building thermal envelopes provides for the possibility for a quantitative comparative assessment of the design principles used in the modern construction sector. The proposed criterion of thermal reliability allows to assess the probable change of the thermal insulation indicators of the envelope structures' system by taking into account the effect of the possible failures of each system element on the occurrence of failures in other elements, and the corresponding change of the thermal insulation properties of the system after the cycles of probable climatic actions.

5 REFERENCES

[1] Bolotin, V. V. (1982). *Methods of probability theory and reliability theory in buildings design*, Stroiizdat, Moscow, 351 p.
[2] Ventsel, E. S. (1988). *Theory of probability and its engineering applications*, Moscow, 479 p.
[3] Levin, B. R. (1978). *Theory of radio engineering systems (mathematical basis)*, Sovietskoie radio, Moscow, 263 p.
[4] Lloid, D. (1964). Reliability, Sovietskoie radio, Moscow, 685 p.
[5] Perelmuter, A. V. (2000). *Selected problems of civil structures reliability and safety*, 2nd revised ed., Stal, Kyiv, 216 p.
[6] Pichugin, S. F. (2009). *Civil structures reliability*, Poltava, ASMI, 452 p.
[7] Kaufman, Ar. (1969). *La confiance technique. Theorie mathematique de la frabelitie*, Dunod, Paris, 79 p.
[8] Farenyuk, G. G. (2009). *Basics of assuring the buildings energy performance and envelopes thermal reliability*, Gama-Print, Kyiv, 216 p.
[9] Farenyuk, G. G. (1983). Experimental investigation of rizopen phenolic plastic foam durability. *Investigations of buildings thermal protection*, NIISF, Moscow, 93-99.
[10] Farenyuk G. G. (2007). Functional design of modern envelope structures. *Construction materials, products and sanitary engineering*, 7, 109-113.

Authors' contacts:

Gennadiy FARENYUK, Doctor of Engineering Sciences
Odessa State Academy of Civil Engineering and Architecture,
Ukraine, 65029, Odessa, 4 Didrihsona str.
State enterprise "State Scientific Research Institute of Building Constructions",
Ukraine, 03037, Kyiv city, 5/2 Preobrazhenska str.
Phone: 0662803754
E-mail: farenyuk@ndibk.gov.ua

ISSN 1846-6168 (Print), ISSN 1848-5588 (Online)
https://doi.org/10.31803/tg-20180929165737

Subject review

GML BASED MANIPULATION OF GEODETIC AND MECHANICAL DATA

Marko ŠLJIVARIĆ, Milan REZO, Nikola KRANJČIĆ, Danko MARKOVINOVIĆ

Abstract: Ever since the Rulebook on cadaster of infrastructure has been published there has been constantly growing need for efficient data manipulation. However, data manipulation has been an issue for a very long period of time. This paper will provide solution in manipulation of geodetic and mechanical data for City of Zagreb gas plant. All the solutions are given in Geography markup language, GML.

Keywords: gas pipeline; geography markup language; geodetic & mechanical data manipulation; Rulebook on Cadaster of infrastructure

1 INTRODUCTION

Since the computation power became sufficient to process geospatial data, many geo-data systems have been developed. Some of the early geo-data systems were BUDS [1], GADS [2, 3], NISP [4] or FIRS [5], all designed to retrieve and display facilities using their own query language and internal data structures [6]. [6] proposed approach on manipulation and display of geographic data where all geographic data is treated as relations. [7] proposed model for storage and manipulation of geographic data called GISER whose main advantage was use of procedure-valued attributes. However, all of the authors were developing their own query languages and data structures. Since this was major issue in interoperability, experts needed to find structured data in order to resolve issues in geo-spatial data organization, interoperability, query and processing. First sign of resolving this issue was with the emergence of Geography Markup Language (GML) in year 2000 [8].

[9] created a GML-based interoperable geographical database for conservation of the lunan stone forest landscape to easily manipulate and query different types of data and after the testing the database concluded that it is interoperable with different spatial functions. [10] proposed a framework for feature-level geospatial data sharing, for transportation network data. [10] concluded that proposed framework has a great potential for sharing, accessing, extracting, transporting and displaying distributed geospatial data at the feature level, all in a web browser. [11] proposed a framework for GML storage, processing and interface for users or applications that need geo-spatial data manipulation service. All of the authors' general conclusions were that the GML is useful tool for providing framework to manipulate geospatial data. This paper will present framework to manipulate geodetic and mechanical data, similar to work done in [10] but with upgraded GML schemas and queries.

2 CASE STUDY

Over the years, geodetic experts have been collecting data for different infrastructure data, such as gas pipelines, water pipelines, communication cables, etc. Faculty of Geodesy in Zagreb has been collecting gas pipeline data for the City of Zagreb gas plant in period from 2005 to 2007. Such data will be used in this paper to show how to accelerate manipulation on such data. In order to develop a solution, what type of data geodetic expert should provide to fulfil the task first needs to be defined. According to the City of Zagreb gas plant, geodetic expert should provide them with four different files. Cartographically well-structured file is file which has all the necessary elements to be used in cadaster and to be manipulated in the GML schema. Fig 1. represents cartographically well-structured CAD file with chartered path of gas line and with mechanical data.

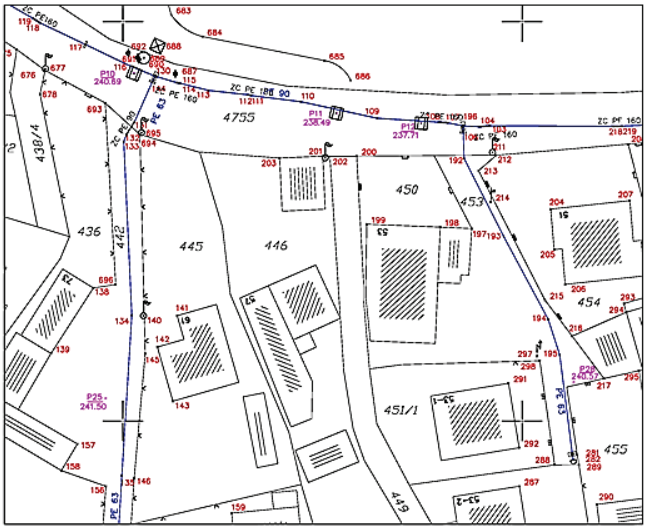

Figure 1 Digital cadaster plan with gas pipeline path

Second file is well defined ASCII file of path or part of the path, as presented in Fig 2. It should contain contractor name, point number, coordinates, altitude, mechanical data code.

Fig 3. shows list of general control network, which is also well defined ASCII file.

The final, fourth file, is list of completed work, with length of gas lines in each of planned path and with information about types of gas lines, as presented in Fig 4.

```
LIN0901063
&COM  GPZ 00000006 PE063       02/07/2005    Krvarić do kćbr67
GeofDT 130   5571404.000 5077843.180  239.3000R  240.450  082 154.30
GeofDT 144   5571403.950 5077843.079  239.3000R  240.450  079 245.88
GeofDT 131   5571401.470 5077837.510  239.9000R  241.040  053 237.71
GeofDT 132   5571400.440 5077835.880  240.1200R  241.220  053 237.71
GeofDT 133   5571400.100 5077834.970  240.2300R  241.410
GeofDT 134   5571401.110 5077813.240  241.6200R  242.720
GeofDT 135   5571399.860 5077793.130  239.8400R  241.000
GeofDT 136   5571399.250 5077783.040  239.4400R  240.600
GeofDT 137   5571399.650 5077775.330  238.9900R  240.090
GeofDT 148   5571400.650 5077768.410  237.9600R  239.060  079 278.29
GeofDT 149   5571401.760 5077761.370  236.9300R  238.030
GeofDT 167   5571403.470 5077753.010  235.6500R  236.800
GeofDT 168   5571406.060 5077742.050  234.0700R  235.170  072 103.27
GeofDT 169   5571404.480 5077741.590  234.2200R  235.370  053 196.07
GeofDT 170   5571402.710 5077741.080  234.2800R  235.430  053 196.07
GeofDT 171   5571400.150 5077739.140  234.0900R  235.190
GeofDT 172   5571383.150 5077733.760  233.6600R  234.760  079 202.52
GeofDT 173   5571381.510 5077733.080  233.4800R  234.570  083 199.29
GeofDT 174   5571381.110 5077732.940  233.4000R  234.490  076 201.22
```

Figure 2 Example of starting LIN file (ASCII file)

```
P1          5571194.420 5077521.550 240.070
P2          5571188.200 5077605.140 237.410
P3          5571172.310 5077667.530 239.710
P25         5571397.840 5077802.840 241.500
P26         5571401.100 5077775.540 240.280
P27         5571403.870 5077735.410 235.020
P28         5571456.480 5077804.890 240.570
GPS2362     5571892.020 5077322.110 178.940
```

Figure 3 List of general control network

```
&COM  GPZ 00000001 PE090       28/07/2005    Krvarić
kD=1149,75 [m], hD=1143,04 [m], dH=-60,9 [m]
&COM  GPZ 00000002 PE063       18/07/2005    Krvarić do kćbr 4/2
kD=120,85 [m], hD=120,6 [m], dH=2,67 [m]
&COM  GPZ 00000003 PE063       06/07/2005    Krvarić do kćbr 18
kD=44,63 [m], hD=44,54 [m], dH=-1,09 [m]
&COM  GPZ 00000004 PE063       18/07/2005    Krvarić prema kćbr 40
kD=10,56 [m], hD=10,41 [m], dH=-1,63 [m]
&COM  GPZ 00000005 PE063       02/07/2005    Krvarić do kćbr 53/2
kD=44,92 [m], hD=44,74 [m], dH=3,29 [m]
&COM  GPZ 00000006 PE063       02/07/2005    Krvarić do kćbr67
```

Figure 4 List of completed work

Having in mind that such structure depends on memory capabilities and PC processing power, next chapters will describe Geography markup language as a better solution to format data and structure. Chapter 4 will provide short overview of new rulebook on cadastre of infrastructure and in Chapter 5 will present proposed GML schema for data management.

3 GEOGRAPHY MARKUP LANGUAGE

The OGC (Open Geospatial Consortium) is an international not-for-profit organization committed to making quality open standards for the global geospatial community. These standards are made through a consensus process and are freely available for anyone to use to improve sharing of the world's geospatial data [12]. OGC standards are used in a wide variety of domains including Environment, Defense, Health, Agriculture, Meteorology, Sustainable Development and many more [13]. Among all the other standards for this paper most interesting standard is one on Geography Markup Language, or shorter GML. The Geography Markup Language (GML) is an XML grammar for expressing geographical features. GML serves as a modelling language for geographic systems as well as an open interchange format for geographic transactions on the Internet. As with most XML based grammars, there are two parts to the grammar – the schema that describes the document and the instance document that contains the actual data. A GML document is described using a GML Schema. This allows users and developers to describe generic geographic data sets that contain points, lines and polygons. However, the developers of GML envision communities working to define community-specific application schemas [14] that are specialized extensions of GML. Using application schemas, users can refer to roads, highways, and bridges instead of points, lines and polygons. If everyone in a community agrees to use the same schema they can exchange data easily and be sure that a road is still a road when they view it [15], or as shown in this paper, gas pipelines.

GML represents expanded XML schema, which can define geospatial object classes, features. GML defines content and it does not shuffle content and its presentation [16]. Feature Types are specified in GML application schema. Main application schema *gml.xsd* contains all other GML schemas, but for the majority of usage *feature.xsd* schema is recommended. Current version of GML is 3.2.2.

Feature.xsd schema contains sub-schemas: ***geometryBasic2d.xsd*** schema which defines basic two dimensional geometry type of data and includes ***geometryBasic0d1d.xsd*** schema for scalar and one dimensional data types as well their connection with values defined in ***measures.xsd*** in which these values are defined. Next there is a sub-schema ***units.xsd*** in which units of values are defined. ***Dictionary.xsd*** schema has all the terminology, and contains ***gmlbase.xsd*** schema where are all other types of simple, complex or abstract data. Simple data types are defined in ***basicTypes.xsd*** schema and how this data links between one and another is defined in ***xlinks.xsd*** schema. ***Temporal.xsd*** schema is component of ***feature.xsd*** schema which gives time component to definition of data.

Other GML schemas in ***gml.xsd*** schema include ***dynamicFeature.xsd*** schema, ***direction.xsd***, ***topology.xsd***, ***geometryComplexes.xsd***, ***geometryAggregates.xsd***, ***geometryPrimitives.xsd***, ***coverage.xsd***, ***valueObjects.xsd***, ***grids.xsd***, ***coordinateReferenceSystems.xsd***, ***datums.xsd***, ***coordinateSystems.xsd***, ***coordinateOperations.xsd***, ***referenceSystems.xsd***, ***dataQuality.xsd***, ***observation.xsd***, ***defaultStyle.xsd*** and ***temporalReferenceSystems.xsd*** and ***temporalTopology.xsd*** schemas.

Fig 5. shows dependence between GML schemas.

As shown on Fig 5. in whole GML there are only seven schemas not depending on any other schema. They are root schemas of GML:

- ***observation.xsd***
- ***dynamicFeature.xsd***
- ***coverage.xsd***
- ***topology.xsd***
- ***defaultStyle.xsd***
- ***coordinateReferenceSystems.xsd***
- ***temporalReferenceSystems.xsd***

Class hierarchy in GML is shown in Fig 6.

On Fig 7 there are presented geometry classes in GML.

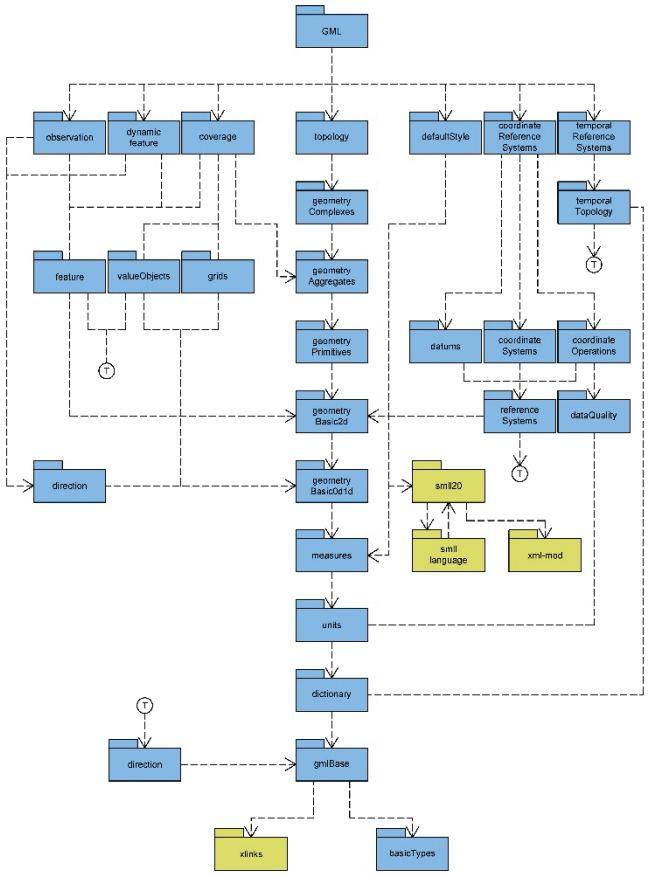

Figure 5 Schema Dependencies [16]

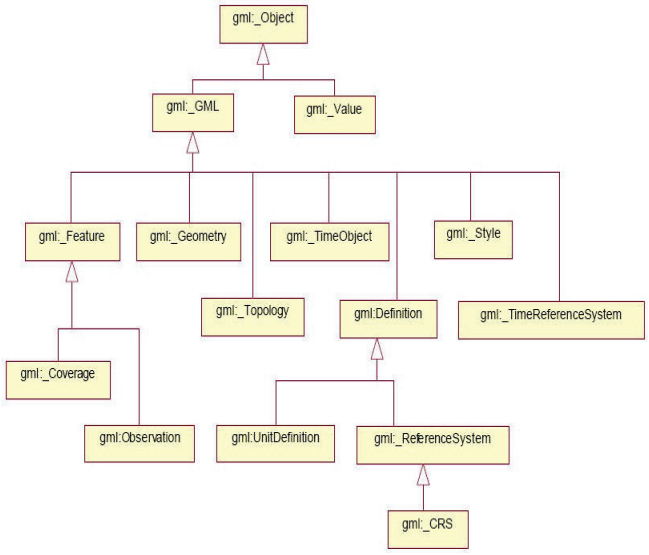

Figure 6 GML Class Hierarchy [16]

4 RULEBOOK ON CADASTER OF INFRASTRUCTURE

On 23rd March 2017 the principal of Croatian state geodetic administration brought out Rulebook on cadaster of infrastructure. In the rulebook, how and which data should be collected for cadaster of infrastructure is pointed out. Since in this paper enhanced manipulation of gas pipeline data is shown, further chapter will only present parts of rulebook regarding gas pipeline. For gas pipeline network it is necessary to obtain data about production, transport, distribution network and connection to such network [17]. Data about basic technical characteristic refers to the type of pressure, material and pipe diameter in millimetres. For every type of infrastructure the data should be collected in Croatian Terrestrial Reference System 1995.55 (HTRS96/TM) and in Croatian Height Reference System 1971.5 (HVRS71). Data about owners, or about administrator of infrastructure that should be collected are name, address, id number and other data necessary for communication such as official mail address, phone number, etc. [17]

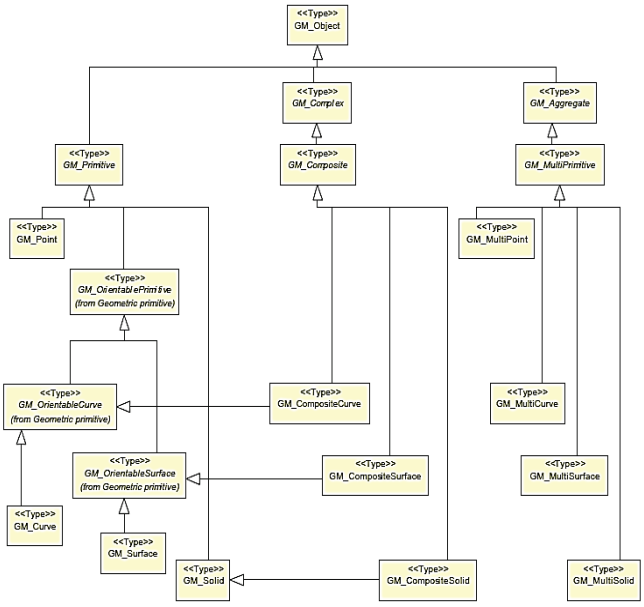

Figure 7 GML Geometry Classes [16]

Cadaster of infrastructure consist of written and numerical part. Written part is:

- list of infrastructure,
- list of owners and infrastructure administrators.

Numerical part is:

- map of infrastructure,
- collection of geodetic elaborate of infrastructure [17]

List of infrastructure contains:

- number of entries within one year and label of confirmed geodetic elaborate of infrastructure of cadaster,
- type of infrastructure and its current use (in usage, abandoned or removed),
- id number of infrastructure and its objects,
- data about owner, or administrator of infrastructure
- names of cadastral municipalities in which infrastructure is settled,
- names of municipalities, settlement and streets in which infrastructure is built,
- house number if the infrastructure is built as home connection,
- length of built infrastructure [17].

List of owners and administrators contains of:

- number of entries of owners or infrastructure administrators,
- data about owners or infrastructure administrators,
- type of infrastructure [17].

Map of infrastructure is graphical plan of infrastructure and related objects of infrastructure. Graphic basic of infrastructural plan is digital orthophoto map in measure 1:2000 or 1:5000 with overlapped digital cadaster map [17].

According to the Rulebook on cadaster of infrastructure geodetic survey contains:

- survey of points of infrastructure in horizontal manner,
- survey of points of infrastructure in vertical manner (for drainage at the bottom of pipe, for other infrastructure at the top of pipes),
- survey of intersections of new infrastructure with existing infrastructure,
- survey of existing infrastructure objects,
- obtaining data about infrastructure owners or infrastructure administrators [17].

Taking the aforementioned into consideration, similar gathering of infrastructural data has been done from 2005 to 2007. Main difference is in geodetic projection since in 2004 was new state horizontal projection datum defined. Since there was a transitional period, the data could be still obtained in old Gauss-Krueger projection.

In the next chapter there is a proposed solution for standardizing process of manipulation of obtained geodetic data for cadaster infrastructure. Main difference in proposed solution is in geodetic projection, but other data is standardized and synced, even in 2005, with new Rulebook of cadaster infrastructure.

5 PROPOSED GML SCHEMA

To begin in standardizing manipulation of geodetic data every well-structured GML the file should start with schema definition. In example below, the schema used is ***feature.xsd***.

```
<?xml version="1.0" encoding="UTF-8"?>
<xs:schema
   xmlns:xs="http://www.w3.org/2001/XMLSchema"
   xmlns:gpz="C:\0000\ProcGeoInf\Oxygen10\"
   xmlns:gml="http://www.opengis.net/gml"
   targetNamespace="C:\0000\ProcGeoInf\Oxygen10\"
   elementFormDefault="qualified">
   <xs:import namespace="http://www.opengis.net/gml"
schemaLocation="feature.xsd"/>
```

In order to standardize processes, after defining schema, what type of data is expected and how that data should be structured in order to develop faster model of processing input data should be defined in GML file. Next example shows defining type for point data.

```
<xs:element name="Point" type="gpz:PointType"
substitutionGroup="gml:_Feature"/>
```

After the whole GML file is completed and data input standardized, the GML should be evaluated. Due to GML basically being XML, it can be evaluated in special software, like XML editor Oxygen 10 or XML Spy. GML document should be well formed and validated. A well-formed document is document that follows the syntax rules specified by the XML 1.0 specification [18]. Valid GML document must be well formed, and it must conform to a document type definition [19]. There are two different document type definition that can be used with GML:

- DTD – The original Document Type Definition
- XML Schema – An XML-based alternative to DTD

In this paper XML Schema *feature.xsd* as document type definition is used. Since the schema is located on official GML pages online, it can be assumed schema does not have errors.

After checking the GML document with SaxonSA and MSXML4.0 modules in Oxygen 10.1 [20], it is clear that GML schema is well formed and validated, while XMLSpy [21] cannot find *SimpleLink* declaration in ***gmlBase.xsd*** schema which reference to schema ***xlinks.xsd*.**

6 RESULTS

After definition of GML file and filing out GML file with data there are preliminary results. In municipality Mikulići there is 11.5 km of main pipeline and GML data takes about 500 kB of memory space on hard disc. In whole cadaster municipality around 5000 home connections were built. Data for each home connection contains ten points and mechanical data for each connection. Total data for municipality Mikulići is around 25 mB. In the City of Zagreb there are forty cadaster municipalities under the jurisdiction of city gas plant. Using simple math there is at least 10 gB of data. This presents a challenge in data manipulation, data safety, speed of searching, modifying and storing such data. Since the GML files are well structured and well defined, above mentioned issues are easily solved with use of transaction technology which is basic in every relation database, object – relation database, or object-oriented database.

7 CONCLUSION

New Rulebook on Cadaster of infrastructure standardize the way data should be gathered. Having in mind that standardizing the process of gathering data results in standardizing the processes of data manipulation. This paper gives an overview of Geography Markup Language, new Rulebook on Cadaster of infrastructure. Proposed GML schema is a direction in which all data manipulation should strive. Main advantage in the data stored using GML is in standardized process of data manipulation, higher data safety and greater speed of searching, modifying and storing such data. Schema and framework proposed in this paper have a better response time and take less memory compared to frameworks proposed in Introduction.

8 REFERENCES

[1] Macri, P. (1973, November). BUDS: The Berkeley Urban Data System. Electronics Research Laboratory, University of California, Berkeley, Memorandum M412.

[2] Christiani, E. J., et al. (1973, March). An Interactive System for Aiding Evaluation of Local Government Policies. *IEEE Transactions on Systems, Man, and Cybernetics*, SMC-3(2), 141-146. https://doi.org/10.1109/TSMC.1973.5408495

[3] Mantey, P. E., et. al. (1973, June). Information for Problem Solving: The Development of an Interactive Geographic Information System. *IEEE Conference on Communication, vol. II*, Seattle, Washington.

[4] Parker, J. L. (1971, November). Information Retrieval with Large Scale Geographic Data Bases," *Proc. 1971 ACM-SIGFIDET Workshop on Data Description, Access and Control*, San Diego, Ca. https://doi.org/10.1145/1734714.1734739

[5] Depta, D. J. & Irwin, G. M. (1974, March). *FIRS II - Design Requirements Component*. Weyerhauser Company, Woods Product Information Systems, Tacoma, Wash.

[6] Berman, R. & Stonebraker, M. GEO-OUEL A System for the Manipulation and Display of Geographic Data, University of California, Berkeley.

[7] Shekhar, S., Coyle, M., Goyal, B., Liu, D.-R., & Sarkar, S. (1997). Data Models in Geographic Information Systems. *Communications of the ACM, 40*(4). https://doi.org/10.1145/248448.248465

[8] http://www.opengeospatial.org/ (Accessed on 21.05.2019.)

[9] Zhang, C., Day, M. J., & Peng, Z-R. (2003). GML-Based Interoperable Geographical Databases. *Cartography, 32*(2), 1-16. https://doi.org/10.1080/00690805.2003.9714249

[10] Peng, Z-R. (2005). A proposed framework for feature-level geospatial data sharing: a case study for transportation network data. International Journal of Geographical Information Science, 19(4), 459-481. https://doi.org/10.1080/13658810512331319127

[11] Wang, W., Wang, F., Qian, Z., & Zhang, L. (2011). GML Data Management: Framework and Prototype. *16th International Conference, DASFAA 2011 International Workshops*, Hong Kong, 101-111. https://doi.org/10.1007/978-3-642-20244-5_10

[12] http://www.opengeospatial.org/standards/gml

[13] Lake, R., Burggraf, D.,Trninic, M., & Rae, L. (2004). *Geography Mark-Up Language: Foundation for the Geo-Web*, New York: Wiley.

[14] http://old.geotools.org/19708.html (Accessed on 21.05.2019.)

[15] http://map.sdsu.edu/geog583/lecture/unit-6.html (Accessed on 21.05.2019.)

[16] Rezo, M. & Šljivarić, M. XML/GML DBMS utemeljeno pohranjivanje i upravljanje geodetskim i strojarskim podacima, Seminarski rad, Geodetski fakultet Zagreb, 2009.

[17] Državna geodetska uprava: Pravilnik o katastru infrastrukture, 2017, NN 29/2017

[18] Son, J. H., Kim, J. S., & Kim, M. H. (2005). Extracting the workflow critical path from the extended well-formed workflow schema. *Journal of Computer and System Sciences*, 70, 86-106. https://doi.org/10.1016/j.jcss.2004.07.001

[19] https://www.w3schools.com/xml/xml_validator.asp (Accessed on 21.05.2019.)

[20] http://www.oxygenxml.com/ (Accessed on 21.05.2019.)

[21] https://www.altova.com/xmlspy-xml-editor (Accessed on 21.05.2019.)

Authors' contacts:

Marko ŠLJIVARIĆ, doc. dr. sc.
European University Brčko,
Technical Faculty,
Bijeljinska cesta 72-74
76100 Brčko, Bosnia and Herzegovina
Tel: +385 91 4444 998
E-mail: marko.sljivaric@gmail.com

Milan REZO, Ph.D. Assistant Professor
University of Zagreb,
Faculty of Geotechnical Engineering,
Hallerova aleja 7,
42000 Varaždin, Croatia
Tel. +385 42 408 950
E-mail: mrezo@gfv.hr

Nikola KRANJČIĆ, mag. ing. geod. et geoinf.
University of Zagreb,
Faculty of Geotechnical Engineering,
Hallerova aleja 7,
42000 Varaždin, Croatia
Tel. +385 42 408 950
E-mail: nkranjcic@gfv.hr

Danko MARKOVINOVIĆ, Ph.D. Assistant Professor
University North,
Jurja Križanića 31b
42000 Varaždin, Croatia
E-mail: danko.markovinović@unin.hr

ISSN 1846-6168 (Print), ISSN 1848-5588 (Online)
https://doi.org/10.31803/tg-20181203125101

Subject review

RESEARCH OF THE OPTIMAL VARIABLE DEFECTS OF THE PREVENTIVE MAINTENANCE OF MEDICINAL EQUIPMENT

Dalibor PONGRAC, Živko KONDIĆ, Veljko KONDIĆ, Marko HORVAT

Abstract: The article clarifies the importance of maintenance in the exploitation of a particular medical device from the aspect of maintaining its availability, reliability and overall functionality. Particularly emphasized is the role of the preventive method or procedures that have a preventive character before the problems arise in the work. Through an analysis of the most common malfunctions and causes that occur during the exploitation, a basis for objective defining and proposing principles has been created – preventive maintenance with special emphasis on preventive maintenance according to an established condition. The article also shows a numerical way of calculating the periodicity of conducting preventive examinations on a particular device.

Keywords: failures; maintenance; maintenance by state; medical devices; preventive maintenance; systems

1 INTRODUCTION

The main task of maintenance is to support the working ability of the technical systems so that they can perform their function. During the period of the use of technical systems, medical devices are exposed to a large number of influential factors, which results in deviations of their features from their default and expected values. In the constant aspiration of the user to keep the working characteristics within the defined limits or to return to the default interval, different maintenance methods have been developed and they differ in their concept, technology and organization [1].

In general terms, technical exploitation systems can be found in two states, both "in operation" and "malfunctioning", that is, the systems may be correct or incorrect, with all faults that may occur.

The maintenance of technical systems includes activities, methods and various techniques to ensure their correct operation in a particular terminal unit to prevent or delay the occurrence of "malfunction".

From this approach to maintenance, three basic methods of maintenance of all technical systems, including the medical devices, can be defined:

1) Prevention,
2) Corrective and
3) Combined methods.

In practice, the choice of the method of the maintenance of technical systems and medical devices is based on the systematic impact analysis and procedures in terms of:

- the overall efficiency of the specific maintenance method,
- the time intervals needed for performing maintenance activities, and
- the interdependence of the total costs and the time of the maintenance activity.

It is obvious that there are many factors that decide which maintenance method to apply in this particular case. The maintenance method must originate from the cause, the failure of component elements or the system as a whole. If the causes of the defects of all constituent components belonging to one device are different, then these different components will also have different maintenance methods that will be most acceptable for each component of the device. In such cases, the optimization of the maintenance method is performed in the most critical part of the system [2].

2 MAINTAINING MEDICAL DEVICES WITH THEIR ASPECTS AND RELIABILITY

The maintenance of medical devices in terms of the dynamics and the content of the activity must be carefully defined and in accordance with the actual needs. Otherwise, negative effects can be obtained. Instead of high reliability and availability, improper planning and implementation, especially complex and long-lasting maintenance procedures, can cause other, additional and even more major failures, and they can significantly reduce reliability and availability while increasing maintenance costs.

2.1 The Term of Availability

Availability is the property of a medical device expressed by the probability of being in a working position, i.e. being able to function satisfactorily at any point in time when required.

2.2 The Term "Reliability"

The reliability of a medical device can be defined as a probability that it will perform the required function under the default conditions and during a given period.

From the above definition of reliability, three basic elements of the definition can be noticed:

- "execution of the required function",
- "in the given time", and
- "under the given working conditions."

Executing a function means that the device has the intended purpose for which it was manufactured and purchased. The default conditions represent the environment (temperature, humidity, etc.) and the default time represents the time period required for satisfactory operation. It can be said that reliability is a characteristic of each technical system, whose initial value depends on a number of factors defined in the development phase.

It is important to note that there can be a fall in the values for the elements, circuits and the system as a whole due to various factors. It is equally important to note that the reliability maintenance activities can be raised by predicting falls of elements, circuits or the system as a whole.

3 CONTEMPORARY METHODS FOR THE MAINTENANCE OF MEDICAL DEVICES

Figure 1 shows the basic methods of the maintenance of medical devices with the corresponding variants [2].

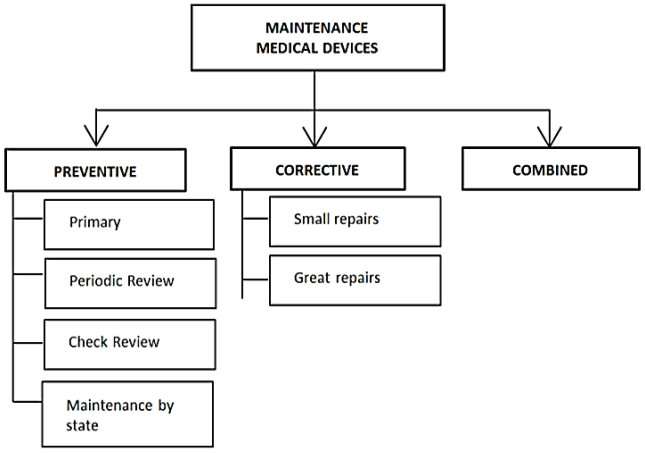

Figure 1 Methods of the maintenance of medical devices

The term preventive maintenance involves a series of actions being taken to prevent the occurrence of the condition "broken", and maintaining medical devices within the functional correctness and in a certain time interval. Preventive actions are then performed before the malfunction occurs, and require, unlike the corrective actions, to be planned and to determine the benefit of their performance.

The good features of preventive maintenance are reflected in the fact that, with particular certainty, the required level of the reliability of the device can be guaranteed. This is shown in Fig. 2, which shows the relation between the reliability curve and the intensity of the failure, with preventive intervention.

The figure shows that the curve of reliability declines over time, and that the failure intensity is a constant value. In the point of time t, periodic inspection of the device was conducted and thus its reliability was taken to the next level R. Hence, the resource of a circuit on a device does not use a fault. In Fig. 2, the drawn part of the surface beneath the curve $R(t)$ represents the area of the unused resource of an assembly of a device. Therefore, the justification of the methods of preventive maintenance must be examined and assessed in each set, because the cost of preventive replacement and works, especially the more expensive and sophisticated equipment, can be considerably higher than the expected results.

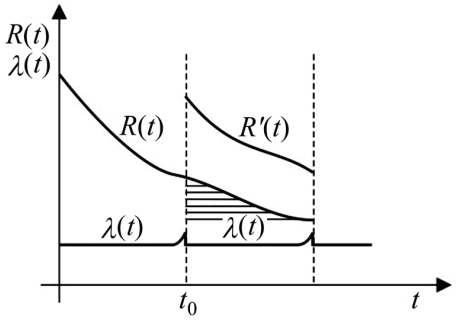

Figure 2 Relationship of reliability and intensity of failure

Preventive maintenance can be accomplished in several ways. This refers to the type and character of preventive maintenance procedures, and then, when the time is determined to carry out these procedures. Considering the fact that in practical situations of the maintenance of medical devices, it is difficult to find a system which applies to only one of these models of preventive maintenance, so usually it is a combination of several different methods. For this reason, the above mentioned principles briefly explain all the above mentioned principles of preventive maintenance.

Basic maintenance covers all methods, which are typically performed by the user of the medical device (operator) and the on-site use of tools and equipment from the composition of the sets of devices. For each specific device, basic maintenance technology should be prescribed if it is not elaborated in the instructions that the manufacturer is obliged to deliver with the device.

Basic maintenance, as the principle of preventive maintenance, should be introduced in all devices. To be effective in practice, it is necessary:

- that operators are perfectly familiar with the device on which they work,
- to specify the correct technology of work so that you know exactly what is being done, when, by whom, how long, how, under which conditions, etc.,
- to determine the person who will oversee the work done during basic maintenance.

Periodic maintenance also refers to preventive maintenance activities that are periodically performed in terms of the review of the critical points and their cleaning (sometimes lubrication) in order to detect or prevent the occurrence of failure. Checks are performed by means of: monitoring, measurement, reading, comparing, and listening to others. In one system, a multiple periodic review can also be planned, e.g.: weekly, monthly inspection, quarterly review, semi-annual review and annual review. These are the variants of preventive examinations, however, it should be noted that they all have the same purpose, but they differ in technology work (content and runtime). Usually, preventive reviews are planned to be performed along with some other

preventive maintenance variants using the manufacturer's recommendations.

A *Check review* by way of preparation and planning is similar to periodic reviews. They differ in their purpose and manner of performance. The purpose of the check review is to determine the ability of medical devices for a particular purpose (accuracy, quality, capacity, etc.) and to determine the safety of the environment (user safety and people in the environment, fire safety, poisoning, pollution, impact, etc.).

Control reviews have a specific way of performing; they have specific accessories that are commonly used (measuring resistance, dimensional accuracy, radiation, etc.). Moreoverm these reviews are specific for their complex procedures of measurements, which often require the special training of the contractor. Most often, they are performed by external associates of authorized specialist institutions according to standard procedures and legal regulations (Technical Protection Act, ISO, EN, HRN, DIN, etc.).

Maintenance by condition is one of the preventive maintenance methods whose decision-making strategy for maintenance activities is based on periodic or continuous control of the device's technical condition in the exploitation process. According to the results of the control, necessary decisions are made and within the scope of the planned maintenance activities. Maintenance by condition is a diagnostic process that enables the technical state of each component or assembly of a particular device to be determined. This process enables insight into the state of the constituent part or assembly or the device as a whole, respectively, it denotes its "state" and allows the permanent planning of replacement or repair of a system based on the actual technical state, increasing the time of the effective operation of the medical device and eliminating unnecessary dangers.

Maintenance by this method is carried out in such a way that first, at certain time intervals, independent of the state of the damage of the component parts of the system, the diagnostic control of the technical condition is performed, and after that, depending on technical condition, activities on the component parts of the device are performed or they remain in the process of exploitation.

The characteristic size of a technical condition, which is typically taken to characterize a change of state, is a physical size that can be mixed and transmitted, most often by analogous means. As a rule, it is the most important size in the process of using the system.

Maintenance by condition, in conjunction with the classical methods of preventative maintenance, provides a close link between the process of changing the technical condition and the process of using the medical device. In practice, there are several methods of maintaining the state. All these methods are classified into two groups:

- maintenance by condition control the level of confidence and
- maintenance by condition with parameter control.

When maintaining by condition with a confidence level control, the constituent condition of the constituent parts and the system as a whole is a permissible level of reliability (R_d), which is most fully expressed by the intensity of the fault and is determined on the basis of the system usage test for a period of 3-5 years. The system is used without restriction of maintenance resources, as long as the actual level of reliability (R_s) exceeds the permissible level of reliability. In the case of $R_s < R_d$, the cause of the fault should be investigated or the maintenance model must be introduced in the condition with the parameter check.

Maintaining by condition of the control parameters provides continuous or periodic control and measurement parameters which determine the technical state of the components or systems. The decision on maintenance activities is made when the value of controlled features reaches the "limit of usability", i.e. before the critical level.

Because of its advantages, the method of maintaining the state is increasingly used in the world, in various technical fields, as evidenced by numerous technical papers by authors from around the world. Benefits are reflected in increasing reliability, which is achieved by reducing the total scope of maintenance work in the case of maintenance. By reducing the total volume of work, future failure risk is reduced relating to the quality of the execution of maintenance procedures, and in this way, they maintain the required level of the reliability of the device. The maintenance costs of the device are then smaller.

The application of the method by condition was manifested particularly in an aircraft, where many general maintenance systems are developed using this method. One of the most famous is the so-called TARAN (Test and Replace as Necessary) system which translates to "Test and Replace if Needed". Similar situations are also in use in other modern technical systems, where many manufacturers have developed their "state tracking" systems (Renault, BMW, etc.).

The difference between the periodic maintenance "by time" and the maintenance method are essential, although both represent preventative activities. While in the case of preventive maintenance by "time", maintenance procedures are carried out after a prescribed time or exploitation resource, regardless of the state of the system, in the maintenance state, the "condition check-up" of the system component elements and maintenance procedures are undertaken only if the values of the parameter values are found beyond the prescribed limits.

4 MEDICAL DEVICE FOR COMPUTER TOMOGRAPHY "ROTHOGRAPH EVO 3D"

Recently, in general and dental medicine, image-based devices are used with Cone Beam Computed Tomography (CBCT) method. It is about reconstructing the tomographic plane of the body; it is a type of radiological image which results in a visual representation of one part of the body or entire body and is generated by ionizing radiant radiation.

Manufacturer of the devices for computer tomography "Rothograph Evo 3D" is the company Villa Sistemi Medicali S.p.A. Buccinasco (MI), Italy, Fig. 3.

Figure 3 Rotograph Evo 3D display

The device is applied in traditional dental medicine and otorhinolaryngology. The specificity of the device is recording heads and the dental jaw (anomalies), the temporomandibular joint (TMJ - temporo-mandibular joint) in 3D (three-dimensional image) and image processing by a computer software called Dental Studio Plus Software 3D. The software provides various possibilities of reconstructing the recorded body parts and depths of view through the layers. The software also provides aesthetic treatment of dentures on the film itself and the addition of implants that the dentist or orthodontist can visualize to the patient's plan of action on the teeth. The device also allows diagnosis, reconstruction of the head and teeth by displaying the volume image. In addition to 3D recording, there is also the ability to record in 2D format. For 3D image capture, the detector performs a rotation of 360° around the patient's head, and the device rotates 180° to produce a panoramic image. The advantage of 3D imaging is to detect any irregularities and gum disease that eliminates the need for additional imaging and unnecessary X-ray radiation.

4.1 Using the Device

The Rotograph Evo 3D is designed for installation in a separate room or is located in a room separated by special lead separators to reduce radiative power. The radius of radiation is 2 m. The operator enters the required parameters for recording via the touch screen or computer and manually adjusts the device to perform recording.

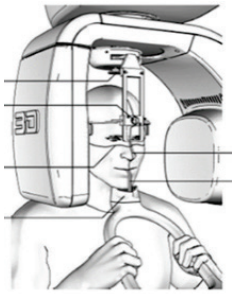

Figure 4 Displays an adjusting of a patient

Fig. 4 shows the patient's access to the device, the movable vertical column is adjusted to the patient's height so that the patient seizes the handle, and the radiology engineer adjusts the face depending on the type of shooting required.

Pressing the exposure button, we get a shot of the patient, the picture is at the same time transferred to the computer and is ready for further processing. The patient can be removed from the device with the radiologist's approval.

4.2 Specifications

Rotograph Evo 3D is listed in Class II B for the European Directive for Medical Devices 93/42, the degree of protection is IPXO. It is manufactured for two types of power supply 220-240 V ~, 110-120 V ~, 50/60Hz.

The device has the ability to adjust the parameters automatically according to the type of shooting and the exposure time depending on the recorded person and the recording type. The X-ray tube head MRE 5 is manufactured by Villa Sistemi Medicali S.p.A., and the X-ray lamp is CEI Bologna (Italy) type OPX 105. The sensitivity range of the sensor is 130×130 mm. The minimum dimensions of the work environment according to the service documentation are 130×120 cm and the recommended dimensions are 130×140 cm without the additional CEPH equipment. [3]

4.3 Dental Studio Plus Software 3D Driver

Using the "Dental Studio Plus 3D" software in Fig. 5, the video is simultaneously displayed on the computer screen. The 3D Reconstruction Module simultaneously reconstructs the volume of the recorded part of the head using a reduction algorithm.

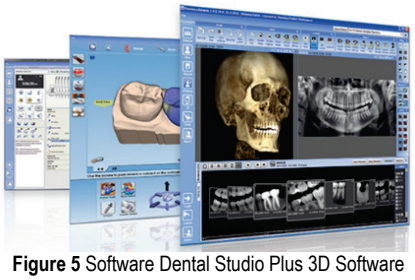

Figure 5 Software Dental Studio Plus 3D Software

The browser software on the screen is visually very practical and adapted to easy viewing and processing images. The software offers the ability to make various useful data such as measurement of the distance between teeth angles, visual implant placement etc.

4.4 Procedures for Preventive Maintenance of the Device

As all medical devices, the Computing Tomography Device Rotograph Evo 3D also must be in the correct state for its full functionality. Therefore, preventive maintenance is required for the safety and efficiency of the device. Preventive maintenance refers to the device operator and service engineer who performs maintenance. For this reason, it is necessary to carry out the verification procedures for the preventive maintenance carried out by the operator and the periodic preventive maintenance performed by the service engineer once a year.

The process of performing preventive maintenance is performed according to a specific procedure prescribed by the manufacturer.

In this case, the following preventative activities are defined:

- Sensor calibration
- Calibrate and adjust the unit and the panorama recording detector
- Partial Volume Calibration
- Calibration of the CEPH ARM (the 2D head recording sensor)
- Set parameters of kV and mA
- Touchscreen calibration.

4.4.1 Sensor Calibration

Sensor calibration is performed using a calibration tool and software to adjust parameter values

All calibrations are performed by performing tests using X-ray, and it is especially important to pay attention to the protection from possible exposure to radiation.

4.4.2 Calibration Procedures and Setting of the Device and Sensor (Detector) for Panorama Recording

To calibrate the device properly, we must take the panoramic shooting first.

The procedure is done in several steps:

1) The unit turns on and the recording type is selected
2) The computer starts up with Dental Studio Plus, the icon on the "CBCT" desktop is pressed and a test program is opened.
3) Selection of the Panoramic exam, setting the special tool shown in Fig. 6 which serves for centring the head and chin support tool for calibrating the sensor in front of the sensor. In this position, the cover is fastened to the sensor.

Figure 6 Special calibration tool

The calibration procedure begins with the recording in the test mode. Set the parameters for shooting an adult 68 kV – 6 mA with a copper filter or recording mode 60 kV – 6 mA without copper filters and computer displays recorded tool that was previously located on the carrier chin.

Use the software to adjust the contrast and brightness. The measuring tape is switched on and the distance between the outer points is measured. The distance between the points must be 91 ± 2 mm, then the distance between the outer and middle points on the left and right sides, which must be half of a total length of 95.5 ± 1 mm, has to be checked. If the measured values are not the same, then the numeric value must be set to "+" or "−" in Service mode under the "Y Axis zero EVO" parameter. The test recording is performed again by surveying the new value and the process is repeated until the moment when they receive the correct values shown in Fig. 7.

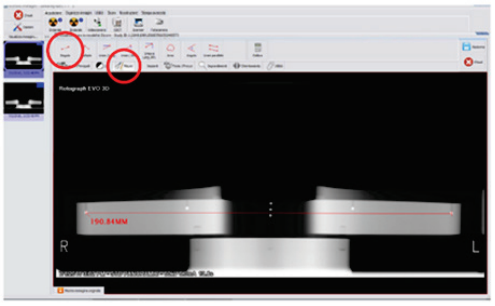

Figure 7 Phantom calibration tool capture and metered points

Entering the Dental Studio software, the "CBCT" application to capture the 3D full volume format will be launched. The centring tool is mounted on the chin carrier, the parameters 66 kV – 6 mA are adjusted and the recording is performed. A portion of the device with the 3D sensor rotates around the 360° tool and the shoot appears on the screen as shown in Fig. 8.

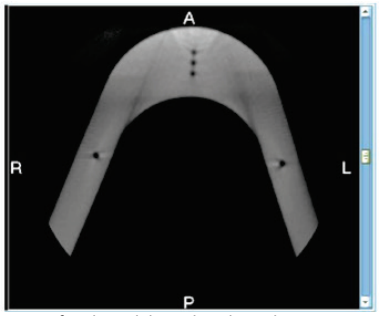

Figure 8 3D images of tools and the point where the measurements are taken

If the portliness is not correct, it is necessary to set the lateral displacement. In order for the portliness to be correct and not to overlap, adjust the parameters according to the instructions in the Service Manual.

4.4.3 Partial Volume Calibration

Partial volume calibration adjusts the mandibular volume (jaw volume). The 3D sensor is selected in the Dental Studio software, then we set the centring tool, the kV and mA settings are adjusted and the mandibular recording on the touch screen is displayed in Fig. 9.

Turn on the "Exam" button and follow the data transfer. Recording tools are read on the screen (Fig. 10) and if necessary, any irregularities are corrected.

In the next step (Fig. 11), the 3D volume of the sinus is recorded.

Any irregularities are re-detected and a corrective procedure is carried out.

Figure 9 Display of a mandibular hinge on the touch screen

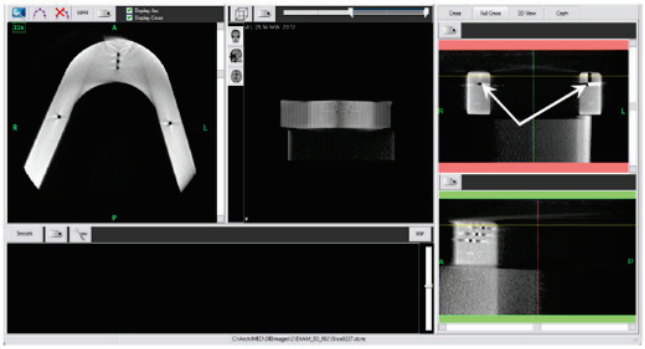

Figure 10 Jaw volume (mandibular) 3D view

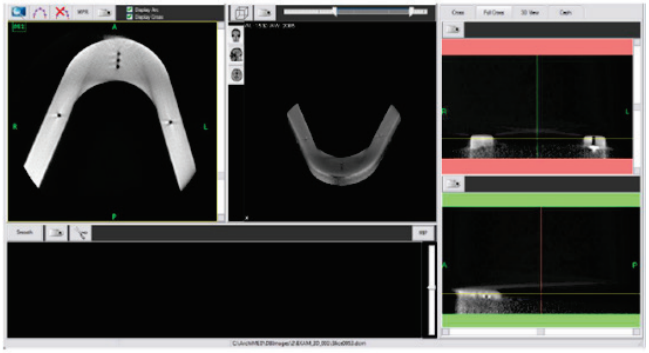

Figure 11 Volume of sinus 3D view, fantasy test

4.4.4 Calibration of the CEPH ARM (2D Head Recording Sensor)

The 2D sensor calibration is also done in the Dental studio software. "CEPH ARM" mode is selected, the kV and mA values are set and the test mode is performed for the X-ray recording. Fig. 12 shows the calibration of 2D sensors using a special phantom head tool.

Figure 12 Calibration of 2D sensors using the head phantom

Vertical earrings are set so that the X-rays must pass through both earrings. Make the exam recording, and if you do not match the two earrings or if they are not symmetrical, the position of the holder is not correct and it is necessary to make a correction as instructed by the Service Manual. Adjusting the collimator (air beam adjustment) is done using the centring tool and the sensor centring software on the computer. Then the X-ray button (exam) is pressed and it visually detects an irregularity if it exists. The line must be vertical with the slot. Entering the service mode for setting the secondary collimator, a recording with the default parameters is performed (60 kV – 6 mA - 0.5 s), and it measures the distance between the canter of the earring and the soft tissue filter. The distance must be about 50 mm.

4.4.5 Setting Parameters of the kV and mA Values

Parameter values can be set on the touch screen or on the computer. The automatic exposure mode (mAs) is adjusted according to the tables in the service documentation.

4.4.6 Touchscreen Calibration

To calibrate the touch screen, a USB memory stick is used, which is inserted in the space provided on the panel. On the main switch, the device is turned on to start the calibration process. The calibration ending is displayed on the touch screen. The device is switched off and then on and the system is ready for operation after it is powered up.

Table 1 The most common causes of the problem with the Rotograph Evo 3D

No.	Causes of work difficulties	Percentage of failures%	Cumulatively
1.	Improper parameterization of kW / mA	40,8	40,8
2.	Computer error	34,4	75,2
3.	X-ray switch button	5,5	81,7
4.	Fuse failure due to voltage oscillation	5,2	85,9
5.	The zero position of the optical rotation sensor	4,1	90
6.	Faulty rails for lifting column	2,9	93,3
7.	Faulty cables	3,3	95,6
8.	Faulty electronics	2,2	98,4
9.	The zero position of the optical rotation sensor	1,4	99,8
10.	Faulty lamp x-tube	0,2	100
Total		100	

5 ROTHOGRAPH EVO 3D REMOVAL OF THE LATEST DAMAGE IN THE WORK OF THE DEVICE

5.1 Analysis of the Most Common Errors in the Work

After installing and putting the device into use, all the data on the problems that have disturbed the normal function of the device are recorded. The dental medicine device Rothograph Evo 3D appeared in the world market in 2009 and it has been technologically upgraded and adapted to the needs and requirements of the users based on user information. The Priority Method (Pareto) analysed the 10 most common causes, i.e. difficulties in the operation of the device mentioned. Tab. 1 shows the causes of difficulty in

the percentage by which the cumulative is obtained. According to the presented table, it is apparent that the first two problems cause almost 80% of the total difficulties of the analysed samples [3].

The diagram shows the frequency of common faults in the operation of the unit (Fig. 13).

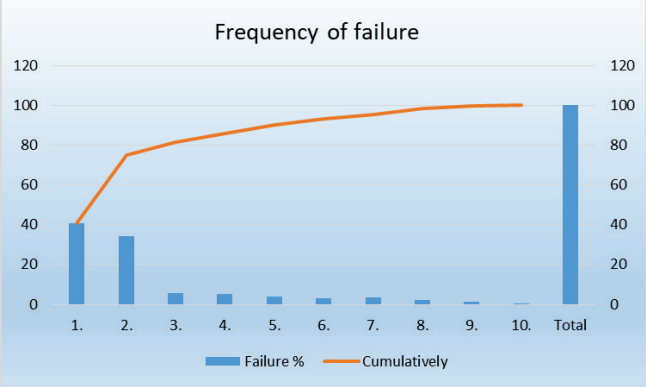

Figure 13 Frequency of malfunctions on the device

The most common cause of malfunctions on the device lies in the incorrect parameterisation and incorrect data entry into the computer by the operator or user of the device.

5.2 Analysis of the Causes of the Above Mentioned Errors

The most common errors in the work on the Rothograph Evo3D will be the analysis of the causes of the error.

Table 2 Description of the cause of the error

No.	FAILURE	DESCRIPTION OF FAILURE
1.	Low quality picture	Incorrectly set parameters kV and mA, incorrect positioning of the patient, improper handling.
2.	Computer error	Incorrect computer, insufficient knowledge of software work, error in communication with the processor, cable problem.
3.	Does not operate the exposure button	Wrench wear, broken button, or defective cable.
4.	The device does not work	Faulty power cable, safety fuse burner, rectifier or module error, PCB board.
5.	Incorrect position sensor	Faulty sensor, improper position of the home position, mechanical damage, motor, PCB board.
6.	The vertical column is not lifted	Roughing of the toothed guide rail, defective engine, PCB board.

According to Tab. 2, the cause of the failure of the device is mostly the same, but there is more to it that requires a good understanding of the operation of the device and the device itself and the experience of the servicer to eliminate the existing problem.

6 DEFINING THE ROTHOGRAPH EVO 3D PREVENTIVE MAINTENANCE PROCEDURES

6.1 Defining Preventive Maintenance Procedures

Based on the conducted analysis, procedures and activities related to the basic maintenance, periodic and control examinations [3-5] are defined (Tab. 3).

Table 3 Activities when viewing the device

Activities	Check review	Periodic review	Basic maintenance
1.Visual view of the devices	●	●	●
2. Outbreaks of external damage (radiation)	●	●	●
3. Installation on the drive parts	●	●	●
4. External cables	●		●
5. Interior cables and wires		●	
6. The stability of the device (wall and floor)	●		●
7. Electricity and lubrication of sliding circuits		●	
8. Lightness indicator light		●	
9. Exposure Parameter Check (kV, mA)		●	
10. Laser Positioning Easy		●	
11. Positioning the 3D Sensor (Calibration)		●	
12. Positioning 2D Sensors (Calibration)		●	
13. Positioning the collimator		●	
14. Sensor Rotation Check		●	●
15. Vertical column lifting	●	●	●
16. X-ray tube control		●	
17. Computer and software control (operating mode)	●	●	●

6.2 Investigating the Frequency of Periodic Reviews

The frequency of periodic inspection and the variants of preventive maintenance for this device, research and calculation of the optimum period of the implementation of preventive examinations [1, 3] was performed.

The essence of the calculation is to determine the momentum and time interval between performing the preventive inspection in order to determine the moment of failure, so that the maximum relative error, made therein, will be a constant at any control. The periodicity is determined without a major error by the most critical part or whole.

The fault of a critical entity is an event that occurs when any of its elements come out of a predefined domain of the working characteristics, Fig. 14.

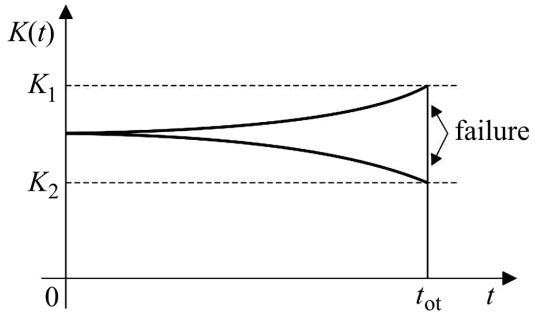

Figure 14 Exit key circuit characteristics from the specification boundary

In Fig. 14, the symbols have the following meanings: t - the operating time of the device; t_{ot} - moment of failure; K - vital characteristic of the most critical entity as a function of the time of use; K_1 and K_2 - the limit of the vital characteristics of the most critical unit of the device that tolerates the change.

From the Fig. 14 it arises, in order to determine as accurately as possible the moment of occurrence of failure, that it is necessary to constantly measure the vital feature of

the most critical of the whole device. However, this is very rarely done in practical work. Much more cases that are frequent are to check the critical entity from time to time and to ascertain whether a critical failure has occurred.

In this case, the actual moment of failure is transformed into a moment of preventive examination. It is understood that such a procedure of determining the time of performing a preventive examination makes a minor or greater mistake, because a critical condition could have occurred immediately before the examination, and much earlier, i.e. immediately after the last review.

The essence of the calculation is to define the time schedules of the inspection so that the maximum relative error of determining the exact failure time remains constant at any inspection.

If on some preventive inspection, a fault was identified on the critical entity (Fig. 15), it means that it will be declared that the critical entity has cancelled you at the time. However, the moment of the real failure of the fault lies somewhere between t_i and Δt_i.

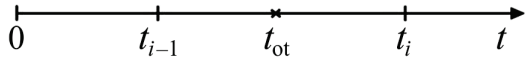

Figure 15 Determining failure on preventive inspection

Mathematical calculations lead to the formula for the first time of performing a preventive examination or the following expression to calculate check-ups.

$$t_i = K_\varepsilon(i) \cdot m_0 \quad (1)$$

$$\Delta t_i = K_\varepsilon^*(i) \cdot m_0 \quad (2)$$

Where: t_i - the time of the first preventive examination (hour); Δt_i - time of the next review (hour); K_ε and K_ε^* - maximum relative error coefficients; m_0 - presumed medium value to failure (hour).

To determine the momentum of the time t_i, when to do the first preventive inspection and at what intervals of time Δt_i, it is necessary to adopt the value of the maximum relative error and the medium value to the fault m_0.

Fig. 16 shows the graph of the coefficient K_ε and K_ε^* for some values of the serial number of the preventive examination (i), and $\varepsilon = 0.10$, $\varepsilon = 0.20$ and 0.30.

The numerical values of the coefficient K_ε and K_ε^* can be calculated for some values of the ordinal number of the preventive review (i), and for the different values of the maximum relative error.

It should be noted that after calculating the values for t_i and Δt_i it is necessary to perform optimization and correction, and than adjust time to real situation. There may also be more errors in the budget if it is adopted by a large value of the maximum relative error and the average error time. Therefore, for the application of this calculation, it is necessary to know the good operation of the device and to have a good theoretical basis for its application.

For specific application, it is necessary to adopt the values of the maximum relative error and to know the mean time to failure. For example, if $\varepsilon = 0.30$ is known and the median time for a failure is 3 years (based on the data from exploitation), t_i and Δt_i can be calculated.

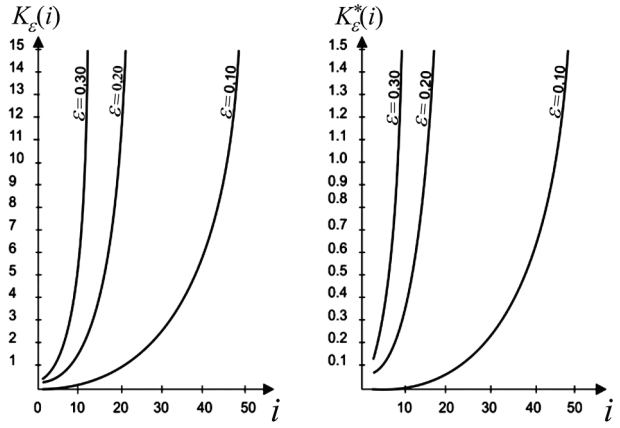

Figure 16 The graph of the coefficient and for some values of the serial number of the preventive review (i), and $\varepsilon = 0.10$, $\varepsilon = 0.20$ and 0.30.

Numerical values for t_i and Δt_i are calculated on the basis of the Eq. (1), and the results are shown in Tab. 4.

Table 4 Numerical values for t_i and Δt_i

I	t_i		Δt_i	
	hours	days	hours	days
1	7884	328.50	2365	98.55
2	11263	469.29	3379	140.79
3	16090	670.41	4827	201.12
4	22985	957.73	6896	287.32
5	32836	1368.18	9851	410,45
6	46909	1954.54	14073	586.36
7	67013	2792.20	20104	837.66
8	95733	3988.86	28720	1196.66
9	136761	5698.38	41028	1709.51
10	195373	8140.54	58612	2442.16

Based on the data from the table, it can be concluded that the first preventive review of the critical entity or the device after being put into use should be performed after 328 days of exploitation, the other after 141 days, the third after 201 days, etc. Due to the simplicity of planning the preventive examinations, and following the maximum admissible values m_0, the following preventive inspection times can be adopted, as shown in Tab. 5.

Table 5 Moments of review

MOMENTS OF REVIEW				
t_0	t_1	t_2	t_3	t_4
months				
0	12	6	6	12

The second method for determining the periodicity of conducting preventive examinations is based on knowing the data from the exploitation of the device in practice. The essence is to know the values of the intensity of the unit malfunction and the average duration of one preventive examination.

If these data are known, then the time of the preventive review can be calculated according to the formula:

$$P_{pp} = \sqrt{\frac{2T_{pp}}{\lambda_{p0}}} \tag{3}$$

Where: λ_{p0} - intensity of system failures (failure/h); T_{pp} - average duration of one preventive examination (h).

The term P_{pp} graphically shows Fig. 17 for some parameter ranges.

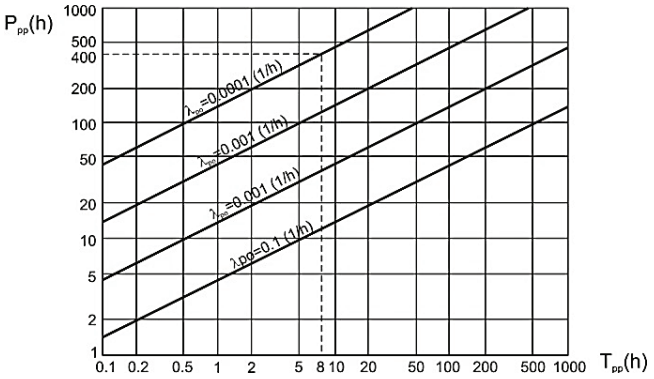

Figure 17 Graphic representation for calculating the periodicity of a preventive examination

For example, a concrete medical device can be taken in exploitation that has the intensity of gradual failures

λ_{p0} = 0.0001 failure/h. It is necessary to determine the optimal period of preventive examinations, which last an average of 8 hours.

From the graphical display, read P_{pp} = 400 hours. The same result is obtained by computing using the expression for optimal periodicity. These results should be commented on. It should be noted that the scope of the preventive review is evaluated over the average time of the execution of a preventive examination, which is closely related to the choice of operations being carried out. This depends on the number of parameters of the device to be controlled, the scope of the disconnection for checking, the metering methods, the control-measuring equipment, the benefits of the metering system or diagnosis, etc. In addition, this method optimizes the maintenance period only from the point of view of a gradual defect, which can be detected by control. A gradual malfunction occurs when some parameter of the device changes gradually from the permissible limits. This entails the need for adjusting or replacing the elements - a cause of a gradual failure. It is clear that preventive action can not affect the occurrence of current malfunctions.

All the operations that make the content of the preventive review should be systematized and grouped for a particular device, paying attention to limitations (maximum time of a preventive review, equipment, personnel qualifications, space, etc.). From such grouped actions, the average time of the preventive examination can be estimated or determined.

In this way, the periodicity of performing a preventive examination is impractical and inoperative, and planning on it would be complex. However, it is the basis for determining the rules on the periodicity of the review.

Actual periodicity comes from estimating and rounding calculation values (always taking into account the experience with such or similar systems) by following the following principles:

- a large number of related devices should have the same periodicity (easier planning, execution, and review control),
- the periodicity has to be determined specifically for devices in continuous work, in occasional work and guarding,
- if the reliability of the device cannot be affected during a preventive review, a review is required only for insight into the condition.

The process of determining the periodicity of a review is an interactive process, and at each stage, it can be repeated and reviewed and the scope of the review can be changed, and thus the viewing time can be changed. The ultimate goal is achieved when objectives with minimal costs, simple planning and maximum reliability of the system are satisfied, all under the conditions and limits.

7 CONCLUSIONS

Maintaining medical devices and technical systems in general is today unimaginable without the use of preventive maintenance methods and in particular the maintenance of the state and the use of modern diagnostic procedures and diagnostic equipment. For these reasons, during the design and development of new devices, designers and constructors require that the development of diagnostic equipment is installed or specifically supplied with medical devices.

This ensures the convenience of the service system and its greater availability and reliability, i.e. increases its overall quality and increases the customer's satisfaction and the satisfaction of the people responsible for its service and maintenance. All this requires the operator's and the maintenance service's enviable technical knowledge, and it also requires from the employers to invest in the procurement of adequate diagnostic equipment and training.

Combined with other preventive methods in maintaining the technical systems, the maintenance based on the state of controlled features has no alternative.

8 REFERENCES

[1] Kondić, Ž., Čikić, A., & Kondić, V. (2013). *Osnove održavanja mehatroničkih sustava 1*, VTŠ, Bjelovar. (in Croatian)

[2] Kondić, Ž., Samardžić, I., Maglić, L., & Čikić, A. (2011). *Pouzdanost industrijskih postrojenja*, Sveučilište Josipa Juraja Strossmayera u Osijeku, Strojarski fakultet u Slavonskom Brodu, Slavonski Brod. (in Croatian)

[3] Pongrac, D. (2017). Održavanje uređaja za računalnu tomografiju "Rotograph Evo 3D". Završni rad br. 353/TGL/2017, Varaždin. (in Croatian)

[4] Villa Sistemi Medicali S.p.A. (2013). *User manual*. Rotograph EVO 3D. Milano, Italija.

[5] Villa Sistemi Medicali, S.p.A. (2013). *Service manual*. Rotograf EVO 3D. Milano, Italija.

Authors' contacts:

Dalibor PONGRAC
University North,
Jurja Križanića 31b, 42000 Varazdin, Croatia
dalibor.pongrac@gmail.com

Živko KONDIĆ
University North,
Jurja Križanića 31b, 42000 Varazdin, Croatia
zkondic@unin.hr

Veljko KONDIĆ
University North,
Jurja Križanića 31b, 42000 Varazdin, Croatia
vkondic@unin.hr

Marko HORVAT
University North,
Jurja Križanića 31b, 42000 Varazdin, Croatia
mhorvat@unin.hr

ISSN 1846-6168 (Print), ISSN 1848-5588 (Online)
https://doi.org/10.31803/tg-20190421134423

Professional paper

THE EQUIPMENT FOR DETERMINING THE IMPACT OF TRAFFIC ENVIRONMENT ON ROAD PAVEMENT

Iryna SOLONENKO

Abstract: The article presents the classification of equipment developed by the author for the research of the operational characteristics of road pavement. The equipment was classified according to the following criteria: type of equipment; type of contact element; mode of interaction with the supporting surface; type of fixture of the suspension element; number of contact elements; sample type; type of load. For illustrations, the classification of the most common equipment was carried out. The research was conducted to compare and select the most rational equipment to study the effect of traffic environment on the road pavement. The research was carried out by the multi-criteria analysis. Based on the conducted research, the most rational installations for conducting experiments were determined.

Keywords: classification; installation; load; multi-criteria analysis; road pavement; traffic environment; wheel

1 INTRODUCTION

The condition of roads is mainly determined by the quality of the road pavement. Basically, the road pavement is influenced by:

- the traffic environment, which depends on the intensity and the combination of vehicles;
- the climatic conditions determined by the location of the examined length of the road (temperature, humidity).

A moving traffic environment, acting on the road pavement, causes various types of defects (wear-at, abrasion, formation of plastic crack, chipping, peeling, etc.) [1-3]. The reason behind the formation of defects depends on the properties of the road pavement materials, the design features of the wheel running gear of cars and the speed of traffic.

The most widespread roads are with a pavement of cement concrete and asphalt concrete. Each of the examined materials of the pavement has its own type of wear and tear. On asphalt, over time, due to the usage of pavements, rutting (plastic deformation of the covering caused by the impact of the wheel) appears on roads.

Rutting leads to a decrease in vehicle traffic safety and impairs vehicle handling (Fig. 1a and 1b) [2, 4].

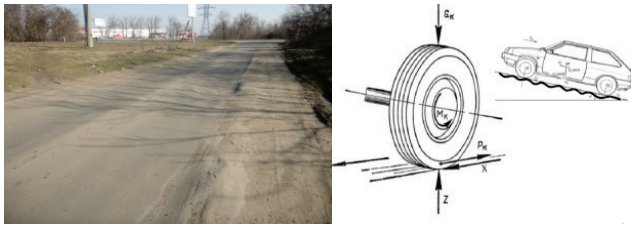

a) b)

Figure 1 Rut on the road: a) the rut on the road; b) wheel action on the road pavement

On roads with asphalt concrete, there are other types of deformations for road pavement: waviness (occurs because of the longitudinal deformations of the road pavement); cracks; pits (caused by vertical deformations of the road pavement).

For hard road surface (cement concrete), the most typical types of wear are: chipping, peeling (caused by the effect of the freeze-thaw temperature); abrasion (occurs to the abrasive effect of the wheels).

2 RESULTS AND DISCUSSION

The study of the influence of the impact of wheel running gear on the road pavement is most often carried out on installations and devices that create dynamic effects on the material pavement. As a rule, these are: laboratory, testing bench, full-size.

Analysis of works [1-13] showed that there is currently no classification for this type of equipment.

The purpose of the research was to develop a classification of equipment that is used to study the effect of transport on road pavements.

To achieve the above-mentioned purposes, the following **problems were resolved**:

- to propose a block diagram of classifications;
- to propose a methodology for the use of classifications;
- to conduct a multi-criteria analysis of the existing stands and equipment;
- to develop a criterion for assessing the properties of the equipment;
- to develop a rating scale of the equipment;
- to develop recommendations for the selection of rational equipment.

In the paper, a classification for the equipment presented in Tab. 1 is proposed. The classification is carried out according to the following criteria: type of equipment; type of contact element; mode of interaction with the supporting surface; type of attachment of the suspension element; number of contact elements; sample type; type of load. Each criterion is divided into classes: With the sample heating; Without the sample heating; Mobile; Rotative; Landfills;

Natural; Flat contact element; Wheel non-deformable; Wheel elastic; The wheel to which the torque is applied; Wheel that is free to roll; Not flexible; Moving translational, Moving rotational, Free, One, Two, More than two; Cuboid, Cylinder, Cuboid and Cylinder; Vertical, Vertical + Horizontal, Vertical + Horizontal + Centrifugal.

Table 1 Classification of the equipment for the study of the operational characteristics of road pavements

No.	Classification of the equipment by signs	Classes of signs
I	TYPE OF EQUIPMENT	
I_1	Laboratory	
I_{12}		With the sample heating
I_{13}		Without the sample heating
I_2	Test-bench	
I_{21}		Mobile
I_{22}		Rotative
I_3	Full-scale	
I_{31}		Landfills
I_{32}		Natural
II	TYPE OF CONTACT ELEMENT	
II_1		Flat contact element
II_2		Wheel non-deformable
II_3		Wheel elastic
III	MODE OF INTERACTION WITH THE MOUNTING SURFACE	
III_1		The wheel to which the torque is applied
III_2		Wheel that is free to roll
IV	TYPE OF ATTACHMENT OF THE SUSPENSION ELEMENT	
IV_1		Not flexible
IV_2		Moving translational
IV_3		Moving rotational
IV_4		Free spin
V	NUMBER OF CONTACT ELEMENTS	
V_1		One
V_2		Two
V_3		More than two
VI	SAMPLE TYPE	
VI_1		Cuboid
VI_2		Cylinder
VI_3		Cuboid and Cylinder
VII	TYPE OF LOAD	
VII_1		Vertical
VII_2		Vertical + Horizontal
VII_3		Vertical + Horizontal + Centrifugal

The combination of the criteria and classes allows you to describe the equipment that is being considered. Example:

$$I_1 + II_2 + III_2 + IV_2 + V_1 + VI_1 + VII_1,$$

Where: I_1 – laboratory; II_2 – wheel non-deformable; III_2 – wheel that is free to roll; IV_2 – the suspension is movable; V_1 – one contact element; VI_1 – the test sample has the form of a cuboid; VII_1 – the load that acts vertically on the contact element.

The examples of the classifications of the existing laboratory equipment are shown in Fig. 2.

Fig. 2 shows installations which have the following characteristics:

- The testing bench for assessing the rutting of the road pavement material - Wheel Tracking Device (Fig. 2a). The testing bench has: the speed of wheel contacts with a sample of pavement in one minute - 42, with a vertical load on the wheel of 520 N, the covering temperature is 60 °C, the pavement thickness is from 40 to 120 mm [2, 4].

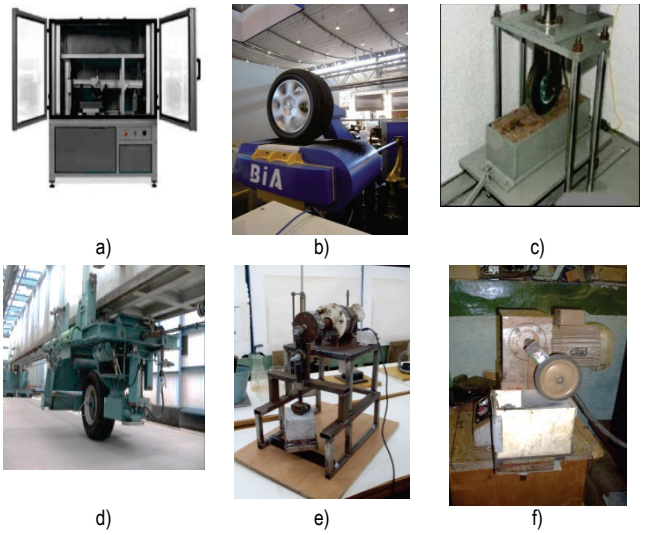

Figure 2 The name of the installation (formula by classifications): a) the testing bench Wheel Tracking Device ($I_1 + II_2 + III_2 + IV_2 + V_1 + VI_1 + VII_1$); b) the testing bench dynamometer BIA ($I13_3 + II_3 + III_1 + IV_1 + V_1 + VI_2 + VII_2$); c) the testing bench of the State Research Institute, Ukraine ($I_{13} + II_3 + III_2 + IV_2 + V_1 + VI_1 + VII_2$); d) one-wheeled installation Lintrack, Netherlands ($I13_3 + II_3 + III_1 + IV_2 + V_1 + VI_1 + VII_2$); e) developed the testing bench by the author BUSOL-1, Odessa, Ukraine ($I_{13} + II_1 + IV_2 + V_1 + VI_3 + VII_1$); f) the testing bench developed by the author BUSOL-2 ($I_{13} + II_3 + III_2 + IV_3 + V_1 + VI_3 + VII_2$)

- The testing bench - the dynamometer BIA, Tolyatti at the plant of LLC "Bia". The testing bench is designed to study the interaction of the vehicle suspension with the road pavement. For road pavement testing, the sample can be made in the form of a cylinder. The testing bench has a wheel load of 7 kN and a treadmill speed of up to 250 km/h (Fig. 2b) [14].
- Installation of the State Research Institute, Ukraine (Fig. 2c). The installation uses reciprocating movements of the tray with the road pavement material with a frequency of 48 passes per 1 minute (50 km/h) [2, 4].
- One-wheel installation Lintrack in the Netherlands. The installation has a wheel load from 15 to 100 kN and a speed of up to 20 km/h (Fig. 2d)) [4].
- The author has developed the testing benches BUSOL-1 and BUSOL-2 (Fig. 2e and 2f) [5]. The testing benches are designed to assess the abrasion and deformation of the road pavement of various types, both in the dry and wet state.

Due to the mobile test benches, research of the physicomechanical and operational characteristics of the road on any of its parts (Fig. 3a) [2, 4] can be conducted.

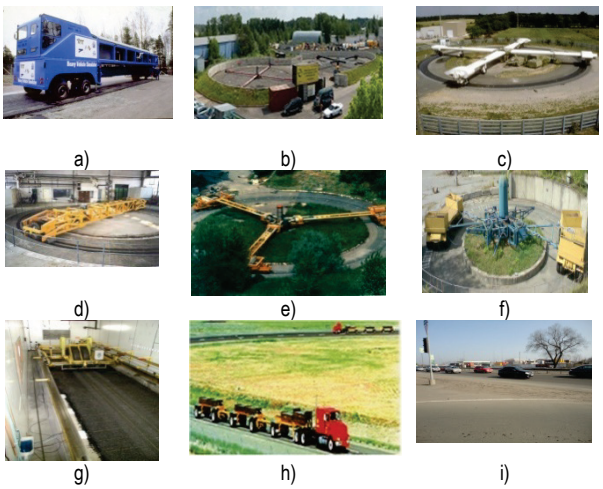

Figure 3 Installations for pavement research: a) The mobile test benches HVS- Mark IV, USA (I_{21} + II_3 + III_1 + IV_2 + V_1+ VI_1 + VII_1); b) The one-wheeled vehicle "Carousel" MADI, Moscow, Russia (I_{22} + II_3 + III_2 + IV_3 + V_3+ VI_1 + VII_2); c) The four-wheeled installation LCPC, France (I_{22} + II_3 + III_1 + IV_2 + V_3+ VI_1 + VII_2); d) The two-wheeled installation in Romania, the city of Iasi (I_{22} + II_3 + III_2 + IV_2 + V_3+ VI_1 + VII_2); e) The two-wheeled installation Vuis-Cestu, Slovakia (I_{22} + II_3 + III_1 + IV_2 + V_3+ VI_1 + VII_2); f) The circular testing bench in Kiev, Ukraine (I_{22} + II_3 + III_1 + IV_2 + V_3+ VI_1 + VII_2); g) The two-wheeled installation Danish Road Testing Machine, Denmark (I_{13} + II_3 + III_1 + IV_2 + V_1+ VI_1 + VII_2); h) The landfills MinRoad, USA (I_{31} + II_3 + IV_4 + V_3+ VI_1 + VII_3); i) The road pavement testing in full-scale conditions (I_{31} + II_3 + IV_4+ V_3 + VI_1 + VII_2)

The use of full-size installations allows a more adequate assessment of the impact of traffic environment on road pavement. They are performed in the form of a rotating installation. Let us examine some of them:

- The one-wheeled installation KUIDM-2 "Carousel" in Moscow, Russia provides a speed of up to 80 km/h (Fig. 3b).
- The four-wheeled rotating installation Laboratoire Central des Ponts and Chaussees (LCPC) was made in France. The installation has: a diameter of rotation of 30 and 40 m; a wheel load of up to 75 kN; the maximum speed of movement of up to 105 km/h (Fig. 3c).
- The two-wheeled installation in Iasi, Romania (Fig. 3d).
- The two-wheeled installation Vuis-Cestu in Slovakia. The installation has: a diameter 32 m; a wheel speed of up to 50 km/h (Fig. 3e).
- The circular testing bench in Kiev, Ukraine. The installation has: a wheel load of up to 75 kN, a wheel speed of up to 40 km/h (Fig. 3f).
- The two-wheeled installation Danish Road Testing Machine (DRTM). The unit has: a wheel load of up to 65 kN; a speed of up to 30 km/h (Fig. 3g).

Apart from the rotating testing bench for the research of the properties of road pavement, test landfills with heavy equipment can be used (Fig. 3h), and testing can be carried out in full-scale conditions (Fig. 3i).

The installations that were shown in the Figs. 2 and 3 were evaluated according to the following criteria: the equipment cost; the research cost; the need for control from the operator's side; the maintenance and repair costs; the price of manufacture and installation of the sample; the ease of use; the measured parameters; the number of the types of coverage; the regulation of sample tests conditions; the protection from environmental exposure; the wheel speed; the cycling of the load.

For the ease of comparison of the testing bench and the installations for each of the criteria, appropriate comparison scales were developed (Tab. 2).

The coded values, descriptions of the testing bench and installations researched in the work are presented in Tab. 3.

Table 2 Criteria and scale rating criteria

No.	Criterion	←the worse Comparison scale the best →				
		1	2	3	4	5
1	The equipment cost	very high	high	medium	low	insignificant
2	The research cost	very high	high	medium	low	insignificant
3	The need for control from the operator's side	two or more people	constant	periodic	start and end of the experience	not required
4	The maintenance and repair costs	very high	high	medium	low	insignificant
5	The price of the manufacture and installation of the sample	very high	high	medium	low	insignificant
6	The ease of use	very low	low	average	high	very high
7	The measured parameters	one	two	three	four	five or more
8	The number of the types of pavement*	one	two	three	four	five or more
9	The regulation of sample tests conditions	unregulated	depending on the environment	temperature change	temperature and humidity	temperature, humidity and contact pressure
10	The protection from environmental exposure	none	from precipitation	partially	in a heated laboratory space	completely
11	The wheel speed	missing	low	medium up to 50 km/h	high 50 km/h and more	very high more than 100 km/h
12	The cycling of the load	there are no 10	low 10-20	average 20-50	high 50-100	very high

one - non-rigid; two - non-rigid, rigid; three - H, R, pavement; four - H, R, P, ground pavement; five - H, R, P, G, paving elements, etc.

The comparison of testing benches and installations were carried out by the method of expert assessments, the results are shown in Tab. 4. The data obtained in Tab. 4 are graphically represented in Fig. 4.

As it was shown by the results of the research presented in Tab. 4 (Fig. 4), the most rational equipment for determining the impact of traffic environment on the road pavement is:

- The laboratory equipment: the Wheel Tracking Device (Fig. 4a); the State Research Institute, Ukraine (Fig. 4b); BUSOL-1, Ukraine (Fig. 4k); м) BUSOL-2 (Fig. 4l).
- The testing bench equipment: the mobile test benches HVS- Mark IV, USA (Fig. 4d); the one-wheeled vehicle "Carousel", Russia (Fig. 4f);
- The natural research: the road pavement testing in full-scale conditions, Odessa, Ukraine (Fig. 4j).

For the first of the installations examined, the disadvantage is the need for the heating of the sample of the material that is being tested. Such installation cannot be used for other types of coverage.

Table 3 The compared testing bench and installations

No.	Formulas of the testing bench and installations	Name of the testing bench and installations
1	$I_{12} + II_2 + III_2 + IV_2 + V_1 + VI_1 + VII_1$	The Wheel Tracking Device, EU (Fig. 2a)
2	$I_{13} + II_3 + III_2 + IV_2 + V_1 + VI_1 + VII_2$	The State Research Institute, Ukraine (Fig. 2f)
3	$I_{12} + II_3 + III_1 + IV_1 + V_1 + VI_2 + VII_2$	The dynamometer stand BIA, Russia (Fig. 2b)
4	$I_{21} + II_3 + III_1 + IV_2 + V_1 + VI_1 + VII_1$	The mobile test benches HVS-Mark IV, USA (Fig. 2a)
5	$I_{13} + II_3 + III_1 + IV_2 + V_1 + VI_1 + VII_2$	The one-wheeled installation Lintrack, Netherlands (Fig. 2d)
6	$I_{22} + II_3 + III_2 + IV_3 + V_3 + VI_1 + VII_2$	The one-wheeled vehicle "Carousel", Russia (Fig. 2b)
7	$I_{22} + II_3 + III_1 + IV_2 + V_3 + VI_1 + VII_2$	The four-wheeled installation LCPC, France (Fig. 2c)
8	$I_{22} + II_3 + III_1 + IV_2 + V_3 + VI_1 + VII_2$	The circular testing bench, Ukraine (Fig. 2f)
9	$I_{31} + II_3 + IV_4 + V_3 + VI_1 + VII_3$	The landfills MinRoad, USA (Fig. 2h)
10	$I_{31} + II_3 + IV_4 + V_3 + VI_1 + VII_2$	The road pavement testing in full-scale conditions (Fig. 2i)
11	$I_{13} + II_1 + IV_2 + V_1 + VI_3 + VII_1$	BUSOL-1, Ukraine (Fig. 2e)
12	$I_{13} + II_3 + III_2 + IV_3 + V_1 + VI_3 + VII_2$	BUSOL-2, Ukraine (Fig. 2f)

Table 4 The comparison of the testing benches and installations

The criterion	1	2	3	4	5	6	7	8	9	10	11	12
The equipment cost	5	3	2	2	4	2	1	2	1	3	5	5
The research cost	4	5	3	3	4	2	1	2	1	4	5	5
The need for control	3	4	2	2	3	2	1	1	1	3	4	4
The maintenance and repair costs	4	4	3	3	3	2	1	2	1	4	4	5
The price of the manufacture and installation of the sample	5	4	3	2	3	2	1	2	1	3	5	5
The ease of use	4	3	4	2	4	3	2	2	3	3	4	5
The measured parameters	5	3	3	4	4	3	2	2	2	5	4	5
The number of the types of pavement*	1	2	2	5	2	2	3	2	3	5	3	4
The regulation of sample tests conditions	4	4	3	2	3	1	1	1	1	1	4	5
The protection from environmental exposure	5	5	5	2	5	1	1	1	1	1	5	5
The wheel speed	3	3	5	3	2	5	5	1	3	5	3	4
The cycling of the load	3	3	5	3	3	4	4	4	5	4	3	5

The installation of the State Scientific Research Institute, Ukraine (Fig. 4b) is deprived of the disadvantages of the above mentioned equipment. The disadvantage of this installation is the low speed of movement of the chute with a sample of material. The equipment BUSOL-1 (Fig. 4b), BUSOL-2 (Fig. 4l) is deprived of the drawbacks of the installations that were examined earlier. Due to it, it is possible to explore samples of asphalt, cement concrete and other types of road pavement. For the experiments, samples of cubic and cylindrical shapes can be used. The samples can be tested dry and wet.

The examined rotating installation (Fig. 4f) provides a speed of up to 50 km/h. The disadvantage of this installation is: very large, occupied space; the high cost of research; the insufficient speed for modeling the interaction of the wheel and the coverage on highways; influence of climatic conditions.

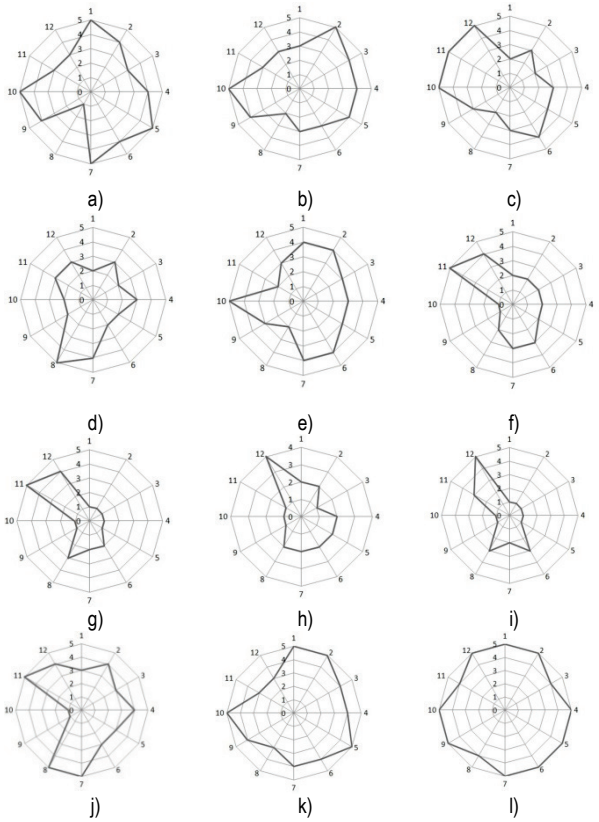

Figure 4 Multicriteria diagrams equipment:
a) The Wheel Tracking Device, EU; b) The State Research Institute, Ukraine; c) The dynamometer stand BIA, Russia; d) The mobile test benches HVS-Mark IV, USA; e) The one-wheeled installation Lintrack, Netherlands; f) The one-wheeled vehicle KUIDM-2 "Carousel", Russia; g) The four-wheeled installation LCPC, France; h) The circular testing bench, Ukraine; i) The landfills MinRoad, USA; j) The road pavement testing in full-scale conditions, Ukraine; k) BUSOL-1, Ukraine; l) BUSOL-2, Ukraine

For a field study (Fig. 4j), the shares should have devices that provide for the number of vehicles: its type, the speed of moving and load on the wheel. The disadvantage of this research is: the inability to control the speed and intensity of the traffic environment; the influence of climatic conditions.

3 CONCLUSIONS

The concluded research enabled the following:

- to offer a classification of equipment for the research of the operational characteristics of road pavements;
- to conduct a multi-criterion analysis of the existing testing benches and installations intended for the study of the road pavement material;
- Based on a multi-criteria analysis, it was recommended to use the following equipment in the scientific and engineering practice: the Wheel Tracking Device; the testing bench of the State Research Institute, BUSOL-1, BUSOL-2; HVS-Mark IV, KUIDM-2 "Carousel" and field study on road pavement.

The use of the considered equipment will significantly reduce the cost and time to conduct research.

4 REFERENCES

[1] Vasiliev, A. P., et al. (2004). Repair and maintenance of highways: Road builder's reference encyclopedia. T. 2. - M.: Informavtodor, p. 507.

[2] Mozgovoy, V. V., Onishchenko, A. N., Prudky, A. V., Kutsman, A. M., Zhukov, A. A., Olkhovy,i B. N., et al. (2010). Experimental evaluation of the stability of asphalt concrete pavement to the formation of rut. *Road machinery*. St. Petersburg, 114-128.

[3] Golovko, S. K., Babinets, A. D., & Fosch, I. V. (2004). Modern approach to the study of the formation of abrasion in asphalt concrete pavements. *Roads and Bridges*, 2, 115-123.

[4] Mozgovoy, V. V., Onishchenko, A. M., Prudky, O. V., Kutsman, O. M., Nevinglovskiy, V. F., et al. (2010). Testing of road constructions on a ring stand - successes, problems, perspectives (part 2). Roadster of Ukraine. *Scientific and Production Magazine, 216*(4), 24-31.

[5] Solonenko, I. P. (2012). Road quality assessment. *Third Scientific and Practical Conference of Young Scientists and Students, ODATRA*, Odessa, Ukraine, 217-220.

[6] Vasilyev, Y. E., Ivachev, A. V., & Bratischev, I. S. (2014). Study of the stability of road construction materials to wear gauge in conditions close to operational. *The Internet Journal "SCIENCE" Release, 24*(5), 1-14. Access mode: http://naukovedenie.ru

[7] Bugaev, S.V. & Solonenko, I. P. (2010). Determination of the change in the mass of the material sample by the amount of volume loss. *Vestnik OGASA*, 39, 50-58.

[8] Solonenko, I. (2019). Coating materials for bike paths. *All-Russian every-month branch magazine "Construction: New technologists - new equipment"*, 1, 32-39.

[9] Solonenko, I. P. (2015). Ensuring performance coatings of concrete for roads, due to their modifications. *Meriding ingineresc, 57*(2), 38-40.

[10] Solonenko, I. P. & Bugaev, S. V. (2017). Determination of the state of a bearing assembly using remote measurement of its heating temperature. *Proceedings of Azerbaijan State Marine Academy*, 2, 171-175.

[11] Solonenko, I. (2016). Influence on the quality of rigid road cover of additives and fillers. *Scientific and technical collection "Automobile roads and road construction"*, 98, 268-278.

[12] Solonenko, I. (2014). Cementno betonski cestovni kolnici. *Tehnički glasnik, 8*(1), 45-47.

[13] Solonenko, I. (2017). Use of cement concrete as a coating for small airfields, heliports and access roads. *XIII International Scientific and Technical Conference "AVIA-2017", NAU*, Kyiv, 23.46-23.50.

[14] Dynamometer with six degrees of freedom. Access mode: http://bia.ru.com/automotive/car-dynamic/6-dof-dynamometer/

Author contacts:

Iryna SOLONENKO, PhD, Head Teacher
Odessa State Academy of Civil Engineering and Architecture,
Ukraine, 65029 Odessa, Didrikhsona St. 4
Tel./Fax: +380974666579
E-mail: odarina08@rambler.ru

ISSN 1846-6168 (Print), ISSN 1848-5588 (Online)
https://doi.org/10.31803/tg-20190503183526

Professional paper

DESIGN AND CALCULATION OF PLANETARY TRANSMISSION WITH BEVEL GEARS

Ivan SABO, Milan KLJAJIN, Mirko KARAKAŠIĆ, Željko IVANDIĆ

Abstract: In this paper, the design and calculation of planetary transmission with bevel gears for road vehicles is presented. It must transfer power to the wheels with the possibility that wheels can rotate at different speeds. The basic calculation of transmission is performed for the drive machine, where an internal combustion engine is chosen, and for the driven machine, which is a car, all forces of resistance are calculated so that the transmission needs to be overcome to move the car. Based on the standard ISO 23509:2016 norm, the calculation of geometry is performed for the input gear pair and it is defined as a hypoid gear pair. For the planetary transmission, a calculation of gear module for bevel gears is first performed, and after that, the geometry is calculated. The calculation of the stress for root stress and Hertz contact pressure is performed for all bevel gears in transmission.

Keywords: bevel gears; design process; planetary transmission

1 INTRODUCTION

At the appearance of the first four-wheeled road vehicles, there was a problem of power transmission from the drive machine to the wheels [1]. When a vehicle is moving over a curved path, the outside wheel must cross more distance at the same time as the inner wheel. If both wheels were connected to the same shaft, one or the other would have to slip. Initially, only one wheel would drive, resulting in a series of disadvantages when transmitting. For this reason, transmissions that transmit power to both wheels appear. They ensure that the wheels rotate at different speeds. The technical solution of this problem is based on the differential planetary transmission with the bevel gears. Differential transmission is characterized by transmissions with one input shaft and multiple output shafts. In this case, it is characterized by with two output shafts, because the power needs to transfer on both wheels. Different wheel rotation speeds provide a planetary transmission [2] that consists of sun and planetary bevel gears. When the vehicle is moving straight, the satellites rotate around the axis of the sun bevel gears. However, when the vehicle is moving on the curved path, then the satellites rotate around the axis of the sun bevel gears and around its axis. In this way, one wheel will rotate if the other wheel is completely blocked.

Figure 1 Open differential [3]

Planetary transmissions with bevel gears can be open and with a limited slip. Differentials with a limited slip can be active and passive.

The open differential has a large opening on the supporter that serves for an easier assembly of the bevel gears (Fig. 1). Using the bolt joint, a driven bevel gear is connected on the supporter flange. This gear is a member of the input gear pair.

Limited slip differentials contain additional machine elements that enable the directioning of the torque to the desired wheel. Active transmissions contain electronic feedback systems, while passive transmissions are fully mechanical. Passive transmissions enable the directioning of the torque from the wheel that rotates faster on a slower rotate wheel (Fig. 2).

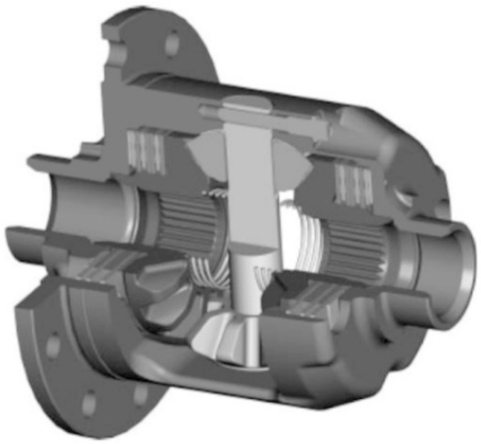

Figure 2 Limited slip differential [3]

Active differentials can direct the torque to any wheel. The basis of the construction is an open differential that has an extra planetary transmission at the output.

The greatest disadvantage of the open differential of a planetary transmission for road vehicles is the inability to direct the torque to the wheel with better adhesion on the

ground. This problem can be explained when the wheels are on surfaces with different friction factors. The rotation moment at the open differential divides equally to the left and right wheel; however, this is not enough to achieve the traction force on the wheel with better adhesion to drive the vehicle. If it is assumed that one wheel is immobile, then the second wheel rotates twice in relation to the supporter. This means that the wheel that has better adhesion on the ground does not gain power from the drive machine because all power is transmitting on the side with less resistance. This disadvantage reduces the traction force of the vehicle. The problem is possible to solve by blocking the transmission of the differential or by increasing the adhesive force on the wheel on the slippery surface.

2 BASIC CALCULATION OF TRANSMISSION

At the beginning, the design of the differential includes a basic calculation. This calculation is important for the determination of the transmission ratio. It is therefore necessary to take into account the data of the drive and the driven machine. The drive machine is an internal combustion engine. The driven machine is a car which includes all forces of resistance important for the calculation of the planetary transmission.

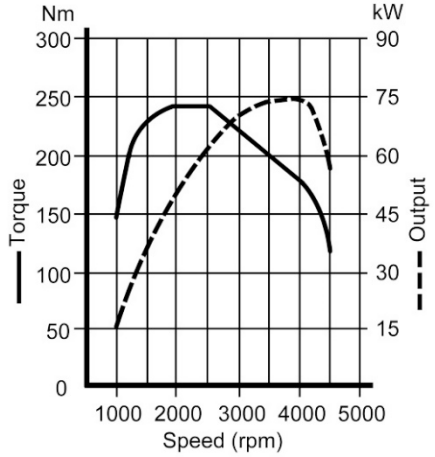

Figure 3 Factory characteristics of the power and torque on the drive machine [4]

Requirements for the calculation and design of the planetary transmission with bevel gears are derived from the requirement list [5]. Following the requirements that are necessary for calculation: the drive machine is an internal combustion engine Volkswagen 1,9 R4 TDI PD with the following technical data [4]: P_m = 74 kW at speed n = 4000 1/min, T_m = 240 Nm at speed n = 1800 - 2400 1/min. The data are graphically presented in the diagram (Fig. 3). Other data are: usability of the gearbox η_m = 0.96, usability of the cardan shaft η_k = 0.98, usability of the differential η_d = 0.97, acceleration of the vehicle a_v = 2.5 m/s^2, maximum vehicle speed at the highest transmission ratio v_{max} = 180 km/h, the vehicle must accelerate from 0 to 100 km/h for 11 seconds, the vehicle mass with the passengers and luggage is m_v = 2100 kg, resisting the rise resistance force from 6°, differential dimensions $l \times w \times h$ = 610 × 400 × 350 mm, the elements for the transfer of power and motion must be bevel gears, the wheel dimensions are 205/55 16, traction force on the drive wheels must be less than the friction force between the wheels and the ground (no slip) and gearbox transmission ratios: i_1 = 3.5, i_2 = 2.1, i_3 = 1.32, i_4 = 0.97, i_5 = 0.76, i_R = 3.55.

2.1 Transmission Load from the Drive Side

When dimensioning design elements, it is necessary to take the maximum load of the drive machine by which the transmission can be loaded [6]. According to the requirement list, for the drive machine for the transmission, the Volkswagen 1.9 R4 TDI PD engine was selected [5]. The technical data for this engine are listed in the previous title and Fig. 3.

2.2 Transmission Load from the Driven Side

The total resistance force of the driven machine is equal to the sum of the rolling resistance force (F_K), rising resistance force (F_P) and inertial force of the vehicle (F_{IN}). For this calculation, the force of air resistance has been neglected. This is because the geometry of the car design is not defined.

The rolling resistance force is generated because of the deformation of the tire at the point of contact with the ground. It is assumed that the vehicle is running on a flat surface without rising. The rolling resistance is then the greatest. The rolling resistance factor for rolling on the asphalt is f_K = 0.02. The weight of the vehicle is:

$$G_V = m_V \cdot g = 2100 \cdot 9.81 = 20601 \text{ N} \quad (1)$$

The rolling resistance force is:

$$F_K = f_K \cdot G_V = 0.02 \cdot 20601 = 412.02 \text{ N} \quad (2)$$

The rising resistance force is a component of the weight force vector that acts in the opposite direction to the motion of the rising vehicle (Fig. 4). The largest rising angle for road vehicles is γ = 6°.

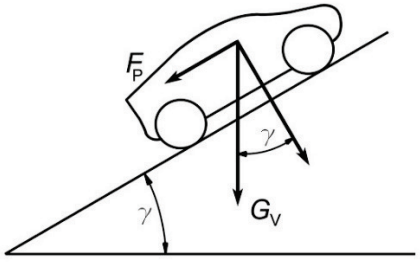

Figure 4 Rising resistance force

The rising resistance force is:

$$F_P = G_V \cdot \sin\gamma = 20601 \cdot \sin 6° = 2153.391 \text{ N} \quad (3)$$

The vehicle's inertial force occurs when the vehicle is accelerating. It is necessary then the vehicle accelerate translational. It is also necessary to accelerate all rotating elements. The contribution factor of rotating masses for the first degree of transmission is $\psi = 1.165$. Hence, the vehicle's inertial force is:

$$F_{IN} = m_V \cdot a \cdot \psi = 2100 \cdot 2.5 \cdot 1.165 = 6116.25 \text{ N} \quad (4)$$

The total resistance force of the driven machine is:

$$F_W = F_K + F_P + F_{IN} = 8681.661 \text{ N} \quad (5)$$

2.3 Calculation of the Transmission Ratio

The scheme of the planetary transmission with bevel gears, derived from the requirement list, is presented in Fig. 5.

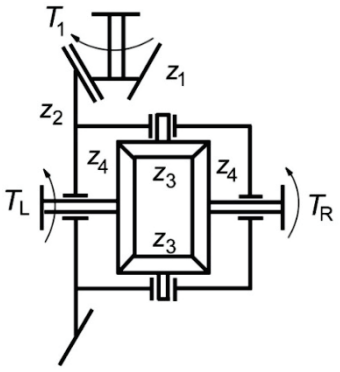

Figure 5 Transmission scheme

For calculating the transmission ratio from the diagram (Fig. 3) for the torque value $T_m = 240$ N·m, the read value of the drive machine number of revolutions is $n = 1800$ l/min. Machine power is then $P_m = 45.24$ kW. The power at the entrance to the planetary transmission is:

$$P_1 = P_m \cdot \eta_m \cdot \eta_k = 45.24 \cdot 0.96 \cdot 0.98 = 42,561 \text{ kW} \quad (6)$$

The angular speed on the first degree of the gearbox transmission is:

$$\omega_1 = \frac{\omega_m}{i_1} = \frac{188.4956}{3.5} = 53.8559 \text{ rad/s} \quad (7)$$

The torque that is transmitting via the cardan shaft to the bevel gear z_1 (Fig. 5) is:

$$T_1 = \frac{P_1}{\omega_1} = \frac{42.561 \times 10^3}{53.8559} = 790.276 \text{ N} \cdot \text{m} \quad (8)$$

The kinematic ratio of the left and right wheel rotation speed:

$$\frac{\omega_L - \omega_2}{\omega_R - \omega_2} = -\frac{z_R}{z_L} = -1 \quad (9)$$

The drive is transmitting via the cardan shaft to the rear wheels of the vehicle. It is assumed that the centre of gravity of the vehicle is at its middle. The centre of gravity is equally far from the front and rear wheels. The distance between the axles of the vehicle is 2700 mm. Therefore, the force on one of the last two wheels of the vehicle equals a quarter of the weight of the vehicle. The amount of this force is $F_a = 5150.25$ N. The friction factor for contact between the tire and surface, in the case of tire-dry asphalt, is $\mu = 0.9$, so the friction force on one wheel equals:

$$F_f = \mu \cdot F_a = 0,9 \cdot 5150.25 = 4635.225 \text{ N} \quad (10)$$

The traction force must be greater than the total resistance force. It must also be smaller than the friction force to avoid slipping. The greatest traction force is:

$$F_{TR} = 2 \cdot F_f = 2 \cdot 4635.225 = 9270.45 \text{ N} \quad (11)$$

Since the planetary transmission is derived as the open differential, the torque is equally divided into the left and right wheel:

$$T_L = T_R = F_f \cdot r_d = 4635.225 \cdot 0.25 = 1160.66 \text{ N} \cdot \text{m} \quad (12)$$

The torque on a large wheel gear z_2, assumed that there are no losses, is:

$$T_2 = T_L + T_R = 1160.66 + 1160.66 = 2321.32 \text{ N} \cdot \text{m} \quad (13)$$

The transmission ratio of bevel gears z_1 and z_2 is:

$$u = \frac{T_2}{T_1} = \frac{2321.32}{790.276} = 2.937 \approx 3 \quad (14)$$

Because of the losses, which are not considered, $u = 3$. The following is the control calculation with losses:

$$\omega_2 = \frac{\omega_1}{u} = \frac{53.8559}{3} = 17.95197 \text{ rad/s} \quad (15)$$

$$P_2 = P_1 \cdot \eta_d = 42.561 \cdot 0.97 = 41.284 \text{ kW} \quad (16)$$

$$T_2 = \frac{P_2}{\omega_2} = \frac{41.284 \times 10^3}{17.95197} = 2299.69 \text{ N} \cdot \text{m} < 2321.3 \text{ N} \cdot \text{m} \quad (17)$$

It can be confirmed that the calculation is exact.

3 CALCULATION OF BEVEL GEARS

3.1 Calculation of the Sun and Planetary Bevel Gear

The bevel gear load is done according to the mean values of the additional gears as the load of virtual gears. The

calculation is the same as the calculation of the gears, only that the intermediate additional gear has the same width as the bevel gear [7]. The bevel gear teeth number are $z_3 = 12$ and $z_4 = 16$. Therefore, the kinematic ratio is $u = 1.33$. The angle between the axes of the bevel gears is $\Sigma = 90°$. The angles of the pitch bevel gears are:

$$\tan\delta_3 = \frac{z_3}{z_4} = \frac{12}{16} = 0,75 \rightarrow \delta_3 = 36.8699° \tag{18}$$

$$\delta_4 = \Sigma - \delta_3 = 90° - 36.8699° = 53.1301° \tag{19}$$

Orientation calculations of the module were performed. The module considering the load of the tooth root is:

$$m \geq 2 \cdot \sqrt[3]{\frac{T_{\max} \cdot \cos\delta_3}{z_3 \cdot \lambda \cdot \sigma_{\mathrm{FP3}}} \cdot Y_{\mathrm{F}}} = \\ = 2 \cdot \sqrt[3]{\frac{1.16 \times 10^6 \cdot \cos 36.8699°}{12 \cdot 22 \cdot 333.3333} \cdot 2.2} = 5.69 \text{ mm} \tag{20}$$

The module considering the load of the tooth flank is:

$$m \geq 2 \cdot \sqrt[3]{\frac{u_{\mathrm{V}}+1}{u_{\mathrm{V}}} \cdot \frac{T_{\max} \cdot \cos^2\delta_3}{z_3^2 \cdot \lambda \cdot \sigma_{\mathrm{HP3}}^2} \cdot Z_{\mathrm{M}}^2 \cdot Z_{\mathrm{HV}}^2 \cdot Z_{\varepsilon \mathrm{V}}^2} = \\ = 2 \cdot \sqrt[3]{\frac{1.77+1}{1.77} \cdot \frac{1.16 \times 10^6 \cdot \cos^2 36.87°}{12^2 \cdot 22 \cdot 1304} \cdot 190^2 \cdot 2.5^2} = \\ = 5.96 \text{ mm} \tag{21}$$

The adopted module of bevel gears is $m = 6$ mm.

3.1.1 Dimensions of the Planetary Bevel Gear

The dimensions are defined with the help of calculations and they determine the geometry of the planetary bevel gear z_3.

Pitch diameter:

$$d_3 = z_3 \cdot m = 12 \cdot 6 = 72 \text{ mm} \tag{22}$$

Radius of gear rack:

$$R_{\mathrm{a}} = \frac{d_3}{2 \cdot \sin\delta_3} = \frac{72}{2 \cdot \sin 36.8699°} = 60 \text{ mm} \tag{23}$$

Face width:

$$b = \frac{R_{\mathrm{a}}}{3} = \frac{60}{3} = 20 \text{ mm} \tag{24}$$

Middle pitch diameter of the bevel gear:

$$d_{\mathrm{m3}} = d_3 - b \cdot \sin\delta_3 = 72 - 20 \cdot \sin 36.87° = 60 \text{ mm} \tag{25}$$

Teeth number of the equivalent gear:

$$z_{\mathrm{v3}} = \frac{z_3}{\cos\delta_3} = \frac{12}{\cos 36.8699°} = 15 \tag{26}$$

Middle module of the bevel gear:

$$m_{\mathrm{m}} = \frac{d_{\mathrm{m3}}}{z_3} = \frac{60}{12} = 5 \text{ mm} \tag{27}$$

Clearance:

$$c = 0.25 \cdot m = 0.25 \cdot 6 = 1.5 \text{ mm} \tag{28}$$

Whole depth:

$$h_3 = h_4 = 2 \cdot m + c = 2 \cdot 6 + 1.5 = 13.5 \text{ mm} \tag{29}$$

Addendum depth for the zero pair of bevel gears:

$$h_{\mathrm{a3}} = h_{\mathrm{a4}} = m = 6 \text{ mm} \tag{30}$$

Dedendum depth for the zero pair of bevel gears:

$$h_{\mathrm{f3}} = h_{\mathrm{f4}} = m + c = 6 + 1.5 = 7.5 \text{ mm} \tag{31}$$

Addendum circle diameter:

$$d_{\mathrm{a3}} = d_3 + 2 \cdot h_{\mathrm{a3}} \cdot \cos\delta_3 = \\ 72 + 2 \cdot 6 \cdot \cos 36.8699° = 81.6 \text{ mm} \tag{32}$$

Teeth face angle:

$$\tan\kappa_{\mathrm{a3}} = \frac{h_{\mathrm{a3}}}{R_{\mathrm{a}}} = \frac{6}{60} = 0.1 \rightarrow \kappa_{\mathrm{a3}} = \kappa_{\mathrm{a4}} = 5.7106° \tag{33}$$

Teeth root angle:

$$\tan\kappa_{\mathrm{f3}} = \frac{h_{\mathrm{f3}}}{R_{\mathrm{a}}} = \frac{7.5}{60} = 0.125 \rightarrow \kappa_{\mathrm{f3}} = \kappa_{\mathrm{f4}} = 7.125016° \tag{34}$$

Face angle of the bevel gear:

$$\delta_{\mathrm{a3}} = \delta_3 + \kappa_{\mathrm{a3}} = 36.8699° + 5.7106° = 42.5805° \tag{35}$$

Inner addendum diameter of the tooth:

$$d_{\mathrm{ia3}} = d_{\mathrm{a3}} - 2 \cdot \frac{b \cdot \sin\delta_{\mathrm{a3}}}{\cos\kappa_{\mathrm{a3}}} = \\ = 81.6 - 2 \cdot \frac{20 \cdot \sin 42.5805°}{\cos 5.7106°} = 54.4 \text{ mm} \tag{36}$$

Pitch diameter of the middle equivalent gear:

$$d_{vm3} = \frac{d_{m3}}{\cos\delta_3} = \frac{60}{\cos 36.8699°} = 75 \text{ mm} \quad (37)$$

Pitch diameter of the equivalent gear:

$$d_{v3} = \frac{d_3}{\cos\delta_3} = \frac{72}{\cos 36.8699°} = 90 \text{ mm} \quad (38)$$

Addendum diameter of the equivalent gear:

$$d_{va3} = d_{v3} + 2 \cdot h_{a3} = 90 + 2 \cdot 6 = 102 \text{ mm} \quad (39)$$

Base diameter of the equivalent gear:

$$d_{vb3} = d_{v3} \cdot \cos\alpha = 90 \cdot \cos 20° = 84.5723 \text{ mm} \quad (40)$$

3.1.2 Dimensions of the Sun Bevel Gear

Dimensions that define the geometry of the sun bevel gear z_4 are determined by expressions that are equivalent to the expressions for determining the dimensions of the bevel gear z_3. It is only necessary to use the members with the index note for the bevel gear z_4. The dimensions of the bevel gear z_4 are presented in Tab. 1.

Table 1 Dimensions of the bevel gear z_4

Name	Mark	Amount
Pitch diameter	d_4	96 mm
Middle pitch diameter	d_{m4}	80 mm
Teeth number of the equivalent gear	z_{v4}	26.6666 mm
Addendum circle diameter	d_{a4}	103.2 mm
Face angle of the bevel gear	δ_{a4}	58.8407°
Pitch diameter of the middle equivalent gear	d_{vm4}	133.33 mm
Pitch diameter of the equivalent gear	d_{v4}	160 mm
Addendum diameter of the equivalent gear	d_{va4}	172 mm
Base diameter of the equivalent gear	d_{vb4}	150.351 mm

3.1.3 Load Calculation of the Tooth Root on the Planetary and Sun Bevel Gear

According to the DIN for the material: the steel for cementing, mark 15CrNi6, has the perm strength in the tooth root of σ_{Flim3} = 500 MPa. The allowed stress in the tooth root is:

$$\sigma_{FP3} = \sigma_{FP4} = \frac{\sigma_{Flim3}}{S_{Flim}} \cdot \frac{Y_m}{Y_{sa}} \cdot K_{FX} \cdot Y_N \cdot Y_R = \\ = \frac{500}{1.5} \cdot \frac{2.1}{1.4} \cdot 1 \cdot 1 \cdot 1.025 = 512.5 \text{ MPa} \quad (41)$$

It was beforehand determined that the planetary transmission will contain four planetary bevel gears. According to that, the force on the tooth is:

$$F_{tm3} = \frac{T_2}{4 \cdot d_{m3}} = \frac{2.3 \times 10^6}{4 \cdot 60} = 9583.333 \text{ N} \quad (42)$$

The stress into the tooth root of the planetary bevel gear is:

$$\sigma_{F3} = \frac{F_{tm3}}{b \cdot m_m} \cdot Y_F \cdot Y_{\varepsilon V} \cdot K_{F\alpha} \cdot K_{F\beta} = \\ = \frac{9583.333}{20 \cdot 5} \cdot 3.25 \cdot 1 \cdot 1 \cdot 1 = 311.4583 \text{ MPa} \quad (43)$$

Since $\sigma_{F3} < \sigma_{FP3}$, the calculation satisfies.

The stress into the tooth root of the sun bevel gear is σ_{F4} = 253.9583 MPa. Since $\sigma_{F4} < \sigma_{FP4}$, the calculation satisfies.

3.1.4 Load Calculation of the Tooth Flank on the Planetary and Sun Bevel Gear

For the material: steel 15CrNi6, which has the perm strength in the tooth flank of σ_{Hlim3} = 1630 MPa, the allowed stress in the tooth flank is:

$$\sigma_{HP3} = \sigma_{HP4} = \frac{\sigma_{Hlim3}}{S_{Hmin}} \cdot K_L \cdot K_{HX} \cdot Z_R \cdot Z_V \cdot Z_N \cdot Z_W = \\ = \frac{1630}{1.25} \cdot 1.05 \cdot 1 \cdot 1 \cdot 1.025 \cdot 1 \cdot 1.1 = 1543.773 \text{ MPa} \quad (44)$$

The stress on the tooth flank of the planetary bevel gear:

$$\sigma_{H3} = Z_M \cdot Z_{HV} \cdot Z_{\varepsilon V} \cdot \sqrt{\frac{u_v + 1}{u_v} \cdot \frac{F_{tm3}}{b \cdot d_{vm3}} \cdot K_{H\alpha} \cdot K_{H\beta}} = \\ = 189.84 \cdot 2.5 \cdot 1 \cdot \sqrt{\frac{1.78 + 1}{1.78} \cdot \frac{9583.33}{20 \cdot 75} \cdot 1 \cdot 1} = \\ = 1499.1262 \text{ MPa} \quad (45)$$

Since $\sigma_{H3} < \sigma_{HP3}$, the calculation satisfies.

The stress into the tooth flank of sun bevel gear is σ_{H4} = 1124.6352 MPa. Since $\sigma_{H4} < \sigma_{HP4}$, the calculation satisfies.

3.2 Hypoid Gears Calculation

This calculation is made according to the ISO 23509:2016 norm. In Tab. 2, the geometric values necessary for the calculation are defined.

Table 2 Input geometry values

Name	Mark	Amount
Shaft angle	Σ	90°
Hypoid offset	a	50 mm
Number of teeth (pinion)	z_1	14
Number of teeth (wheel)	z_2	42
Outer pitch diameter of wheel	d_{e2}	270 mm
Wheel face width	b_2	40 mm
Mean spiral angle of wheel	β_{m2}	35°
Cutter radius	r_{c0}	115 mm

Since the calculation is very extensive, the calculation is made using the Excel spreadsheet calculator (Fig. 6). In This figure is presented only as a part of the calculation. The calculation contains an iteration procedure for the determination of the condition $|R_{\text{mint}} - R_{\text{m1}}| < 0.0001 \cdot R_{\text{m1}}$. Before the iteration procedure, it is necessary to determine the next parameters: gear ratio $u = 3$, hypoid dimension factor $F = 1$, wheel pitch angle $\delta_2 = 62.68°$ and pinion pitch angle $\delta_1 = 25.29°$. R_{m1} is calculated according to the expression:

$$R_{\text{m1}} = \frac{d_{\text{m1}}}{2 \cdot \sin \delta_1} \tag{46}$$

R_{mint} is calculated according to:

$$R_{\text{mint}} = \frac{A_3 \cdot A_4}{A_5 \cdot A_6 + A_3 \cdot A_7} \tag{47}$$

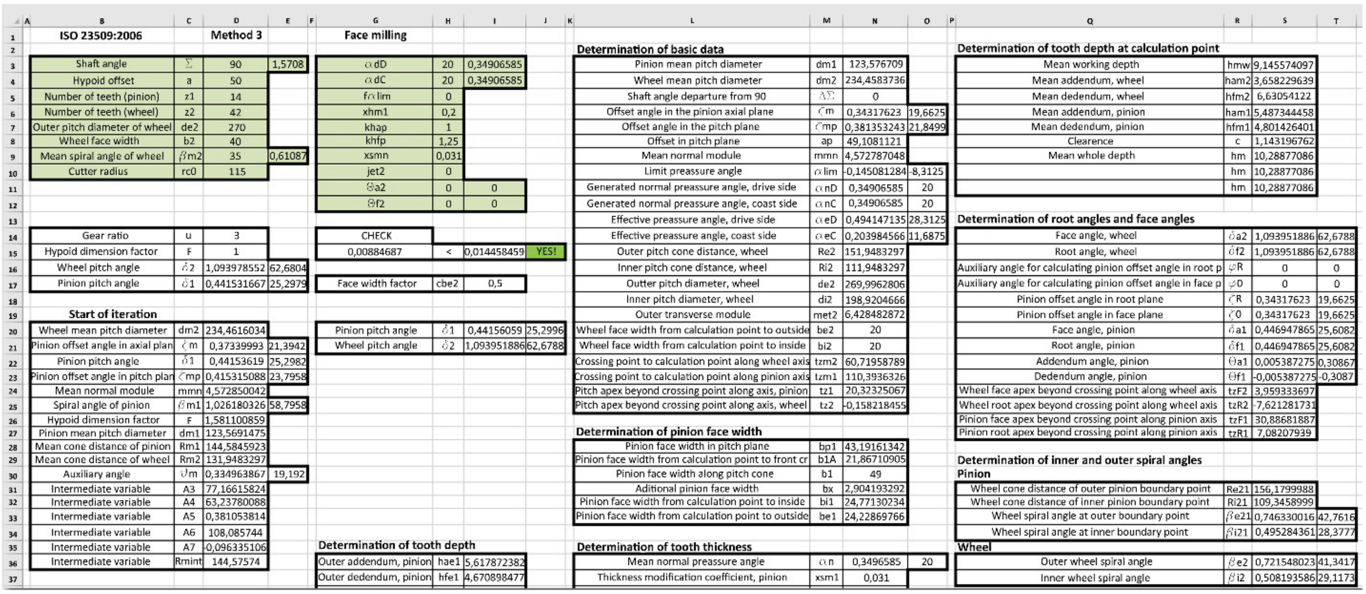

Figure 6 Hypoid gears calculation in Excel

Table 3 Remaining geometric dimensions

Outer pitch cone distance, pinion	Re1	168,81329
Inner pitch cone distance, pinion	Ri1	119,81329
Outer pitch diameter, pinion	de1	144,2850201
Inner pitch diameter, pinion	di1	102,4046327
Outside diameter, pinion	dae1	154,4430979
Outside diameter, wheel	dae2	273,3543739
Outer root diameter, pinion	dfe1	135,8392337
Outer root diameter, wheel	dfe2	263,9097366
Inner addendum diameter diameter, pinion	dai1	112,0853911
Inner addendum diameter diameter, wheel	dai2	202,2785598
Inner dedendum diameter diameter, pinion	dfi1	93,48152686
Inner dedendum diameter diameter, wheel	dfi2	192,8339226
Crossing point to crown along axis, pinion	txo1	129,8976525
Crossing point to crown along axis, wheel	txo2	66,6490006
Crossing point to front crown along axis, pinion	txi1	85,71025773
Crossing point to front crown along axis, wheel	txi2	48,28988394
Pinion whole depth, perpendicular to the root cone	ht1	10,28877086

Along with the calculation, the Excel spreadsheet contains the next calculation points: calculation of the basic geometric sizes of bevel gears, the mean tooth depth calculation, calculation of the face and root angles, face width calculation of the pinion gear, calculation of the inner and outer spiral angle, calculation of the inner and outer depth of teeth, teeth thickness calculation and calculation of the remaining geometric dimensions. The results of the last calculation point are presented in Tab. 3. The obtained results are expressed in millimetres.

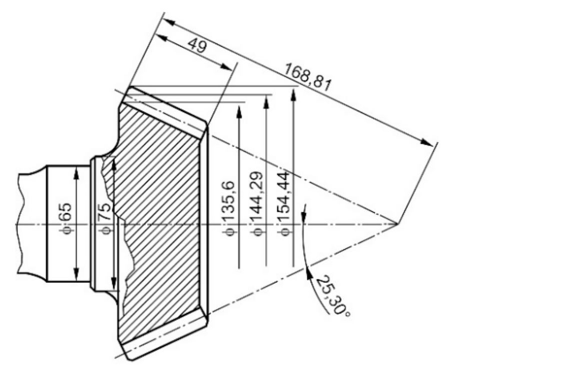

Figure 7 Pinion gear

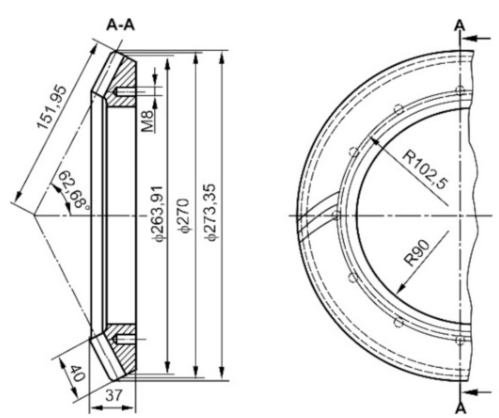

Figure 8 Wheel gear

A detailed analytical calculation, with all the necessary expressions, is presented in [5].

According the calculation, the pinion and wheel bevel gear are designed. The dimensions are presented in Fig. 7 and Fig. 8.

3.2.1 Load Calculation of the Tooth Root and the Flank of the Pinion Hypoid Gear

For the material of the pinion sun gear, according to the DIN, the 17CrNiMo6 steel for cementing was selected. The amounts of the perm strength for the tooth root and flank are $\sigma_{\text{Flim1}} = 500$ MPa and $\sigma_{\text{Hlim1}} = 1630$ MPa. The allowed stress on the tooth root is:

$$\sigma_{\text{FP1}} = \frac{\sigma_{\text{Flim1}}}{S_{\text{Flim}}} \cdot \frac{Y_{\text{m}}}{Y_{\text{sa}}} \cdot K_{\text{FX}} \cdot Y_{\text{N}} \cdot Y_{\text{R}} = \\ = \frac{500}{1.5} \cdot \frac{2.1}{1.6} \cdot 1 \cdot 1 \cdot 1{,}025 = 448.4375 \text{ MPa} \tag{48}$$

The force on the tooth is:

$$F_{\text{mt1}} = \frac{2 \cdot T_{\text{1}}}{d_{e1}} = \frac{2 \cdot 790271.8}{144.285} = 10954.3168 \text{ N} \tag{49}$$

It follows that:

$$\sigma_{\text{F01}} = \frac{F_{\text{mt1}}}{b_{\text{1}} \cdot m_{\text{mn}}} \cdot Y_{\text{Fa}} \cdot Y_{\text{sa}} \cdot Y_{\varepsilon} \cdot Y_{\beta} = \\ = \frac{10954.316}{49 \cdot 4.572} \cdot 3.25 \cdot 1.6 \cdot 0.364 \cdot 0.75 = 69.38 \text{ MPa} \tag{50}$$

The amount of stress on the tooth root is:

$$\sigma_{\text{F1}} = \sigma_{\text{F01}} \cdot K_{\text{A}} \cdot K_{\text{V}} \cdot K_{\text{F}\alpha} \cdot K_{\text{F}\beta} = \\ = 69.383 \cdot 1.5 \cdot 1.05 \cdot 1 \cdot 1 = 109.2184 \text{ MPa} \tag{51}$$

Since $\sigma_{\text{F1}} < \sigma_{\text{FP1}}$, the calculation satisfies.

The allowed stress on the tooth flank is:

$$\sigma_{\text{HP1}} = \frac{\sigma_{\text{Hlim1}}}{S_{\text{Hmin}}} \cdot K_{\text{L}} \cdot K_{\text{HX}} \cdot Z_{\text{R}} \cdot Z_{\text{V}} \cdot Z_{\text{N}} \cdot Z_{\text{W}} = \\ = \frac{1630}{1.25} \cdot 1.05 \cdot 1 \cdot 1 \cdot 1.05 \cdot 1 \cdot 1.1 = 1581.426 \text{ MPa} \tag{52}$$

It follows that:

$$\sigma_{\text{H01}} = Z_{\text{H}} \cdot Z_{\text{E}} \cdot Z_{\varepsilon} \cdot Z_{\beta} \cdot Z_{\text{K}} \cdot \sqrt{\frac{F_{\text{tm1}}}{b_{\text{1}} \cdot d_{\text{v1}}} \cdot \frac{u_{\text{v}} + 1}{u_{\text{v}}}} = \\ = 1.79 \cdot 189.8 \cdot 1 \cdot 0.71 \cdot 0.85 \cdot \sqrt{\frac{10954.3}{49 \cdot 159.5} \cdot \frac{5.91 + 1}{5.91}} = \\ = 266.9 \text{ MPa} \tag{53}$$

The amount of stress on the tooth flank is:

$$\sigma_{\text{H1}} = \sigma_{\text{H01}} \cdot \sqrt{K_{\text{A}} \cdot K_{\text{V}} \cdot K_{\text{H}\alpha} \cdot K_{\text{H}\beta}} = \\ = 266.9106 \cdot \sqrt{1.5 \cdot 1.05 \cdot 1 \cdot 1} = 334.9701 \text{ MPa} \tag{54}$$

Since $\sigma_{\text{H1}} < \sigma_{\text{HP1}}$, the calculation satisfies.

3.2.2 Load Calculation of the Tooth Root and the Flank of the Wheel Gear

For the material of the wheel gear, according to the DIN, the 16MnCr5 steel for cementing was selected. The amounts of the perm strength for the tooth root and the flank are $\sigma_{\text{Flim2}} = 460$ MPa and $\sigma_{\text{Hlim2}} = 1630$ MPa.

According to the Eq. (48), the allowed stress on the tooth root for the wheel gear is $\sigma_{\text{FP2}} = 370.8427$ MPa. According to the Eq. (49), the force on the tooth is $F_{\text{mt2}} = 17037.2705$ N. Hence, according to the Eq. (50), it follows that $\sigma_{\text{F02}} = 147.6882$ MPa. The stress on the tooth root, according to Eq. (51), is $\sigma_{\text{F2}} = 232.6089$ MPa. Since $\sigma_{\text{F2}} < \sigma_{\text{FP2}}$, the calculation satisfies.

According to Eq. (52), the allowed stress on the tooth flank for the wheel gear is $\sigma_{\text{HP2}} = 1543.773$ MPa. Hence, according to the Eq. (53), it follows that $\sigma_{\text{H02}} = 303.3964$ MPa.

The stress on the tooth flank, according to Eq. (54), is $\sigma_{\text{H2}} = 380.7595$ MPa. Since $\sigma_{\text{H2}} < \sigma_{\text{HP2}}$, the calculation satisfies.

According to the calculation, a planetary transmission with bevel gears was modelled in CAD. The 3D model is presented in Fig. 9.

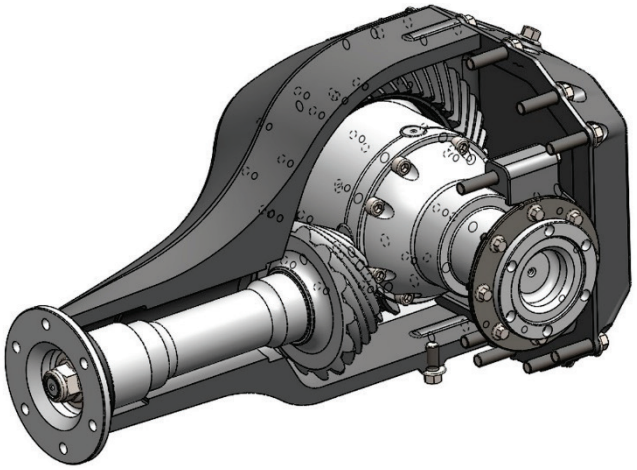

Figure 9 Planetary differential for road vehicles

4 CONCLUSION

The differential designed in this paper must enable different rotation speeds on the wheels when they are entering in the bend. Therefore, the most important part of this transmission is planetary transmission, consisting of sun and planetary bevel gears. Bevel gears in comparison with other type of gears have lower loads and usability with more complex geometry and fabrication process. Hence, they

should be installed in the first degree of the transmission because the smallest torques are there. In this case, they are at the end of the transmission chain and this creates additional problems in the dimensioning process. The momentum of the internal combustion engine first increases in the gearbox, and then it increases in the input gear pair. This ultimately leads to a very high amount of torque that planetary gears have to convey. For this reason, instead of two satellites, a four-satellite construction has been designed to allow the planetary transmission unload.

The load calculation of the tooth root and flank on the planetary bevel gears is based on the stress calculation of the equivalent virtual gears. Some influential factors are taken in value 1 even though their real value is lower. This results with a higher security of the calculation, since the bevel gears have a lower load than the other types of gears. These are the factors such as the load contribution factor, factor of the degree of overlap and the load distribution factor in the root and on the flank tooth. Because of this and the higher amount of torque, there have been a greater number of gear modules in the orientation calculation. Since the dimensions of the differential are limited, a smaller differential is designed with a smaller number of teeth. The stress results were therefore increased, because it could not go for a solution with larger modules or a larger number of teeth. This would result with the dimension increase of the differential. Although the stress results are of higher amounts, the results of the calculation are satisfying because they are lower than the permitted values.

The input gear pair is defined as a hypoid gear pair. This pair has a much quieter pace when transmitting high power and speed. They have a higher degree of overlap and a good grip even in the case of mild improper distribution of the load. The load calculation of the tooth root and the flank on the hypoid gear pair is based on the calculation of the equivalent virtual helical gears. The results are satisfactory and the gears are well dimensioned. Due to the rough calculation of the hypoid pair based on the calculation of virtual gears, it can be concluded that the actual stresses are lower than the calculated. This is because the curved teeth in relation to the helical teeth can carry higher loads and higher speeds with a better degree of overlap.

5 REFERENCES

[1] Damjanović, M., Popović, V., & Simović, S. (2016). Fluctuation of the dynamic load nature in the power transmission train. *Tehnički vjesnik - Technical gazette*, *23*(3), 741-748. https://doi.org/10.17559/TV-20141127151825

[2] Wu, Y.-C. & Chen, L.-A. (2015). Design of an 8 – speed internal gear hub with a rotary control mechanism for bicycles. *Tehnički vjesnik - Technical gazette*, *22*(4), 865-871. https://doi.org/10.17559/TV-20131225075135

[3] Crolla, D., Foster, E. D., Kobayashi, T., & Vaughan, N. (2015). *Encyclopedia of Automotive Engineering*. New Jersey, John Wiley & Sons.

[4] https://www.myarchive.us/richc/VW_TDI_with_PumpeDuse.pdf

[5] Sabo, I. (2016). *Konstruiranje planetarnog prijenosnika sa stožnicima za cestovna vozila*. Slavonski Brod, Strojarski fakultet u Slavonskom Brodu.

[6] Kljajin, M., Ivandić, Ž., & Karakašić, M. (2018). *Elementi strojeva-zbirka projektno-konstrukcijskih zadataka*. Strojarski fakultet u Slavonskom Brodu.

[7] Oberšmit, E. (1982). *Ozubljenja i zupčanici*. Zagreb, Sveučilišna naklada Liber.

Authors' contacts:

Ivan SABO, mag. ing. mech.
Mechanical Engineering Faculty in Slavonski Brod
Trg Ivane Brlić-Mažuranić 2, 35000 Slavonski Brod, Croatia
E-mail: isabo@sfsb.hr

Milan KLJAJIN, Full professor with tenure
1) Mechanical Engineering Faculty in Slavonski Brod
Trg Ivane Brlić-Mažuranić 2, 35000 Slavonski Brod, Croatia
E-mail: mkljajin@sfsb.hr

2) University North,
Jurja Križanića 31b, 42000 Varaždin, Croatia
E-mail: mkljajin@unin.hr

Mirko KARAKAŠIĆ, Associate professor
Mechanical Engineering Faculty in Slavonski Brod
Trg Ivane Brlić-Mažuranić 2, 35000 Slavonski Brod, Croatia
E-mail: mirko.karakasic@sfsb.hr

Željko IVANDIĆ, Full professor with tenure
Mechanical Engineering Faculty in Slavonski Brod
Trg Ivane Brlić-Mažuranić 2, 35000 Slavonski Brod, Croatia
E-mail: zivandic@sfsb.hr

ISSN 1846-6168 (Print), ISSN 1848-5588 (Online)
https://doi.org/10.31803/tg-20190514132701

Professional paper

ESTIMATION OF PROCESS CAPABILITY BASED ON CONTINUOUS AND ATTRIBUTE DATA

Biserka RUNJE, Živko KONDIĆ, Amalija HORVATIĆ NOVAK, Zdenka KERAN

Abstract: In the paper, a process capability and process performance analyses for continuous and attribute data are conducted by using an industry example. The inner diameter of the bearing rings is analysed by applying the normal capability analysis for the continuous data and by applying the binomial capability analysis for the attribute data. In order to quantify the process performance and process capability for continuous and attribute data, the sigma level or the process sigma is calculated. This represents an alternative method to calculating process capability indices and process performance indices.

Keywords: attribute data; continuous data; process capability; process performance; sigma level

1 INTRODUCTION

Process capability can be defined as the ability of the process to produce products/services which satisfy the requirements and needs determined by the customers themselves. Process capability studies can be conducted by using either the continuous or attribute data [1]. Continuous data is quantitative data and can contain an infinite number of values. Attribute data is data that has the quality or attribute characteristic that can be counted for recording and for the analysis.

Before process capability could be assessed, the process needed to be brought under control [2-4]. In the paper, the *p* control chart and *X* bar - *R* control chart were used to bring and keep the process under statistical control. The capability of attribute data was estimated by using the binomial distribution while the capability of continuous data was estimated by using the normal distribution. In order to compare a variable process to an attribute process, a sigma level (*Z*-score and *Z*.Bench) was used [5-7].

2 PROCES CAPABILITY ANALYSIS

The paper tracks the daily production of rings ($N = 100$ pcs) for a period of 25 days. The control of the production process was carried out through the application of the "100% control" process on the inner diameter of the bearing rings (LSL = 62.943 mm ≤ inner diameter ≤ USL = 63.050 mm). The diameter of the ring was controlled through the use of the "go – no go" method and the number of non-conforming units was ascertained (Tab. 1). The results of the non-conforming units under the lower specification limits (LSL) and above the upper specification limits (USL) are presented in Tab. 1.

Table 1 Number of non-conforming units

	Number of non-conforming units												
LSL	2	0	0	0	0	0	0	0	0	0	1	0	0
USL	0	1	2	0	2	0	1	2	1	0	1	2	0
	Number of non-conforming units												
LSL	0	0	0	0	0	1	0	0	0	1	0	0	
USL	1	1	0	0	0	1	2	0	1	0	1	1	

Considering the attributive nature of the data, the *p* control chart was used to ascertain whether the process was stable and in control. Parallel to these actions, five rings were randomly selected from the process each day and their inner diameter was measured. Results are presented in Tab. 2.

Table 2 Inner diameter in mm

Sample No.				
1.	2.	3.	4.	5.
62.986	62.997	62.980	62.967	63.017
62.963	63.024	63.012	62.989	62.992
62.980	63.013	62.971	63.017	62.994
62.996	63.010	62.974	62.989	63.010
62.973	63.014	62.996	62.968	62.995
Sample No.				
6.	7.	8.	9.	10.
62.980	63.017	62.997	62.997	62.999
63.018	62.975	62.981	62.985	62.983
63.017	62.981	63.043	63.020	62.994
62.989	62.998	63.008	63.013	63.022
62.967	62.990	63.017	62.964	62.995
Sample No.				
11.	12.	13.	14.	15.
63.026	62.969	63.043	62.984	63.006
63.026	63.013	63.046	62.958	62.993
62.977	62.993	62.987	63.010	63.002
62.984	63.010	63.027	63.028	62.958
62.999	62.998	62.986	62.961	63.014
Sample No.				
16.	17.	18.	19.	20.
62.990	62.986	62.993	63.044	62.985
62.987	62.993	63.002	62.926	62.989
62.988	62.994	62.989	63.033	63.021
63.009	63.010	63.031	63.003	63.008
63.003	63.001	62.979	63.009	63.014
Sample No.				
21.	22.	23.	24.	25.
63.013	63.009	62.973	62.973	63.044
62.978	63.028	62.987	62.987	63.008
63.018	62.998	62.939	62.939	62.992
63.017	63.001	63.003	63.003	62.999
62.974	62.980	62.998	62.998	62.989

Taking into account the fact that this analysis deals with continuous data, the *X* bar - *R* control chart was used to ascertain the stability of the process. The capability of attribute data was calculated by using the binomial

distribution, while the capability of continuous data was calculated by using the normal distribution via the Minitab trial version. The Binomial Process Capability Report is presented in Fig. 1.

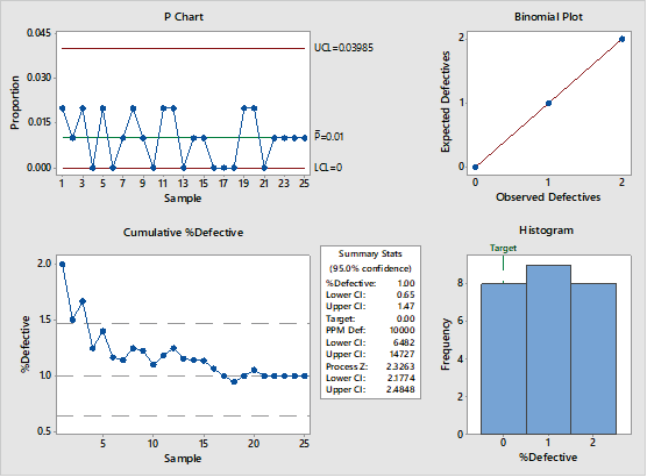

Figure 1 Binomial Process Capability Report

The *p* chart indicates that there are no data points exceeding the control limits. The chart of the cumulative estimate of the mean percentage of defective items (% defect) demonstrates that the estimate of the overall defective rate appears to be stabilizing around 1%, but additional data may need to be collected in order to verify this. The process *Z* equals 2.33. The process *Z* (the sigma capability of a process) is the capability index. The larger the process *Z* is, the better the process is performing. Process Z is computed from the average probability *P* by determining the value from a standard normal (0, 1) distribution so that the area to the right of the value is the average *P* [8-9].

The results of the process control using the *X* bar – *R* control chart are shown in Figs. 2a) and 2b), while the process capability report (normal) is shown in Fig. 3.

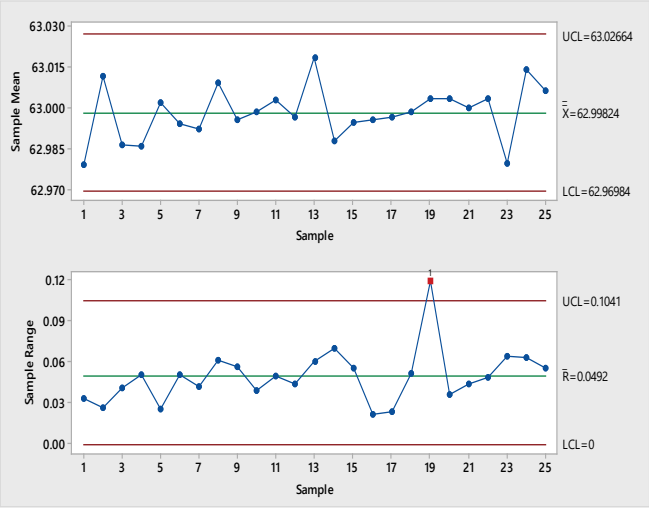

Figure 2 a) *X* bar – *R* control charts - Process not under control

In Fig. 2a), the displayed process is not stable, hence it makes no sense to calculate its capability. In such a case, the cause of process instability needs to be investigated and removed. Fig. 2b), on the other hand, displays a process which is stable and under control.

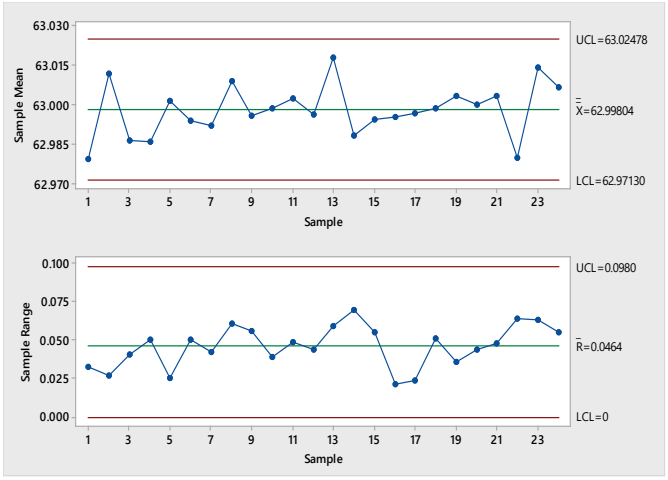

Figure 2 b) *X* bar – *R* control charts - Process under control

In accordance with the process capability report (Fig. 3), capability assessments were conducted by calculating the potential capability (process capability) and overall capability (process performance). As shown in Fig. 3, the data follow a normal distribution.

Instead of potential capability indices *Cp* and process performance indices *Pp*, the sigma level *Z*.Bench (potential) *and* sigma level *Z*.Bench (overall) were calculated.

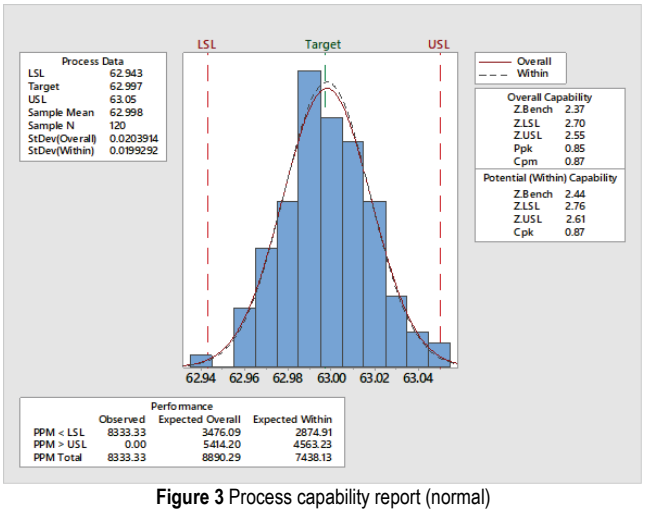

Figure 3 Process capability report (normal)

Z. Bench is defined by the Eq. (1).

$$Z.\text{Bench} = \phi^{-1}(1 - P_1 - P_2) \quad (1)$$

Where:

$$P_1 = \text{Prob}(X < \text{LSL}) = 1 - \phi(Z.\text{LSL}) \quad (2)$$

$$P_2 = \text{Prob}(X > \text{LSL}) = 1 - \phi(Z.\text{USL}) \quad (3)$$

ϕ - cumulative distribution function of a standard normal distribution

ϕ^{-1} - inverse of a cumulative distribution function of a standard normal distribution

Z.LSL - measure of sigma capability in relation to the upper specification limit
Z.USL - measure of sigma capability in relation to the lower specification limit

Sigma capability in relation to the lower specification limit *Z.LSL* and sigma capability in relation to the upper specification limit *Z.USL* are defined by Eqs. (4) and (5).

$$Z.\mathrm{LSL} = \frac{\bar{x} - LSL}{\sigma}, \tag{4}$$

$$Z.\mathrm{USL} = \frac{USL - \bar{x}}{\sigma}. \tag{5}$$

Where: $\bar{x}$ – arithmetic mean, σ – standard deviation.

The Process capability report (Fig. 3) shows that the process mean (62.998 mm) is slightly larger than the target (62.996 mm) and both tails of the distribution fall outside the specification limits. This means that there are rings whose diameter is below the lower specification of 63.943 mm or greater than the upper specification of 63.050 mm. The *Ppk* index equals 0.85, indicating that the process has to be improved by reducing variability and by centering the process on the target. In the case of this production process, its large variation represents the main challenge in assuring process quality, while the process being slightly off target is a secondary issue [10-11]. The benchmark *Z* statistics is computed by determining the *Z* value using the standard normal (0.1) distribution [8-9]. The *Z* benchmark describes the sigma capability of a process. *Z* LSL and *Z* USL measure how the process is performing against the specification limits [8-9]. *Z* Bench equals 2.37.

The *Z* score resulting from the analysis of the attribute data amounts to 2.33 and it is very close to the value of the *Z* Bench obtained from the analysis of the continuous data which is equal to 2.37. It can therefore be concluded that both analyses reached similar conclusions in regard to the sigma level of the process.

3 CONCLUSION

The procedure for estimating process capability depends on the data types used. In the first step, it is necessary to check whether the data type is continuous or attributive. In the second step, stability has to be checked by using control charts for continuous or attribute data. Depending on the type of data, the normal capability or binomial capability procedure should be applied. The process capability and process performance can be conducted via the calculation of process capability indices, as well as process performance indices and the sigma level. The sigma level or process sigma represents a good measuring tool that can be used to quantify the ability of process performance of the continuous or attribute data. The process sigma or sigma level is a universal benchmark that can be used to measure the quality of different processes.

4 REFERENCES

[1] https://support.minitab.com/en-us/minitab/18/help-and-how-to/quality-and-process-improvement/capability-analysis/supporting-topics/data-and-data-assumptions/data-types-for-capability-analysis/

[2] Deming, W. E. (1982). *Quality, Productivity and Competitive Position*, MIT Press, Cambridge.

[3] Quentin, B. (2010). *Lean Six Sigma & Minitab: The Complete Toolbox Guide for All Lean Six Sigma Practitioners*, OPEX Resources, Winchester.

[4] Antony, J., Antony, F. J., Kumar, M., & Cho, B. R. (2007). Six Sigma in Service Organizations: Benefits, Challenges and Difficulties, Common Myths, Empirical Observation and Success Factors. *International Journal of Quality & Reliability Management*, *24*(3), 294-311. https://doi.org/10.1108/02656710710730889.

[5] Kotz, S. & Johnson, N. L. (1993). *Process Capability Indices*, Chapman & Hall, London. https://doi.org/10.1007/978-1-4899-4465-8

[6] Harris, T. J. & Ross, W. H. (1991). Statistical Process Control Procedures for Correlated Observations, *Canadian Journal of Chemical Engineering*, *69*(1), 48-57. https://doi.org/10.1002/cjce.5450690106

[7] Runje, B., Medić, S., Kondić, Ž., Alar, Ž., & Tunjić, Đ. (2012). Statistical process control of fire-resistant coating production based on thickness measurements. *Tehnicki Vjesnik-Technical Gazette*. *19*(3), 589-593.

[8] https://analyse-it.com/docs/user-guide/process-capability/z-benchmark

[9] https://support.minitab.com/en-us/minitab/18/help-and-how-to/quality-and-process-improvement/capability-analysis/supporting-topics/capability-metrics/process-z-values-for-attribute-capability/

[10] Sommerville, S. & Montgomery, D. C. (1996). Process Capability Indices and Non-Normal Distribution. *Quality Engineering*, *9*(2), 305-316. https://doi.org/10.1080/08982119608919047

[11] Relyea, D. B. (2011). *The Practical Application of the Process Capability Study: Evolving from Product Control to Process Control*, CRC Press, Boca Raton.

Authors' contacts:

Biserka RUNJE, Ph.D. Prof.
University of Zagreb,
Faculty of Mechanical Engineering and Naval Architecture,
Ivana Lučića 5, 10000 Zagreb, Croatia
biserka.runje@fsb.hr

Živko KONDIĆ, Ph.D. Prof.
University North,
104 brigade 3, 42000 Varaždin, Croatia
zivko.kondic@unin.hr

Amalija HORVATIĆ NOVAK, Ph.D.
University of Zagreb,
Faculty of Mechanical Engineering and Naval Architecture,
Ivana Lučića 5, 10000 Zagreb, Croatia
amalija.horvatic@fsb.hr

Zdenka KERAN, Ph.D. Assis. Prof.
University of Zagreb,
Faculty of Mechanical Engineering and Naval Architecture,
Ivana Lučića 5, 10000 Zagreb, Croatia

ISSN 1846-6168 (Print), ISSN 1848-5588 (Online)
https://doi.org/10.31803/tg-20.....

14pt
14pt

ARTICLE TITLE ONLY IN ENGLISH (Style: Arial Narrow, Bold, 14pt)

14pt

Ivan HORVAT, Thomas JOHNSON (Style: Arial Narrow, Bold, 11pt)

11pt
11pt

Abstract: Article abstract contains maximum of 150 words and is written in the language of the article. The abstract should reflect the content of the article as precisely as possible. TECHNICAL JOURNAL is a trade journal that publishes scientific and professional papers from the domain(s) of mechanical engineering, electrical engineering, civil engineering, multimedia, logistics, etc., and their boundary areas. This document must be used as the template for writing articles so that all the articles have the same layout. (Style: Arial Narraw, 8pt)

8pt

Keywords: keywords in alphabetical order (5-6 key words). Keywords are generally taken from the article title and/or from the abstract. (Style: Arial Narraw, 8pt)

10pt
10pt

1 ARTICLE DESIGN
(Style: Arial Narrow, Bold, 10pt)

10pt

(Tab 6 mm) The article is written in Latin script and Greek symbols can be used for labelling. The length of the article is limited to eight pages of international paper size of Letter (in accordance with the template with all the tables and figures included). When formatting the text the syllabification option is not to be used.

10pt

1.1 General Guidelines
(Style: Arial Narrow, 10pt, Bold, Align Left)

10pt

The document format is Letter with margins in accordance with the template. A two column layout is used with the column spacing of 10 mm. The running text is written in Times New Roman with single line spacing, font size 10 pt, alignment justified.

Article title must clearly reflect the issues covered by the article (it should not contain more than 15 words).

Body of the text is divided into chapters and the chapters are divided into subchapters, if needed. Chapters are numbered with Arabic numerals (followed by a period). Subchapters, as a part of a chapter, are marked with two Arabic numerals i.e. 1.1, 1.2, 1.3, etc. Subchapters can be divided into even smaller units that are marked with three Arabic numerals i.e. 1.1.1, 1.1.2, etc. Further divisions are not to be made.

Titles of chapters are written in capital letters (uppercase) and are aligned in the centre. The titles of subchapters (and smaller units) are written in small letters (lowercase) and are aligned left. If the text in the title of the subchapter is longer than one line, no hanging indents.

10pt

Typographical symbols (bullets), which are being used for marking an item in a list or for enumeration, are placed at a beginning of a line. There is a spacing of 10pt following the last item:

- Item 1
- Item 2
- Item 3

10pt

The same rule is valid when items are numbered in a list:

1. Item 1
2. Item 2
3. Item 3

10pt

1.2 Formatting of Pictures, Tables and Equations
(Style: Arial Narrow, 10pt, Bold, Align Left)

10pt

Figures (drawings, diagrams, photographs) that are part of the content are embedded into the article and aligned in the centre. In order for the figure to always be in the same position in relation to the text, the following settings should be defined when importing it: text wrapping / in line with text.

Pictures must be formatted for graphic reproduction with minimal resolution of 300 dpi. Pictures downloaded from the internet in ratio 1:1 are not suitable for print reproduction because of unsatisfying quality.

10pt

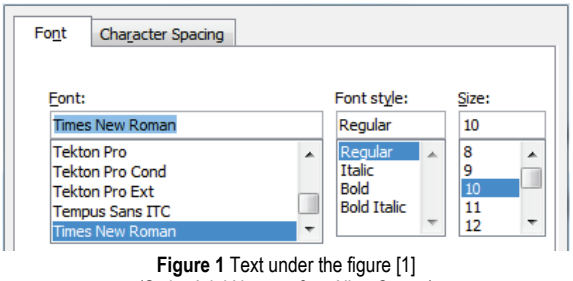

Figure 1 Text under the figure [1]
(Style: Arial Narraw, 8pt, Align Centre)

10pt

The journal is printed in black ink and the figures have to be prepared accordingly so that bright tones are printed in a satisfactory manner and are readable. Figures are to be in colour for the purpose of digital format publishing. Figures in the article are numbered with Arabic numerals (followed by a period).

Text and other data in tables are formatted - Times New Roman, 8pt, Normal, Align Center.

When describing figures and tables, physical units and their factors are written in italics with Latin or Greek letters,

while the measuring values and numbers are written upright.
10pt

Table 1 Table title aligned centre
(Style: Arial Narraw, 8pt, Align Centre)

	1	2	3	4	5	6
ABC	ab	ab	ab	ab	ab	ab
DEF	cd	cd	cd	cd	cd	cd
GHI	ef	ef	ef	ef	ef	ef

10 pt

Equations in the text are numbered with Arabic numerals inside the round brackets on the right side of the text. Inside the text they are referred to with equation number inside the round brackets i.e. ".... from Eq. (5) follows ...." (Create equations with MathType Equation Editor - some examples are given below).
10pt

$$F_{\text{avg}}(t,t_0)=\frac{1}{t}\int_{t_0}^{t_0+t}F\big(q(\tau),p(\tau)\big)\,\mathrm{d}\tau, \tag{1}$$

10pt

$$\cos\alpha+\cos\beta=2\cos\frac{\alpha+\beta}{2}\cdot\cos\frac{\alpha-\beta}{2}. \tag{2}$$

10pt

Variables that are used in equations and also in the text or tables of the article are formatted as *italics* in the same font size as the text.

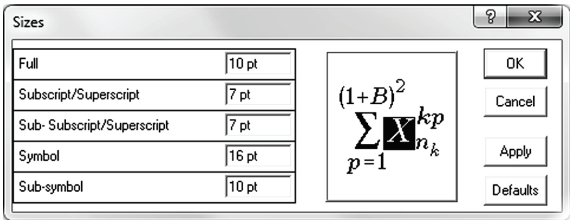

Figure 2 The texts under figures
(Style: Arial Narraw, 8pt, Align Centre)

Figures and tables that are a part of the article have to be mentioned inside the text and thus connected to the content i.e. „ … as shown in Fig. 1…" or „data from Tab. 1…" and similar.
10pt

2 PRELIMINARY ANNOTATION

10pt

Article that is offered for publication cannot be published beforehand, be it in the same or similar form, and it cannot be offered at the same time to a different journal. Author or authors are solely responsible for the content of the article and the authenticity of information and statements written in the article.

Articles that are accepted for publishing are classified into four categories: original scientific papers, preliminary communications, subject reviews and professional papers.

Original scientific papers are articles that according to the reviewer and the editorial board contain original theoretical or practical results of research. These articles need to be written in such a way that based on the information given, the experiment can be repeated and the results described can be achieved together with the author's observations, theoretical statements or measurements.

Preliminary communication contains one or more pieces of new scientific information, but without details that allow recollection as in original scientific papers. Preliminary communication can give results of an experimental research, results of a shorter research or research in progress that is deemed useful for publishing.

Subject review contains a complete depiction of conditions and tendencies of a specific domain of theory, technology or application. Articles in this category have an overview character with a critical review and evaluation. Cited literature must be complete enough to allow a good insight and comprehension of the depicted domain.

Professional paper can contain a description of an original solution to a device, assembly or instrument, depiction of important practical solutions, and similar. The article need not be related to the original research, but it should contains a contribution to an application of known scientific results and their adaptation to practical needs, so it presents a contribution to spreading knowledge, etc.

Outside the mentioned categorization, the Editorial board of the journal will publish articles of interesting content in a special column. These articles provide descriptions of practical implementation and solutions from the area of production, experiences from device application, and similar.
10pt

3 WRITING AN ARTICLE

10pt

Article is written in the English language and the terminology and the measurement system should be adjusted to legal regulations, standards (ISO 80 000 series) and the SI international system of units. The article should be written in third person.

Introduction contains the depiction of the problem and an account of important results that come from the articles that are listed in the cited literature.

Main section of the article can be divided into several parts or chapters. Mathematical statements that obstruct the reading of the article should be avoided. Mathematical statements that cannot be avoided can be written as one or more addendums, when needed. It is recommended to use an example when an experiment procedure, the use of the work in a concrete situation or an algorithm of the suggested method must be illustrated. In general, an analysis should be experimentally confirmed.

Conclusion is a part of the article where the results are being given and efficiency of the procedure used is emphasized. Possible procedure and domain constraints where the obtained results can be applied should be emphasized.
10pt

4 RECAPITULATION ANNOTATION

10pt

In order for the articles to be formatted in the same manner as in this template, this document is recommended for use when writing the article. Finished articles written in MS Word for Windows and formatted according to this

template must be submitted using our The Paper Submission Tool (PST) (https://tehnickiglasnik.unin.hr/authors.php) or eventually sent to the Editorial board of the Technical Journal to the following e-mail address: tehnickiglasnik@unin.hr

The editorial board reserves the right to minor redaction corrections of the article within the framework of prepress procedures. Articles that in any way do not follow these authors' instructions will be returned to the author by the editorial board. Should any questions arise, the editorial board contacts only the first author and accepts only the reflections given by the first author.

10pt

5 REFERENCES (According to APA)

10pt

The literature is cited in the order it is used in the article. Individual references from the listed literature inside the text are addressed with the corresponding number inside square brackets i.e. "… in [7] is shown …". If the literature references are web links, the hyperlink is to be removed as shown with the reference number 8. Also, the hyperlinks from the e-mail addresses of the authors are to be removed. In the literature list, each unit is marked with a number and listed according to the following examples (omit the subtitles over the references – they are here only to show possible types of references):

9pt

[1] See http://www.bibme.org/citation-guide/apa/

[2] See http://sites.umuc.edu/library/libhow/apa_examples.cfm

[3] (Style: Times New Roman, 9pt, according to APA)

[4] Amidzic, O., Riehle, H. J., & Elbert, T. (2006). Toward a psychophysiology of expertise: Focal magnetic gamma bursts as a signature of memory chunks and the aptitude of chess players. *Journal of Psychophysiology, 20*(4), 253-258. https://doi.org/10.1027/0269-8803.20.4.253

[5] Reitzes, D. C. & Mutran, E. J. (2004). The transition to retirement: Stages and factors that influence retirement adjustment. *International Journal of Aging and Human Development, 59*(1), 63-84. Retrieved from http://www.baywood.com/journals/PreviewJournals.asp?Id=0091-4150

[6] Jans, N. (1993). *The last light breaking: Life among Alaska's Inupiat Eskimos*. Anchorage, AK: Alaska Northwest Books.

[7] Miller, J., & Smith, T. (Eds.). (1996). *Cape Cod stories: Tales from Cape Cod, Nantucket, and Martha's Vineyard*. San Francisco, CA: Chronicle Books.

[8] Chaffe-Stengel, P. & Stengel, D. (2012). *Working with sample data: Exploration and inference*. https://doi.org/10.4128/9781606492147

[9] Freitas, N. (2015, January 6). People around the world are voluntarily submitting to China's Great Firewall. Why? Retrieved from http://www.slate.com/blogs/future_tense/2015/01/06/tencent_s_wechat_worldwide_internet_users_are_voluntarily_submitting_to.html

(Style: Times New Roman, 9pt, according to APA)

10pt

10pt

Authors' contacts:

8pt

Full Name, title
Institution, company
Address
Tel./Fax, e-mail

8pt

Full Name, title
Institution, company
Address
Tel./Fax, e-mail

DESIGN2020

16th INTERNATIONAL DESIGN CONFERENCE

MAY, 18-21 2020 - CAVTAT - DUBROVNIK - CROATIA

TOPICS

DESIGN METHODS
- Requirements Engineering
- Design for X
- Ecodesign implementation
- Design for additive manufacturing
- Product service engineering
- Computational design synthesis
- Engineering design in mechatronics
- Change management

DESIGN PROCESSES
- Configuration and modularisation
- Modelling and management of engineering processes
- Product development models and strategies
- Conceptual design cognition
- Design for product life cycle
- Resilient processes

INFORMATION & KNOWLEDGE
- Design knowledge and collaboration
- Collaborative systems
- Representations of design information
- Decision making and decision support
- Knowledge intensive design
- Artificial intelligence in design
- Data driven design

THEORY AND RESEARCH METHODS
- Empirical studies of design and design support
- New approaches to the design theories
- Design science research methods
- Design theory

ENGINEERING DESIGN PRACTICE
- Geometrical modelling, simulation and tolerancing
- Simulation based design
- Optimisation
- Visualisation and virtualisation

DESIGN INNOVATION
- Creativity and ideation
- Innovation methods and tools
- Open innovation
- Social innovation

DESIGN2020

SYSTEMS ENGINEERING
- Defining a systems approach
- Managing structural complexity
- Simulation within complex systems
- Complex systems design
- Interdependencies in complex systems
- Model-based systems engineering (MBSE)
- Cyber-physical systems design

ORGANISATION & MANAGEMENT
- Organisational understanding of product development
- Multi-product development
- Life cycle management
- Market and business implications
- Global product development
- Globalisation, legislation, remanufacturing

DESIGN SUPPORT TOOLS
- Tools for DfX and product development
- IT in product development
- Usage and integration of supportive technologies
- Virtual product development
- PDM/PLM

SOCIOTECHNICAL ISSUES
- Approaches to socio-technical systems design
- Human factors in design
- Socially responsible design
- Technology and sustainable development
- Life science and design for healthcare

HUMAN BEHAVIOUR
- Cooperation and collaboration
- Designer's attitudes and skills
- Human thinking
- Emotional engineering

INDUSTRIAL DESIGN
- User-centred design
- Aesthetics and visual impressions
- User interaction design

DESIGN EDUCATION
- Design education strategy
- Tools and environments for design education
- Project-based education

INVITATION

By tradition, DESIGN Conference is a forum for discussion and further development of all aspects of design knowledge from cognition and philosophy to methods and tools, from research theory to practice.

The goal of DESIGN Conference is to bring together researchers and practitioners who have worked on or thought about engineering and industrial design from a variety of perspectives, disciplines, and fields: engineering, aesthetics, ergonomics, psychology, sociology and the like.

Programme Chairs welcome the high-quality submissions covering substantial, original and previously unpublished research.

Rigour academic research should provide designers with the next generation of method and tools that will be appropriate to the demands. The paper submitted should address the key questions of the DESIGN 2020 conference. What are the new advances in design theory and research? How to improve design methodologies and tools, projects and processes, development of products and services? Which competencies, information, and communication technologies are needed? What is the impact on everyday design work? What social and legal issues should be considered? How we can harmonize the research outcomes so they can be transferred to design practice?

Applied, theoretical and results-oriented papers from both academia and industry, based on thorough analysis or argumentation, will all be considered for the conference programme.

The submitted papers should fit into one of the proposed conference topics. It is expected that these specific topics are extensive and non-exhaustive.

A list of examples is added for illustrating the core topics. It is required explicitly from all contributors to show how they are contributing to the overall research within these areas.

A detailed description of topics and instructions for online submission are available at **www.designconference.org**

REVIEWING POLICY

The papers will be accepted on the double-blind review basis made by the members of the Scientific Advisory Board.

The review criteria will be the novelty and level of contribution, validity of conclusions, industrial or application perspective and formal qualities of the contribution.

DESIGN Conference papers are indexed in SCOPUS and WOS - CPCI and referenced in CrossRef with DOI identifier.

Selected papers will be recommended for publication in international journals.

PROGRAMME

The DESIGN Conference provides an interactive environment where participants proactively create opportunities to share design knowledge and new cross-disciplinary research that leads to innovation.

PLENARY SESSIONS
The new ideas and visions will be presented by the keynote speakers.

TOPIC-ORIENTED SESSIONS
Will host papers selected around common research questions in order to foster discussion.

WORKSHOPS
DESIGN 2020 workshops will promote the integration of different views, approaches, and methods. Workshop coordinators could invite selected presentations and demonstrations in order to stimulate the debate as well as to propose any format of delivery that inspires interaction. The workshops will be organised on the 18th of May.

PH.D. STUDENTS' FORUM
The forum will be a unique opportunity for younger researchers and Ph.D. students to discuss their research questions and ideas with experienced researchers, practitioners and R&D managers in order to facilitate their research efforts.

THE DESIGN DEBATE
The purpose of the design debate is to investigate in a forensic manner some key topics that affect the engineering design research community. Two opponents and the debate moderator will be distinguished key players in the community presenting evidence for or against a particular topic.

INDUSTRIAL FORUM
The industrial forum will be an opportunity to discuss industrial views, needs and expectations of design research, tracing the emerging trends in industrial innovation and the right strategies for a sustainable future. The forum will offer a platform for debate among decision-makers, practitioners and academics about the future of design research, needs and expectations.

1. Full paper submission deadline **November, 15 2019**
2. Final acceptance of papers **January, 27 2020**
3. Publish-ready papers **February, 21 2020**
4. Final Conference programme **April, 2020**
5. **DESIGN 2020 Conference May, 18-21 2020**

CONFERENCE VENUE

Hotel Croatia Cavtat
Frankopanska ul. 10, 20210 Cavtat, Croatia

PROGRAMME CHAIRS

John Clarkson
University of Cambridge, United Kingdom

Tim McAloone
Technical University of Denmark, Denmark

Julie Stal-Le Cardinal
CentraleSupélec, Paris, France

Mario Štorga
University of Zagreb, Croatia

Christian Weber
Technical University Ilmenau, Germany

Dorian Marjanović
University of Zagreb, Croatia

ORGANISING SECRETARIAT ADDRESS

DESIGN Conference Secretariat
Faculty of Mechanical Engineering and Naval Architecture

Ivana Lučića 5, 10 000 Zagreb, Croatia
Phone: +385 1 6168 432

design2020@fsb.hr
www.designconference.org

the Design Society a worldwide community

cad lab

FSB 100

TEHNIČKI GLASNIK / TECHNICAL JOURNAL – GODIŠTE / VOLUME 13 – BROJ / NUMBER 2

LIPANJ 2019 / JUNE 2019 – STRANICA / PAGES 81-164

Sveučilište
Sjever

SVEUČILIŠTE SJEVER / UNIVERSITY NORTH – CROATIA – EUROPE

ISSN 1846-6168 (PRINT) / ISSN 1848-5588 (ONLINE)

TEHNICKIGLASNIK@UNIN.HR – HTTP://TEHNICKIGLASNIK.UNIN.HR